UNESP – Universidade Estadual Paulista

“Júlio de Mesquita Filho”

Instituto de Química

JÉSSICA VERGER NARDELI

Revestimentos de poliuretanos derivados de óleos vegetais com e sem adição de inibidores de corrosão: propriedades químicas, estruturais e de resistência à corrosão

Araraquara

2020

JÉSSICA VERGER NARDELI

Revestimentos de poliuretanos derivados de óleos vegetais com e sem adição de inibidores de corrosão: propriedades químicas, estruturais e de resistência à corrosão

Tese apresentada ao Instituto de Química, Universidade Estadual Paulista, como parte dos requisitos necessários para obtenção do título de Doutora em Química

Orientador: Prof. Dr. Assis Vicente Benedetti
Coorientador: Prof. Dr. Sidney José Lima Ribeiro
Coorientadora Exterior: Fátima Montemor

Araraquara
2020

FICHA CATALOGRÁFICA

Nardeli, Jéssica Verger
N223r Revestimentos de poliuretanos derivados de óleos vegetais com e sem adição de inibidores de corrosão: propriedades químicas, estruturais e de resistência à corrosão / Jéssica Verger Nardeli. – Araraquara: [s.n.], 2020
150 p.: il.

Tese (doutorado) – Universidade Estadual Paulista, Instituto de Química
Orientadora: Assis Vicente Benedetti
Coorientador: Sidney José Lima Ribeiro
Coorientadora: Fátima Montemor

1. Revestimentos protetores. 2. Corrosão. 3. Revestimento em metal. 4. Ligas de alumínio. 5. Eletroquímica. I. Título.

Bibliotecária Responsável: Ana Carolina Gonçalves Bet – CRB8/8315

UNIVERSIDADE ESTADUAL PAULISTA

Câmpus de Araraquara

CERTIFICADO DE APROVAÇÃO

TÍTULO DA TESE: "Revestimentos de poliuretanos derivados de óleos vegetais com e sem adição de inibidores de corrosão: propriedades químicas, estruturais e de resistência à corrosão"

AUTORA: JÉSSICA VERGER NARDELI
ORIENTADOR: ASSIS VICENTE BENEDETTI

Aprovada como parte das exigências para obtenção do Título de Doutora em QUÍMICA, pela Comissão Examinadora:

Prof. Dr. ASSIS VICENTE BENEDETTI
Departamento de Físico-Química / Instituto de Química - UNESP - Araraquara

Profª Drª MARINA MAGNANI
Departamento de Físico-Química / Instituto de Química - UNESP - Araraquara

Dr. ANTONIO APARECIDO PUPIM FERREIRA
Departamento de Química Analítica / Instituto de Química - UNESP - Araraquara

Prof. Dr. ZEKI NAAL
Departamento de Física e Química / Faculdade de Ciências Farmacêuticas - USP - Ribeirão Preto

Prof. Dr. PAULO OLIVI
Departamento de Química / Faculdade de Filosofia, Ciências e Letras - USP - Ribeirão Preto

Araraquara, 29 de junho de 2020

DADOS CURRICULARES

Dados pessoais

Nome: Jéssica Verger Nardeli
Nome em citações bibliográficas: NARDELI, J. V., Nardeli, Jéssica V.
Endereço profissional: Universidade Estadual Paulista “Júlio de Mesquita Filho”, UNESP, Instituto de Química, IQ, Araraquara, SP, Brasil, Rua Francisco Degni, 55, Bairro Quitandinha – 14800-060.
E-mail para contato: jeh.nardeli@gmail.com

Formação acadêmica/titulação

2020 Doutorado em Química (Conceito CAPES 7) com período sanduíche

Universidade Estadual Paulista “Júlio de Mesquita Filho”, UNESP, Instituto de Química, IQ, Araraquara, SP, Brasil.
Título: Revestimentos de poliuretanos derivados de óleos vegetais com e sem adição de inibidores de corrosão: propriedades químicas, estruturais e de resistência à corrosão.
Orientador: Dr. Assis Vicente Benedetti
Coorientador: Dr. Sidney José Lima Ribeiro
Bolsista: Fundação de Amparo à Pesquisa do Estado de São Paulo – FAPESP
Processo FAPESP: 2015/10554-9

Instituto Superior Técnico, Lisboa, Portugal. (1 ano)
Título: Avaliação da propriedade "*self-healing*" de revestimentos de poliuretanos derivados de óleos vegetais com e sem adição de inibidores de corrosão com recurso a técnicas eletroquímicas localizadas e estudo das propriedades químicas, estruturais.
Supervisora: Dra. Fátima Montemor
Bolsista: Fundação de Amparo à Pesquisa do Estado de São Paulo – FAPESP
Processo FAPESP: 2018/09040-9

2014 Mestrado em Química (Conceito CAPES 7) com período sanduíche

Universidade Estadual Paulista “Júlio de Mesquita Filho”, UNESP, Instituto de Química, IQ, Araraquara, SP, Brasil.
Título: Estudo eletroquímico de revestimentos ambientalmente amigáveis para proteção da liga de alumínio ASTM 1200.
Orientador: Dr. Assis Vicente Benedetti
Coorientador: Dr. Cecilio Sadao Fugivara
Bolsista: Fundação de Amparo à Pesquisa do Estado de São Paulo – FAPESP

Processo FAPESP: 2012/22431-0

Instituto Superior Técnico, Lisboa, Portugal. (4 meses)
Título: Estudo do mecanismo de corrosão pelas técnicas de SVET e LEIS em revestimentos ambientalmente amigáveis aplicados na liga de alumínio ASTM 1200.
Supervisora: Dra. Fátima Montemor
Bolsista: Fundação de Amparo à Pesquisa do Estado de São Paulo – FAPESP
Processo FAPESP: 2013/23060-9

2012 Graduação em Bacharelado em Química com atribuições tecnológicas

Universidade Federal da Grande Dourados, UFGD, Dourados, Brasil.
Título: Síntese, caracterização físico-química e biológica de acetatos básicos de Cu^{2+} e Fe^{3+} para o controle de *Aedes Aegypti* (Diptera: Culicidae).
Orientador: Dr. Eduardo José de Arruda
Bolsista: Conselho Nacional de Desenvolvimento Científico e Tecnológico - CNPq

Formação complementar

2018 - 2019 Doutorado Sanduíche.
Instituto Superior Técnico de Lisboa, IST, Portugal.
Bolsista: Fundação de Amparo à Pesquisa do Estado de São Paulo.

2017 - 2017 Miniaturização - Equipamentos portáteis, eletrodos impressos e técnicas.
Universidade Federal do ABC, UFABC, Santo André, Brasil.

2017 - 2017 Espectroscopia de Impedância Eletroquímica (EIS): Abordagem completa.
Universidade Estadual Paulista Júlio de Mesquita Filho, UNESP, São Paulo, Brasil.

2017 - 2017 Microscopia confocal.
Universidade Estadual Paulista Júlio de Mesquita Filho, UNESP, São Paulo, Brasil

Experiência internacional

1) Instituto Superior Técnico, Lisboa, Portugal.
Projeto: Avaliação da propriedade *"self-healing"* de revestimentos de poliuretanos derivados de óleos vegetais com e sem adição de inibidores de corrosão com recurso a técnicas eletroquímicas localizadas e estudo das propriedades químicas, estruturais.
Supervisora: Dra. Fátima Montemor
Bolsista: Fundação de Amparo à Pesquisa do Estado de São Paulo – FAPESP
Processo FAPESP: 2018/09040-9
Período: 1 ano (2018-2019)

2) Instituto Superior Técnico, Lisboa, Portugal.
Projeto: Estudo do mecanismo de corrosão pelas técnicas de SVET e LEIS em revestimentos ambientalmente amigáveis aplicados na liga de alumínio ASTM 1200.
Supervisora: Dra. Fátima Montemor
Bolsista: Fundação de Amparo à Pesquisa do Estado de São Paulo – FAPESP
Processo FAPESP: 2013/23060-9
Período: 4 meses (2014)

Produção bibliográfica

Trabalhos publicados em anais de evento (completo)

1) NARDELI, J. V.; FUGIVARA, C. S.; BENEDETTI, A. V.
Caracterização de revestimentos orgânicos: E_{OCP}, EIS, FTIR, ângulo de contato e SEM/EDS In: 22º Congresso Brasileiro de Engenharia e Ciência dos Materiais - CBECIMAT, 2016, Materiais poliméricos, Natal/RN.

2) NARDELI, J. V.; BENEDETTI, A. V.; FUGIVARA, C. S.
Estudo eletroquímico de revestimentos orgânicos derivados de óleos vegetais: E_{OCP}, LP, CP, EIS, LEIS e SVET In: INTERCORR - Congresso internacional de Corrosão, 2016, Búzios/RJ. Corrosão. ABRACO - Associação Brasileira de Corrosão.

Trabalhos publicados em anais de eventos (resumo expandido)

1) NARDELI, J. V.; SILVA, T. P. G.; FUGIVARA, C. S.; BENEDETTI, A. V.
Determinação da energia livre de superfície para revestimentos contra corrosão. 57º Congresso Brasileiro de Química - CBQ, 2017, Gramado/RS.

Trabalhos publicados em anais de evento (resumo)

1) NARDELI, J. V.; FUGIVARA, C. S.; TARYBA, M.; MONTEMOR, M.F.; BENEDETTI, A. V.
Proteção eficaz contra a corrosão por revestimento de poliuretano *self-healing* para AA2024. XXIV Congreso de la Sociedad Iberoamericana de Electroquímica, 2020, Montevideo/Uruguay. Corrosão.

2) NARDELI, J. V.; FUGIVARA, C. S.; TARYBA, M.; MONTEMOR, M.F.; BENEDETTI, A. V.
Smart coating based on polyurethane for AA2024: localized study of anti-corrosion performance. Simpósio Brasileiro de Eletroquímica e Eletroanalítica (SIBEE), 2019, Ribeirão Preto/SP. Tratamento, Corrosão E Proteção de Superfícies (TCPS).

3) NARDELI, J. V.; FUGIVARA, C.S.; TARYBA, M.; MONTEMOR, M.F.; BENEDETTI, A. V.
Zn containing polymer coatings for AA7475: localized study of anti-corrosion performance. European Corrosion Congress - EUROCORR, 2019, Seville. Organic coatings.

4) NARDELI, J. V.; FUGIVARA, C. S.; BENEDETTI, A. V.
Correlation of surface free energy and hydrophobicity of aluminum alloy with and without corrosion resistant organic coatings. 233rd ECS MEETING, 2018, Seattle, WA. Corrosion.

5) BARROS, J. J.; NARDELI, J. V.; BENEDETTI, A. V.; SUEGAMA, P. H.
Electrochemical study of sustainable coatings applied for the protection of aluminum alloy 1200. 1ª Reunião Bienal da Sociedade Brasileira de Eletroquímica e Eletroanalítica, 2018, Ribeirão Preto/SP. Corrosion.

6) NARDELI, J. V.; FUGIVARA, C. S.; BENEDETTI, A. V.
Evaluation of barrier properties of organic coatings by electrochemical permeation and electrochemical methods. 233rd ECS MEETING, 2018, Seattle, WA. Corrosion.

7) NARDELI, M. V.; NARDELI, J. V.; PAIM, L. L.
Characterization of the polyaniline film on composite electrodes of graphite/carbon nanotubes by cyclic voltammetry and SEM. Marco Inicial da Sociedade Brasileira de Eletroquímica e Eletroanalítica - SBEE, 2017, São Bernardo do Campo. Engenharia Eletroquímica.

8) NARDELI, J. V.; FUGIVARA, C.S.; BENEDETTI, A.V.
Effect of corrosion inhibitors in 3.5% NaCl solution on Al alloy protection coated with organic coatings. XXI Simpósio Brasileiro de Eletroquímica e Eletroanalítica, 2017, Natal/RN. Eletroquímica e materiais.

9) NARDELI, M. V.; NARDELI, J. V.; SA, A. C.; PAIM, L. L.
Eletropolimerização e caracterização por voltametria cíclica do filme de polianilina na superfície de eletrodos compósitos de grafite modificados com nanotubos de carbono funcionalizados. 14° Congresso Brasileiro de Polímeros, 2017, Águas de Lindóia/SP. Nanocompósitos poliméricos.

10) NARDELI, J. V.; FUGIVARA, C.S.; BENEDETTI, A. V.
Permeation Study of electrolytes in organic coatings. 5th International Conference on Multifunctional, Hybrid and Nanomaterials, 2017, Lisboa/PT. Organic coatings.

11) NARDELI, J. V.; FUGIVARA, C. S.; BENEDETTI, A. V.
Study of corrosion coatings: electrolyte permeation and roughness measurements. Marco Inicial da Sociedade Brasileira de Eletroquímica e Eletroanalítica - SBEE, 2017, São Bernardo do Campo. Engenharia Eletroquímica.

12) NARDELI, J. V.; FUGIVARA, C. S.; BENEDETTI, A. V.
Caracterização de revestimentos orgânicos: E_{OCP}, EIS, FTIR, ângulo de contato e SEM/EDS. 22º Congresso Brasileiro de Engenharia e Ciência dos Materiais - CBECIMAT, 2016, Materiais poliméricos, Natal/RN.

13) NARDELI, J. V.; FUGIVARA, C. S.; MONTEMOR, M. F.; BENEDETTI, A. V.
Estudo eletroquímico de revestimentos orgânicos derivados de óleos vegetais: E_{oc}, LP, CP, EIS, LEIS e SVET. INTERCORR - Congresso internacional de Corrosão, 2016, Búzios/RJ, Tratamento de superfície.

14) NARDELI, J. V.; FUGIVARA, C. S.; MONTEMOR, M. F.; BENEDETTI, A. V.
Trabalho de pesquisa desenvolvido no instituto de química. Mulheres na Ciência: O gênero na pós-graduação, 2016, Araraquara. Trabalho de pesquisa desenvolvido no instituto de química.

Apresentação de trabalho e/ou palestra

1) NARDELI, JÉSSICA V.; FUGIVARA, C. S.; TARYBA, M.; MONTEMOR, M. F.; BENEDETTI, A. V.
Proteção eficaz contra a corrosão por revestimento de poliuretano *self-healing* para AA2024, 2020.
Local: Montevideo/Uruguay. Evento: XXIV Congreso de la Sociedad Iberoamericana de Electroquímica.

2) NARDELI, J. V.; FUGIVARA, C. S.; TARYBA, M.; MONTEMOR, M. F.; BENEDETTI, A. V.

Smart coating based on polyurethane for AA2024: localized study of anti-corrosion performance, 2019.
Local: Ribeirão Preto/SP. Evento: Simpósio Brasileiro de Eletroquímica e Eletroanalítica (SIBEE).

3) NARDELI, J. V.; FUGIVARA, C. S.; TARYBA, M.; MONTEMOR, M. F.; BENEDETTI, A. V.
Zn containing polymer coatings for AA7475: localized study of anti-corrosion performance, 2019.
Local: Seville, Spain. Evento: EUROCORR 2019 - European Corrosion Congress – EUROCORR.

4) NARDELI, J. V.; FUGIVARA, C. S.; BENEDETTI, A. V.
Correlation of Surface Free Energy and Hydrophobicity of Aluminum Alloy with and without Corrosion Resistant Organic Coatings, 2018.
Local: Seattle, WA. Evento: 233rd ECS MEETING - The Electrochemical Society.

5) NARDELI, J. V.; FUGIVARA, C. S.; BENEDETTI, A. V.
Evaluation of Barrier Properties of Organic Coatings by Electrochemical Permeation and Electrochemical Methods, 2018.
Local: Seattle, WA. Evento: 233rd ECS MEETING - The Electrochemical Society.

6) NARDELI, M. V.; NARDELI, J. V.; PAIM, L. L.
Characterization of the polyaniline film on composite electrodes of graphite/carbon nanotubes by cyclic voltammetry and SEM, 2017.
Local: São Bernardo do Campo/SP. Evento: Marco Inicial da Sociedade Brasileira de Eletroquímica e Eletroanalítica – SBEE.

7) NARDELI, J. V.; FUGIVARA, C. S.; BENEDETTI, A. V.
Effect of corrosion inhibitors in 3.5% NaCl solution on Al alloy protection coated with organic coatings, 2017.
Local: Natal/RN. Evento: XXI Simpósio Brasileiro de Eletroquímica e Eletroanalítica – SIBEE.

8) NARDELI, M. V.; NARDELI, J. V.; SA, A.C.; PAIM, L.L.
Eletropolimerização e caracterização por voltametria cíclica do filme de polianilina na superfície de eletrodos compósitos de grafite modificados com nanotubos de carbono funcionalizados, 2017.
Local: Águas de Lindóia/SP. Evento: 14º Congresso Brasileiro de Polímeros.

9) NARDELI, J. V.; FUGIVARA, C. S.; BENEDETTI, A. V.
Estudo de revestimentos contra corrosão: permeação de eletrólitos e medidas de rugosidade, 2017.
Local: São Bernardo do Campo/SP. Evento: Marco Inicial da Sociedade

Brasileira de Eletroquímica e Eletroanalítica - SBEE.

10) NARDELI, J. V.; FUGIVARA, C. S.; BENEDETTI, A. V.
Permeation Study of electrolytes in organic coatings, 2017.
Local: Lisboa/Portugal. Evento: 5th International Conference on Multifunctional, Hybrid and Nanomaterials.

11) NARDELI, J. V.; FUGIVARA, C. S.; BENEDETTI, A. V.
Study of corrosion coatings: electrolyte permeation and roughness measurements, 2017.
Local: São Bernardo do Campo/SP. Evento: Marco Inicial da SBEE - Marco Inicial da Sociedade Brasileira de Eletroquímica e Eletroanalítica.

Participação em eventos científicos

1) Simpósio Brasileiro de Eletroquímica e Eletroanalítica (SIBEE). Ribeirão Preto/SP, 2019.

2) VI Encontro Dia Mundial da Sensibilização para a Corrosão. Lisboa/Portugal, 2019.

3) 5th International Conference on Multifunctional, Hybrid and Nanomaterials. Lisboa/Portugal, 2017.

4) Curso de Espectroscopia de Impedância Eletroquímica (EIS), Fundamentos, Aplicações e Instrumentação – INTERPRISE, Araraquara/SP, 2017.

5) II Segunda Pedagógica do ENDOC - Encontro de docentes. Araraquara/SP, 2017.

6) Marco Inicial da Sociedade Brasileira de Eletroquímica e Eletroanalítica – SBEE. São Bernardo do Campo/SP, 2017.

7) 22º Congresso Brasileiro de Engenharia e Ciência dos Materiais – CBECIMAT. Natal/RN, 2016.

8) Caracterização e síntese dos componentes das cápsulas de fosfoetanolamina para o MCTI. Araraquara/SP, 2016.

9) Desafios atuais para a Ciência e a Tecnologia Brasileiras. Araraquara/SP, 2016.

10) I Workshop Sobre Análise Térmica: Fundamentos e Aplicações. Araraquara/SP, 2016.

11) INTERCORR - Congresso internacional de Corrosão. Búzios/RJ, 2016.

12) Instabilidades cinéticas em eletrocatálise, Araraquara/SP, 2016.

13) Mulheres na Ciência: O gênero na pós-graduação. Araraquara/SP, 2016.

Organização de evento

1) Colaboradora do minicurso “Voltametria cíclica: da teoria à prática” durante a 1ª Escola de Verão em Química – Universidade Estadual Paulista “Júlio de Mesquita Filho” (UNESP), Araraquara/SP.

Participação em banca de comissões julgadoras

1) XXXI Congresso de Iniciação Científica - CIC da Universidade Estadual Paulista “Júlio de Mesquita Filho” - UNESP, Instituto de Química de Araraquara – IQ, Araraquara/SP, 2019.

2) XXIX Congresso de Iniciação Científica - CIC da Universidade Estadual Paulista “Júlio de Mesquita Filho” - UNESP, Instituto de Química de Araraquara – IQ, Araraquara/SP, 2017.

Conselho Editorial

1) Editora Atena (2020 – atual)

Revisor de periódico

1) Journal of The Electrochemical Society (2020 – atual)

2) Journal of Solid State Science and Technology (2020 – atual)

3) Polymers (2020 – atual)

4) Corrosion (2019 – atual)

5) Current Nanoscience (2020 – atual)

6) Advanced Engineering Forum (2019 – atual)

Capítulos de livros publicados

1) **NARDELI, J. V.**; FUGIVARA, C. S.; MONTEMOR, F.; BENEDETTI, A. V. Smart coating for corrosion protection of aluminium alloys: global and localized study of anti-corrosion performance, Chapter 1, p. 1-14, In: A diversidade de debates na pesquisa em química 2, Editora Atena, 2020. Qualis L3

Artigos completos publicados/submetidos em periódicos indexados:

1) **NARDELI, J. V.**; FUGIVARA, C. S.; BENEDETTI, A. V.
Correlation between hydrophobicity and susceptibility to corrosion associating measures of contact angle and testing with *aluminon*., (2020) em correção.

2) **NARDELI, J. V.**; FUGIVARA, C. S.; BENEDETTI, A. V.
Assessment of electrolytes permeation through barrier membranes and coatings before application on materials surfaces. **Corrosion Engineering, Science and Technology**, (2020) em revisão. Qualis A2, Fator de impacto: 1,706

3) **NARDELI, J. V.**; FUGIVARA, C. S.; TARYBA, M.; MONTEMOR, M. F.; BENEDETTI, A. V. Self-healing ability based on hydrogen bonds in organic coatings for corrosion protection in aluminum alloys. **Corrosion Science**, (2020) em revisão. Qualis A1, Fator de impacto: 6,479

4) **NARDELI, J. V.**; FUGIVARA, C. S.; TARYBA, M.; MONTEMOR, M. F.; BENEDETTI, A. V. Biobased self-healing polyurethane coating with Zn micro-flakes for corrosion protection of AA7475. **Chemical Engineering Journal**, (2020) em revisão. Qualis A1, Fator de impacto: 10,652

5) **NARDELI, J. V.**; FUGIVARA, C. S.; TARYBA, M.; MONTEMOR, M. F.; BENEDETTI, A. V. Novel healing coatings based on natural-derived polyurethane modified with tannins for corrosion protection of AA2024-T3. **Corrosion Science**, 162 (2020) 108213. Qualis A1, Fator de impacto: 6,479

6) **NARDELI, J. V.**; FUGIVARA, C. S.; PINTO, E. R. P.; POLITO, W. L.; MESSADDEQ, Y.; RIBEIRO, S. J. L.; BENEDETTI, A. V. Preparation of polyurethane monolithic resins and modification with a condensed tannin-yielding self-healing property. **Polymers**, 11 (2019) 1890. Qualis A1, Fator de impacto: 3,426

7) **NARDELI, J. V.**; FUGIVARA, C. S.; TARYBA, M.; PINTO, E. R. P.; MONTEMOR, M. F.; BENEDETTI, A. V. Tannin: a natural corrosion inhibitor for aluminum alloys. **Progress in Organic Coatings**, 135 (2019) 368-381. Qualis A1, Fator de impacto: 4,469

8) **NARDELI, J. V.**; SNIHIROVA, D.; MONTEMOR, M. F.; FUGIVARA, C. S.; PINTO, E. R. P.; MESSADDEQ, Y.; BENEDETTI, A. V. Localised corrosion assessement of crambe-oil-based polyurethane coatings applied on the ASTM 1200 aluminum alloy. **Corrosion Science**, 111 (2016) 422-435. Qualis A1, Fator de impacto: 6,479

Dedicatória

Aos meus pais e minhas irmãs por sempre me apoiarem, ajudarem e permanecerem ao meu lado.

Agradecimentos

A ***Deus***, por sempre me conceder forças para continuar rompendo os obstáculos do cotidiano.

Aos meus pais, ***Marcos e Nadir***, e irmãs, ***Marielle e Fernanda*** - minha base, por estarem sempre ao meu lado apoiando e contribuindo no meu conhecimento pessoal e profissional, por tudo o que eu sou, por terem me proporcionado educação e amor pelos estudos.

Ao ***Prof. Dr. Assis Vicente Benedetti***, que sempre será meu exemplo de pessoa, orientador e pesquisador, agradeço imensamente pela orientação, paciência, confiança, disposição, ensinamentos que possibilitaram meu amadurecimento científico, pessoal e encanto pela pesquisa.

A ***Profª. Drª. Fátima Montemor***, que sempre será meu exemplo de pesquisadora, pela orientação, confiança, ensinamentos, reconhecimento científico, incentivo e acolhimento durante o estágio de pesquisa no exterior desenvolvido no Instituto Superior Técnico de Lisboa, Portugal.

Ao ***Prof. Dr. Sidney José Lima Ribeiro***, pela confiança e contribuição na infraestrutura laboratorial, na qual possibilitou o desenvolvimento inicial do trabalho de doutorado. Ao ***Prof. Dr. Cecílio Sadao Fugivara*** pela disposição, ensinamentos e apoio no laboratório. Ao ***Prof. Dr. Younes Messaddeq*** pela contribuição na infraestrutura laboratorial. Ao ***Prof. Dr. Eduardo José de Arruda*** pelos ensinamentos, incentivo pela pesquisa desde a iniciação científica. A ***Profª. Drª. Patrícia Hatsue Suegama*** por apresentar-me a pesquisa na área de corrosão.

Ao amor da minha vida, pelo apoio, compreensão e incentivo nesta jornada, e a todos os amigos da Unesp de Araraquara e aos membros do ***Grupo de Eletroquímica e Materiais – GEMAT*** do Instituto de Química pelo apoio e amizade.

A todos os pesquisadores do ***Grupo de Estudos de Corrosão e Efeitos Ambientais – GECEA*** do Instituto Superior Técnico de Lisboa pela parceria e acompanhamento durante o estágio de pesquisa.

Meus queridos amigos e professores (Brasil e Portugal): Dr. Tarcio, Dr. Haroldo, Dr. Fernando, Ms. Riberto, Prof. Dr. Elton, Ms. Raone, Jéssica, Profª. Drª. Fabiola, Prof. Dr. Adriano, Profª. Drª. Fabiana, Profª. Drª. Carmem, Ms. Mahboobeh, Drª. Maryna, Ms. Joana, Ms. Roma, Ms. Yegor, Ms. Mirela, Dr. Kiko, Prof. Dr. João Salvador, Profª. Drª. Alda, Prof. Dr. Genilson e Profª. Drª. Ranuzy.

À ***Fundação de Amparo à Pesquisa do Estado de São Paulo - FAPESP***, pelas bolsas concedidas que possibilitaram a excelente execução do projeto e apresentação dos resultados em congressos nacionais e internacionais. Bolsa de Doutorado no Brasil (Processo FAPESP: 2015/10554-9) e Bolsa Estágio de Pesquisa no Exterior – BEPE (Processo Fapesp: 2018/09040-9).

"Mudam-se os tempos, mudam-se as vontades,
Muda-se o ser, muda-se a confiança;
Todo o mundo é composto de mudança,
Tomando sempre novas qualidades.
A persistência é o menor caminho do êxito"

Prólogo

Esta tese doutoral baseou-se em vários experimentos iniciais para o desenvolvimento da formulação dos revestimentos. Assim, avaliou-se o efeito de vários inibidores em solução (estigmasterol, aguapé e tanino condensado); alguns se mostraram propensos a possível aplicação na incorporação dos revestimentos, no entanto, a quantidade extraída de estigmasterol e aguapé não era suficiente para atender as necessidades do projeto. Dessa forma nos limitamos e exploramos outro inibidor orgânico (tanino condensado: polímeros de flavan-3-ol), cujo efeito foi explorado quando: i) adicionado em solução e ii) contato com formulações de revestimentos que falharam. A partir de uma série de medidas eletroquímicas convencionais e localizadas, complementadas com cálculos computacionais, permitiram a escolha do inibidor tanino condensado, este trabalho foi publicado na revista Progress in Organic Coatings. Em paralelo ao estudo da escolha do inibidor, foram realizados experimentos com o propósito de optar por uma matriz polimérica mais eficiente no impedimento da permeação de eletrólitos. Portanto, foram realizados experimentos com resinas monolíticas em célula de permeação e os resultados nos permitiram optar pela escolha da matriz mais apropriada. Tendo concluído os experimentos iniciais de escolha do inibidor e matriz polimérica, teve início a etapa de desenvolvimento dos revestimentos poliméricos com base na literatura, conforme descrito no Capítulo I, e na sequência esses revestimentos foram aplicados na proteção da liga de alumínio AA2024-T3 contra corrosão, sendo avaliados com ênfase no efeito *self-healing* (Capítulos II, III e IV).

Resumo

Os revestimentos de poliuretano (PU) foram preparados a partir de óleos vegetais (crambe e mamona) e modificados pela incorporação de inibidores de corrosão (tanino condensado). A reação foi monitorada caracterizando os produtos intermediários (poliéster e pré-polímero). O poliéster foi caracterizado pela solubilidade em metanol, índice de acidez, grupos hidroxila e espectroscopia no infravermelho por transformada de Fourier com refletância total atenuada (FTIR), e o pré-polímero foi caracterizado por teor de sólido, teor de solvente, isocianato livre (NCO) e FTIR. Os revestimentos de PU foram caracterizados por FTIR e absorção de água. Esses revestimentos foram aplicados sobre as ligas de alumínio com extensômetro. O processo de cura foi conduzido em temperatura ambiente (~25 ^{o}C). A espessura dos revestimentos foi determinada por microscopia eletrônica de varredura (SEM) e a adesão foi avaliada pela Norma ASTM D3359. Após a caracterização química e morfológica dos revestimentos foi realizado o estudo eletroquímico. A resistência à corrosão e o processo de degradação do filme (longevidade da ação do revestimento), foram estudadas por medidas de potencial em circuito aberto (E_{OCP}) e espectroscopia de impedância eletroquímica (EIS) em solução aquosa 0,6 mol L^{-1} NaCl com o tempo de imersão. Foram empregadas técnicas eletroquímicas localizadas como espectroscopia de impedância eletroquímica local (LEIS) em solução aquosa 0,005 mol L^{-1} NaCl e as técnicas de varredura com eletrodo vibrante (SVET) e de varredura com eletrodo íon-seletivo (SIET), em solução aquosa 0,05 mol L^{-1} NaCl durante 24 h. Os resultados demonstram que os revestimentos modificados com tanino condensado fornecem proteção eficaz contra a corrosão ($|Z| \sim 10^{11} \Omega\ cm^2$) apresentam efeito *self-healing* atribuído à formação de novas ligações de hidrogênio. As técnicas eletroquímicas local forneceram informação decisiva sobre o mecanismo de inibição da corrosão. Com tudo isso, o trabalho se diferencia e se destaca por conter uma variedade de formulações que utilizam como matéria-prima produtos naturais (óleo de crambe, óleo de mamona, inibidor de corrosão – tanino condensado) que oferecem efeito *self-healing*, garantindo um proteção efetiva contra corrosão da liga AA2024-T3 mesmo quando a superfície é submetida a defeitos artificiais.

Abstract

Polyurethane (PU) coatings were prepared from vegetable oils (crambe and castor) and modified by the incorporation of corrosion inhibitors (condensed tannins). The reaction was monitored by characterizing the intermediate products (polyester and prepolymer). Polyester was characterized by solubility in methanol, acidity index, hydroxyl groups and attenuated total reflectance Fourier transform infrared spectroscopy (FTIR), and the prepolymer was characterized by solid content, solvent content, free-isocyanate (NCO) groups and FTIR. PU coatings were characterized by FTIR and water uptake. These coatings were applied on aluminum alloys with an extensometer. The curing process was carried out at room temperature (~25 ^{o}C). The thickness of the coatings was determined by scanning electron microscopy (SEM) and the adhesion was assessed using the ASTM D3359 standard. After the chemical and morphological characterization of the coatings, the electrochemical study was carried out. The corrosion resistance and the film degradation process (longevity of the coating action) were studied by open circuit potential measurements (E_{OCP}) and electrochemical impedance spectroscopy (EIS) in 0.6 mol L^{-1} NaCl aqueous solution with the immersion time. Localized electrochemical techniques were also used, such as local electrochemical impedance spectroscopy (LEIS) in 0.005 mol L^{-1} NaCl aqueous solution and scanning techniques with vibrating electrode (SVET) and with ion-selective electrode (SIET), in aqueous solution 0.05 mol L^{-1} NaCl for 24 h. The results demonstrate that the modified tannin coatings provide effective protection against corrosion ($|Z| \sim 10^{11} \Omega\ cm^2$) and have a self-healing effect, attributed to the formation of new hydrogen bonds. The local electrochemical techniques provided decisive information about the corrosion inhibition mechanism. Therefore, the present study is different and stands out for containing a variety of formulations that use natural products as raw material (crambe oil, castor oil, corrosion inhibitor - condensed tannin) that offer self-healing effect guaranteeing effective protection against corrosion of the AA2024-T3 aluminum alloy even when the surface is subjected to artificial scratch.

LISTA DE FIGURAS

Figura 1. Classificação das ligas de alumínio (ABNT NBR ISO 209)..... 34
Figura 2. Ligas de alumínio que são utilizadas na estrutura da aeronave..... 35
Figura 3. Os principais ácidos graxos presentes nos óleos..... 38
Figura 4. Equação da reação básica para a formação de um poliuretano 40
Figura 5. Ilustração geral do efeito *self-healing* nos polímeros modificados 40
Figura 6. Sistema reacional utilizado para desenvolvimento das resinas / revestimentos de poliuretano 46
Figura 7. Esquema para obter as resinas monolíticas de PU e PU-modificado com tanino condensado (Capítulo I)..... 47
Figura 8. Extensômetro TKB Erichsen instruments® utilizado para aplicar as resinas na superfície do substrato..... 47
Figura 9. Espectros de ATR-FTIR para: matéria prima (óleo de crambe (CO) e mamona (CAO)), poliéster, pré-polímero, inibidor tanino condensado (TAN) e revestimentos (referência e modificado). 118
Figura 10. Inicialização do efeito *self-healing* para os revestimentos apresentados nos (a) Capítulo II – maior concentração de tanino e (b) Capítulo III – menor concentração de tanino. 126
Figura 11. Ilustração do mecanismo de proteção quando aplicado um defeito artificial na superfície do revestimento referência e revestimento modificado com tanino condensado. 127
Figura 12A. Reações de obtenção do poliéster por meio da modificação do óleo de crambe. 143
Figura 13A. Reações de obtenção do pré-polímero por meio da modificação do óleo de mamona..... 144
Figura 14A. Reações de obtenção da resina de PU. 145
Figura 15A. Reações de obtenção da resina de PU-modificado com tanino condensado..... 146

LISTA DE ABREVIATURAS, SIGLAS E SÍMBOLOS

PU – Poliuretano, Polyurethane

CO – Óleo de crambe, Crambe oil

CAO – Óleo de mamona, Castor oil

TAN – Tanino, Tannin

I_{OH} – *Hydroxyl groups*, Índice de hidroxila,

NCO – *Isocyanate*, Isocianato

Eq. – *Equation*, Equação

h – *Hours*, Hora

Hz – Hertz

kV – Quilovolt

A – Ampère

T – *Temperature*, Temperatura

wt.% - *Weight*, Peso

t – *Time*, Tempo

%*W* – *Water uptake*, Absorção de água

m_t – *Weight after immersion*, Massa após imersão

m_0 – *Initial weight*, Massa inicial

ASTM – *American Society for Testing and Materials*

ABNT – Associação Brasileira de Normas Técnicas

AA – *Aluminum Association,* Associação de Alumínio

OM – *Optical microscopy* - Microscopia óptica

ATR-FTIR – *Attenuated total reflectance Fourier transform infrared spectroscopy*, espectroscopia no infravermelho por transformada de Fourier com refletância total atenuada

SEM – *Scanning electron microscopy* - Microscopia eletrônica de varredura

EDX – *Energy dispersive X-ray (EDX) analysis*, Análise por espectroscopia de dispersão de energia de raios-X

E_{OCP} – *Open circuit potential* - Potencial em circuito aberto

EIS – *Electrochemical impedance spectroscopy*, Espectroscopia de impedância eletroquímica

|*Z*| – *Impedance modulus*, Módulo de impedância

vs. – *Versus*

Ω – *Ohm*

G – *Giga*

EEC – *Equivalent electrical circuit*, Circuito elétrico equivalente

R_{CT} – *Charge transfer resistance*, Resistência de transferência de carga

R_{PO} – *Coating pore resistance*, Resistência dos poros do revestimento

CPE_{dl} – *Constant phase element associated with the* double layer, Elemento de fase constante associado a dupla camada

CPE_{coat} – *Constant phase element associated with the coating*, Elemento de fase constante associado ao revestimento

LEIS – *Localized electrochemical impedance spectroscopy*, Espectroscopia de impedância eletroquímica localizada

ρ – *Conductivity*, Condutividade

A – *Admittance,* Admitância

A_0 – *Initial Admittance*, Admitância inicial

SVET – *Scanning vibrating electrode technique*, Técnica de varredura com eletrodo vibrante

SIET– S*canning ion-selective electrode technique*, Técnica de varredura com eletrodo íon-seletivo

i – *Current density*, Densidade de corrente

SUMÁRIO

Estado da arte 27
1 Objetivos e organização da tese 32
2 Introdução 32
2.1 O alumínio e suas ligas 32
2.1.1 O alumínio 32
2.1.2 Ligas de alumínio 33
2.2 Revestimentos de poliuretano e efeito *self-healing* 36
2.2.1 Revestimentos de poliuretano 37
2.2.2 Efeito *self-healing* 40
2.3 Técnicas eletroquímicas convencionais e locais para estudar a capacidade de inibição da corrosão 42
3 Parte experimental 44
3.3.1 Absorção de água (*water uptake*) 48
3.3.2 Espectroscopia na região de infravermelho por transformada de Fourier com acessório de refletância total atenuada (ATR-FTIR) 49
3.3.3 Espessura dos revestimentos 49
3.3.4 Testes de adesão 49
3.3.5 Ângulo de contato 50
3.3.6 Microscopia óptica (OM) 50
3.3.7 Microscopia eletrônica de varredura (SEM / EDX) 50
3.4 Estudo eletroquímico 51
3.4.1 Potencial em circuito aberto (E_{OCP}) e espectroscopia de impedância eletroquímica (EIS) 51
3.4.2 Espectroscopia de impedância eletroquímica localizada (LEIS) .. 51
3.4.3 Técnica de varredura com eletrodo vibrante (SVET) e com eletrodo íon seletivo (SIET) 52
CAPÍTULO I: Preparação das resinas monolíticas 54
CAPÍTULO II: Aplicação dos revestimentos para proteção contra corrosão da liga AA2024-T3 76
CAPÍTULO III: Desenvolvimento de *smart-coating* (revestimento inteligente) para proteção contra corrosão 89
CAPÍTULO IV: Estudo do efeito do inibidor em solução 102
4 Discussão 117
4.1 Preparação das resinas monolíticas 117
4.2 Aplicação dos revestimentos na proteção contra corrosão 118

5 Conclusões 129
Referências bibliográficas 132
Apêndice I 143
Apêndice II 147
Apêndice III 148
Apêndice IV 150

Estado da arte

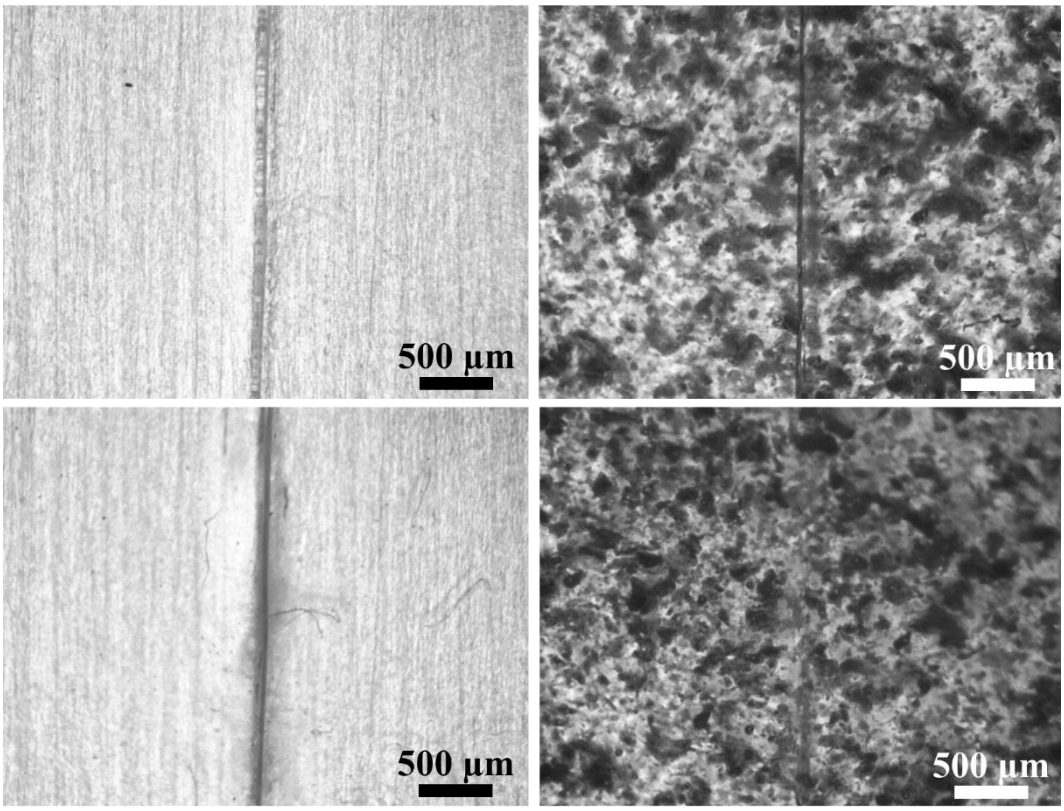

POLÍMEROS *SELF-HEALING*

Essas imagens de microscopia óptica apresentam uma redução drástica na corrosão de uma chapa de alumínio (AA2024-T3) revestida com um revestimento modificado (à direita) em comparação com um revestimento referência. Ambas as amostras foram arranhadas e colocadas em NaCl a 0,005 mol L^{-1} por 25 horas. No revestimento modificado, o arranhão recuperou completamente - efeito *self-healing* (autocura), enquanto no revestimento referência, o arranhão permanece até o substrato.

Jéssica V. Nardeli et al., Corrosion Science, 162 (2020) 108213

Revestimentos costumam ser eficientes para proteção contra corrosão de diferentes substratos metálicos ao oferecerem uma barreira física que impede o contato do substrato com as espécies corrosivas. Entretanto, quando ocorre desgaste ou defeito nos revestimentos, os substratos ficam expostos e sofrem o processo de corrosão. Nesse contexto, os revestimentos com propriedade *self-healing* são eficientes quando o revestimento apresenta alguma falha pois o

revestimento é capaz de recuperar a área danificada sem intervenção externa, mas sim por um efeito autônomo da própria matriz polimérica. Para obter o efeito *self-healing*, o revestimento conta com incorporação de aditivos que inibem a corrosão por meio da recuperação da matriz polimérica que está associada à formação de novas ligações química.

A composição dos revestimentos tem despertado grande interesse devido aos efeitos dependentes da formulação e ao emprego de substâncias oriundas de fontes renováveis (óleos e inibidores de corrosão) contribuindo no arranjo estrutural que possibilita diversas aplicações potenciais como revestimentos protetores contra corrosão. Atualmente, alguns exemplos de revestimentos com base científica e tecnológica são apresentados na tabela abaixo que faz um paralelo da composição e resistência no estudo contra corrosão. Além disso, a adição de inibidores de corrosão na estrutura polimérica do revestimento pode ser interessante para avaliar o ganho na propriedade barreira, como no processo *self-healing* no âmbito do desenvolvimento de novos revestimentos, cujo efeito *self-healing* ocorra de forma autônoma por meio da formação de novas ligações na estrutura química do revestimento.

O inibidor de corrosão tanino condensado foi explorado para estudar as propriedades de interação com a superfície metálica, em específico alumínio, por meio de cálculos computacionais e testes em laboratório, considerando o efeito da adição em solução e em contato com a matriz polimérica (Prog. Org. Coat. 135 (2019) 368-381). Com relação ao contato com a estrutura polimérica, os revestimentos foram extensivamente estudados com o objetivo de desenvolver uma nova estrutura para aplicação na proteção contra corrosão de superfícies metálicas. Em particular, as pesquisas se concentraram nos inibidores naturais (estigmasterol, aguapé e tanino condensado).

O grande interesse no estudo de sistemas de poliuretano que combinam compostos à base de óleos vegetais com inibidor de corrosão deve-se à variedade de aplicações possíveis devido às suas excelentes propriedades e a substituição por materiais de fontes não-renováveis. De fato, a contribuição acentuada da incorporação do tanino na matriz polimérica mostrou o efeito *self-healing* tanto na resina monolito (Polymers 11 (2019) 1890), como na resina aplicada na liga de alumínio AA2024 (Corros. Sci. 162 (2020) 108213). Os ensaios convencionais de corrosão comprovaram resistência relativamente

elevada (|Z| ~ 10^{11} Ω cm²) quando comparado a diferentes sistemas já relatados na literatura (Tabela abaixo). Os ensaios de corrosão localizada permitiram o registro da diminuição da corrosão na região do defeito que em combinação com as análises de superfície por microscopia óptica e eletrônica de varredura permitiram a observação do efeito *self-healing* (Figura acima), propriedade interessante em aplicações visando a proteção da superfície metálica.

Comparação com outros trabalhos

Revestimento	Impedância (Ω cm^2)	Referência
Vanadia-based coatings	1x10^3	Surf. Coat. Technol. 206 (2012) 3686–3692
Chitosan	1x10^3	Mater. Lett. 66 (2012) 302–304
Bisphenol A based benzoxazine/Polyurethane/SiO_2	2x10^4	J. Mater. Sci 55 (2020) 2215-2225
Chitosan with inhibitor 2-mercaptobenzothiazole	1x10^5	ECS Electrochem. Lett. 2 (2013) C19-C22
Chitosan with cerium nitrate	1x10^5	Prog. Org. Coat. 75 (2012) 8-13
Polypyrrole/TiO_2 nanocomposite coating	1x10^5	Ceram. Int. 39 (2013) 5639-5650
Organic coating Li_2CO_3-loaded	1x10^5	Corros. Sci. 140 (2018) 272-285
Poly(methyl methacrylate) (PMMA) microcapsules filled with linseed oil (LO)	1x10^5	Prog. Org. Coat. 132 (2019) 288-297
Epoxy/TiO_2 porous particles	1x10^5	Prog. Org. Coat. 74 (2012) 418-426
PDDA/PAA multilayer coatings	1x10^5	Colloid. Surf. A 476 (2015) 48–56
Chitosan	1x10^6	J. Mater. Chem., 21 (2011) 4805
Chitosan+Ce/hybrid sol-gel	1x10^6	J. Mater. Chem., 21 (2011) 4805
Graphene oxide	1x10^6	Prog. Org. Coat. 129 (2019) 285-291
Sol-Gel Coating Modified with La and Mo-Enriched Zeolites (La+Mo coating)	1,4x10^6	J. Electrochem. S. 161 (2014) C215-C222
Alkyd varnish coating (AVC) with isophorone diisocyanate (IPDI) microcapsules	1x10^6	J. Mater. Chem. A, 2014, 2, 1914–1921
Coatings containing isophorone diisocyanate microcapsules	1x10^6	Corros. Sci. 80 (2014) 528–535
Sol-gel/Hydroxyapatite particles	1x10^6	ACS Appl. Mater. Interfaces 2 (2010) 3011- 3022
Chitosan with 2-Mercaptobenzothiazole	1x10^7	Surf. Coat. Techol. 226 (2013) 51-59
Polyaniline/poly (γ-glycidoxypropyltrimethoxysilane) bi-layer coating	1x10^7	Surf. Coat. Technol. 337 (2018) 1-11

Anion-exchanging hydrotalcite compounds dispersed as a particulate additive in organic resins	$1x10^7$	Prog. Org. Coat. 47 (2003) 174-182
Polydopamine functionalized graphene oxide nanocomposites/waterborne polyurethane	$1x10^7$	Eur. Polym. J. 120 (2019) 109249
Polyurethane with polycaprolactone	$3x10^7$	Chem. Eng. J. 368 (2019) 1033-1044
Voltage-controlled plasma electrolytic oxidation (PEO) coatings	$1x10^7$	Mater. Des. 120 (2017) 36-46
Methyl methacrylate (MMA)/ PVD/TEOS	$1x10^7$	Prog. Org. Coat. 65 (2009) 37-43
Nafion	$1x10^7$	Appl. Energy 112 (2013) 1126–1130
Inhibitor containing multilayered urea formaldehyde microcapsules (MLUFMCs)	$1x10^7$	J. Mater. Sci. 54 (2019) 12079–12094
Polyurethane with PLA/MBT	$1x10^8$	Prog. Org. Coat. 130 (2019) 235-243
Polyurethane with einforced with 3-(triethoxysilyl)propyl isocyanate	$1x10^8$	Prog. Org. Coat. 136 (2019) 105243
Inorganic/Organic Hybrids	$1x10^8$	Prog. Org. Coat. 134 (2019)209-218
Waterborne coatings	$1x10^8$	Prog. Org. Coat. 82 (2015) 1–6
Coatings modified with combinations of layered double hydroxides and cerium molibdate nanocontainers filled with corrosion inhibitors	$1x10^8$	Electrochim. Acta 60 (2012) 31-40
Epoxy/Urea formaldeyde capsules	$1x10^8$	Prog. Org. Coat. 70 (2011) 142-149
Silane/CeO_2 nanoparticles	$1x10^8$	Prog. Org. Coat. 63 (2008) 330-337
Epoxy/Layered double hydroxides, cerium molybdate	$1x10^8$	Electrochim. Acta 60 (2012) 31-40
Polyurethane coating	$1x10^8$	Corros. Sci. 111 (2016) 422-435
Polyurethane coating with inhibitor in solution	$1x10^8$	Prog. Org. Coat. 135 (2019) 368-381
Acrylated polycaprolactone polyurethanes	$1x10^9$	ACS Appl. Mater. Interfaces 7 (2015) 175-183
Polyether imide (PEI) in N,N-dimethylacetamide (DMAc)	$1x10^9$	Acta Biomater. 9 (2013) 8660-8670
Novel healing coating: Polyurethane with condensed tannin (Presente trabalho)	**$1x10^{11}$**	**Corros. Sci. 162 (2020) 108213**

A possibilidade de melhorar o efeito barreira, incluindo efeito *self-healing* baseados na incorporação de inibidor de corrosão na matriz polimérica possibilitou a aplicação do revestimento na proteção contra corrosão da liga AA2024-T3. A síntese incorporando o inibidor de corrosão diretamente na estrutura polimérica sem capsulas abre perspectivas muito promissoras para aplicações em outras superfícies. A presente tese é o resultado da totalidade de estudos/ensaios e testes (análise da membrana/monolito em célula de

permeação, efeito do aditivo quando incorporado em solução, efeito da estrutura com relação à composição dos segmentos rígidos e flexíveis) que permitiram conhecimento mais profundo do sistema polimérico, possibilitando, assim, a realização de modificações da estrutura polimérica por meio da incorporação de aditivos contra corrosão, visando aprimorar o desempenho contra corrosão e o efeito *self-healing* (autocura).

1 Objetivos e organização da tese

Objetivos

Investigar e sintetizar revestimentos orgânicos a partir do óleo de crambe e óleo de mamona sem e com aditivos (tanino condensado). Aplicar os revestimentos na superfície da liga AA2024-T3 para proteção contra corrosão e avaliar o comportamento eletroquímico por meio de técnicas convencionais e localizadas. Preparar e caracterizar revestimentos orgânicos de poliuretano sem e com aditivo (tanino condensado). Caracterizar revestimentos orgânicos antes da aplicação na superfície metálica. Depositar o revestimento orgânico sobre a liga AA2024-T3. Caracterizar e estudar a eletroquímica da interface AA2024-T3 / solução NaCl e AA2024-T3 / revestimentos orgânicos / solução NaCl e avaliar a eficiência desses revestimentos na proteção da liga AA2024-T3 contra a corrosão em diferentes concentrações de NaCl. Avaliar a propriedade *self-healing* dos revestimentos orgânicos.

Organização da tese

A tese está organizada nos seguintes capítulos:

O Capítulo I descreve a preparação de revestimentos orgânicos.
Os Capítulos II e III descrevem a aplicação de diferentes formulações de revestimentos orgânicos na proteção contra corrosão da liga AA2024-T3.
O Capítulo IV descreve o estudo do efeito do inibidor em solução.

2 Introdução

2.1 O alumínio e suas ligas

2.1.1 O alumínio

O alumínio é o terceiro metal mais abundante e o segundo metal mais consumido do mundo [1]. O alumínio é um material muito versátil, leve, pois apresenta baixa densidade (2,7 g cm^{-3}), maleável, dúctil, apto para a fundição e mecanização, possui alta resistência mecânica, muito boa resistência à corrosão atmosférica e à ação de alguns compostos químicos [2].

O alumínio apresenta resistência à corrosão maior que a maioria dos outros metais; sua afinidade por oxigênio é extremamente importante, pois à temperatura ambiente, há a formação de uma película passiva de óxido na sua superfície que protege o metal especialmente contra a corrosão [3].

Apesar de o alumínio puro possuir baixa resistência mecânica, ser maleável e frágil, suas ligas com pequenas quantidades de cobre, magnésio, manganês, silício e outros elementos químicos apresentam características adequadas às mais diversas aplicações. As ligas constituem o material principal para a produção de muitos componentes dos aviões e foguetes [2].

2.1.2 Ligas de alumínio

A classificação do alumínio e suas ligas, segundo ABNT NBR ISO 209 [4], baseia-se em um sistema de quatro dígitos [5] que foi inicialmente proposto pela *Aluminum Association,* Associação de Alumínio (AA) [6,7].

A **Figura 1** apresenta um esquema referente a classificação das ligas de alumínio segundo a ABNT NBR ISO 209 [4]. Existem duas maneiras para se aumentar a resistência mecânica das ligas de alumínio: via tratamento térmico ou via encruamento (deformação à frio) (**Figura 1**).

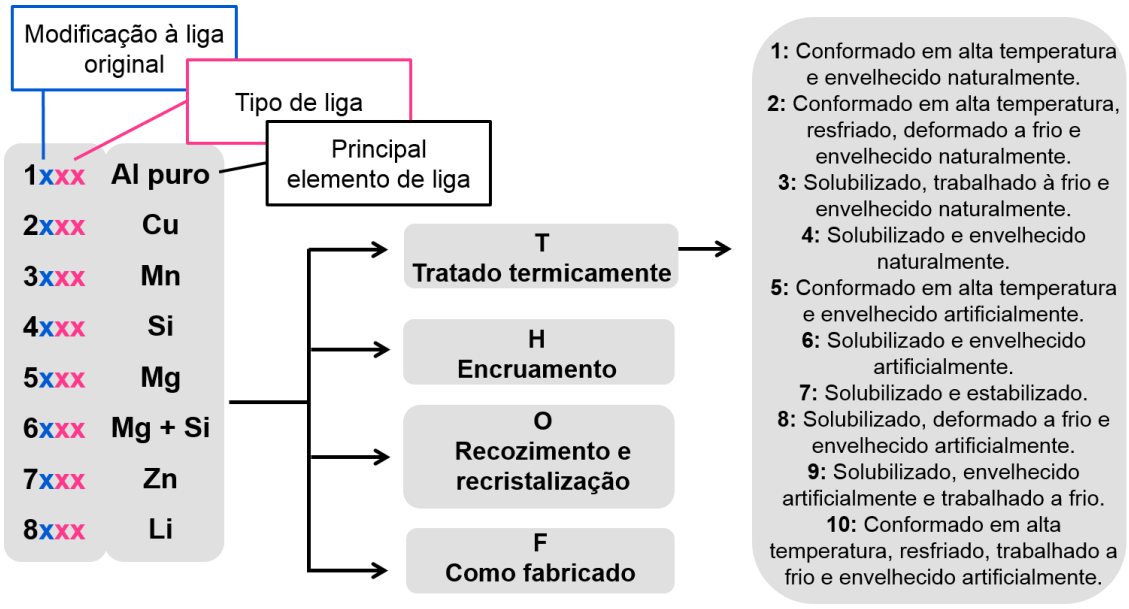

Figura 1. Classificação das ligas de alumínio segundo a ABNT NBR ISO 209. Fonte: adaptado [4].

A resistência à corrosão das ligas de alumínio depende da microestrutura heterogênea das adições de elementos de liga e tratamentos térmicos [8,9]. Dentro deste contexto, apresenta-se algumas informações pertinentes ao principal elemento de liga, em que o primeiro dígito indica o grupo dos elementos que determinam as características da liga:

Série 1xxx. Alumínio ≥ 99.00%. Caracteriza-se pela excelente resistência à corrosão generalizada, alta condutividade térmica e elétrica, baixa resistência mecânica e excelente usinabilidade.

Série 2xxx. O cobre é o principal elemento de liga, tendo o magnésio como segundo elemento adicional. A resistência à corrosão é menor do que as demais ligas. As ligas 2xxx são usadas para rodas de caminhões e aeronaves e fuselagem de aeronaves.

Série 3xxx. O manganês é o segundo componente majoritário de liga, pertence ao grupo de ligas não tratáveis termicamente, mas possui resistência mecânica em média 20% maior do que as ligas da série 1xxx, devido a conter ao redor de 1,5% Mn.

Série 4xxx. O silício é o principal elemento depois do alumínio. A porcentagem de silício pode ser de até 12% diminuindo o ponto de fusão da liga. Por esta razão, este tipo de liga é usado para soldas.

Série 5xxx. Tem o magnésio como componente majoritário depois do alumínio. Possui boas características para solda e boa resistência à corrosão, inclusive em ambiente marítimo, e por isso pode ser usada em casco de navios e barcos.

Série 6xxx. Possui silício e magnésio aproximadamente nas proporções de formação de Mg_2Si, o que a torna termicamente tratável. Possui resistência mecânica média (menor que as séries 2xxx e 7xxx), possui boa resistência à corrosão e pode ser usada para soldas.

Série 7xxx. O zinco, principal componente depois do alumínio, pode variar de 1 a 8%. A adição de pequena porcentagem de Mg torna possível o tratamento térmico, que promove melhor combinação de resistência mecânica e à corrosão, e tenacidade à fratura.

Série 8xxx. A liga 8xxx possui grande variedade de elementos em sua composição, mas frequentemente caracteriza-se por possuir de 2,4 a 2,8% de lítio. Essa liga tem como aplicação o desenvolvimento de estrutura de aviões e aeronaves espaciais.

A **Figura 2** apresenta um exemplo de aplicação das ligas de alumínio, neste caso na estrutura da aeronave.

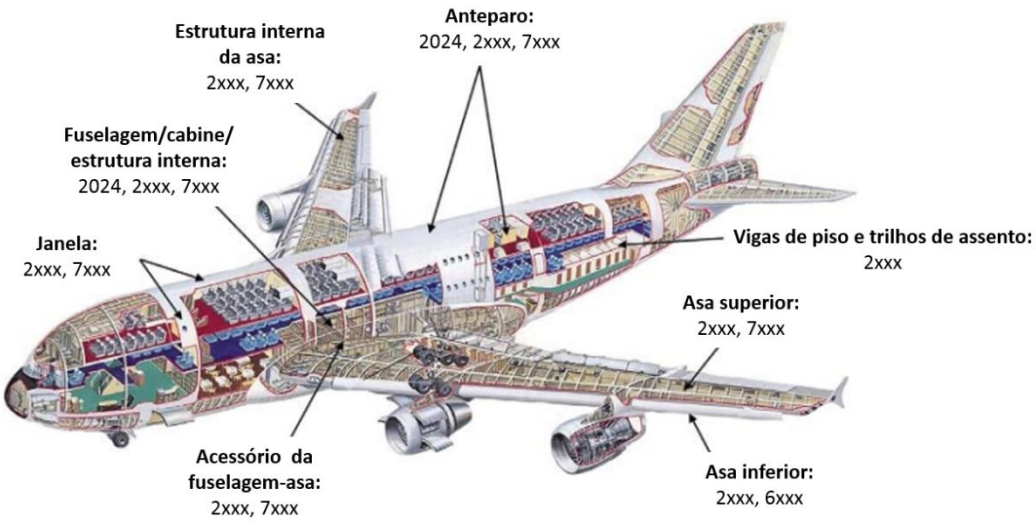

Figura 2. Ligas de alumínio que são utilizadas na estrutura da aeronave. Fonte: adaptado [10].

Conhecendo as classificações das ligas de alumínio e os tipos de tratamento térmico (**Figura 1**), juntamente com um exemplo de aplicação (**Figura**

2), designa-se a liga de alumínio de interesse neste trabalho como: liga AA2024-T3, onde o cobre (com teores entre 3,8% – 4,9%) é o principal elemento de liga, tendo o magnésio como segundo elemento adicional (com teores entre 1,2% – 1,8%), e foi solubilizada, trabalhada à frio e envelhecida naturalmente. Os elementos de liga (cobre e magnésio) são adicionados para aumentar a resistência mecânica da liga. No entanto, apesar da influência positiva da adição dos elementos de liga na resistência mecânica, eles são diretamente responsáveis pela redução na resistência à corrosão das ligas AA2024-T3 [11]. Uma vez que, a natureza, concentração e distribuição de partículas intermetálicas de segunda fase é um fator dominante que controla os mecanismos e a cinética de corrosão localizada, pois as características eletroquímicas das partículas podem diferir daquelas da matriz circundante, o que pode tornar a liga suscetível à corrosão localizada [8,9]. Outras partículas intermetálicas presentes na liga AA2024-T3 são: Al-Cu-Fe-Mn, Al-Cu-Mg.

A liga AA2024-T3 é particularmente suscetível à corrosão devido à presença da fase S rica em Cu e Mg, que é a fase mais sensível à corrosão [12]. A fase S (Al_2CuMg) é a fase intermetálica mais abundante na liga AA2024-T3 [13]. Esses precipitados desempenham um papel fundamental no processo de corrosão, pois atuam como locais preferenciais de nucleação de corrosão. Quando a fase S rica em Cu se dissolve, há abertura de vales da matriz de Al ao redor das partículas de Al_2CuMg, principalmente como resultado de sua autodissolução [14]. A corrosão da liga AA2024-T3 em soluções de NaCl é um processo complexo, envolvendo reações químicas e eletroquímicas que incluem a dissolução da fase S e a oxidação de Al a Al^{3+}, Mg a Mg^{2+}, oxidação e deposição de Cu, e redução de O_2 e H_2O para OH^- [13].

2.2 Revestimentos de poliuretano e efeito self-healing

A função de um revestimento é fornecer uma proteção contra corrosão ao substrato metálico e contra riscos ou lesões quando em contato com o meio ambiente. A eficiência da proteção do substrato contra qualquer deterioração natural depende de fatores como a qualidade do revestimento e os ambientes de corrosão a que serão submetidos. Além dessas prerrogativas, necessárias a qualquer revestimento, é extremamente desejável que utilize precursores

naturais, e que sua aplicação e degradação não resultem em uma fonte de poluição ou contaminação do ambiente.

Dentro deste contexto, diferentes abordagens têm sido estudadas para minimizar os problemas de corrosão na liga AA2024 [15-18] e as mais eficazes são baseadas no uso de revestimentos orgânicos, ou seja, primer modificado com aditivos anticorrosivos [19-23]. O mecanismo de proteção normalmente combina as boas propriedades de barreira das matrizes orgânicas (***item 1.2.1***), que dificultam a absorção de água e espécies corrosivas, com a presença de aditivos anticorrosivos que inibem a corrosão por meio do efeito *self-healing* (***item 1.2.2***).

2.2.1 Revestimentos de poliuretano

A vida moderna depende de polímeros, desde os materiais usados na fabricação de aviões, carros até aqueles com aplicações sofisticadas na medicina. No entanto, a maioria dos polímeros são derivados petroquímicos [24]. A resina de poliuretano (PU) é um dos materiais amplamente utilizados com grande potencial para aplicações multiuso devido às excelentes propriedades físicas, químicas e mecânicas [25-31]. O processamento industrial desses compostos ainda é amplamente realizado com base no processamento de indústrias petroquímicas, em que as matérias-primas derivadas de gás natural e petróleo são limitadas e não podem ser renovadas [32]. É importante lembrar que alguns polímeros petroquímicos são biodegradáveis, ou seja, que pode ser destruído por um agente biológico, e nem todos os polímeros bioderivados são biodegradáveis [24]. Os poliuretanos também são aplicados em superfícies metálicas, formando revestimentos de barreira para protegê-los contra a corrosão em ambientes agressivos [33,34].

Nos últimos anos, houve um interesse crescente no desenvolvimento de revestimentos poliméricos sustentáveis que reduzam o uso de polímeros à base de derivados petroquímicos [35]. Os interesses industriais e dos consumidores no desenvolvimento de materiais verdes a partir de abundantes recursos renováveis aumentaram à medida que estão prontamente disponíveis, de baixo custo, não tóxicos e biodegradáveis [36]. O óleo de crambe da planta *Crambe*

abyssinica preenche essas características e é composto por diferentes ácidos graxos, com propriedades específicas, ausentes em outras matérias-primas, sendo considerado biocompatível e biodegradável [37,38]. *Crambe abyssinica* é uma planta que também pode fornecer uma matéria-prima adequada para produtos de maior valor, como polímeros, aditivos de polímeros, surfactantes, produtos de cuidados pessoais e produtos farmacêuticos [39-41]. O óleo de mamona é inerente biodegradável, de baixo custo, quase não tóxico, industrialmente favorável [37,38] e facilmente disponível [42,43]. É um dos recursos renováveis mais importantes para a produção de polímeros, incluindo a preparação de poliuretanos [44], substituindo produtos à base de petróleo (matéria-prima derivada de petróleo). A **Figura 3** ilustra os principais ácidos graxos presentes nos óleos.

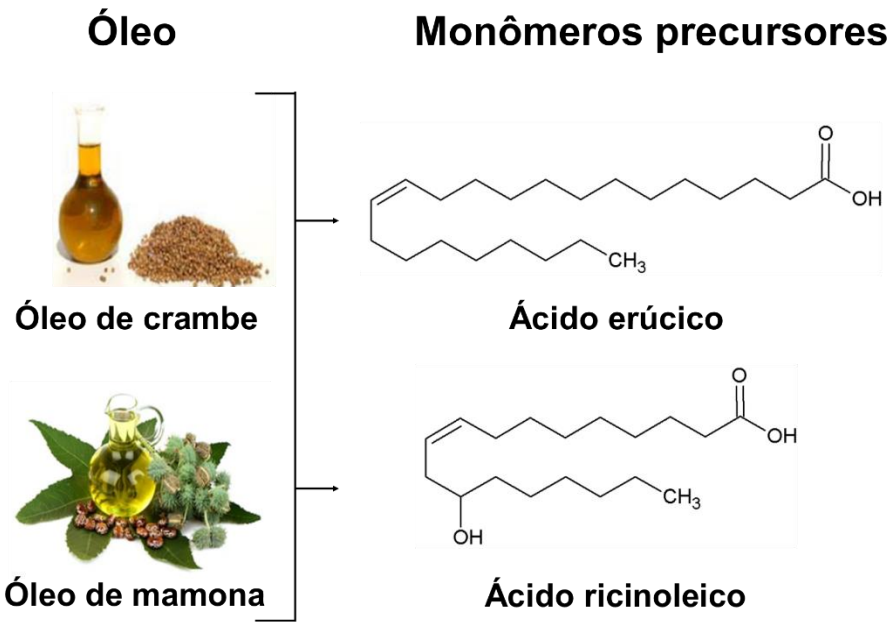

Figura 3. Os principais ácidos graxos presentes nos óleos. Fonte: autor [45].

O óleo de crambe é o componente mais importante do poliéster e o óleo de mamona do pré-polímero.

Os estudos iniciais de poliuretano à base de óleo de crambe indicaram grande dependência da resposta eletroquímica com a natureza da composição da resina [46,47]. Verificou-se que, após aplicar um defeito artificial na superfície do revestimento e investigar o efeito *self-healing* (capacidade de autorreparação/autocura) por medidas localizadas (LEIS e SVET), a propriedade

de autocura estava presente no revestimento que apresentava menor propriedade barreira nos estudos de EIS na ausência de defeito [23]. Por outro lado, o revestimento que apresentou melhor resistência à corrosão observado pelos resultados de EIS não apresentaram a propriedade de autocura [23]. Isso chamou nossa atenção para investigar a resistência à corrosão de diferentes formulações de revestimentos, alterando os componentes e suas proporções. Além dos componentes básicos (óleo de crambe, óleo de mamona e diisocianato alifático), dois outros componentes do revestimento são o trimetilolpropano (TMP), um agente de reticulação [48,49] e o anidrido ftálico (PhA) que participa da poliesterificação e facilmente reage com grupos OH presentes em TMP e mono ou diglicerídeos. Essa reação resulta na formação de poliésteres (segmento flexível) [48,49]. Em seguida, optamos, inicialmente, por usar quantidades diferentes do agente de reticulação (TMP), mantendo constante a massa de PhA, fabricando dois poliésteres diferentes [23]. Em seguida, a ideia foi estudar o efeito do agente de reticulação na resistência à corrosão do revestimento. A outra parte que compõe os revestimentos é o pré-polímero, obtido por reação de diisocianato de hexametileno (HDI, que contém grupos terminais bifuncionais de NCO) com grupos OH de diferentes fontes para produzir o segmento rígido. A resina final é obtida fazendo reagir os segmentos flexíveis e rígidos na proporção escolhida de poliéster e pré-polímero.

O HDI representa a classe mais importante de poliisocianatos usada atualmente na fabricação de resinas de poliuretano. As resinas preparadas com diisocianatos alifáticos oferecem excelente resistência a produtos químicos e ao amarelamento [50,51]. Essa é uma das principais vantagens do uso de diisocianatos alifáticos em comparação com os aromáticos, cujas resinas sofrem oxidação mais facilmente, principalmente quando expostas à luz UV, do que aquelas preparadas com diisocianatos alifáticos [52]. O HDI pode reagir com muitos produtos químicos e levar a formação de uretano e alofanato [53]. A **Figura 4** mostra a equação da reação básica para a formação do poliuretano a partir do HDI.

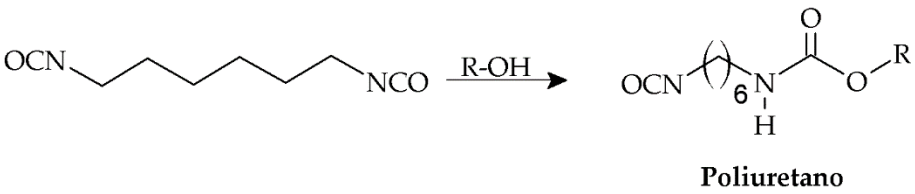

Figura 4. Equação da reação básica para a formação de um poliuretano [autora, 2020].

No entanto, as peças revestidas com PU são suscetíveis a danos durante a exposição ao longo do tempo. Nas regiões em que o revestimento foi danificado, a propagação da corrosão e a delaminação do revestimento podem causar perdas severas e sérios danos ao material não revestido. Para prevenir e minimizar a atividade de corrosão, os revestimentos são tipicamente modificados com aditivos anticorrosivos.

2.2.2 Efeito Self-healing

O efeito *self-healing* é definido como: "*A capacidade de um material curar (recuperar/reparar) danos de forma automática e autônoma, ou seja, sem nenhuma intervenção externa*" [54]. O efeito *self-healing* pode estar relacionado à integração física ou química dos componentes reparadores do polímero [55,56]. A busca por polímeros *self-healing* aumentou devido à necessidade de prolongar a vida útil de materiais suscetíveis à corrosão.

A **Figura 5** representa esquematicamente o mecanismo geral de autorreparação (*self-healing*).

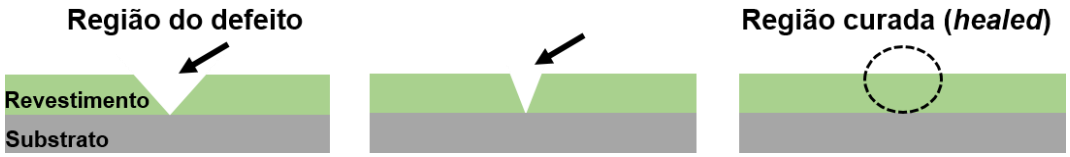

Figura 5. Ilustração geral do efeito self-healing nos polímeros modificados [57].

Estão sendo desenvolvidas novas estratégias de sistemas *self-healing* de proteção contra corrosão, os quais necessitam de investigação dos fundamentos do processo de inibição de corrosão. Uma das estratégias mais exploradas na

área de revestimentos *self-healing* e que mostra potencial de proteção é o encapsulamento de agentes funcionais, com capacidade de cicatrização/regeneração, em sistemas nanoestruturados que são dispersos na matriz do revestimento [58-61].

Outra estratégia que contribui com o desenvolvimento de revestimentos *self-healing* é a adoção de sistemas de revestimentos contendo pigmentos anticorrosivos [62,63] que podem impedir ou reparar o processo de corrosão; uma vez que a principal função do revestimento protetor, isto é, a proteção contra a corrosão, seja recuperada.

A maneira mais viável de introduzir inibidores de corrosão nos revestimentos é adicioná-los/incorporá-los durante o processo de síntese. Neste caso são indispensáveis estudos prévios para garantir que o inibidor não tenha um efeito prejudicial às propriedades de barreira do revestimento [64]. Esses estudos são essenciais também para que as propriedades de barreira não sejam interrompidas ou a capacidade de proteção contra a corrosão do revestimento modificado diminua consideravelmente conforme já relatado [65,66].

Durante anos, a aplicação de pigmentos à base de cromato tem sido a estratégia mais utilizada para conferir efeitos de reparação contra corrosão em revestimentos orgânicos aplicados em diferentes partes metálicas e, em particular, na liga AA2024. No entanto, o impacto negativo dos compostos de cromo no ambiente e na saúde humana levou à substituição de cromatos por outros pigmentos, um problema em muitas aplicações, mas ainda permitido em aplicações aeronáuticas [67]. Atualmente, a tendência é substituir os compostos que contêm cromato por inibidores ambientalmente amigáveis, não-tóxicos e biodegradáveis [68] e introduzir capacidade de *self-healing* nos revestimentos de proteção à corrosão [69]. Diversos estudos têm explorado a ação de extratos vegetais como inibidores de corrosão em solução para proteger diferentes substratos metálicos [70-74]. Esses extratos contêm uma variedade de produtos orgânicos naturais, tais como óleos essenciais, taninos, entre outras substâncias ativas ricas em grupos -OH que foram relatadas como inibidores de corrosão eficazes [75-77]. A demanda por inibidores de corrosão mais ecológicos está aumentando o interesse pelos taninos, que efetivamente protegem as ligas de alumínio da corrosão [78-80]. Os taninos podem ser usados para modificar as matrizes orgânicas e espera-se que esta estratégia reforce as propriedades de

barreira, enquanto introduz a capacidade de *self-healing* no revestimento quando este é danificado. Desta forma, o tanino condensado foi incorporado à síntese dos nossos sistemas.

Os taninos são classificados em dois grupos: condensados e hidrolisáveis. O tanino hidrolisável é composto principalmente de ácido gálico, enquanto o tanino condensado é composto por polímeros de flavan-3-ol [77,81] e é amplamente utilizado para produzir adesivos e espumas [82] e muitos polímeros à base de tanino, usando diferentes endurecedores [83]. Taninos são antioxidantes polifenólicos naturais [84] e contêm vários grupos hidroxila adjacentes e exibem afinidades específicas para muitos íons metálicos [84]. O tanino, quando adicionado ao eletrólito ou no primer, protege as superfícies metálicas contra a corrosão [21, 85-90], e quando o tanino encapsulado foi adicionado às películas sol-gel de metiltrimetoxissilano e tetraetilortosilicato, mas quando diretamente adicionado à película sol-gel foi lixiviado [79]. No entanto, quando o tanino condensado foi diretamente incorporado à resina de poliuretano derivada do óleo de crambe conferiu a propriedade de autocura ao revestimento e a lixiviação do tanino foi insignificante [13], o que atribuiu a este material excelente proteção da liga AA2024 contra a corrosão em soluções de cloreto [13].

Este trabalho tem como objetivo formular, preparar e caracterizar revestimentos de poliuretano não modificados [23,46,91] e modificados com tanino condensado, usado como inibidor de corrosão de alumínio e ligas de alumínio [13], e demonstrar o efeito de *self-healing* quando o mesmo é incorporado na formulação, pois aumenta significativamente a vida útil de revestimentos resistentes à corrosão nos quais foram aplicados defeitos artificiais na superfície.

Portanto, com o propósito de aprimorar o efeito barreira dos revestimentos de poliuretano, estudou-se o efeito da incorporação de pigmentos anticorrosivos a fim de aumentar a quantidade de grupos hidroxila na estrutura final da resina e desenvolver um revestimento *self-healing*.

2.3 Técnicas eletroquímicas convencionais e locais para estudar a capacidade de inibição da corrosão

Proteção efetiva contra corrosão e efeito *self-healing* dependem da resposta do revestimento modificado. Para entender melhor essa combinação, é de suma importância combinar diferentes ferramentas eletroquímicas para extrair informações relevantes sobre a evolução das propriedades barreira do revestimento. Portanto, o objetivo principal desta parte do trabalho de tese é investigar o efeito da adição do tanino condensado (estrutura química representada na **Figura 12A**) na estrutura do revestimento e avaliar seu desempenho como agente anticorrosivo. Para isso, foi aplicada a técnica eletroquímica convencional de espectroscopia de impedância eletroquímica (EIS), a qual fornece informações médias da superfície atribuíveis ao comportamento de toda a superfície do eletrodo. Assim, as técnicas eletroquímicas convencionais dificilmente fornecem informações sobre o comportamento da corrosão localizada ou sobre o tempo e os mecanismos de início da corrosão em microescala. No entanto, as técnicas localizadas, as quais abrangem as análises de espectroscopia de impedância eletroquímica localizada (LEIS) e as técnicas de varredura com eletrodo vibrante (SVET) e com eletrodo íon-seletivo (SIET) são apropriadas para investigar efeitos locais de corrosão.

Técnicas eletroquímicas localizadas revelam detalhes do processo de corrosão com resolução microscópica [92]. A espectroscopia de impedância localizada (LEIS) é uma poderosa ferramenta eletroquímica que pode medir a admitância nas proximidades da interface, fornecendo informações valiosas sobre os fenômenos de corrosão local e sua propagação ou inibição [16,93,94]. O SVET pode identificar regiões anódicas e catódicas com base nas distribuições locais de densidade de corrente e a micropotenciometria (SIET) monitora a distribuição de espécies iônicas de interesse, em particular as que influem no pH do meio próximo à superfície [92,95-98]. Assim, a combinação de técnicas localizadas e médias de superfície se constitui em ferramenta poderosa para desvendar detalhes dos mecanismos que governam a proteção contra corrosão.

A capacidade de proteção contra corrosão dos revestimentos com tanino condensado foi comparada com um revestimento referência (com a mesma matriz polimérica, sem adição de tanino condensado). Estudos complementares foram realizados por microscopia eletrônica de varredura (SEM) e espectroscopia de energia dispersiva de raios-X (EDX). As combinações de

todas as técnicas forneceram informações valiosas sobre o mecanismo de proteção contra corrosão da liga AA2024-T3 em meio contendo cloreto.

3 Parte experimental

Nesta sessão experimental abordaremos a formulação das resinas monolíticas / revestimentos, sistema reacional, técnicas de caracterização de superfície e estudo eletroquímico. Outras informações tais como reagentes, caracterização da matéria-prima (óleos de crambe e mamona) e detalhes experimentais relacionados a síntese constam no Capítulo I [45], as principais reações de obtenção das resinas / revestimentos são descritas no Apêndice I.

3.1 Formulação dos revestimentos

A preparação do revestimento foi realizada em três etapas (**Figura 6** – sistema reacional). Etapa (1) preparação do poliéster, etapa (2) preparação do pré-polímero e etapa (3) preparação do revestimento por meio da mistura dos produtos obtidos na etapa (1) e (2).

As resinas que serão descritas no Capítulo I possuem a mesma composição dos revestimentos descritos no Capítulo II. Sendo que, no Capítulo I, as resinas foram denominadas *PU-resin* e *PU-modified resin* e no Capítulo II, os revestimentos (resinas aplicadas na liga AA2024-T3) foram denominados *Reference coating* e *Tannin-modified coating*. Portanto, dois revestimentos foram preparados: **referência** (*PU-resin*, Capítulo I; *Reference coating*, Capítulo II) e **modificado com tanino condensado** (*PU-modified resin*, Capítulo I; *Tannin-modified coating*, Capítulo II). **Formulação do revestimento referência**: na etapa (1) o poliéster foi preparado pela reação de transesterificação do óleo de crambe (CO, 1 mol, 997,6 g), trimetilolpropano (TMP, 3 mol, 402,3 g), anidrido ftálico (PhA, 3 mol, 444,3 g), hidroxitolueno butilado (BHT 2,26 x 10^{-3} mol, 0,50 g, antioxidante) e hidróxido de lítio (LiOH, 0,01 mol, 0,25 g, catalisador) sob agitação e aquecimento a 240 °C por 5 h em atmosfera de nitrogênio. Nesta etapa reacional ocorreu a formação de glicerina (produto secundário) que foi

removido com a vidraria Dean-Stark (**Figura 6**). O progresso da reação foi monitorado por teste de solubilidade em metanol (3 mL metanol / 1 mL poliéster) e índice de acidez (mg KOH / g de poliéster). Quando o poliéster foi totalmente solubilizado em metanol e o índice de acidez foi menor do que 30, a reação foi concluída. Na etapa (2) o pré-polímero foi preparado com óleo de mamona (CAO, 0,42 mol, 125,3 g), trimetilolpropano (TMP, 0,35 mol, 46,93 g), hidroxitolueno butilado (BHT, 0,01 mol, 2,20 g), propileno glicol (PG, 0,16 mol, 12,17 g), acetato de n-butila (BA, 3,83 mol, 444,89 g), etilenoglicol (EGA, 1,45 mol, 191,61 g), diisocianato de hexametileno (HDI, 3,11 mol, 523,08 g) sob agitação e aquecimento a 60 °C por 6 h em atmosfera de nitrogênio. CO e CAO são polióis, TMP é agente entrecruzador, PhA que participa da poliesterificação e reage facilmente com grupos -OH de TMP, HDI contém grupos terminais -NCO bifuncionais, PG, BA, EGA são extensores de cadeia, BHT é antioxidante usado por causa das ligações insaturadas do óleo de mamona, LiOH é catalisador. Na etapa (3) os produtos obtidos nas etapas (1) e (2) foram reagidos entre si na presença do catalisador octoato de estanho (SO, 1%) sob agitação durante 10 min para produzir o **revestimento referência** (*PU-resin*, Capítulo I; *Reference coating*, Capítulo II). Para o **revestimento modificado com tanino condensado** (*PU-modified resin*, Capítulo I; *Tannin-modified coating*, Capítulo II), as etapas (1) e (2) foram exatamente as mesmas descritas acima e na etapa (3) foi adicionado tanino condensado ($8,83 \times 10^{-3}$ mol, 2,10 g).

No Capítulo III, os revestimentos aplicados na liga AA2024-T3 foram denominados *Unmodified coating* e *Modified coating*. Portanto, dois revestimentos foram preparados: **Formulação do revestimento referência** (*Unmodified coating*, Capítulo III): na etapa (1) o poliéster foi preparado pela reação de transesterificação do óleo de crambe (CO, 1 mol, 997,6 g), trimetilolpropano (TMP, 3 mol, 402,3 g), anidrido ftálico (PhA, 3 mol, 444,3 g), hidroxitolueno butilado (BHT $2,26 \times 10^{-3}$ mol, 0,50 g) e hidróxido de lítio (LiOH, 0,01 mol, 0,25 g) sob agitação e aquecimento a 240 °C por 5 h em atmosfera de nitrogênio. Na etapa (2) o pré-polímero foi preparado com óleo de mamona (CAO, 0,64 mol, 191,0 g), trimetilolpropano (TMP, 0,53 mol, 71,07 g), hidroxitolueno butilado (BHT, 0,01 mol, 2,20 g), propileno glicol (PG, 0,25 mol, 19,02 g), acetato de n-butila (BA, 5,75 mol, 667,92 g), etilenoglicol (EGA, 2,17 mol, 286,76 g), diisocianato de hexametileno (HDI, 4,66 mol, 783,79 g) sob

agitação e aquecimento a 60 °C por 6 h em atmosfera de nitrogênio. Na etapa (3) os produtos obtidos nas etapas (1) e (2) foram reagidos entre si na presença do catalisador octoato de estanho (SO, 1%) sob agitação durante 10 min para produzir o **revestimento referência** (*Unmodified coating*, Capítulo III). Para o **revestimento modificado com tanino condensado** (*Modified coating*, Capítulo III), as etapas (1) e (2) foram exatamente as mesmas descritas acima e na etapa (3) foi adicionado tanino condensado (2,10 x 10^{-3} mol, 0,50 g).

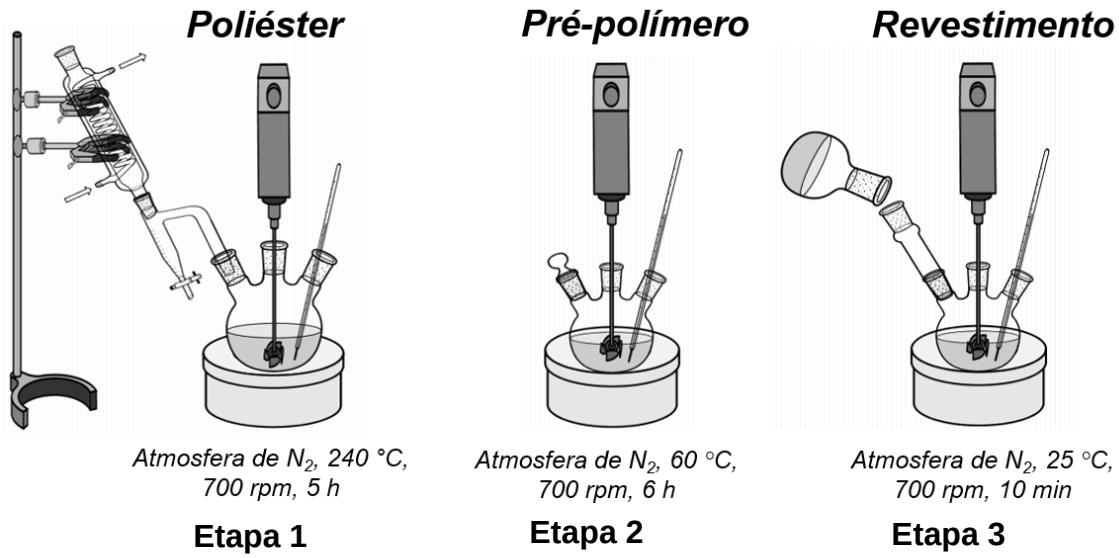

Figura 6. Sistema reacional utilizado para desenvolvimento das resinas / revestimentos de poliuretano. Fonte: autor [45].

Os revestimentos descritos no Capítulo I (denominados *PU* e *PU-modified*) foram estudados na forma de resina monolítica e o esquema de obtenção é representado na **Figura 7**. O substrato de Teflon® foi limpo com água deionizada e acetona e deixado secar (~ 25 °C). A resina foi aplicada no substrato usando um extensômetro (TKB Erichsen instruments®) (**Figura 8**) e foi mantida a ~ 25 °C por 24 h para permitir a evaporação do solvente.

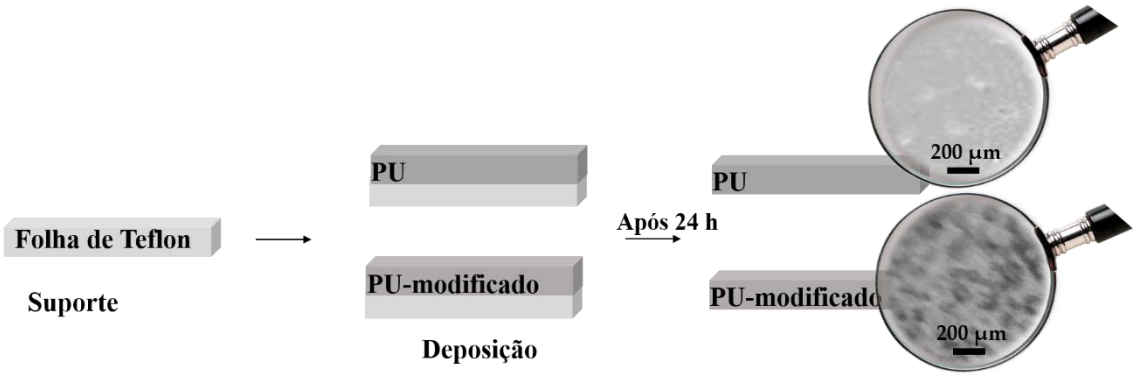

Figura 7. Esquema para obter as resinas monolíticas de PU e PU-modificado com tanino condensado (Capítulo I). Fonte: autor [45].

Figura 8. Extensômetro TKB Erichsen instruments® utilizado para aplicar as resinas na superfície do substrato.

Os revestimentos descritos nos Capítulos II e III foram aplicados sobre placas AA2024-T3 (100 mm x 100 mm x 2 mm) usando um extensômetro (TKB Erichsen instruments®) e a cura foi a 25 °C por 48 h.

3.2 Preparação do substrato

A composição química do substrato AA2024-T3 (Embraer) está representada na **Tabela 1**. A composição foi determinada por análise EDX (FEG-SEM JSM7001F, JEOL acoplado com detector elementar Oxford (England) modelo INCA 250) com 25 kV de energia e a média de medições em triplicata.

Tabela 1. Composição química do substrato AA2024-T3.

Composição (%massa)	AA2024-T3
Cu	4,40
Mn	0,52
Mg	1,38
Fe	0,16
Zn	0,06
Si	< 0,06
Cr	< 0,06
Ti	< 0,06
Al	Balanço

O pré-tratamento da superfície (100 mm x 100 mm x 2 mm) antes da aplicação dos revestimentos incluiu uma etapa de polimento com lixa de carbeto de silício (#280, #320, #400, #1200, #1500, #2000) seguido por lavagem em água desionizada, acetona e secagem em estufa por 24 h a 120 °C.

3.3 Caracterização da superfície

3.3.1 Absorção de água (water uptake)

A absorção de água foi determinada pela imersão dos revestimentos livres (monolitos, revestimentos referência e modificado com tanino condensado) em água desionizada à temperatura ambiente e cálculo da percentagem de absorção de água desionizada com medidas na microbalança de cristal de quartzo (Sartorius® MC5 Micro Balance). Antes e após 0,25 h, 0,5 h, 0,75 h, 1 h e 2 h de exposição à água desionizada, o ganho de massa (m_t) foi medido e a absorção de água (%*W*) foi expressa pela Equação 1 [13]:

$$\%W = \frac{m_t - m_0}{m_0} \times 100 \qquad \text{(Eq. 1)}$$

em que m_o / mg é a massa inicial do revestimento e m_t / mg é a massa do revestimento após a imersão em água desionizada por um certo tempo.

3.3.2 Espectroscopia na região de infravermelho por transformada de Fourier com acessório de refletância total atenuada (ATR-FTIR)

Os revestimentos foram estudados por meio de ATR-FTIR usando um espectrofotômetro Vertex70 Bruker com um acessório de Reflectância Total Atenuada (varredura = 64, varredura de energia de 400 a 4000 cm^{-1}, resolução = 2 cm^{-1}).

3.3.3 Espessura dos revestimentos

A espessura dos revestimentos foi determinada a partir de amostras embutidas na transversal e analisadas por meio da microscopia eletrônica de varredura (SEM) usando microscópio FEG-SEM JEOL modelo JSM 7001F usando 25 kV.

3.3.4 Testes de adesão

Testes de aderência do revestimento ao substrato, baseados na norma ASTM D3359 [99], foram realizados utilizando cortador de hastes cruzadas Elcometer 107. Utilizou-se 6 dentes com espaçamento de 1 mm. Um padrão de 6 seções transversais (~ 20 mm) perpendiculares ao material revestido foi aplicado até atingir o substrato. Em seguida, a fita adesiva Elcometer T1079358 foi aplicada sobre o padrão de corte e foi removida. Com o auxílio de uma lupa foi avaliado o desprendimento do revestimento. A superfície do revestimento foi visualmente comparada com a escala padrão (**Tabela 2**) da norma ASTM D3359 [99] e a adesão é graduada de acordo com a porcentagem de área removida.

Tabela 2. Classificação dos resultados do teste de adesão (adaptado da norma ASTM D3359 [99]).

Classificação	% Área removida	Superfície analisada
5B	Nenhum 0%	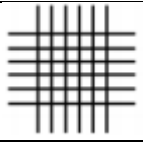

4B	Menor que 5%	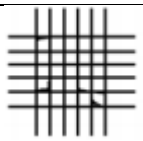
3B	5 – 15%	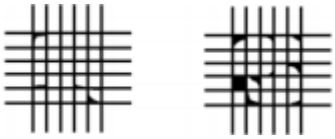
2B	15 – 35%	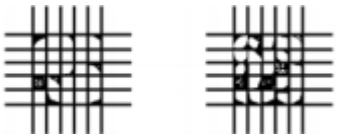
1B	35 – 65%	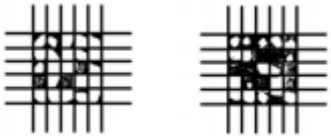
0B	Maior que 65%	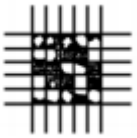

3.3.5 Ângulo de contato

A hidrofobicidade da superfície das amostras foi caracterizada por um Dataphysics OCA20. O ângulo de contato estático da água foi medido em triplicata colocando-se uma gota de água desionizada Milli-Q de 17 µL (resistividade de 18,2 MΩ cm) na superfície da amostra.

3.3.6 Microscopia óptica (OM)

Imagens de microscopia óptica dos revestimentos foram obtidas no Microscópio digital modelo LEICA DMS300 e estereomicroscópio Carl ZEISS Jena (Oberkochen, Germany) acoplado a um computador e ao software TOP VIEW® (SPECwise, Inc., West Palm Beach, FL, USA) [100].

3.3.7 Microscopia eletrônica de varredura (SEM / EDX)

As superfícies dos revestimentos foram analisadas antes e após os testes de imersão por SEM e EDX, usando um microscópio JSM 7001F modelo FEG-SEM JEOL (acoplado com detector elementar Oxford (England) modelo INCA 250) com energia de aceleração de 2 kV e 15 kV.

3.4 Estudo eletroquímico

A condutividade da solução de NaCl foi medida usando um condutivímetro EUTECH INSTRUMENTS PC700.

As amostras revestidas foram cortadas usando uma guilhotina (GH0-0420, Adira). Para as medidas convencionais de E_{OCP} e EIS, a área geométrica do eletrodo de trabalho foi de 1 cm^2, enquanto nos estudos localizados LEIS e SVET/SIET a área geométrica foi de ~10 mm^2 e ~0.9 mm^2, respectivamente.

3.4.1 Potencial em circuito aberto (E_{OCP}) e espectroscopia de impedância eletroquímica (EIS)

Medidas convencionais de E_{OCP} e EIS em liga AA2024-T3 revestidas e não revestidas foram realizados em uma célula eletroquímica convencional de três eletrodos (modelo K0235, PAR). Utilizou-se como eletrodo de trabalho a liga AA2024-T3 revestida ou não (área geométrica de 1 cm²), Ag|AgCl|KCl $_{3\ mol\ L\text{-}1}$, como eletrodo de referência, e uma espiral de Pt como eletrodo auxiliar. Todos os potenciais foram medidos em relação ao eletrodo de referência Ag|AgCl|KCl. As medidas de E_{OCP} foram registradas por 24 h antes da primeira medida de EIS e entre cada experimento de EIS até o final dos ensaios. As medidas de impedância eletroquímica foram realizadas usando um potenciostato / galvanostato Gamry REF600, obtidas no intervalo de frequência de 100 kHz a 10 mHz, aplicando uma amplitude de sinal senoidal de 10 mV rms sobre E_{OCP}, e registrando 10 pontos / década de frequência. Os espectros de EIS foram registrados em função do tempo de imersão até se observar uma diminuição acentuada do valor de E_{OCP}, isto é, até as propriedades de barreira dos revestimentos serem deterioradas. O eletrólito foi uma solução aquosa 0,6 mol L^{-1} NaCl, e as medidas foram realizadas a 25 °C.

Os dados experimentais de EIS foram testados quanto à consistência com as condições de Kramers-Kronig e ajustados usando o modelo de circuito elétrico equivalente (EEC) com o software Z-View®.

3.4.2 Espectroscopia de impedância eletroquímica localizada (LEIS)

A técnica LEIS foi utilizada para medir a admitância de um defeito artificial na amostra revestida quando imersa em solução 0,005 mol L^{-1} NaCl. O defeito

tinha aproximadamente 5 mm de comprimento x 0,3 mm de largura e foi aplicado com um bisturi, atingindo o metal. As medições de LEIS foram realizadas com uma interface eletroquímica Solartron 1286, um analisador de resposta em frequência Solartron 1250 acoplado a uma estação eletroquímica Uniscan. Foi utilizada uma configuração de cinco eletrodos: eletrodo de calomelano saturado (SCE) como eletrodo de referência, substrato revestido como eletrodo de trabalho, rede de platina como eletrodo auxiliar e sonda LEIS (bi-eletrodo de Pt) para medir o gradiente de potencial local, acima da superfície. A configuração personalizada da sonda LEIS usada nesse experimento foi descrita em detalhes anteriormente [13,57]. Os valores de admitância foram registrados em cada ponto de varredura sobre toda a área exposta, incluindo o defeito. A área varrida foi de 5060 µm × 2000 µm para o revestimento referência e 5000 µm × 2000 µm para o revestimento modificado com tanino condensado (Capítulo II, revestimentos denominados *Reference* e *Tannin-modified*). A área varrida foi de 5048 µm × 2000 µm para o revestimento referência e 5106 µm × 2000 µm para o revestimento modificado com tanino condensado (Capítulo III, revestimentos denominados *Unmodified* e *Modified*). Uma frequência de 5 kHz foi usada durante o mapeamento do LEIS. Portanto, os mapas LEIS (área de varredura: 32 pontos x 16 linhas) foram obtidos em solução aquosa 0,005 mol L^{-1} NaCl (condutividade constante, ρ = 0,000548 S cm^{-1}) a cada 1 h por 25 h de imersão.

3.4.3 Técnica de varredura com eletrodo vibrante (SVET) e com eletrodo íon seletivo (SIET)

As medições SVET / SIET quase simultâneas foram realizadas utilizando um aparelho da Applied Electronics Inc., controlado pelo software ASET (Science Wares). O defeito, atingindo o substrato, foi aplicado usando um bisturi. As medidas foram realizadas em uma região de 22 pontos × 38 linhas, gerando 836 pontos para o revestimento referência e 22 pontos × 41 linhas, gerando 902 pontos para revestimento modificado com tanino condensado. Uma sonda isolada Pt-Ir (Microprobe), com platina preta depositada em uma ponta esférica de 12 µm de diâmetro foi utilizada como eletrodo vibrante durante as medições SVET. A microssonda foi colocada (100 ± 2) µm acima da superfície, vibrando nos planos vertical (Z) e horizontal (X). As frequências de vibração da sonda correspondentes foram de 124 Hz e 325 Hz, respectivamente. As medidas foram

realizadas durante a imersão das amostras revestidas em solução aquosa 0,05 mol L^{-1} NaCl (condutividade constante, ρ = 0,00540 S cm^{-1}) a 25 °C.

O SIET foi utilizado para as medidas micropotenciométricas. As medições de pH locais foram realizadas utilizando um microeletrodo de vidro capilar com um diâmetro de orifício de ponta de (1,8 ± 0,2) µm; o pH local foi mapeado (50 ± 2) µm acima da superfície. Foi utilizada uma membrana à base de ionóforos pH seletiva com faixa de trabalho de pH estendida, especialmente desenvolvida para aplicações em corrosão [13]. O eletrodo de referência externo foi um eletrodo de Ag|AgCl| 0,05 mol L^{-1} NaCl e soluções tampão comerciais foram utilizadas para a calibração. O coeficiente angular de Nernst foi de (-55,1 ± 0,5) mV/pH. O potencial de referência foi registrado no eletrólito a granel antes e depois de cada medição, a fim de levar em conta possíveis desvios. A área varrida foi de 1,64 mm × 1,68 mm.

CAPÍTULO I:

Preparação das resinas monolíticas

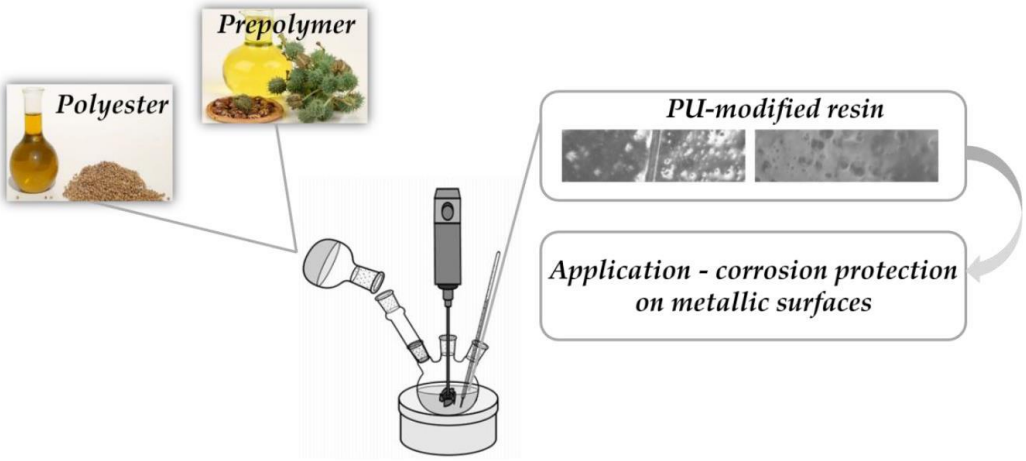

Este capítulo fornece uma visão geral do preparo e caracterização das resinas monolíticas de poliuretano. São denominadas resinas monolíticas por não estarem aplicadas a uma superfície. Uma das motivações para explorar as propriedades contra corrosão de revestimentos é o estudo prévio das resinas monolíticas. Finalmente, a etapa inicial do trabalho de pesquisa é explicada. Esta seção é publicada como artigo de síntese: J.V. Nardeli, C.S. Fugivara, E.R.P. Pinto, W.L. Polito, Y. Messaddeq, S.J.L. Ribeiro, A.V. Benedetti. "Preparation of polyurethane monolithic resins and modification with condensed tannin yielding self-healing property" na revista Polymers v. 11, p.1890, 2019.

Reproduced with permission from [J.V. Nardeli, C.S. Fugivara, E.R.P. Pinto, W.L. Polito, Y. Messaddeq, S.J.L. Ribeiro, A.V. Benedetti. Preparation of polyurethane monolithic resins and modification with condensed tannin yielding self-healing property. POLYMERS. v.11, p.1890, 2019] Copyright 2019 MDPI Polymers

polymers

MDPI

Article

Preparation of Polyurethane Monolithic Resins and Modification with a Condensed Tannin-Yielding Self-Healing Property

Jéssica Verger Nardeli [1,*], Cecílio Sadao Fugivara [1], Elaine Ruzgus Pereira Pinto [2], Wagner Luiz Polito [2], Younes Messaddeq [2], Sidney José Lima Ribeiro [2] and Assis Vicente Benedetti [1,*]

[1] Department of Physical-chemistry, Institute of Chemistry, São Paulo State University (UNESP), PO Box 355, Araraquara 14801-970, SP, Brazil; sadao.fugivara@unesp.br

[2] Department of General and Inorganic Chemistry, Institute of Chemistry, São Paulo State University (UNESP), PO Box 355, Araraquara 14801-970, SP, Brazil; elainerpp@gmail.com (E.R.P.P.); politowl@iqsc.usp.br (W.L.P.); younes.messaddeq@copl.ulaval.ca (Y.M.); sidney.jl.ribeiro@unesp.br (S.J.L.R.)

* Correspondence: jeh.nardeli@gmail.com (J.V.N.); assis.v.benedetti@unesp.br (A.V.B.)

Received: 21 October 2019; Accepted: 13 November 2019; Published: 15 November 2019

Abstract: Resins of polyurethane were prepared from vegetable oils (crambe and castor) and modified by adding green corrosion inhibitor (condensed tannin). The oils were characterized by gas chromatography with flame-ionization detection (GC-FID), attenuated total reflectance Fourier transform infrared spectroscopy (FTIR-ATR) and thermogravimetric analysis (TGA). The reaction was monitored by characterizing the intermediate products (polyester and prepolymer). The polyester was characterized by solubility in methanol, acidity index, hydroxyl groups and FTIR-ATR, and the prepolymer was characterized by solid content, solvent content, isocyanate (NCO) groups and FTIR-ATR. The formation of PU resins was confirmed by FTIR-ATR and TGA, and the presence of tannin particles incorporated in the coating can be observed by optical microscopy (OM). The absence of the band attributed to NCO in FTIR-ATR spectra of the resins confirmed the complete reaction between polyester and prepolymer. The OM observation and a video demonstrate that Polyurethane (PU)-modified with condensed tannin resin presents self-healing effect, probably through the formation of new hydrogen bonds when in contact with deionized water. Therefore, these results open possibilities for new synthetic routes aiming at improving the very important self-healing property for protecting metals and their alloys against corrosion, extending significantly the metallic materials lifetime as previously demonstrated by our group.

Keywords: condensed tannin; self-healing; polyurethane resins; condensed tannin-modified PU resin; crambe oil; castor oil

1. Introduction

Modern life relies on polymers, from the materials that are used to make airplanes and cars to those with sophisticated applications in medicine. However, most polymers are derived from petrochemicals [1]. Polyurethane (PU) resin is one of the widely used materials with great potential for multipurpose applications due to its excellent physical, chemical, and mechanical properties [2–8]. Industrial processing of these compounds is still widely carried out by relying on the processing of petrochemical industries, where raw materials derived from natural gas and petroleum are limited and cannot be renewed [9]. It is important to remember that some petrochemical polymers are biodegradable, and not all bioderived polymers will be biodegraded [1]. Polyurethanes are also

Reproduced with permission from [J.V. Nardeli, C.S. Fugivara, E.R.P. Pinto, W.L. Polito, Y. Messaddeq, S.J.L. Ribeiro, A.V. Benedetti. Preparation of polyurethane monolithic resins and modification with condensed tannin yielding self-healing property. POLYMERS. v.11, p.1890, 2019] Copyright 2019 MDPI Polymers.

applied on metal surfaces forming barrier coatings to protect them against corrosion in aggressive environments [10,11].

In recent years there has been a growing interest in developing sustainable polymer coatings that reduce the use of petrochemical-based polymers [12]. Industrial and consumer interests in the development of green materials from abundant renewable resources have increased as they are readily available, of low cost, nontoxic and biodegradable [13]. Crambe oil from *Crambe abyssinica* plant fills these characteristics and is composed of different fatty acids, with specific properties, which are absent in other raw materials, being considered biocompatible and biodegradable [14,15]. *Crambe abyssinica* is a plant that can also provide a suitable raw material for higher-value products, such a, polymers, polymer additives, surfactants, personal care products and pharmaceuticals [16–18]. Castor oil is inherent biodegradable, of low cost, almost non-toxic, industrially [14,15] favorable, and easily available [19,20]. It is one of the most important renewable resources to produce polymers, including the preparation of polyurethanes [21], replacing petroleum-based products. Figure 1 illustrates the main fatty acids present in oils.

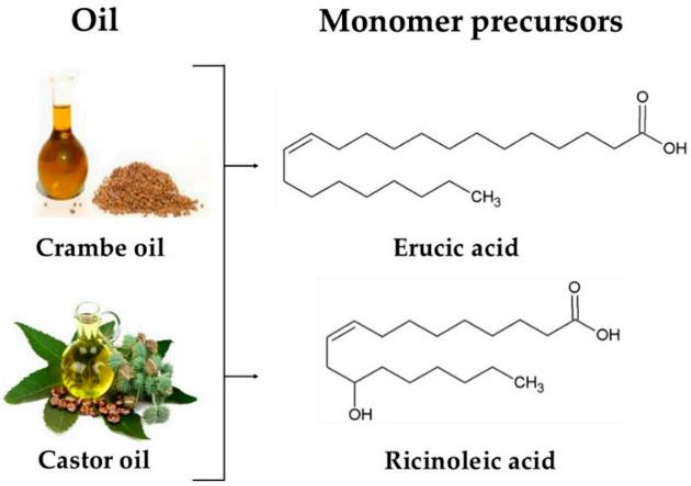

Figure 1. The main fatty acids present in oils.

Crambe oil is the most important component of polyester, and castor oil of the prepolymer.

Why and how the resins here studied were drawn? The initial studies of crambe oil-based polyurethane indicated great dependence of the electrochemical response on the nature of the resin composition [22,23], and it was also observed that after applying a scratch on the coating surface, the self-healing property was present in a resin-based coating, in which the pristine was less resistant to corrosion [24]. Conversely, the pristine that showed better corrosion resistance did not present the self-healing property [24]. This has called our attention to investigate the corrosion resistance of different coatings formulations by changing the components and their proportions. Besides the base components (crambe and castor oils, and aliphatic diisocyanate), two other components of the coating are trimethylolpropane (TMP), a crosslinking agent [25,26], and phthalic anhydride (PhA) that takes part in the polyesterification and easily reacts with OH groups present in TMP and mono- or diglycerides. This reaction results in polyesters formation (flexible segment) [25,26]. Then, we choose, initially, to use two different quantities of the crosslinking agent (TMP) maintaining constant the mass of PhA, fabricating two different polyesters [24]. Then, the idea was to study the effect of the crosslinking agent on the corrosion resistant ability of the coating. The other part composing the coatings is the prepolymer, which is obtained by reacting hexamethylene diisocyanate (HDI, which contains bifunctional NCO terminal groups) with OH groups from different sources to produce the rigid segment. The final resin is obtained by reacting both flexible and rigid segments in a chosen polyester and prepolymer proportion.

HDI represents the most important class of polyisocyanates used today in the fabrication of polyurethane resins. Resins prepared with aliphatic diisocyanates provide excellent resistance to chemicals and to yellowing [27,28]. This is one of the main advantages of using aliphatic diisocyanates compared to aromatic ones, whose resins undergo oxidation easier, especially when exposed to UV light, than those prepared from aliphatic diisocyanates [29]. HDI can react with many chemicals [30] and in our system the main reactions of HDI to form the prepolymer are drawn in Figure 2.

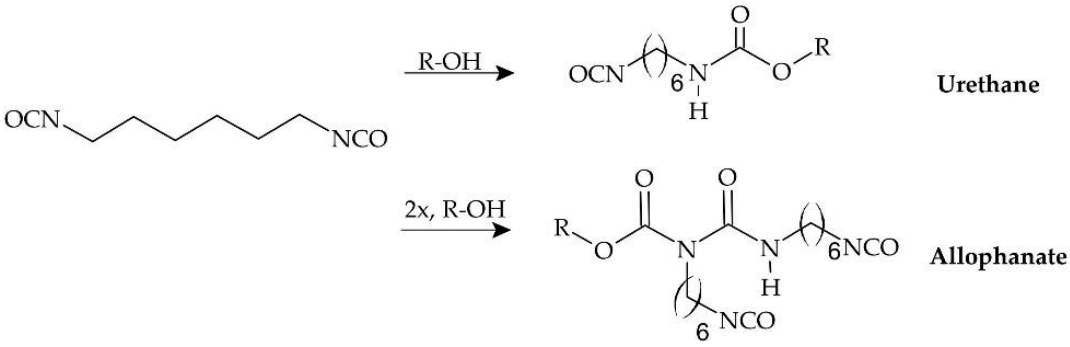

Figure 2. Main reactions of prepolymer in the curing process [30], modified by the authors.

In order to increase the amount of hydroxyl groups in the final resin structure and develop a smart coating, condensed tannin was incorporated into the synthesis.

Tannin in vascular plants occurs as two types, condensed and hydrolysable. Hydrolysable tannin is made up primarily of gallic acid while condensed tannin is made up from three-ring flavanols [31] and is largely used to produce adhesives, foams, biofoams [32] and many tannin-based polymers using different hardeners [33]. Tannins are natural polyphenolic antioxidants [34] and contain multiple adjacent hydroxyl groups and exhibit specific affinities for many metal ions [34]. Tannin, when added to the electrolyte or in the primer, protects metallic surfaces against corrosion [35–41], and when encapsulated tannin was added to sol–gel films of methyltrimethoxysilane and tetraethylorthosilicate, but when directly added to the sol–gel film was leaching [42]. However, when condensed tannin was directly incorporated to the crambe oil-derived polyurethane resin have conferred the self-healing property to the coating and tannin leaching was negligible [43], which attributed to this material excellent protection of AA2024 alloy against corrosion in chloride solutions.

This work aims at formulating, preparing and characterizing PU resins unmodified [22,24] and modified with condensed tannin used as corrosion inhibitor of aluminum and aluminum alloys [43], and demonstrating the self-healing effect in the condensed-tannin-modified PU resin monoliths, which significantly increases the service life of corrosion-resistant coatings with artificial defects or damaged in service. The investigation of self-healing property in monoliths when compared to the coated substrate may give insight about the influence of the metallic substrate in the corrosion resistance performance of the coating.

2. Materials and Methods

2.1. Materials

Crambe oil (CO) provided by Foundation Mato Grosso do Sul (Campo Grande, Brazil) [44], castor oil (CAO) provided by Asher® (São Carlos, Brazil), condensed tannin species extracted from mimosa (*Acacia mearnsii*) [45,46] provided by TANAC® (Montenegro, Brazil). Trimethylolpropane (TMP, CAS number 77-99-6), phthalic anhydride (PhA, CAS number 85-44-9), butylated hydroxyl toluene (BHT, CAS number 128-37-0), lithium hydroxide (LiOH, CAS number 1310-65-2), propylene glycol (PG, CAS number 57-556), n-butyl acetate (BA, CAS number 123-86-4), ethyl glycol acetate (EGA, CAS number 111-15-9), hexamethylene diisocyanate (HDI, CAS number 212-485-8), stannous octoate (SO, CAS

number 301-10-0) were used to prepare the organic resin. All reagents and solvents are analytical grade and were purchased from Sigma-Aldrich® (St. Louis, MO, USA).

2.2. Characterization Techniques

2.2.1. Raw Materials

Quantification by Gas Chromatography with Flame-Ionization Detection (GC-FID)

For this analysis, both vegetable oils were transesterified to form methyl esters (Scheme 1). The reactions were carried out in a flask equipped with a reflux condenser, and the raw material (50 g) that remained under stirring and heating was introduced until reaching a temperature of 70 °C. In parallel, amounts of potassium hydroxide catalyst (KOH, 0.5g) and methanol (CH_3OH, 91 mL) were added and homogenized. The reaction was kept under constant stirring at a temperature of (70 ± 5) °C for 3 h at reflux. At the end of the reactions, the product was separated from glycerol, excess methanol, catalyst and other soluble impurities in the polar environment, followed by washing of the methyl esters and subsequently analyzed/quantified by gas chromatograph equipped with a flame ionization detector (GC-FID). The methyl esters were dissolved in heptane and the analysis performed in a Shimadzu GC-2010 GC-FID (Kyoto, Japan) and a Zebron ZB -5HT column (30 m × 0.32 mm × 10 μm), helium (carrier gas with velocity 54.0 cm s^{-1}), stationary phase 5% phenyl and 95% dimethyl polycyclohexanol No. 314134.

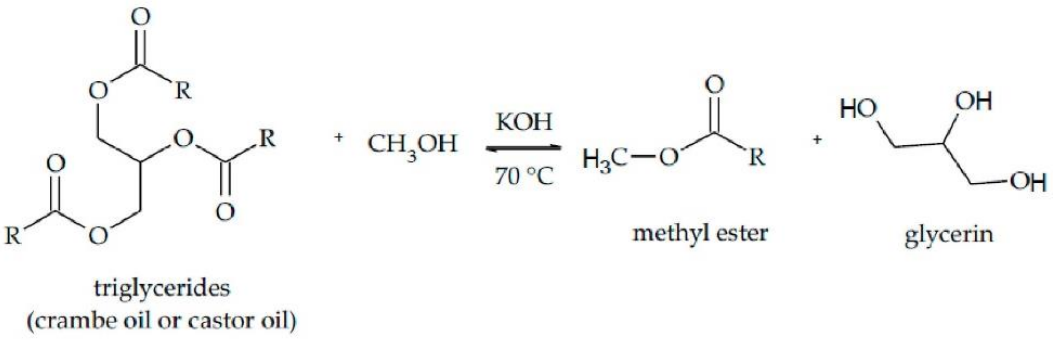

Scheme 1. Transesterification of vegetable oils to form methyl esters.

Attenuated Total Reflectance Fourier Transform Infrared Spectroscopy (FTIR-ATR)

Raw materials (crambe and castor oil), the intermediates (polyester, prepolymer) and final products (PU resin, and PU-modified resin) were analyzed by means of a FTIR-ATR using a Vertex70 Bruker spectrophotometer (Billerica, MA, USA) with an Attenuated Total Reflectance accessory (scans = 64, energy scanning from 590 to 4000 cm^{-1}, resolution = 4 cm^{-1}).

2.2.2. Polyester

Hydroxyl Groups

This analysis confirms whether the modification reaction of crambe oil was successful by determining the quantity of hydroxyl groups added to the chemical structure. The quantity of hydroxyl groups was determined in triplicate according to ASTM E222 [47] and calculated using Equation (1):

$$I_{OH} = \frac{V_B + \left(\frac{m_{sm} \times V_{IAl}}{m_{IAl}}\right) - V_{KOH}}{m_{sm}} \times 56.1 \quad (1)$$

where V_B = volume of alcoholic KOH standard solution necessary to titrate the blank (oil) (mL); V_{KOH} = volume of the alcoholic KOH standard solution necessary to titrate the sample (mL);

V_{IAl} = volume of the standard solution of alcoholic KOH spent on I_{Al} (mL); m_{sm} = sample mass (g); m_{IAl} = sample mass (g) for the determination of index acid (I_{AI}).

2.2.3. Prepolymer

Solid Content and Solvent Content

The solid content was determined for the prepolymer and indicates the quantity of remaining reagent after the solvent curing and evaporation process [25,26]. For analysis, Petri dishes were used. Each Petri dish was weighed empty followed by the addition of an amount of prepolymer (~1 g). The samples were then kept at room temperature (25 ± 5) °C for 24 h. The calculation was performed according to Equations (2) and (3).

$$\text{Solid content } (\%) = \frac{\text{dry prepolymer mass (g)}}{\text{mass of the liquid prepolymer (g)}} \times 100 \quad (2)$$

$$\text{Solvent content } (\%) = 100 - (\text{solid content}) \quad (3)$$

NCO Groups

The quantity of NCO groups was determined in triplicate according to ASTM D2572 [48,49] and calculated according to Equation (4). The NCO groups defines the mass percentage of isocyanate groups that are available to react with polyester, water, etc.

$$\%\text{NCO} = \frac{[(B - V) \times N \times 0.0420]}{W} \times 100 \quad (4)$$

where B = volume of HCl solution used to titrate the blank (without the sample) (mL); V = volume of HCl solution used to titrate the sample (mL); N = concentration of HCl solution; W = sample mass (g).

2.2.4. PU Resin and PU-Modified Resin

PU resin and PU-modified resin were characterized by FTIR-ATR.

Raman Spectroscopy

All the samples were also analyzed by solid state Raman using a Fourier transform Raman spectrometer (Bruker RAMII model, Billerica, MA, USA). For each Raman spectrum, 200 scans were performed in the range of 4000–500 cm^{-1} with a resolution of 4 cm^{-1}. The source of radiation was a leisure with a wavelength of 1064 nm and a power of 100 mW with acquisition time of 6 min.

Thermogravimetric Analysis (TGA)

The thermal stability of raw materials (vegetable oils) and resins (PU and PU-modified) was analyzed by thermogravimetric analyzer (TGA, Hitachi STA 7200, Tokyo, Japan), performed from 25 °C to 550 °C at 10 °C min^{-1} under nitrogen gas at a flow rate of 100 mL min^{-1}.

Optical Microscopy (OM)

The surface of resins with an artificial scratch (size 1000 μm × 60 μm) using a scalpel blade was recorded during 4 h of immersion in a thin layer of deionized water using a system [50] that allows to monitor the surface with a stereomicroscope Carl ZEISS Jena (Oberkochen, Germany) coupled to a computer and TOP VIEW® software (SPECwise, Inc., West Palm Beach, FL, USA).

3. Results and Discussion

3.1. Characterization of Raw Material

3.1.1. Quantification by Gas Chromatography with Flame-Ionization Detection (GC-FID)

Results from GC-FIG of methyl esters (crambe and castor) are shown in Table 1. The results suggest that the major component for crambe methyl esters is derived mainly from erucic acid (13-*cis*-docosenoic acid), while for castor methyl esters, the largest component is ricinoleic acid (12-hydroxy-9-*cis* octadecenoic).

Table 1. Results of compositional analysis profile of the methyl esters of crambe and castor oils.

Correspondent Fatty Acid	Chemical Name	Crambe	Castor
		(%)	
Palmitic acid	hexadecanoic acid	3.5	1.2
Stearic acid	octadecanoic acid	1.7	0.9
Oleic acid	*cis*-9-octadecenoic acid	15.1	3.6
Ricinoleic acid	12-hydroxy-9-*cis* octadecenoic acid	-	94.9
Linoleic acid	*cis*-,*cis*-9,12-octadecadienoic acid	7.4	6.2
Linolenic acid	*cis*,9,12,15-octadecatrienoic acid	5.1	0.7
Arachidic acid	eicosanoic acid	1.9	-
Gadoleic acid	*cis*,9-eicosenoic acid	6.9	0.5
-	11,14-Eicosadienoic acid	0.4	-
Behenic acid	docosanoic acid	3.6	-
Erucic acid	13-*cis*-docosenoic acid	52.9	-
DHA	*cis*-4,7,10,13,16,19-docosahexanoic acid	1.1	-
Lignoceric acid	tetracosanoic acid	5.2	-
-	*cis*-15-tetracenoic acid	2.3	-

3.1.2. Attenuated Total Reflectance Fourier Transform Infrared Spectroscopy (FTIR-ATR)

Figure 3 illustrates the FTIR-ATR spectrum for crambe oil, castor oil and tannin and the main attributions of the different bands in FTIR-ATR (normalized intensity of bands) stand out.

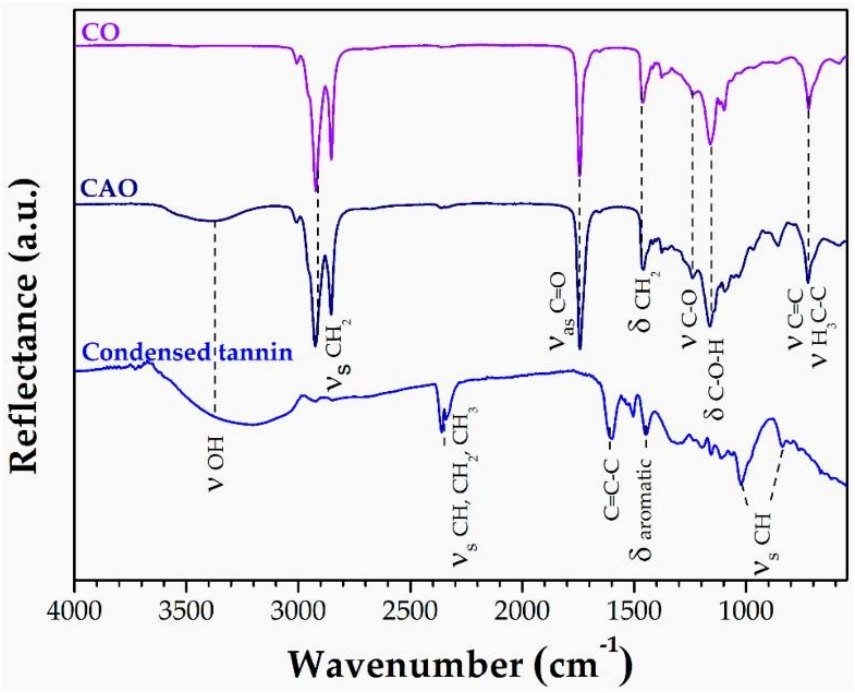

Figure 3. FTIR-ATR spectra for the crambe oil, CO (—), castor oil, CAO (—) and condensed tannin (—).

The FTIR-ATR spectrum of crambe oil evidences the absence of –OH band, as expected because crambe oil has no hydroxyl in its structure; the spectrum for castor oil evidences the presence of –OH (3425 cm^{-1}). In the case of condensed tannin, the absence of band C=O (~1700 cm^{-1}) [40,43] confirms that the structure is a condensed (condensed tannin) [51] and contributes to the insertion of OH (~3340 cm^{-1}) that favors the self-healing effect when the resin is applied to protect aluminum alloys [43].

3.1.3. Thermogravimetric Analysis (TGA)

Representative dynamic thermogravimetric analysis (TGA) results of crambe oil and castor oil are shown in Figure 4.

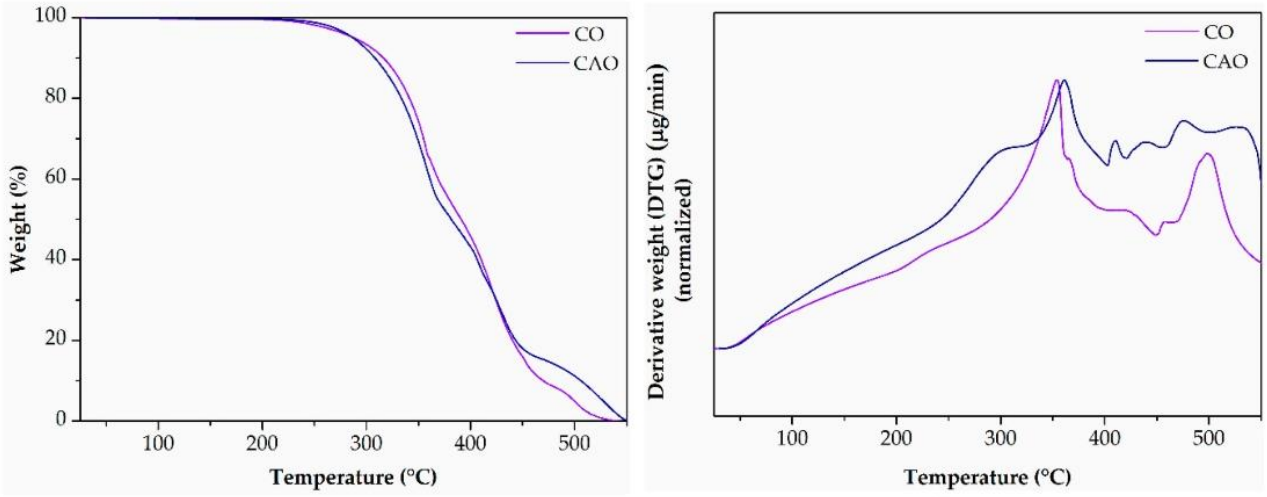

Figure 4. TGA weight loss (**a**) and derivatives of TGA data (**b**) of crambe oil, CO (—), castor oil, CAO (—).

Crambe and castor oils exhibit no appreciable weight loss before 250 °C, indicating good thermal stability. The most stable raw material was crambe oil-CO (300 °C), followed by castor oil-CAO (294.4 °C). Both oils presented thermal decomposition in three consecutive stages between 245–535 °C (crambe oil-CO) and 240–555 °C (castor oil-CAO). These values indicate high purity of oils, with no presence of inorganic compounds. DTG curves present a series of exothermic events, which are attributed to the oxidative degradation of organic matter (oil structure).

3.2. Main Chemical Reactions for the Polyester and Prepolymer Preparation and Products Characterization

3.2.1. Polyester Preparation

Polyester was produced by reacting a vegetable oil and oxygenated solvents based on literature with modifications [43,52,53]. Crambe oil (CO, 1995.2 g), trimethylolpropane (TMP, 804.6 g), butylated hydroxyl toluene (BHT, 1.0 g) and lithium hydroxide (LiOH, 0.50 g) under stirring and heating at 240 °C for 5 h in N_2 atmosphere, and glycerin (a by-product) was removed during the reaction with Dean-Stark (Figure 5a and Scheme 2). The reaction progress was monitored by the methanol solubility test (3 mL methanol/1 mL polyester) and acidity index (mg KOH/g of polyester). When the polyester was totally solubilized in methanol and the acidity index was lower than 30, the reaction was completed, and the synthesis stopped. After 5 h of reaction, the temperature was lowered to 150 °C and phthalic anhydride (PhA, 888.6 g) was added under stirring and heating at 150 °C for 2 h in N_2 atmosphere (Figure 5a and Scheme 3).

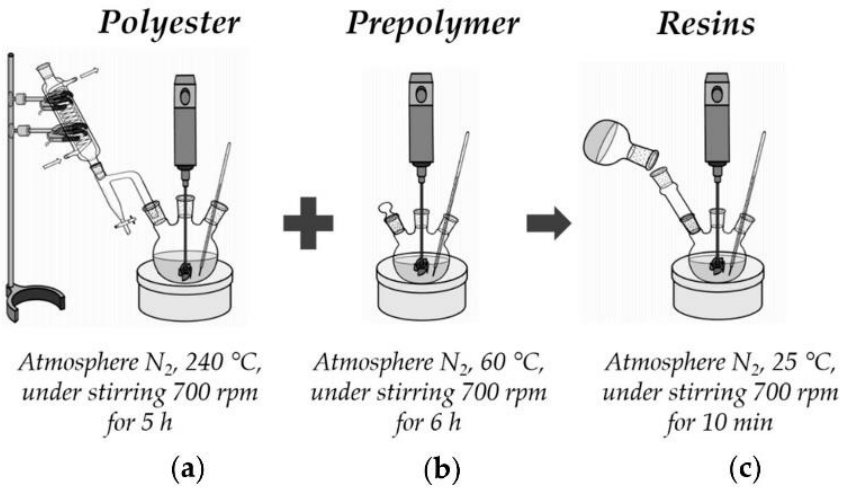

Figure 5. Reaction system for: (**a**) polyester, (**b**) prepolymer and (**c**) PU and PU-modified resins.

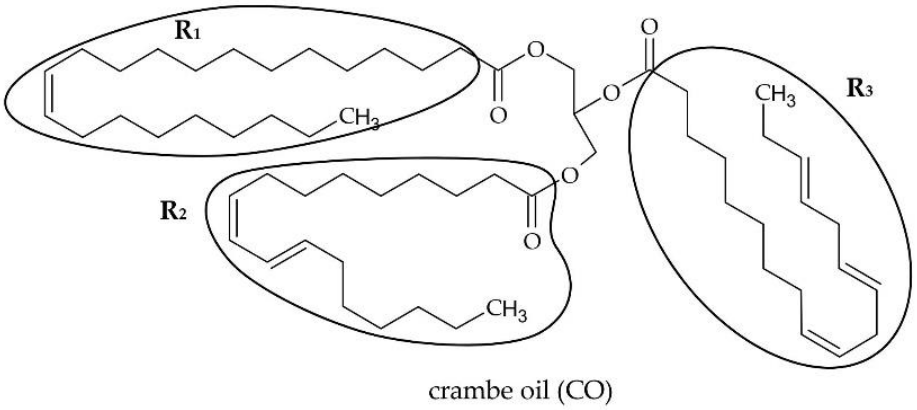

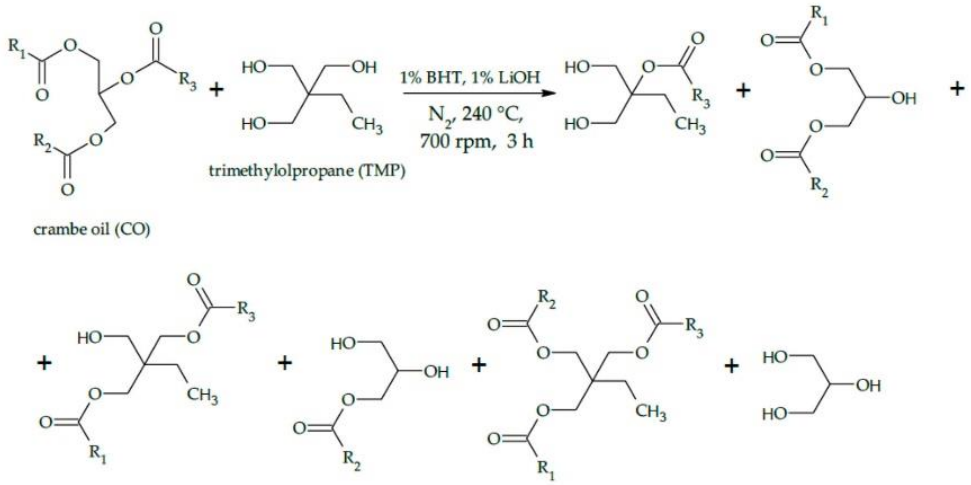

Scheme 2. First step of modification of crambe oil.

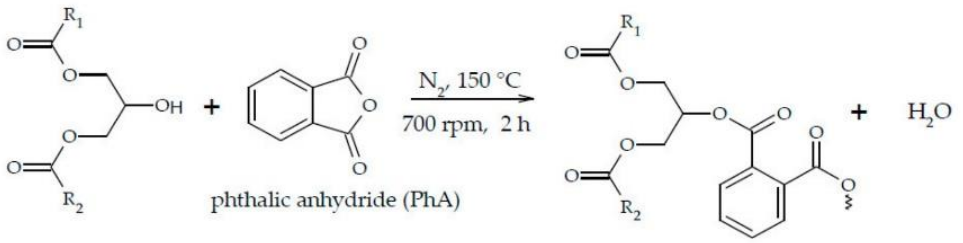

Scheme 3. Reaction that occurs with all products formed in Scheme 2, especially with the –OH for polyester formation.

3.2.2. Prepolymer Preparation

Prepolymer was produced by reacting a vegetable oil and oxygenated solvents based on literature with modifications [43]. The prepolymer was prepared with castor oil (CAO, 250.6 g), trimethylolpropane (TMP, 93.86 g), butylated hydroxy toluene (BHT, 4.40 g), propylene glycol (PG, 24.34 g), n-butyl acetate (BA, 889.78 g), ethyl glycol acetate (EGA, 383.22 g), hexamethylene diisocyanate (HDI, 1046.16 g) under stirring and heating at 60 °C for 6 h in N_2 atmosphere (Figure 5b and Scheme 4).

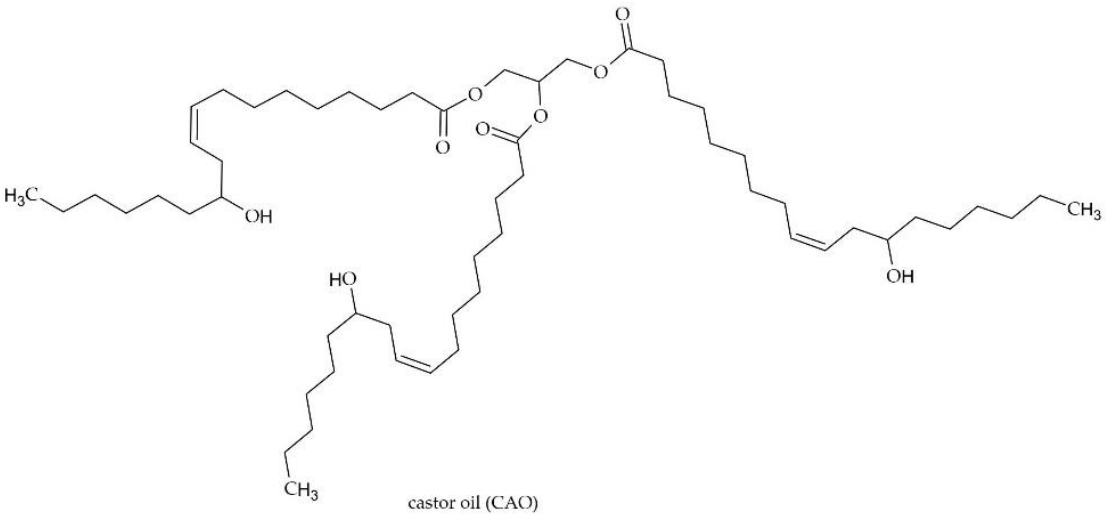

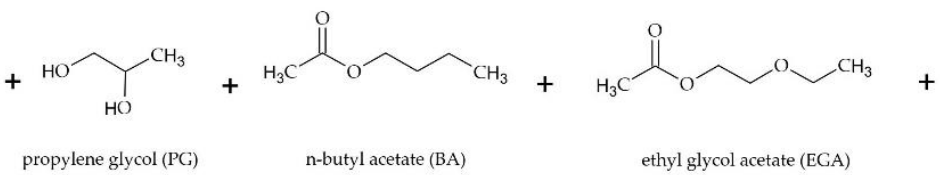

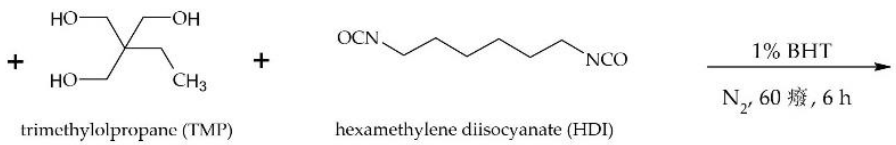

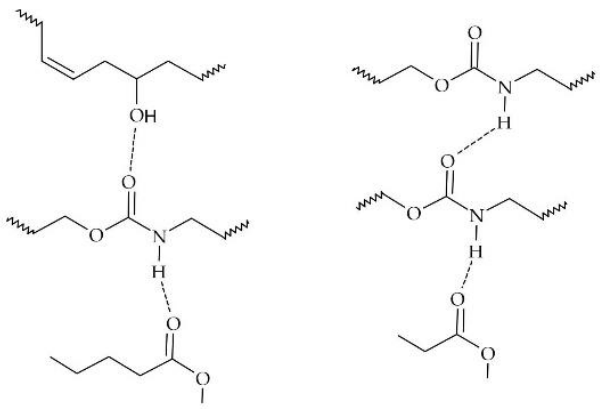

Scheme 4. Prepolymer obtaining reaction.

3.2.3. Characterization of Polyester and Prepolymer

Hydroxyl Groups, Solid Content, Solvent Content, and NCO Groups

Table 2 shows the physicochemical properties for the polyester (hydroxyl groups) and prepolymer (solid content and solvent content, NCO groups).

Table 2. Physicochemical properties of polyester and prepolymer.

Properties			
Polyester		**Prepolymer**	
Hydroxyl groups (mg KOH/g sample)	151.6	**Solid content (%)**	56.1
		Solvent content (%)	43.8
		NCO groups (%)	6.26

Crambe oil has no hydroxyl in its chemical structure, so the structure is modified by transesterification with trimethylolpropane (TMP). The hydroxyl groups (I_{OH}) are all considered hydroxyls present in the chemical structure of the modified polyester. Thus, the result of the hydroxyl groups (151.6 mg KOH/g sample) confirms the modification of the raw material (crambe oil). According to the literature [26] the greater the quantity of free hydroxyls, the more the reaction medium is conducive to carrying out chain cross-linking reactions.

The prepolymer presented 56.1% solid and 43.8% solvent, being higher than values found in the literature [54,55], but like those discussed by Mannari and Massingill [56]. These values indicate a decrease in the amount of volatile organic compounds. The NCO groups is also an important feature for prepolymers, for example, for commercial application normally the NCO groups corresponds to a maximum of 20% [57] and this work achieved 6.26%. From this index, the required amount of hydrogen donor groups was calculated according to the NCO/OH molar ratio studied for each coating.

Attenuated Total Reflectance Fourier Transform Infrared Spectroscopy (FTIR-ATR)

Figure 6 illustrates the FTIR-ATR spectrum for polyester and prepolymer and the main attributions of the different bands in FTIR-ATR (normalized intensity of bands) stand out.

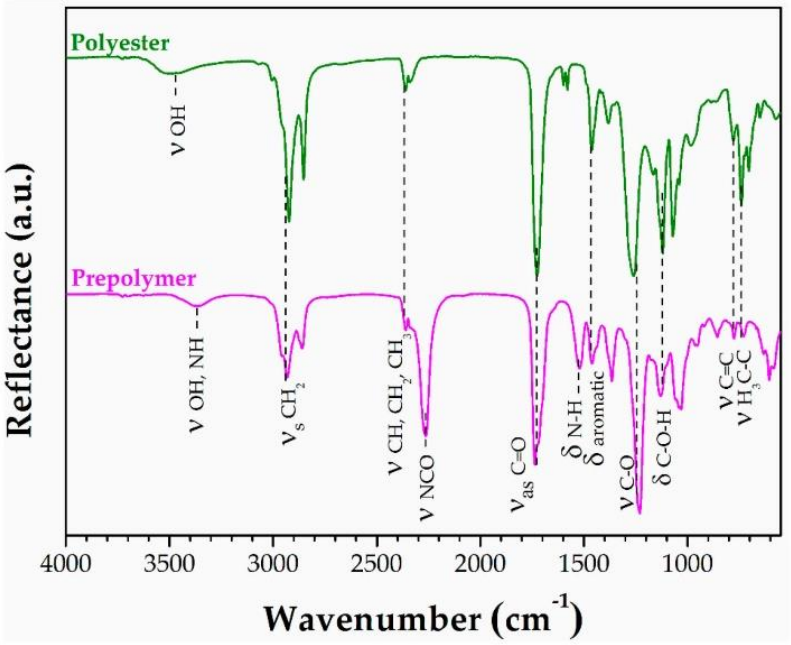

Figure 6. FTIR-ATR spectra for the polyester (—) and prepolymer (—).

The FTIR-ATR spectrum of polyester confirms the effectiveness of the crambe oil modification reaction (Schemes 2 and 3) by the presence of the –OH (3489 cm^{-1}) band. The FTIR-ATR spectrum of prepolymer shows the presence of the characteristic NCO (2270 cm^{-1}) band of free isocyanate groups in the chemical structure (Scheme 4) [58,59].

3.3. Preparation and Characterization of PU and PU-Modified Resins

3.3.1. Preparation of Polyurethane Resins

Polyester and prepolymer react in the presence of a catalyst, stannous octoate (SO, 1%), under stirring for 10 min to produce the PU resin (Figure 5c and Scheme 5). For the PU-modified resin, steps 1 and 2 were exactly the same as for the reference coating, except that condensed tannin was added (4.20 g) in the last step of the resin formulation (Figure 5c and Scheme 6).

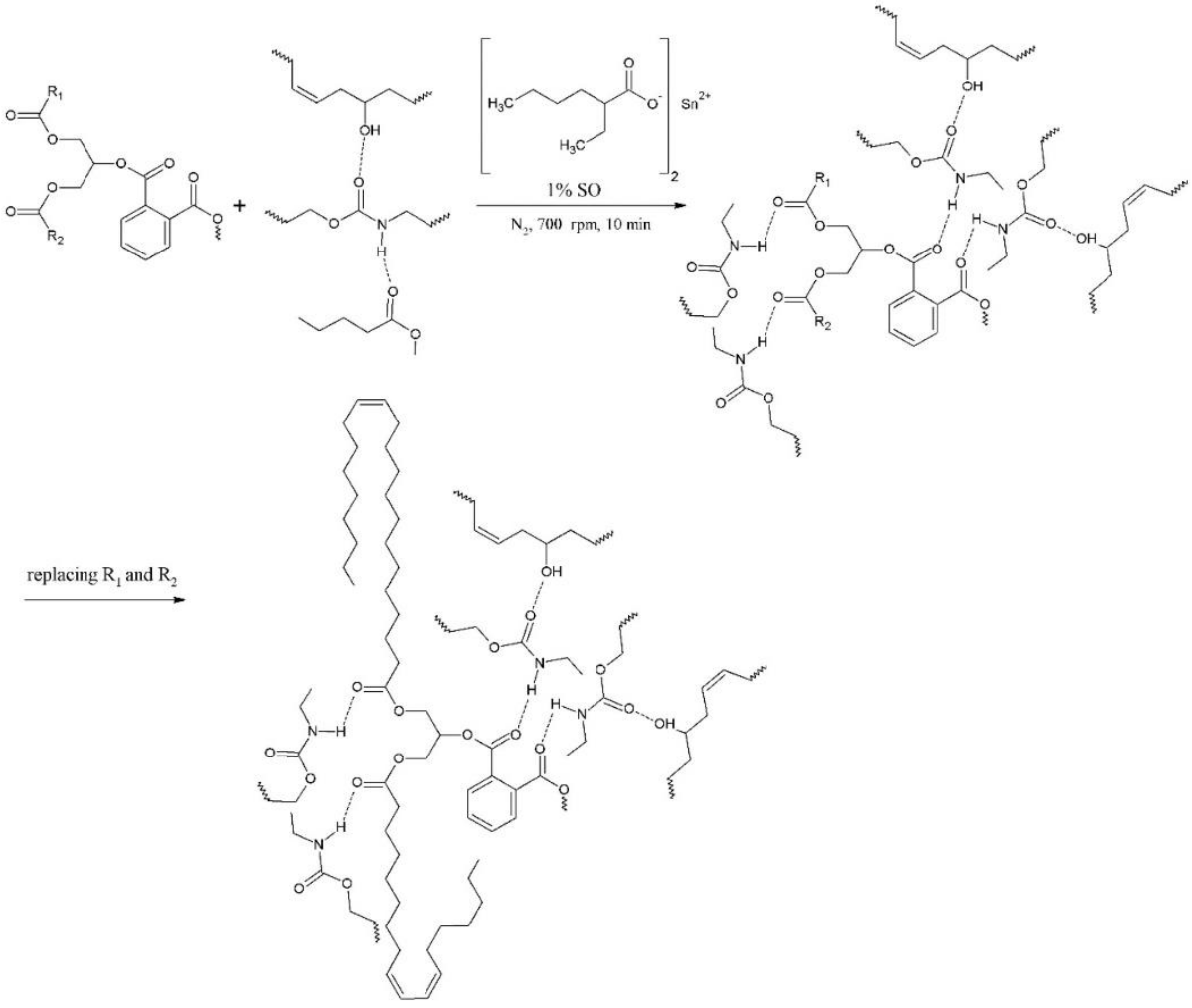

Scheme 5. Preparation of PU-resin.

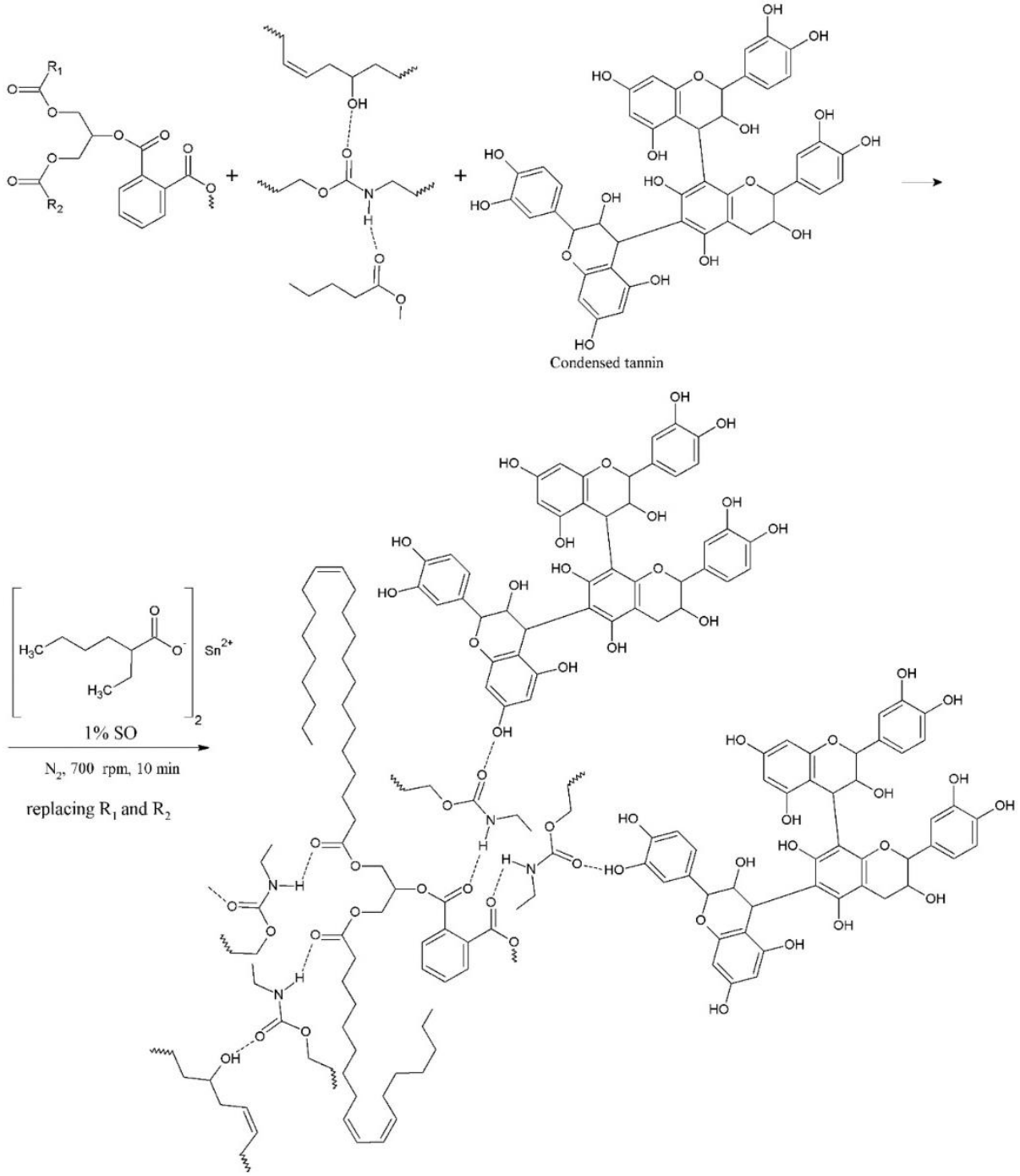

Scheme 6. Preparation of PU-modified resin.

Figure 7 shows a scheme to obtain the monolithic resins. The Teflon sheet substrate was cleaned with deionized water and acetone and allowed to dry (~25 °C). The PU and PU-modified resins formulation was then cast using an applicator on the Teflon sheet substrate. The resin applied on the substrate was kept at room temperature (~25 °C) for 24 h to allow the solvent to evaporate.

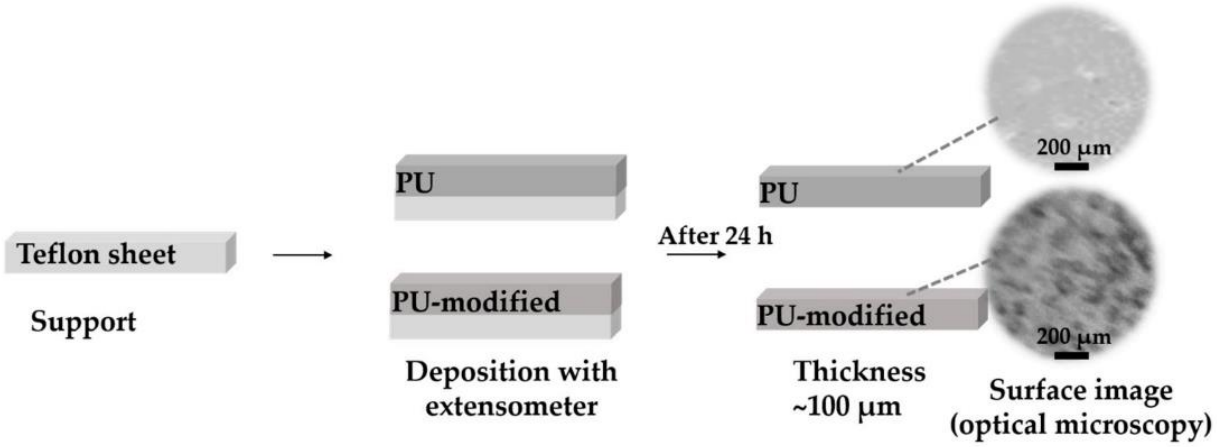

Figure 7. Scheme to obtain the monolithic resins of the PU and PU-modified with condensed tannin.

3.3.2. Characterization of PU and PU-Modified Resins

Attenuated Total Reflectance Fourier Transform Infrared Spectroscopy (FTIR-ATR)

Figure 8 illustrates the FTIR-ATR spectrum for PU and PU-modified resins and the main attributions of the different bands in FTIR-ATR (normalized intensity of bands) stand out.

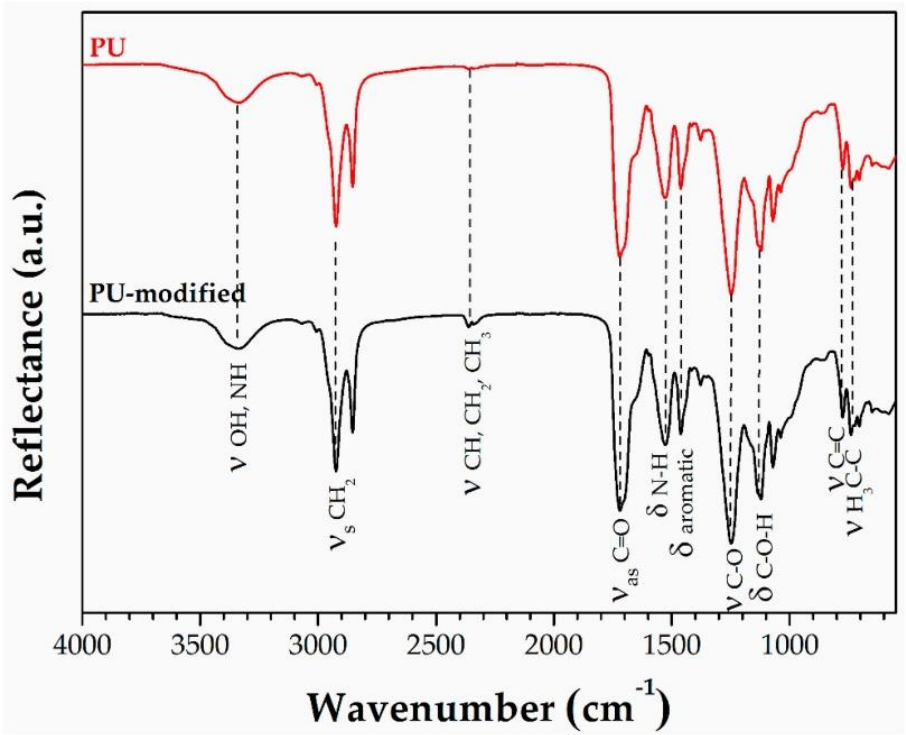

Figure 8. FTIR-ATR spectra for the PU resin (—) and PU-modified resin (—).

In the FTIR-ATR spectrum of PU-resin, it was noted in the band attributed to NCO-free groups that some disappeared, indicating/confirming the complete reaction between the polyester and prepolymer (Schemes 5 and 6) [60]. These spectra are similar, but not the same, as presented by our group in previous studies [43], where the resin was applied on aluminum alloy, and in the present work the monoliths were analyzed. PU and PU-modified resins contain the characteristic bands of –OH (3346 cm^{-1}), N–H (3340 and 1527 cm^{-1}), C=O (1720 cm^{-1}), C–O (1249 cm^{-1}), O–H (1246 cm^{-1}) and –O–H (1120 cm^{-1}) bonds, which clearly show the formation of a urethane linkage [48].

Thermogravimetric Analysis (TGA)

Representative dynamic thermogravimetric analysis (TGA) results of PU and PU-modified resins are shown in Figure 9. Table 3 presents the attributions to the mass loss.

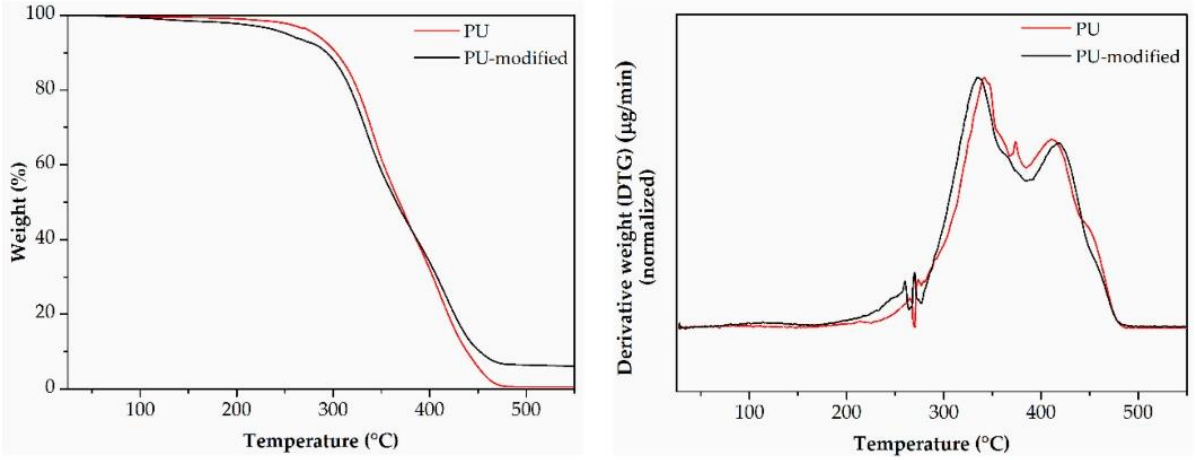

Figure 9. TGA weight loss (**a**) and derivatives of TGA data (**b**) of PU resin (—) and PU-modified resin (—).

Table 3. Attributions to the different thermal events.

Temperature (°C)	Weight Loss Due to:
260–350	Decomposition of active H sources (chain extenders)
360–490	Breakup of isocyanate (rigid segment) of the polyester (flexible segment)
200–650 (two steps)	Decomposition of polyurethane (PU)

The PU and PU-modified resins exhibit no significant weight loss before 250 °C, indicating good thermal stability, as already observed for CO and CAO. Two not well-defined peaks are observed between ~260 and ~490 °C. The weight loss in the 260–350 °C range can be referred to the decomposition of chain extensors [61]; in the 360–490 °C interval, the thermal events can be associated with the breakup of prepolymer (rigid segment) of the polyester (flexible segment) [61] and 200–650 °C (two steps) can be referred to decomposition of polyurethane (PU) to form CO_2 and water [62].

Raman Spectroscopy

Figure 10 shows the Raman spectrum for the resins (normalized for the intensities).

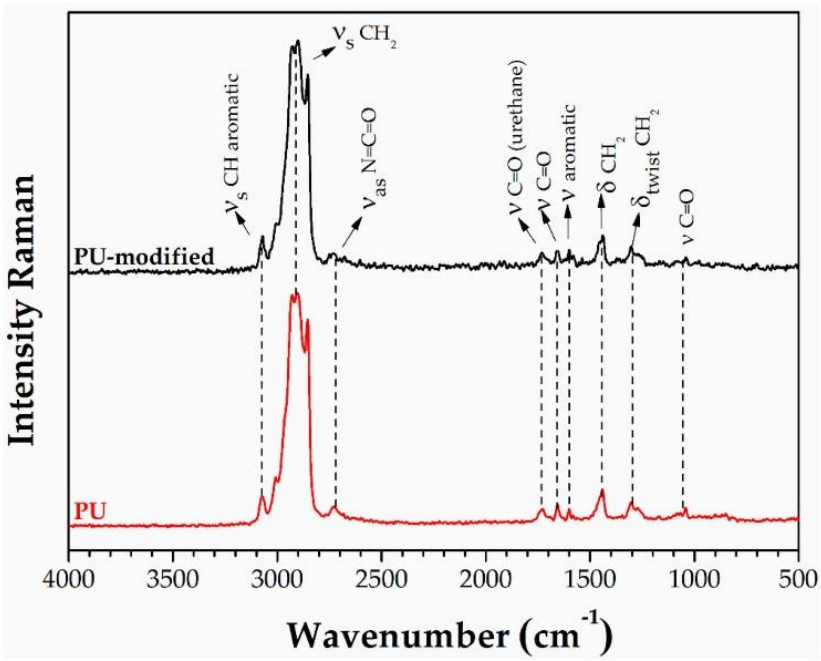

Figure 10. Raman spectra for the PU-blank and PU-modified (with intensity normalized).

Note the presence of some more intense bands, which are characteristic of the formed polymer. The assignments of the bands were made according to previous studies on polyurethanes [63–68].

Artificial Defected Monoliths in Contact with Deionized Water

Figure 11 shows the surface OM images of the PU and the condensed tannin-modified PU monolith obtained before and after immersion in deionized water when an artificial defect was made on the surface.

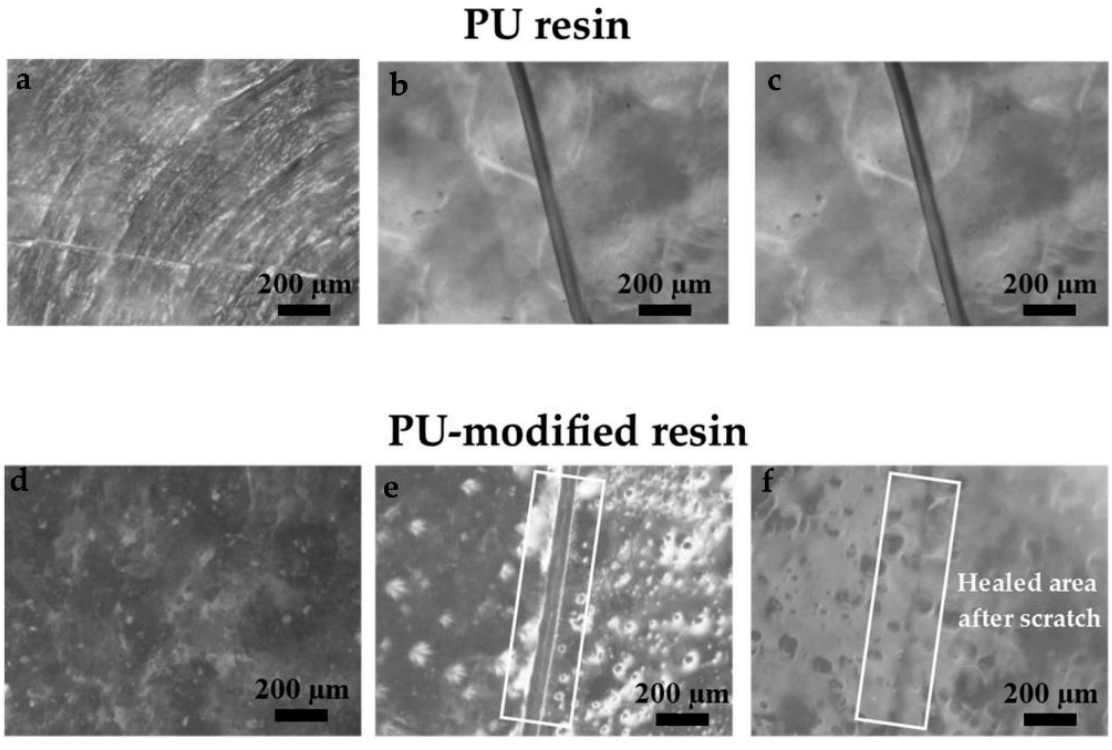

Figure 11. OM images of PU and condensed tannin-modified PU monoliths for the prepared surfaces (**a**,**d**) and after applying an artificial defect before (**b**,**e**) and after 4 h of immersion in deionized water (**c**,**f**).

This figure clearly shows that for the PU the defect remained intact after immersion of the monolith in deionized water while for the condensed tannin-modified PU monolith the defect disappeared after some time in contact with deionized water. To demonstrate this process, videos (Figure S1) were recorded of both artificial-defected surfaces during the contact with deionized water for 4 h and it is clear that the defect remained almost unchanged for PU, while for the modified PU, the defect began to close by the movement of the coating walls limited by the defect until completely closing the defect after some immersion time. Other works have also studied the self-healing effect by microscopic images [59,69–71].

3.3.3. Self-Healing Effect

The above-described results (Figure 11 and Figure S1) allow us to propose that the incorporation of condensed tannin in the monolithic resin is responsible for the self-healing effect. The closing of the walls of the artificial defect in a condensed tannin-modified PU monolith was also observed when this type of coating was applied on AA2024 [43]. Tannin-modified PU monolith (100-µm thick) with a scratch of the 1000 µm long × 60 µm wide × 100 µm deep was automatically repaired when immersed in deionized water. When the modified resin was applied on AA2024, the healing effect was described based on hydrogen bond cleavage, then followed by the formation of a new hydrogen bond and confirmed by electrochemical localized techniques [43]. When tannin-modified PU was placed in contact with water, the swelling of the coating was insignificant, and the self-healing effect was observed, indicating that the self-healing mechanism can be the formation of hydrogen bonds. The FTIR-ATR (Figure 8) suggests an increase of the number of hydrogen bonds after adding condensed tannin to the PU resin. The FTIR-ATR spectrum of the tannin-modified PU monoliths with an artificial defect after having the defect repaired by immersion in water also indicates the increase of the intensity of the band attributed to hydrogen bond, demonstrating that the self-healing effect is based on hydrogen bond generation (Figure 12).

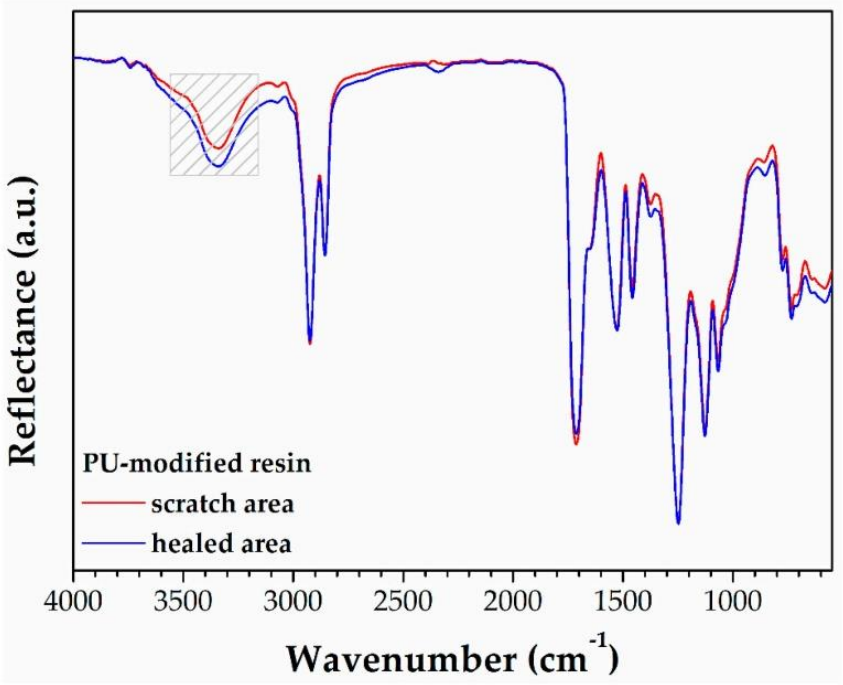

Figure 12. FTIR-ATR spectra of the modified-PU monolith with artificial defect and after having the defect repaired by immersion in water.

It is very important to demonstrate that the self-healing property is a characteristic of the monolith, i.e., a property free of any metallic surface contribution. Therefore, the self-healing effect may be interpreted considering that the free OH groups present in tannin and some others created in the

polyurethane by interacting with tannin when in contact with water or humidity allows the formation of new hydrogen bonds. Figure 13 schematizes the possibilities of hydrogen bonding formation between the flexible and rigid segments and condensed tannin.

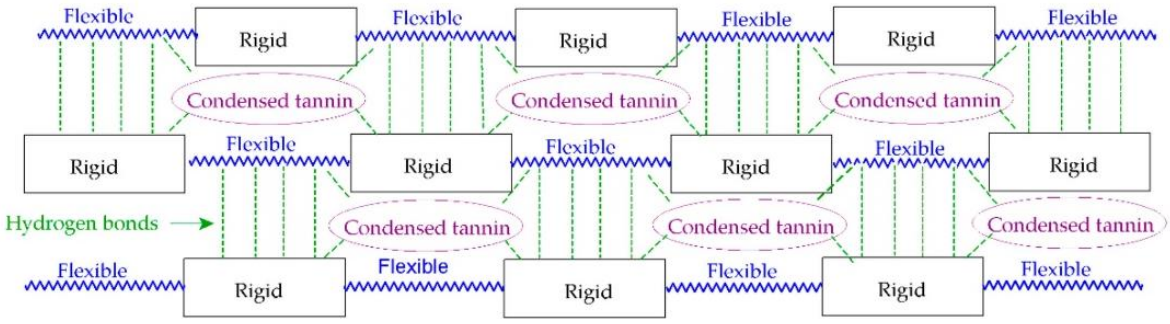

Figure 13. Scheme of hydrogen bonds between flexible and rigid segments of PU and hydrogen bonds between tanning and both segments.

Therefore, the self-healing of the condensed tannin-modified PU coating is understood to function as follows: when an artificial defect or damage is produced on the coating surface, the humidity, water or aqueous solutions rapidly makes new hydrogen bonds—mainly with the tannin and the flexible segment of the polymer. This opens the possibility of hydrogen bond formation with the rigid segment of the polymer; therefore, the healing effect is based on hydrogen bond cleavage followed by new hydrogen bond formation. It is worth remembering that many of the properties of tannins are based on their ability to form hydrogen bonds [51,72]. Interactions involving the formation of new hydrogen bonds between a viscous system (here the polyester, prepolymer and nonmodified resin) in combination with a condensed tannin led to the formation of a flexible structure [1,73,74], mainly due to the greater proportion of polyester, more active than prepolymer, leading to a higher probability to form new hydrogen bonds with condensed tannin.

3.4. Applications of the PU and PU-Modified Resins

Special self-healing polyurethane coatings play an important role in the protection of aluminum alloys against corrosion in aggressive aqueous media, mainly in those containing chloride ions [21,22]. Polyurethane-based coatings were applied to protect AA1200 alloy and some formulation offered good barrier effect for 1 year of immersion in 3.5 wt % NaCl solution [22].

The resins synthesized in this work were applied on aluminum alloy AA2024-T3 for protecting it against corrosion and the self-healing effect investigated by electrochemical measurements in scratch zone [43]. The efficiency of the incorporation of tannin in the polyurethane resin (condensed tannin-modified PU) was already proved by FTIR-ATR and by the combination of localized electrochemical techniques with surface analysis (in the scratch and scratch-free zones). When immersion in NaCl 0.005 mol L^{-1} occurred, the self-healing effect start to act after 2–3 h and the coating was completely recovered at around 7 h of immersion in 3.5 wt % NaCl.

These results open a large window of applications of modified-PU resins in terms of their possible incorporation with other materials with different properties, such as corrosion inhibitors (encapsulated or not), reinforcing materials to increase the wear resistance, materials able to modify the hydrophobicity of the surface and to modify other properties of PU resins. As a consequence, modified-PU resins can be used to extend the lifetime of different metallic surfaces working in aqueous aggressive media or subjects, tribocorrosion conditions, as well as many other applications.

4. Conclusions

In this work, polyurethane (PU) produced from vegetable oils and condensed tannin-modified PU resin were successfully obtained and characterized by different chemical and physical techniques.

The formation of polyester through the modification of the crambe oil was confirmed by the determination of quantity of hydroxyl groups (151.6 mg KOH/g sample) and the prepolymer formation by the disappearance of the free NCO groups of hexamethylene diisocyanate.

FTIR-ATR spectra confirmed that a condensed tannin was used. FTIR-ATR spectra were efficient in confirming the formation of polyester, prepolymer, PU and condensed tannin-modified PU resins, also reinforced by Raman spectra.

The good thermal stability of resins was confirmed by thermogravimetric analysis, since no appreciable weight loss below 250 °C was observed.

These studies open many possibilities for new vegetable oils-based polyurethane formulations and modified-polyurethane resins that can be used to extend the lifetime of different metallic surfaces, as well as the ability to work in aqueous aggressive media due to the generation of the self-healing property, or to better equip many other applications in materials science.

Supplementary Materials: The following are available online at http://www.mdpi.com/2073-4360/11/11/1890/s1, Figure S1 contains videos a and b.

Author Contributions: Conceptualization, J.V.N. and A.V.B.; methodology, J.V.N.; C.S.F.; E.R.P.P.; W.L.P.; Y.M. and S.J.L.R.; writing—original draft preparation, J.V.N.; writing—review and editing, J.V.N.; S.J.L.R. and A.V.B.; visualization, E.R.P.P.; W.L.P.; Y.M. and S.J.L.R.; supervision, A.V.B.; funding acquisition, J.V.N.

Funding: J.V. Nardeli author thanks the São Paulo state agency FAPESP (Process: 2015/10554-9 and 2018/09040-9) for scholarships.

Acknowledgments: The authors are grateful TANAC S.A. by providing the inhibitors. The authors thank Multiuser Chemical Analysis Laboratory and CEMPEQC of IQ-UNESP the possibility of using the laboratory for analysis FTIR-ATR, Raman and GC-FID; Centro de Química Estrutural, CQE, Instituto Superior Técnico de Lisboa, Portugal the possibility of using the laboratory for termogravimetric analysis. The authors would like to thank Profa. Dra. Isabele Rodrigues Nascimento for the fruitful discussions about organic reactions.

Conflicts of Interest: The authors declare no conflict of interest.

References

1. Zhu, Y.; Romain, C.; Williams, C.K. Sustainable polymers from renewable resources. *Nature* **2016**, *540*, 354–362. [CrossRef] [PubMed]
2. Rahman, M.M.; Rabbani, M.M.; Saha, J.K. Polyurethane and Its Derivatives. In *Functional Polymers: Polymers and Polymeric Composites: A Reference Series*; Mazumder, J., Sheardown, M.H., Al-Ahmed, A., Eds.; Springer: Cham, Switzerland, 2019. [CrossRef]
3. Szmechtyk, T.; Sienkiewicz, N.; Woźniak, J.; Strzelec, K. Polyurethanes as self-healing materials. *Curr. Chem. Lett.* **2015**, *4*, 61–66. [CrossRef]
4. Yang, Z.; Shuai, B.; Zhang, X.; Yu, H.; Zhang, H.; Jia, Y.; Zhang, C.; Guan, X. Fabrication and performance of a polyurethane hybrid composite with waste red mud. *Polym. Compos.* **2019**, *40*, 2424–2431. [CrossRef]
5. Khalid, T.; Albasha, L.; Qaddoumi, N.; Yehia, S. Feasibility Study of Using Electrically Conductive Concrete for Electromagnetic Shielding Applications as a Substitute for Carbon-Laced Polyurethane Absorbers in Anechoic Chambers. *IEEE Trans. Antenn. Propag.* **2017**, *65*, 2428–2435. [CrossRef]
6. Zhang, C.; Shuai, B.; Zhang, X.; Hu, X.; Zhang, H.; Jia, Y.; Yang, Z.; Guan, X. Polyurethane/Red Mud Composites with Flexibility, Stretchability, and Flame Retardancy for Grouting. *Polymers* **2018**, *10*, 906. [CrossRef]
7. Xiang, X.J.; Qian, J.W.; Yang, W.Y.; Fang, M.H.; Qian, X.Q. Synthesis and properties of nanosilica-reinforced polyurethane for grouting. *J. Appl. Polym. Sci.* **2006**, *100*, 4333–4337. [CrossRef]
8. Yang, Z.; Zhang, X.; Liu, X.; Guan, X.; Zhang, C.; Niu, Y. Flexible and stretchable polyurethane/waterglass grouting material. *Constr. Build. Mater.* **2017**, *138*, 240–246. [CrossRef]
9. Zaimahwati; Yuniati; Jalal, R.; Rihayat, T.; Zhafiri, S. Synthesis and Characterization Thermal of Polyurethane/MMT from Castor Oil Polyols for Coating. *Iop Conf. Ser. Mater. Sci. Eng.* **2019**, *536*, 1–8. [CrossRef]
10. Zhao, Z.; Guo, L.; Feng, L.; Lu, H.; Xu, Y.; Wang, J.; Xiang, B.; Zou, X. Polydopamine functionalized graphene oxide nanocomposites reinforced the corrosion protection and adhesion properties of waterborne polyurethane coatings. *Eur. Polym. J.* **2019**, 109249. [CrossRef]

11. Ye, X.; Wang, Z.; Ma, L.; Wang, Q.; Chu, A. Zinc oxide array/polyurethane nanocomposite coating: Fabrication, characterization and corrosion resistance. *Surf. Coat. Technol.* **2019**, *358*, 497–504. [CrossRef]
12. Garrison, T.F.; Kessler, M.R. *Chap 3—Plant Oil-Based Polyurethanes, Bio-Based Plant Oil Polymers and Composites*; Samy, A., Madbouly, C.Z., Kessler, M.R., Eds.; William Andrew Publishing: Norwich, NY, USA, 2016; pp. 37–54. [CrossRef]
13. Alam, M.; Akram, D.; Sharmin, E.; Zafar, F.; Ahmad, S. Vegetable oil based eco-friendly coating materials: A review article. *Arab. J. Chem.* **2014**, *7*, 469–479. [CrossRef]
14. Pfister, D.P.; Xia, Y.; Larock, R.C. Recent advances in vegetable oil-based polyurethanes. *Chem. Sus. Chem.* **2011**, *4*, 703–717. [CrossRef]
15. Panda, S.S.; Panda, B.P.; Nayak, S.K.; Mohanty, S. A Review on Waterborne Thermosetting Polyurethane Coatings Based on Castor Oil: Synthesis, Characterization, and Application. *Polym. Plast. Technol. Eng.* **2018**, *57*, 500–522. [CrossRef]
16. Gällstedt, M.; Pettersson, H.; Johansson, T.; Newson, W.R.; Johansson, E.; Hedenqvist, M.S. Film Extrusion of *Crambe abyssinica*/Wheat Gluten Blends. *J. Vis. Exp.* **2017**, *119*, e54770. [CrossRef]
17. Rasel, H.; Johansson, T.; Gällstedt, M.; Newson, W.; Johansson, E.; Hedenqvist, M. Development of bioplastics based on agricultural side-stream products: Film extrusion of Crambe abyssinica/wheat gluten blends for packaging purposes. *J. Appl. Polym. Sci.* **2016**, *133*, 42442. [CrossRef]
18. Arbenz, A.; Avérous, L. Tannins: A Resource to Elaborate Aromatic and Biobased Polymers. In *Biodegradable and Biobased Polymers for Environmental and Biomedical Applications*; Susheel, K., Avérous, L., Eds.; Wiley: Hoboken, NJ, USA, 2016; Chapter 4. [CrossRef]
19. Madbouly, S.A.; Otaigbe, J.U. Rheokinetics of thermal-induced gelation of waterborne plyurethane dispersions. *Macromolecules* **2005**, *38*, 10178–10184. [CrossRef]
20. Madbouly, S.A.; Xia, Y.; Kessler, M.R. Rheological behavior of environmentally friendly castor oil-based waterborne polyurethane dispersions. *Macromolecules* **2013**, *46*, 4606–4616. [CrossRef]
21. Karak, N.; Rana, S.; Cho, J.W. Synthesis and characterization of castor-oil-modified hyperbranched polyurethanes. *J. Appl. Surf. Sci.* **2009**, *112*, 736–743. [CrossRef]
22. Nardeli, J.V.; Fugivara, C.S.; Benedetti, A.V. Environmentally Friendly coatings applied on aluminum alloy ASTM 1200. In Proceedings of the 64th Annual Meeting of the International Society of Electrochemistry, Santiago de Querétaro, Mexico, 8–13 September 2013; International Society of Electrochemistry: Lausanne, Switzerland, 2013; Volume 1.
23. Nardeli, J.V.; Fugivara, C.S.; Taryba, M.; Montemor, M.F.; Benedetti, A.V. Zn containing polymer coatings for AA7475: Localized study of anti-corrosion performance. In Proceedings of the the European Corrosion Congress–EUROCORR, Sevilha, Spain, 9–13 September 2019.
24. Nardeli, J.V.; Snihirova, D.V.; Fugivara, C.S.; Montemor, M.F.; Pinto, E.R.P.; Messaddeq, Y.; Benedetti, A.V. Localised corrosion assessement of crambe-oil-based polyurethane coatings applied on the ASTM 1200 aluminum alloy. *Corros. Sci.* **2016**, *111*, 422–435. [CrossRef]
25. Talbert, R. *Paint Technology Handbook*; CRC Press: Boca Raton, FL, USA, 2007; ISBN 9781574447033.
26. Fazenda, J.M.R. *Tintas, Ciência e Tecnologia*; Abrafati: São Paulo, Brazil, 2009; ISBN 9788521204749.
27. Xie, F.; Zhang, T.; Bryant, P.; Kurusingal, V.; Colwell, J.M.; Laycock, B. Degradation and stabilization of polyurethane elastomers. *Prog. Polym. Sci.* **2019**, *90*, 211–268. [CrossRef]
28. Rosu, D.; Rosu, L.; Cascaval, C.N. IR-change and yellowing of polyurethane as a result of UV irradiation. *Polym. Deg. Stab.* **2009**, *94*, 591–596. [CrossRef]
29. The Chemistry of Polyurethane Coatings—A General Reference Manual, Bayer® Material Science. Available online: http://digitalcollections.library.cmu.edu/awweb/awarchive?type=file&item=488891 (accessed on 1 May 2019).
30. Golling, F.E.; Pires, R.; Hecking, A.; Weikard, J.; Richter, F.; Danielmeier, K.; Dijkstra, D. Polyurethanes for corrosion & adhesives—Chemistry & applications. *Polym. Int.* **2019**, *68*, 848–855. [CrossRef]
31. Hernes, P.J.; Benner, R.; Cowie, G.L.; Goñi, M.A.; Bergamaschi, B.A.; Hedges, J.I. Tannin diagenesis in mangrove leaves from a tropical estuary: A novel molecular approach. *Geochim. Cosmochim. Acta* **2001**, *65*, 3109–3122. [CrossRef]
32. Pizzi, A. Tannin-Based Biofoams-A Review. *JRM* **2019**, *7*, 477–492. [CrossRef]
33. Tondi, G. Tannin-Based Copolymer Resins: Synthesis and Characterization by Solid State 13C NMR and FT-IR Spectroscopy. *Polymers* **2017**, *9*, 223. [CrossRef]

34. Banu, K.; Shimura, T.; Sadeghi, S. Selective detection and recovery of gold at tannin-immobilized non-conducting electrode. *Anal. Chim. Acta* **2015**, *853*, 207–213. [CrossRef]
35. Peres, R.S.; Cassel, E.; Azambuja, D.S. Black wattle tannin as steel corrosion inhibitor. *Int. Sch. Res. Net.* **2012**, *2012*, 1–9. [CrossRef]
36. Martinez, S.; Štagljar, I. Correlation between the molecular structure and the corrosion inhibition efficiency of chestnut tannin in acidic solutions. *J. Molec. Struc.* **2003**, *640*, 167–174. [CrossRef]
37. Martinez, S. Inhibitory mechanism of mimosa tannin using molecular modeling and substitutional adsorption isotherms. *Mater. Chem. Phys.* **2002**, *77*, 97–102. [CrossRef]
38. Michael, N.C.; Olubunmi, J.A. The corrosion inhibition of mild steel in sulphuric acid solution by flavonoid (catechin) separated from Nypa fruticans Wurmb leaves extract. *Sci. J. Chem.* **2014**, *2*, 27–32. [CrossRef]
39. Rahim, A.A.; Rocca, E.; Steinmetz, J.; Kassim, M.J.; Adnan, R.; Ibrahim, M.S. Mangrove tannins and their flavanoid monomers as alternative steel corrosion inhibitors in acidic medium. *Corros. Sci.* **2007**, *49*, 402–417. [CrossRef]
40. Nardeli, J.V.; Fugivara, C.S.; Taryba, M.; Pinto, E.R.P.; Montemor, M.F.; Benedetti, A.V. Tannin: A natural corrosion inhibitor for bare and coated aluminum alloys. *Prog. Org. Coat.* **2019**, *135*, 368–381. [CrossRef]
41. Matamala, G.; Smeltzer, W.; Droguett, G. Comparison of steel anticorrosive protection formulated with natural tannins extracted from acacia and from pine bark. *Corros. Sci.* **2000**, *42*, 1351–1362. [CrossRef]
42. Dalmoro, V.; Santos, C.; Santos, J.H.Z. Chap. 20: Smart coatings for corrosion protection. In *Industrial Applications for Intelligent Polymers and Coatings*; Springer: Berlin, Germany, 2016; pp. 417–435. [CrossRef]
43. Nardeli, J.V.; Fugivara, C.S.; Taryba, M.; Montemor, M.F.; Ribeiro, S.J.L.; Benedetti, A.V. Novel healing coatings based on natural-derived polyurethane modified with tannins for corrosion protection of AA2024-T3. *Corros. Sci.* **2019**, in press. [CrossRef]
44. Fundação MS (Mato Grosso do Sul Foundation for Research and Dissemination of Agricultural Technologies). Available online: http://www.fundacaoms.org.br/ (accessed on 1 May 2019).
45. Grasel, F.S.; Ferrão, M.F. A rapid and non-invasive method for the classification of natural tannin extracts by near-infrared spectroscopy and PLS-DA. *Anal. Methods* **2016**, *8*, 644–649. [CrossRef]
46. Peres, R.S.; Armelin, E.; Alemán, C.; Ferreira, C.A. Modified tannin extracted from black wattle tree as an environmentally friendly antifouling pigment. *Ind. Crop. Prod.* **2015**, *65*, 506–514. [CrossRef]
47. *ASTM E222 Standard Test Methods for Hydroxyl Groups Using Acetic Anhydride Acetylation*; American Society for Testing Materials: West Conshohocken, PA, USA, 2010.
48. Alrashed, M.M.; Jana, S.; Soucek, M.D. Corrosion performance of polyurethane hybrid coatings with encapsulated inhibitor. *Prog. Org. Coat.* **2019**, *130*, 235–243. [CrossRef]
49. *ASTM D2572 Standard Test Method for Isocyanate Groups in Urethane Materials or Prepolymers*; American Society for Testing Materials: West Conshohocken, PA, USA, 2010.
50. Alencar, M.A.S.; Benedetti, A.V.; Fugivara, C.S.; Messaddeq, Y. Construção de célula eletroquímica para observação de amostras *in situ* em estereomicroscópio. *Quim. Nova* **2010**, *33*, 1394–1397. [CrossRef]
51. Grasel, F.S.; Ferrão, M.F.; Wolf, C.R. Development of methodology for identification the nature of the polyphenolic extracts by FTIR associated with multivariate analysis. *Spectrochim. Acta A Mol. Biomol. Spectrosc.* **2016**, *153*, 94–101. [CrossRef]
52. Pinto, E.R.P. Modificação de óleo Vegetais e de Origem Animal para a Síntese de Poliésteres e Poliuretanos com Baixo teor de Compostos Orgânicos Voláteis. Ph.D. Thesis, Universidade Estadual Paulista Júlio Mesquita Filho (UNESP), Araraquara/SP, Brasil, 2012.
53. Pinto, E.R.P.; Polito, W.L.; Ribeiro, S.J.L.; Messaddeq, Y. Hydroxylated polyester resin synthesizing from crambe oil by mass polymerization. In Proceedings of the 102nd AOCS Annual Meeting & Expo. 2011, Cincinnati, OH, USA, 1–4 May 2001.
54. Yeganeh, H.; Shamekhi, M.A. Novel polyurethane insulating coatings based on polyhydroxyl compounds, derived from glycolysed PET and castor oil. *J. Appl. Polym. Sci.* **2006**, *99*, 1222–1233. [CrossRef]
55. Moeini, H.R. Synthesis and properties of novel polyurethane-urea insulating coatings from hydroxyl-terminated prepolymers and blocked isocyanate curing agent. *J. Appl. Polym. Sci.* **2009**, *112*, 3714–3720. [CrossRef]
56. Mannari, V.M.; Massingill, J.L. Two-component high-solid polyurethane coating systems based on soy polyols. *J. Coat. Technol. Res.* **2006**, *3*, 151–157. [CrossRef]

57. Tecnologia dos Poliuretanos. Available online: https://www.poliuretanos.com.br/Cap7/73Tintas.htm (accessed on 1 May 2019).
58. Haghdadeh, P.; Ghaffari, M.; Ramezanzadeh, B.; Bahlakeh, G.; Saeb, M.R. Polyurethane coatings reinforced with 3-(triethoxysilyl)propyl isocyanate functionalized graphene oxide nanosheets: Mechanical and anti-corrosion properties. *Prog. Org. Coat.* **2019**, *136*, 105243. [CrossRef]
59. Fan, W.; Zhang, Y.; Li, W.; Wang, W.; Zhao, X.; Song, L. Multi-level self-healing ability of shape memory polyurethane coating with microcapsules by induction heating. *Chem. Eng. J.* **2019**, *368*, 1033–1044. [CrossRef]
60. Han, Y.; Hu, J.; Xin, Z. Facile preparation of high solid content waterborne polyurethane and its application in leather surface finishing. *Prog. Org. Coat.* **2019**, *130*, 8–16. [CrossRef]
61. Koh, E.; Kim, N.K.; Shin, J.; Kim, Y.W. Polyurethane Microcapsules for Self-Healing Paint Coatings. *RSC Adv.* **2014**, *4*, 15830–15834. [CrossRef]
62. Brochu, A.B.; Chyan, W.J.; Reichert, W.M. Microencapsulation of 2-octylcyanoacrylate tissue adhesive for self-healing acrylic bone cement. *J. Biomed. Mater. Res. B* **2012**, *100*, 1764–1772. [CrossRef]
63. Miller, C.E.; Archibald, D.D.; Myrick, M.L.; Angel, S.M. Determination of physucal properties of reaction-injection-molded polyurethanes by NIR-FT-Raman spectroscopy. *Appl. Spectrosc.* **1990**, *44*, 1297–1300. [CrossRef]
64. Romanova, V.; Begishev, V.; Karmanov, V.; Kondyurin, A.; Maitz, M.F. Fourier transform Raman and Fourier transform infrared spectra of cross-linked polyurethaneurea films synthesized from solutions. *J. Raman Spectrosc.* **2002**, *33*, 769–777. [CrossRef]
65. Janik, H.; Palys, B.; Petrovic, Z.S. Multiphase-separated polyurethanes studied by micro-raman spectroscopy. *Macromol. Rapid Commun.* **2003**, *24*, 265–268. [CrossRef]
66. Parnell, S.; Min, K.; Cakmak, M. Kinetic studies of polyurethane polymerization with Raman spectroscopy. *Polymer* **2003**, *44*, 5137–5144. [CrossRef]
67. Weakley, A.T.; Warwick, P.C.T.; Bitterwolf, T.E.; Aston, D.E. Multivariate analysis of micro-raman spectra of thermoplastic polyurethane blends using principal component analysis and principal component regression. *Appl. Spectrosc.* **2012**, *66*, 1269–1278. [CrossRef] [PubMed]
68. Bruckmoser, K.; Resch, K. Investigation of ageing mechanisms in thermoplastic polyurethanes by means of IR and Raman spectroscopy. *Macromol. Symp.* **2014**, *339*, 70–83. [CrossRef]
69. Navarchian, A.H.; Najafipoor, N.; Ahangaran, F. Surface-modified poly(methyl methacrylate) microcapsules containing linseed oil for application in self-healing epoxy-based coatings. *Prog. Org. Coat.* **2019**, *132*, 288–297. [CrossRef]
70. Khan, A.; Ubaid, F.; Fayyad, E.M.; Ahmad, Z.; Shakoor, R.A.; Montemor, M.F.; Kahraman, R.; Mansour, S.; Hassan, M.K.; Hasan, A.; et al. Synthesis and properties of polyelectrolyte multilayered microcapsules reinforced smart coatings. *J. Mater. Sci.* **2019**, *54*, 12079–12094. [CrossRef]
71. Chaudhari, A.B.; Tatiya, P.D.; Hedaoo, R.K.; Kulkarni, R.D.; Gite, V.V. Polyurethane Prepared from Neem Oil Polyesteramides for Self-Healing Anticorrosive Coatings. *Ind. Eng. Chem. Res.* **2013**, *52*, 10189–10197. [CrossRef]
72. Hailong, F.; Wang, J.; Jin, Z. Tough, Swelling-Resistant, Self-Healing, and Adhesive Dual-Cross-Linked Hydrogels Based on Polymer–Tannic Acid Multiple Hydrogen Bonds. *Macromolecules* **2018**, *51*, 1696–1705. [CrossRef]
73. Burattini, S.; Colquhoun, H.M.; Fox, J.D.; Friedmann, D.; Greenland, B.W.; Harris, P.J.F.; Hayes, W.; Mackay, M.E.; Rowan, S.J. A self-repairing, supramolecular polymer system: Healability as a consequence of donor–acceptor π–π stacking interactions. *Chem. Commun.* **2009**, *44*, 6717–6719. [CrossRef]
74. Mauldin, T.C.; Kessler, M.R. Self-healing polymers and composites. *Int. Mater. Rev.* **2010**, *55*, 317–346. [CrossRef]

© 2019 by the authors. Licensee MDPI, Basel, Switzerland. This article is an open access article distributed under the terms and conditions of the Creative Commons Attribution (CC BY) license (http://creativecommons.org/licenses/by/4.0/).

Material suplementar no Apêndice II

CAPÍTULO II:

Aplicação dos revestimentos para proteção contra corrosão da liga AA2024-T3

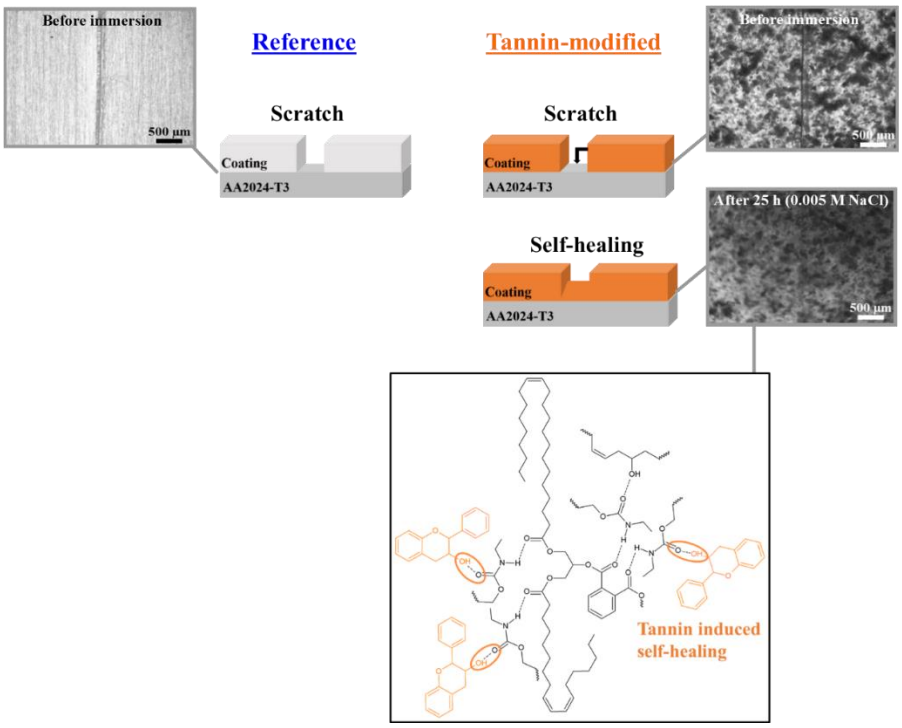

Este capítulo fornece um estudo detalhado da aplicação dos revestimentos na proteção contra corrosão da liga AA2024-T3. Aborda diferentes técnicas eletroquímicas convencionais e localizadas, as quais permitem o estudo detalhado do sistema em questão. O efeito self-healing é confirmado por meio de análises de microscopia óptica, eletrônica de varredura e representado por meio de um vídeo. Esta seção é publicada como artigo: J.V. Nardeli, C.S. Fugivara, M. Taryba, M.F. Montemor, S.J.L. Ribeiro, A.V. Benedetti. "Novel healing coatings based on natural-derived polyurethane modified with tannins for corrosion protection of AA2024-T3" na revista Corrosion Science v. 162, p.108213, 2020.

Reproduced with permission from [J.V. Nardeli, C.S. Fugivara, M. Taryba, M.F. Montemor, S.J.L. Ribeiro, A.V. Benedetti. Novel healing coatings based on natural-derived polyurethane modified with tannins for corrosion protection of AA2024-T3. CORROSION SCIENCE. v.162, p.108213, 2020] Copyright 2019 Elsevier Ltd. Corrosion Science.

Corrosion Science 162 (2020) 108213

Contents lists available at ScienceDirect

Corrosion Science

journal homepage: www.elsevier.com/locate/corsci

Novel healing coatings based on natural-derived polyurethane modified with tannins for corrosion protection of AA2024-T3

Jéssica V. Nardeli[a,b,*], Cecilio S. Fugivara[a], Maryna Taryba[b], M.F. Montemor[b], Sidney J.L. Ribeiro[a], Assis V. Benedetti[a,*]

[a] Universidade Estadual Paulista-UNESP, Instituto de Química, 14800-060, Araraquara, SP, Brazil
[b] Centro de Química Estrutural-CQE, DEQ, Instituto Superior Técnico, Universidade de Lisboa, Av. Rovisco Pais, 1049-001, Lisboa, Portugal

ARTICLE INFO

Keywords:
Functional coatings
Self-healing
Corrosion protection
AA2024-T3

ABSTRACT

Polyurethane coatings derived from crambe and castor oil formulated with different proportions of additives were modified with tannin and applied on AA2024-T3 coupons. The coatings were characterized by water uptake and attenuated total reflectance Fourier transform infrared spectroscopy (FTIR-ATR). The thickness of the coatings was determined by scanning electron microscopy (SEM) and adhesion was evaluated by the ASTM D3359 standard. The barrier properties and corrosion protection ability were assessed by open circuit potential (E_{OCP}) and electrochemical impedance spectroscopy (EIS). The self-healing ability of the coatings was studied by localized impedance spectroscopy (LEIS) and by the scanning vibrating electrode technique coupled with the scanning ion-selective electrode technique (SVET/SIET). The measurements demonstrate that tannin-modified coatings provide effective corrosion protection due to polymer healing and the results give important highlights concerning the mechanism of corrosion inhibition.

1. Introduction

The aluminum alloy AA2024 is a prime material for application in aircraft parts because of its favorable strength to weight ratio. However, this alloy is particularly susceptible to corrosion due to the presence of the Cu and Mg rich S-phase, which is the most corrosion sensitive phase [1] in this alloy. Different approaches have been pursued to minimize corrosion problems in the AA2024 alloy [2–5] and the most effective ones are based on the use of organic coatings, namely primers modified with different anti-corrosion pigments [6–10]. The corrosion protection mechanism typically combines the good barrier properties of organic matrices, which prevent water and corrosive species uptake, with the presence of anti-corrosion additives that inhibit corrosion.

However, coated parts are susceptible to damage during service and over the time, corrosion propagation and coating delamination may cause serious damages of the bare material. To prevent and to minimize corrosion activity, coatings are typically modified with anti-corrosion pigments. For years, chromate-based pigments have been used to impart corrosion healing effects to organic coatings applied on different metallic parts and, in particular, on the AA2024. However, the detrimental impact of chromate compounds on the environment and human health has boosted the search of alternatives. Although chromates have been already replaced in many applications, they are still allowed in aeronautical applications [11]. Therefore, the tendency nowadays is to search for novel environmentally friendly alternatives, based on non-toxic and biodegradable inhibitors [12] and to introduce self-healing ability in the protective coatings [13]. Several studies have explored the action of corrosion inhibitors obtained from plant extracts as additives in aggressive solutions [14–18]. Such extracts contain a variety of natural organic products such as essential oils, tannins, flavones and flavonoids, among other active substances, rich in –OH groups, that have been reported as effective corrosion inhibitors [19–21]. The quest for more ecological corrosion inhibitors has been raising interest on tannins, which effectively protect aluminum alloys from corrosion [22–24]. Tannins can be introduced during formulation of organic matrices and are expected to reinforce barrier properties, while introducing healing ability in the coating when damaged.

Effective corrosion protection, and consequent self-repair effects, depend on the response of the modified coating. To better understand this combination, it is of outmost importance to combine different electrochemical tools to extract relevant information concerning the evolution of the coating barrier properties. Therefore, the main goal of this work is to investigate the effect of addition of tannin in the coating structure and to evaluate its anti-corrosion performance. For this

* Corresponding authors at: Universidade Estadual Paulista-UNESP, Instituto de Química, 14800-060, Araraquara, SP, Brazil.
E-mail addresses: jessica.nardeli@unesp.br (J.V. Nardeli), assis.v.benedetti@unesp.br (A.V. Benedetti).

https://doi.org/10.1016/j.corsci.2019.108213
Received 29 May 2019; Received in revised form 3 September 2019; Accepted 7 September 2019
Available online 10 September 2019
0010-938X/ © 2019 Elsevier Ltd. All rights reserved.

Reproduced with permission from [J.V. Nardeli, C.S. Fugivara, M. Taryba, M.F. Montemor, S.J.L. Ribeiro, A.V. Benedetti. Novel healing coatings based on natural-derived polyurethane modified with tannins for corrosion protection of AA2024-T3. CORROSION SCIENCE. v.162, p.108213, 2020] Copyright 2019 Elsevier Ltd. Corrosion Science.

purpose, electrochemical impedance spectroscopy (EIS), localized electrochemical impedance spectroscopy (LEIS), and scanning vibrating electrode technique (SVET) coupled with the scanning ion-selective electrode technique (SIET) were used. The corrosion protection ability of the new coating was compared with a reference coating, without tannin addition. Complementary studies were performed by scanning electron microscopy (SEM) and energy dispersive X-ray (EDX) analysis. The combination of all these techniques provided valuable insights into the corrosion protection mechanism of tannin modified coatings.

2. Experimental

2.1. Samples

2.1.1. AA2024-T3 substrate

The weight composition of the AA2024-T3 plates (supplied by Embraer) was: 4.40% Cu, 0.52% Mn, 1.38% Mg, 0.16% Fe, 0.06% Zn, (Si, Cr and Ti < 0.06%), and balance Al. This composition was determined by EDX analysis (FEG-SEM JSM7001 F, JEOL using a light elements detector, by Oxford (England) model INCA 250) at an accelerating voltage of 25 kV and represents the average of triplicate measurements.

The pre-treatment of the AA2024-T3 plates (100 mm × 100 mm × 2 mm) prior coating application included a polishing step with silicon carbide sandpaper (#280, #320, #400, #1200, #1500, #2000) followed by washing in distilled water and acetone and then drying in oven for 24 h at 120 °C. After surface preparation coatings were applied by means of a TKB Erichsen Instruments No. AJ03/06 extensometer and subjected to cure at room temperature for 48 h.

2.1.2. Organic coating formulation

The coating formulation involved two steps: preparation of polyester and preparation of pre-polymer. Two sets of coatings were prepared: the reference (without tannin) and the tannin-modified ones. In step 1 (Eq. (1)), the polyester was prepared via the transesterification reaction of crambe oil (CO, 1 mol, 997.6 g), trimethylolpropane (TMP, 3 mol, 402.3 g), phthalic anhydride (PhA, 3 mol, 444.3 g), butylated hydroxyl toluene (BHT, 2.26×10^{-3} mol, 0.50 g) and lithium hydroxide (LiOH, 0.01 mol, 0.25 g) under stirring and heating at 240 °C for 5 h in N_2 atmosphere. Glycerin (a by-product) was removed during the reaction with Dean-Stark. The reaction progress was monitored by the methanol solubility test (3 mL methanol/1 mL polyester) and acidity index (mg KOH/g of polyester). When the polyester was totally solubilized in methanol and the acidity index was lower than 30, the reaction was completed, and the synthesis stopped.

$$\mathrm{CO + TMP + PhA + BHT + LiOH \rightarrow polyester + glycerin + H_2O} \quad (1)$$

In step 2 (Eq. (2)), the prepolymer was prepared with castor oil (CAO, 0.42 mol, 125.3 g), trimethylolpropane (TMP, 0.35 mol, 46.93 g), butylated hydroxy toluene (BHT, 0.01 mol, 2.20 g), propylene glycol (PG, 0.16 mol, 12.17 g), n-Butyl acetate (BA, 3.83 mol, 444.89 g), ethyl glycol acetate (EGA, 1.45 mol, 191.61 g), hexamethylene diisocyanate (HDI, 3.11 mol, 523.08 g) under stirring and heating at 60 °C for 6 h in N_2 atmosphere. CO and CAO are polyols, TMP is the crosslinking agent, PhA takes part in the polyesterification and easily reacts with OH groups from TMP and mono or diglycerides, HDI contains bifunctional NCO terminal groups, PG, BA, EGA are chain extenders, BHT is the antioxidant used because of the unsaturation bonds of castor oil.

$$\mathrm{CAO + TMP + BHT + PG + BA + EGA + HDI \rightarrow prepolymer} \quad (2)$$

The products obtained in steps 1 and 2 reacted in presence of a catalyst, stannous octoate (SO, 1%), under stirring for 10 min to produce the reference coating (Eq. (3)). For the tannin-modified coating, steps 1 and 2 were exactly the same as for the reference coating, except that tannin was added (8.83×10^{-3} mol, 2.10 g) in the last step of the coating formulation (Eq. (4)).

$$\mathrm{polyester + prepolymer + SO \rightarrow reference\ coating} \quad (3)$$

$$\mathrm{polyester + prepolymer + tannin + SO \rightarrow tannin - modified\ coating} \quad (4)$$

The coatings were applied onto the cleaned AA2024-T3 coupons (100 mm × 100 mm) using an adjustable applicator (TKB Erichsen instruments®) and cured at 25 °C for 48 h.

2.2. Coating and surface characterization

2.2.1. Water uptake

Water uptake was determined by immersing free films (reference coating and tannin-modified) in deionized water at room temperature and following calculation of deionized water absorption percentage using a quartz crystal microbalance (Sartorius® MC5 Micro Balance). Before and after 0.25 h, 0.5 h, 0.75 h, 1 h and 2 h of exposure to deionized water, the amount of gained weight (m_t) was measured and the water uptake (%W) determined according to Eq. (5) [25]:

$$\%W = \frac{m_t - m_0}{m_0} \times 100 \quad (5)$$

where m_o (mg) is the initial weight of the coating and m_t (mg) is the weight after immersion in deionized water for certain time.

2.2.2. Attenuated total reflectance Fourier transform infrared spectroscopy (FTIR-ATR)

Both coatings were studied by means of FTIR-ATR using a Vertex70 Bruker spectrophotometer with an Attenuated Total Reflectance accessory (scans = 64, energy scanning from 590 to 4000 cm^{-1}, resolution $= 2\,cm^{-1}$).

2.2.3. Thickness of coatings

The thickness of the coatings was determined from cross-section images obtained with scanning electron microscopy (SEM) using FEG-SEM JEOL model JSM 7001 F microscope using 25 kV.

2.2.4. Adhesion tests

Adhesion tests based on ASTM D3359-09 [26] were performed employing Elcometer 107 Cross Hatch Cutter. 6 teeth, 1 mm spacing tool was used. A pattern of 6 cross sections (˜ 20 mm) at right angles to the coated material was applied until reaching the substrate. Then, Elcometer T1079358 adhesive tape was applied over the cut pattern and it was removed. With the aid of a magnifying glass the detachment of the coating was evaluated. The surface of the coating was visually compared to the standard scale shown in ASTM D3359-09 and adhesion is graded according to the percentage of area removed.

2.2.5. Optical microscopy images

Optical microscopy images of the coatings were obtained using a digital LEICA model DMS300 microscope.

2.2.6. Scanning electron microscopy (SEM)

The coating surface was analyzed before and after testing by SEM and EDX analysis using a FEG-SEM JEOL model JSM 7001 F microscope at an accelerating voltage of 15 kV or 20 kV. The EDX detector from the FEG-SEM JEOL is a light elements detector, by Oxford (England) model INCA 250.

2.3. Electrochemical studies

The conductivity of the NaCl solution was measured using an EUTECH INSTRUMENTS PC700 conductometer.

For the open circuit potential and electrochemical impedance spectroscopy measurements the working electrode geometrical area was 1 cm^2, while for LEIS and SVET/SIET studies areas of 10 mm^2 and

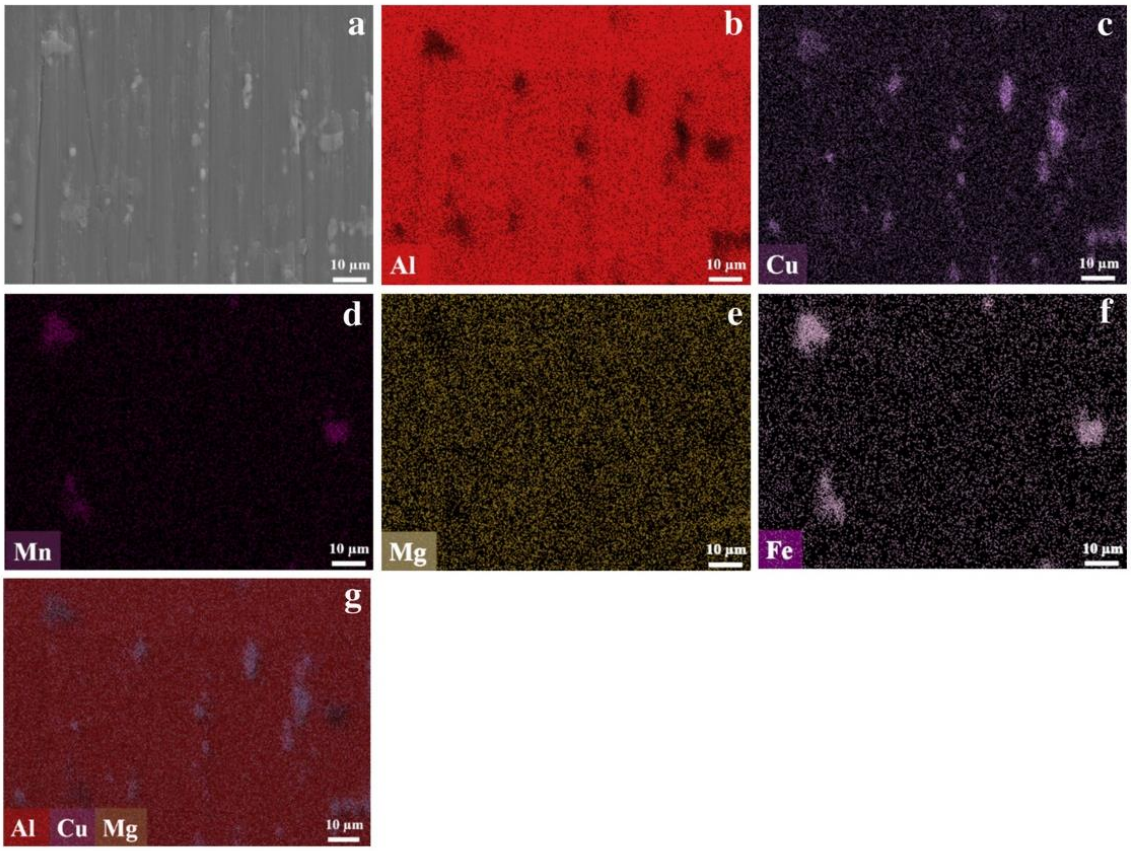

Fig. 1. (a) SEM images of the AA2024-T3 surface; (b, c, d, e, f) EDX elemental maps of Al, Cu, Mn, Mg and Fe and (g) S-phase.

1 mm^2 were used, respectively.

2.3.1. Open circuit potential (E_{OCP}) and electrochemical impedance spectroscopy (EIS)

E_{OCP} and conventional EIS experiments on coated and uncoated AA2024-T3 were carried out in a conventional three-electrode electrochemical cell (model K0235, PAR). The bare and the coated AA2024-T3 (geometrical area of 1 cm^2) were used as working electrode, Ag|AgCl|KCl 3 mol L^{-1} was used as reference electrode, and a Pt spiral as counter electrode. E_{OCP} measurements were taken for 24 h before the first EIS measurement and between each EIS measurement until the end of the test. EIS measurements were performed using a GAMRY REF600 potentiostat/galvanostat by applying 10 mV(r.m.s.) sinusoidal potential perturbation signal to E_{OCP}, from 100 kHz to 10 mHz, recording 10 points/frequency decade. The impedance spectra were recorded as function of the immersion time until observing a sharp decrease of the E_{OCP} values, i.e., until the barrier properties of the coatings were deteriorated. The electrolyte was an unstirred and non-deaerated 0.6 mol L^{-1} NaCl aqueous solution, and the measurements were conducted at 25 °C.

All EIS experimental data were validated by applying the Kramers-Kronig conditions and fitted using an equivalent electrical circuit (EEC) and the Z-View® software.

2.3.2. Localized electrochemical impedance spectroscopy (LEIS)

LEIS was used to measure the admittance over an artificial defect (scratch) when the coated sample was immersed in 0.005 mol L^{-1} NaCl. The working electrode area was 10 mm^2 and a defect with approximately 5 mm long × 0.3 mm wide was created with a scalpel, reaching the bare metal. LEIS measurements were carried out using a Solartron 1286 electrochemical interface and a Solartron 1250 frequency response analyzer coupled with a Uniscan electrochemical station. A five electrode configuration electrochemical cell was used: saturated calomel electrode (SCE) as reference electrode, coated substrate as working electrode, platinum mesh as counter electrode, and a Pt bi-electrode serving as LEIS probe to measure the local potential gradient in solution, above the surface. The customized configuration of the LEIS probe used in this experiment has been described in detail elsewhere [10,27]. Admittance values were obtained in each scan point over the whole exposed area including the defect. The scanned area was 5060 µm × 2000 µm for the reference coating and 5000 µm × 2000 µm for the tannin-modified coating. A frequency of 5 kHz was used during LEIS mapping. Therefore, the LEIS maps (area scan: 32 points x 16 lines) were taken in 0.005 mol L^{-1} NaCl aqueous solution (constant conductivity ρ = 0.000548 S cm^{-1}) every hour, during 25 h of immersion.

2.3.3. Scanning vibrating electrode technique (SVET) and scanning ion-selective electrode technique (SIET)

Quasi-simultaneous SVET/SIET measurements of the coated samples were performed using an apparatus from Applicable Electronics Inc., controlled by the ASET software (Science Wares). The measurements were performed in a 22 × 38 grid, generating 836 points for the reference coating and 22 × 41 grid, generating 902 points for tannin-modified coating. An insulated Pt–Ir probe (MicroProbe), with platinum black deposited on a spherical tip of 15 µm diameter was used as vibrating electrode. The microprobe was placed 100 ± 2 µm above the surface, vibrating in vertical (Z) and horizontal (X) planes; the corresponding probe vibration frequencies were of 124 Hz and 325 Hz, respectively. Measurements were taken during the immersion of the coated samples in 0.05 mol L^{-1} NaCl aqueous solution (constant conductivity ρ = 0.00540 S cm^{-1}) at 25 °C.

SIET was used for the micro-potentiometric measurements. Local pH measurements were carried out using a glass capillary microelectrode with a tip orifice diameter of 1.8 ± 0.2 µm; the local pH was mapped 50 ± 2 µm above the surface. A pH selective ionophore-based

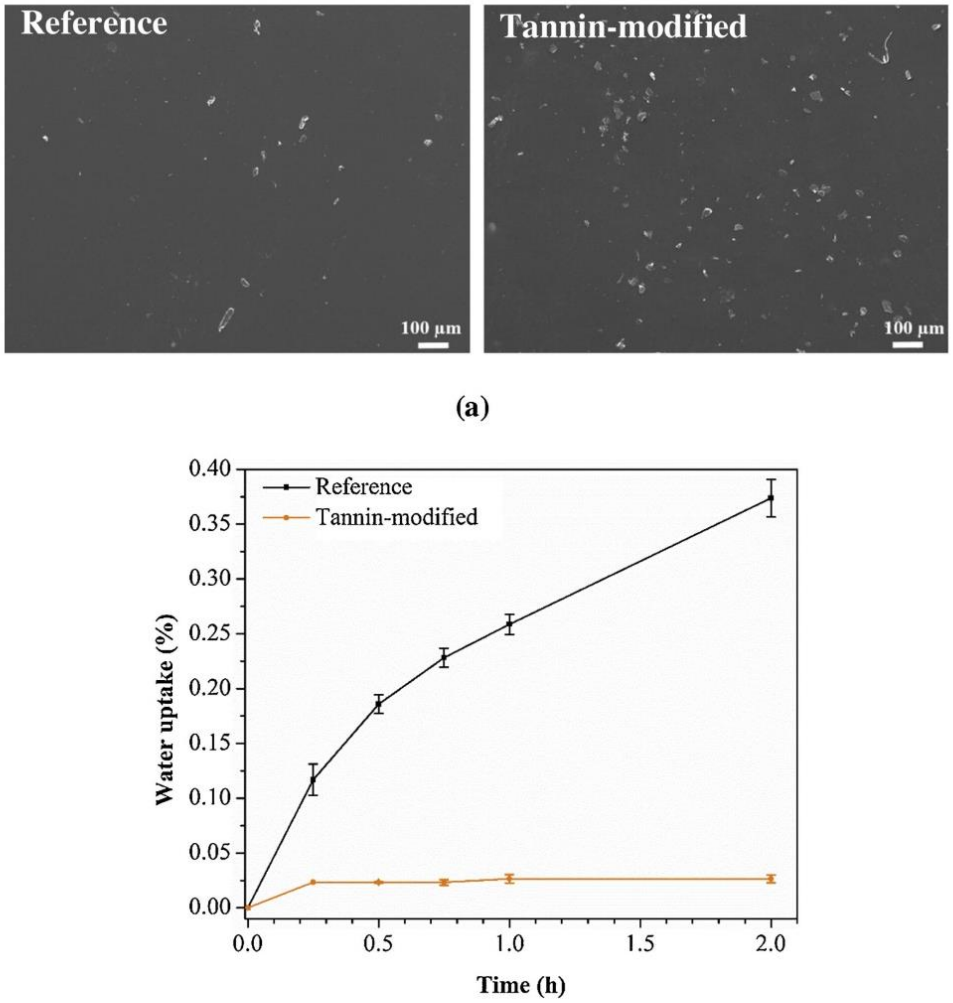

Fig. 2. (a) SEM image from the surface of reference and tannin-modified coatings and (b) water uptake evolution for the reference and tannin-modified coatings.

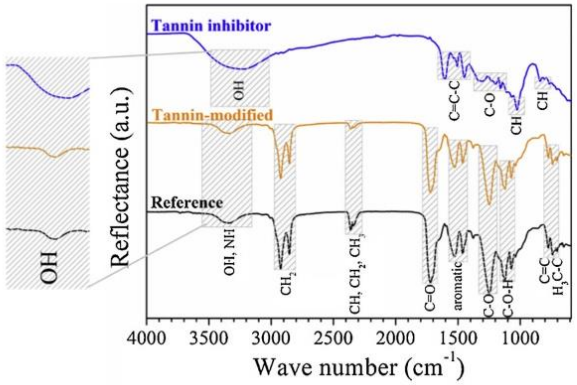

Fig. 3. FTIR-ATR spectra for the tannin, reference coating and tannin-modified coating.

membrane with extended pH working range, specially developed for corrosion applications was used [28]. The external reference electrode was a homemade Ag|AgCl|0.05 mol L^{-1} NaCl mini electrode and commercial buffer solutions were used for calibration. The Nernstian slope was -55.1 ± 0.5 mV/pH. The reference potential was recorded in the bulk electrolyte before and after each measurement in order to account for possible potential drift. The scanned areas of the coated samples were 0.96 mm x 1.38 mm (reference coating) and 0.99 mm x 1.85 mm (tannin-modified coating). In each coating a line scratch defect, 1.1–1.2 mm long, was created using a surgery blade (scalpel).

3. Results and discussion

3.1. Surface characterization

3.1.1. AA2024-T3 substrate

Fig. 1 shows a SEM micrograph of the alloy AA2024-T3 and the respective EDX elemental mapping that evidence the main metals in the alloy, particularly in the intermetallics: Al (Fig. 1b), Cu (Fig. 1c), Mn (Fig. 1d), Mg (Fig. 1e) and Fe (Fig. 1f). The S-phase (Al_2CuMg), the most abundant intermetallic phase in the AA2024-T3 represents ca. 60% of the precipitates and covers around 2.5–3% of the surface area [29]. This abundance was clearly evidenced in Fig. 1**c** and Fig. 1**g** where Cu-rich precipitates, with dimensions typically below 10 µm can be observed. These precipitates play a key role in the corrosion process, because they act as preferential corrosion nucleation sites. Moreover, when the Cu-rich S-phase dissolves, there is trenching of the Al matrix around the Al_2CuMg particles mainly as result of its self-dissolution

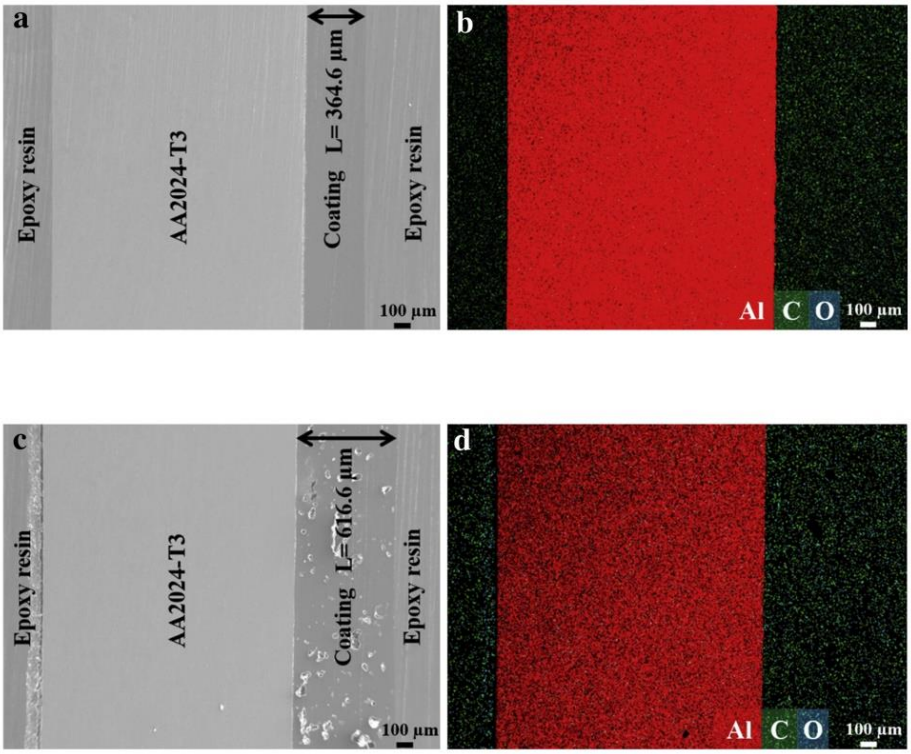

Fig. 4. SEM of a cross-section and EDX elemental maps of Al, C and O of (a, b) reference and (c, d) tannin-modified coatings.

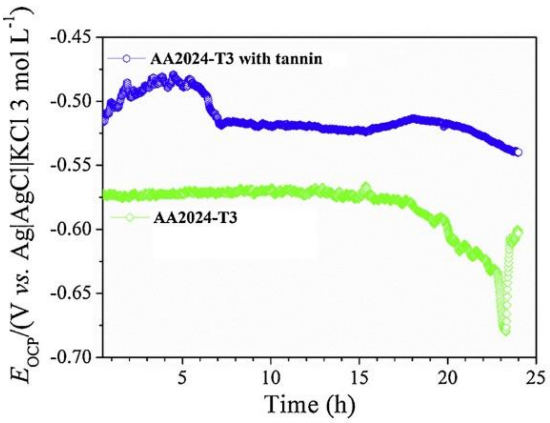

Fig. 5. E_{OCP} *vs.* time for the AA2024-T3 alloy immersed during 24 h in 0.6 mol L^{-1} NaCl without and with addition of tannin.

[30]. The presence of Mn and Fe precipitates was also observed - Fig. 1d and f. These intermetallics are also susceptible to localized corrosion activity. Overall, the different precipitates observed in Fig. 1 constitute preferential sites for corrosion onset. Corrosion of AA2024-T3 in NaCl solutions is a complex process, involving chemical and electrochemical processes that include dissolution of the S-phase and oxidation of Al to Al^{3+}, Mg to Mg^{2+}, oxidation and re-deposition of Cu, and reduction of dissolved O_2 and H_2O to OH^-. A detailed study on the corrosion mechanism of the S-phase and its role regarding pitting initiation can be found elsewhere [29,30].

3.1.2. Reference and tannin-modified coatings

The water uptake of the free standing coatings is depicted in Fig. 2b. Polyurethane yields urethane groups, which form an H-bonding hard phase that retards water absorption [31]. In this case, the reference coating displays $\%W = 0.37$, while the tannin-modified coating displays $\%W = 0.02$. This result suggest that the presence of the tannin increases significantly the number of hydrogen bonds and, consequently, it delays water absorption for more than one order of magnitude. One of the main advantages of organic solvent-based polyurethane coatings is the high-water resistance compared to waterborne polyurethane coatings [25].

3.1.2.1. Attenuated total reflectance Fourier transform infrared spectroscopy (FTIR-ATR). Fig. 3 illustrates the FTIR-ATR spectrum for tannin and for the reference and tannin-modified coatings and depicts the values of the different bands in FTIR-ATR spectra (normalized intensity of bands).

The spectrum for tannin shows a band at 3282 cm^{-1} which is attributed to the presence of hydroxyl groups. Other stretching that can be identified are C=C–C at 1608 cm^{-1}, 1506 cm^{-1}, 1450 cm^{-1}, characteristic of aromatic compounds; C–O at 1315 cm^{-1}, 1239 cm^{-1}, 1202 cm^{-1} and C–H in-plan and C–H out-of-plan, respectively occurring at 1020 cm^{-1} and 845 cm^{-1} [32–35].

The band of hydroxyl groups predominates in polyesters and can be detected at 3356 cm^{-1}, accounting for hydrogen bonds formation [36,37]. However, the band at 3356 cm^{-1} can be influenced by the urethane bond, because it has the N–H stretching from the urethane (–NH–CO–O) bond [38]. So, this band could be also related to hydrogen bond of some free hydroxyl with secondary amine from urethane. The water uptake also influences this band as can be seen for longer immersion times.

The absence of the band at ca. 2270 cm^{-1} shows that NCO-free groups of the prepolymer can be consumed during the preparation of the coating and cure reactions [38,39]. The main NCO-free consumption reactions are allophanate and biuret bonds formation, and the reaction with water from humidity during the cure process. The IR bands at 1542 and 1718 cm^{-1} are characteristic of the aromatic ring present in PhA and N–H vibration from the urethane (–NH–CO–O) bond [38].

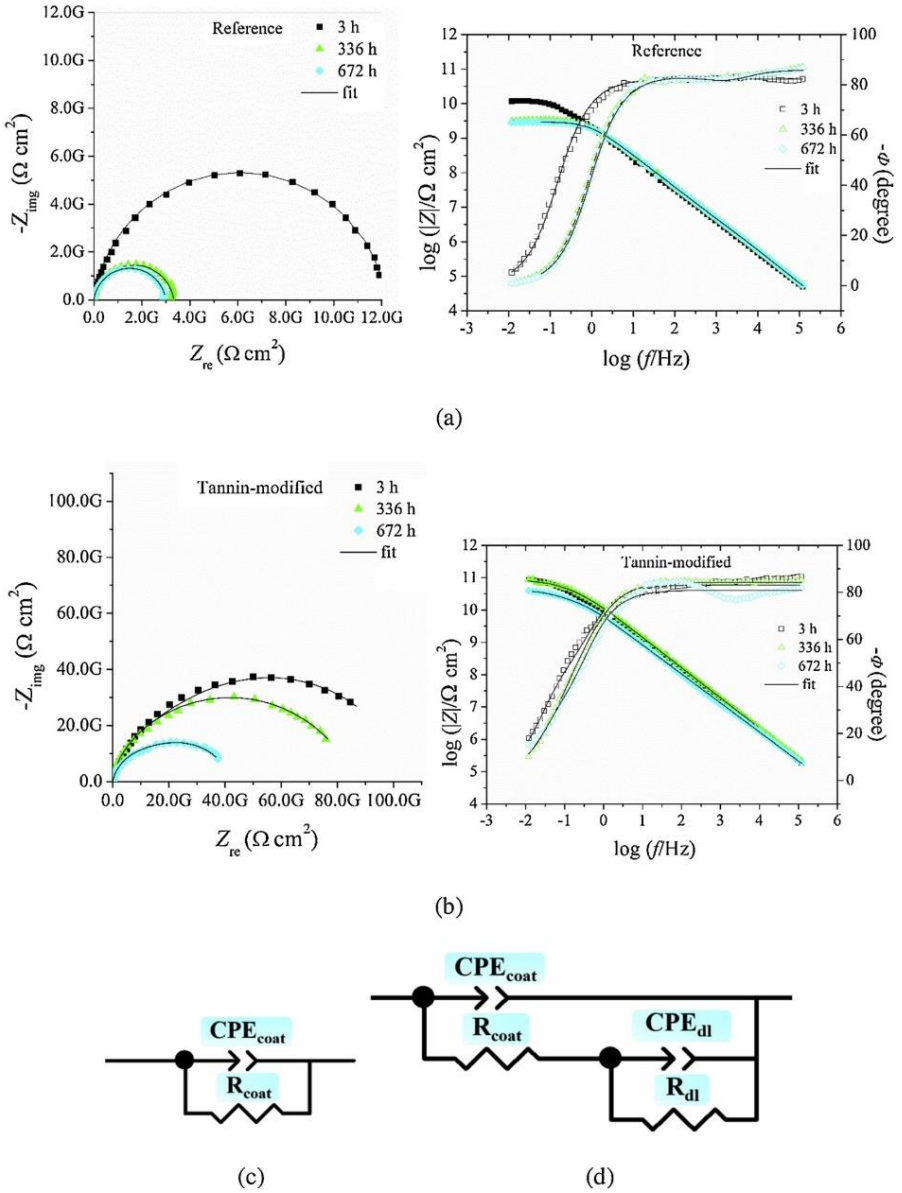

Fig. 6. Nyquist and Bode plots for the samples coated with (a) reference coating and (b) tannin-modified coating after 3 h, 336 h and 672 h of immersion in 0.6 mol L^{-1} NaCl, (c, d) Equivalent electrical circuits used to fit the EIS data where (c) used only for reference coating after 3 h of immersion.

Other bands between 1400-1000 cm^{-1} can be attributed to the stretching of C—O (ester), and C—O—C, and angular deflection of H—O—C and C—H bonds also present in all oils and polyesters [36].

The spectra of reference coating and tannin-modified coatings provide several spectral details, evidencing some similarities. The ratio of the areas under the peak assigned to the -OH group for tannin-modified coating / reference coating is near 50 (inset Fig. 3), indicating that the hydroxyls group increase significantly with the addition of tannin. Moreover, this ratio is 1.2 for C—O group; 1.7 for C—O—H group and 3.2 for C=C bond. The most important contribution of tannin to the coating is an important increase of the number of -OH containing groups, which, undoubtedly will affect the barrier properties and polymeric matrix behavior when damaged.

3.1.2.2. Coating thickness. SEM images of the cross-sections and the EDX elemental mapping (Al, C, O) on similar areas in the reference and tannin-modified coatings are presented in Fig. 4. The average thickness of the reference coating is 364 ± 1 μm and that of the tannin-modified coating is 616 ± 1 μm. The coatings evidence homogeneity and good adhesion to the substrate (AA2024-T3) and do not show presence of defects or features such as cracks or voids.

3.1.2.3. Adhesion tests. To confirm the adhesion properties of the reference coating and tannin-modified coating to the AA2024-T3 substrate, coated samples were submitted to the tape pull-off test (ASTM D3359-09). These results (5B - maximum adhesion) evidence the excellent adhesion of the reference and tannin-modified coatings onto the AA2024-T3 substrate; this result is in agreement with the observations from Fig. 4.

Table 1
EEC parameters used to fit the EIS diagrams obtained in 0.6 mol L^{-1} NaCl for reference coating and tannin-modified coating applied on AA2024-T3 alloy.

Time	Reference							Reference	
	Elements							Elements	
	Value without normalization							Value with normalization	
	CPE-T_{coat} /10^{-11} (S cm^{-2} s^n)	n_1	R_{po} /10^9 (Ω cm^2)	*CPE-T_{dl}* /10^{-11} (S cm^{-2} s^n)	n_2	R_{ct} /10^9 (Ω cm^2)	χ^2/10^{-3}	R_{po}/10^9 (Ω cm)	R_{ct}/10^{10} (Ω cm)
3 h	8.76	0.91	12.3				2.19	337.0	
336 h	5.11	0.94	0.042	1.70	0.83	3.27	1.53	1.15	8.96
672 h	5.08	0.94	0.030	1.60	0.84	2.93	1.40	0.82	8.03
Time	Tannin-modified							Tannin-modified	
	Elements							Elements	
	Value without normalization							Value with normalization	
	CPE-T_{coat} /10^{-11} (S cm^{-2} s^n)	n_1	R_{po} /10^{10} (Ω cm^2)	*CPE-T_{dl}* /10^{-11} (S cm^{-2} s^n)	n_2	R_{ct} /10^{10} (Ω cm^2)	χ^2/10^{-3}	R_{po}/10^{11} (Ω cm)	R_{ct}/10^{11} (Ω cm)
3 h	1.87	0.92	4.30	4.07	0.79	6.13	12.1	6.97	9.94
336 h	1.44	0.93	3.69	2.69	0.65	4.96	1.50	5.98	8.04
672 h	2.87	0.89	2.43	12.9	0.82	1.74	10.4	3.94	2.82

*to discard possible influences of the coating thickness on the resistance values, both R_{po} and R_{ct} values were divided by the corresponding coating thickness (resistance normalized by the coating thickness).

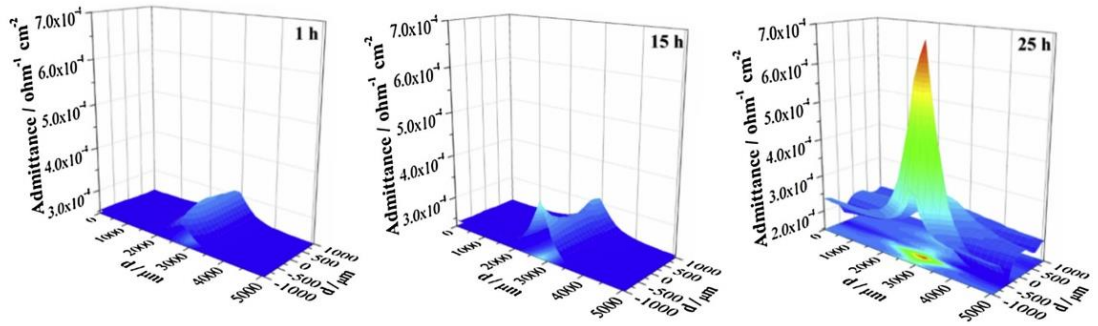

Fig. 7. LEIS maps of the AA2024-T3 alloy coated with the reference coating during immersion in aerated 0.005 mol L^{-1} NaCl solution at different immersion times.

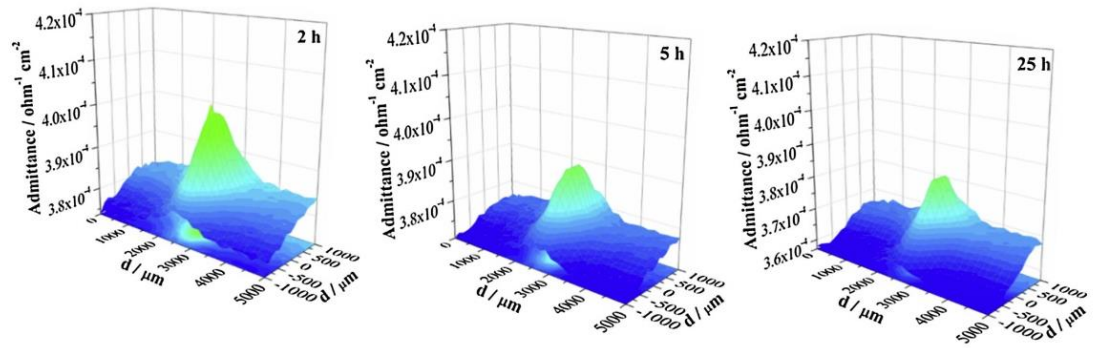

Fig. 8. LEIS maps of the AA2024-T3 alloy coated with the tannin-modified coating during immersion in aerated 0.005 mol L^{-1} NaCl solution at different immersion times.

3.2. Electrochemical study

3.2.1. Open circuit potential (E_{OCP}) and electrochemical impedance spectroscopy (EIS)

Fig. 5 depicts the evolution of E_{OCP} *vs.* time in 0.6 mol L^{-1} NaCl for the bare AA2024-T3 alloy exposed to NaCl without and with addition of tannin (8.83×10^{-3} mol). For the bare AA2024-T3 alloy, the E_{OCP} values are close to −0.60 V, while in the tannin-containing NaCl the values are more anodic: ~ −0.53 V. This ennoblement of the E_{OCP} suggests that, in these experimental conditions, tannin works predominantly as anodic inhibitor.

Fig. 6a and b show a set of representative Nyquist and Bode plots for the reference and tannin-modified coatings obtained after 3 h, 336 h and 672 h of immersion in 0.6 mol L^{-1} NaCl. The EIS measurements reflect the changes occurring in the coating barrier properties and at the metal/coating interface.

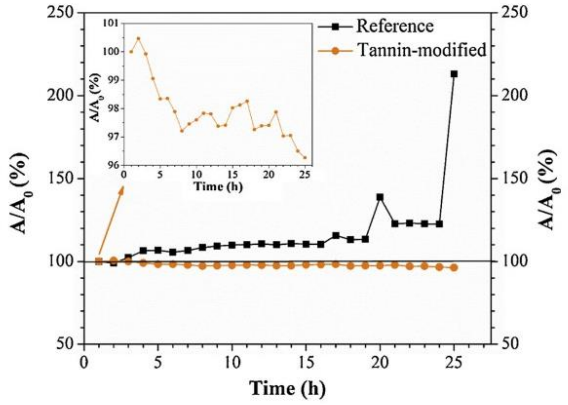

Fig. 9. Ratio between the maximum admittances values determined at a certain time and the maximum initial admittance values for each sample (reference coating and tannin-modified coating) during immersion in 0.005 mol L^{-1} NaCl solution. Inset: tannin-modified coating (magnified scale).

In the high frequency region of Fig. 6a, the Bode plots show a broad time constant with phase angle values close to -85°, as expected when coatings provide good barrier properties. At low frequencies a resistive plateau can be observed. The impedance magnitude ($|Z|$) for reference coating decreases from values around 1.0×10^{10} Ω cm^2 to values near 2.6×10^9 Ω cm^2 after 672 h of immersion (Fig. 6b). However, for the tannin-modified coating the initial $|Z|$ values are one order of magnitude higher and over the time they decrease from approximately 1.0×10^{11} Ω cm^2 to 4.1×10^{10} Ω cm^2, being always above of those of the reference coating.

The equivalent circuits used to quantify the impedance data are depicted in Fig. 6c. In this combination, R_{coat} and R_{dl} can be assigned respectively to the coating pore resistance and the charge transfer resistance; R_s, the electrolyte resistance, was not included because it could be not assessed within the studied frequency range; CPE_{coat} and CPE_{dl} are the constant phase elements associated with the coating and double layer, respectively. Constant phase elements were used here instead of pure capacitances because of the deviations from an ideal capacitor behavior. The parameters estimated after fitting the experimental results are presented in Table 1.

All the values confirm the superior barrier properties of the tannin-modified coatings.

3.2.2. Localized electrochemical impedance spectroscopy (LEIS)

Figs. 7 and 8 show the evolution of the admittance values over an area containing the artificial defect formed on the reference and tannin-modified coatings, respectively. The reference coating - Fig. 7 shows increasing corrosion activity over time, as expected when the bare Al alloy is exposed to NaCl. For the tannin modified coating there is some activity over the defect, but it remains weaker and tends to vanish over the time - Fig. 8.

To better compare both samples Fig. 9 depicts the evolution of the maximum admittance over the defect determined at each instant over the initial maximum admittance value. Thus, values below 100% indicate healing of corrosion while values above account for increased surface activity. Both samples showed similar corrosion activity at early stages and the one coated with the tannin-containing coating showed weaker and more stable activity over time, indicating that the substrate remains protected, probably due to coating recovery as confirmed by optical microscopy (Fig. S1, Supplementary material) and SEM imaging (Fig. 10b). For the reference coating there is a gradual increase of the admittance over time that becomes more marked after 20 h of immersion, evidencing stronger corrosion activity as confirmed by optical microscopy and SEM imaging (Fig. 10a).

Before immersion and also at the end of the immersion tests (25 h in 0.005 mol L^{-1} NaCl) both defects were observed via optical microscopy, SEM imaging and EDX analysis. Fig. 10 shows that for the reference coating, the corrosion process propagated from the defect underneath the surrounding coating. In contrast, for the tannin-modified coating this effect could not be detected probably due to improved corrosion protection and recovery of the coating barrier properties as suggested by SEM and EDX analysis (Fig. 10b).

For the reference coating (Fig. 10a), the EDX analysis in the spot 1 (scratched zone) shows the following elemental composition: C (61.4 wt.%), O (32.6 wt.%) and Al (5.80 wt.%). At the spot 2 (scratch-free zone) the elemental composition is C (75.0 wt.%), O (24.6 wt.%) and Al (0.29 wt.%). The quantity of Al in the exposed alloy is higher than in the coated part, as expected. These results indicate coating damage over time. For the tannin-modified coating (Fig. 10b), the EDX analysis in the spot 1 (scratched zone) shows the presence of C (80.3 wt.%), O (19.5 wt.%) and Al (0.12 wt.%) and in the spot 2 (scratch-free zone) the composition is C (70.8 wt.%), O (28.9 wt.%) and Al (0.22 wt.%). The quantity of Al is similar, indicating that the tannin-modified coating recovers over the defect, an effect that can be attributed to the self-healing property imparted by tannin, as suggested in Fig. 9.

3.2.3. Scanning vibrating electrode technique (SVET) and scanning ion-selective electrode technique (SIET)

Figs. 11 and 12 present the results of quasi-simultaneous current density and pH measurements (immersion in 0.05 mol L^{-1} NaCl) after 1 h, 8 h and 24 h for the reference coating and after 1 h, 7 h and 24 h for the tannin-modified coating.

The sample coated with the reference coating (Fig. 11) revealed weak corrosion activity inside the defect during the immersion period. This activity was enough to induce slight alkalization over the defect at the end of the immersion test, 24 h. It is worth to mention that cathodic activity could not be detected by the SVET probe, probably because the coating thickness hinders the detection of negatively charged species formed underneath the coating. However, since pH microelectrodes are characterized by higher sensitivity they can detect pH alkalization, which confirm local corrosion activity.

Interestingly, the corrosion activity observed over the sample coated with tannin-modified coating was higher compared to the reference sample during the first 7–10 h of immersion (Fig. 12). Both, current density and pH distributions indicate an early increase of the anodic activity until 7 h of immersion and then, after a sudden activity drop, the defect remains inactive until the end of the immersion test.

The lower activity over the scratch in the reference coating when compared to the tannin-modified coating possibly has the following explanation. Due to the scratch, chlorides and dissolved oxygen from the electrolyte reaches the substrate where anodic dissolution of Al accompanied by reduction of oxygen occur locally. Over the time the phenomena propagates underneath the coating leading to cathodic delamination, more pronounced in case of the reference coating. However, the properties of the coating, and particularly its ability to form new hydrogen bonds, repair the damaged coating areas and delay corrosion propagation. This effect is even more pronounced in the presence of tannin and can be explained by the increased number of –OH groups (confirmed by FTIR, Fig. 3) in the structure of the coating, which may repair damaged areas. The repair mechanism is likely to involve the formation of new hydrogen bonds between hydroxyl groups from tannin and/or oxygen from groups exiting in the polyurethane matrix. This repair of the coating, ultimately inhibits corrosion activity over defects.

Fig. 13a and b present the SEM images and EDX analysis for the reference coating and for the tannin-modified coatings, respectively, after the SVET/SIET (24 h of immersion) measurements. The results evidence that the substrate has been exposed and oxidized and that the Al (scratch zone) content is higher in the reference coating (Fig. 13a). For the tannin-modified coating (Fig. 13a) the scratch zone does not reveal the presence of aluminum confirming the self-healing effect, in

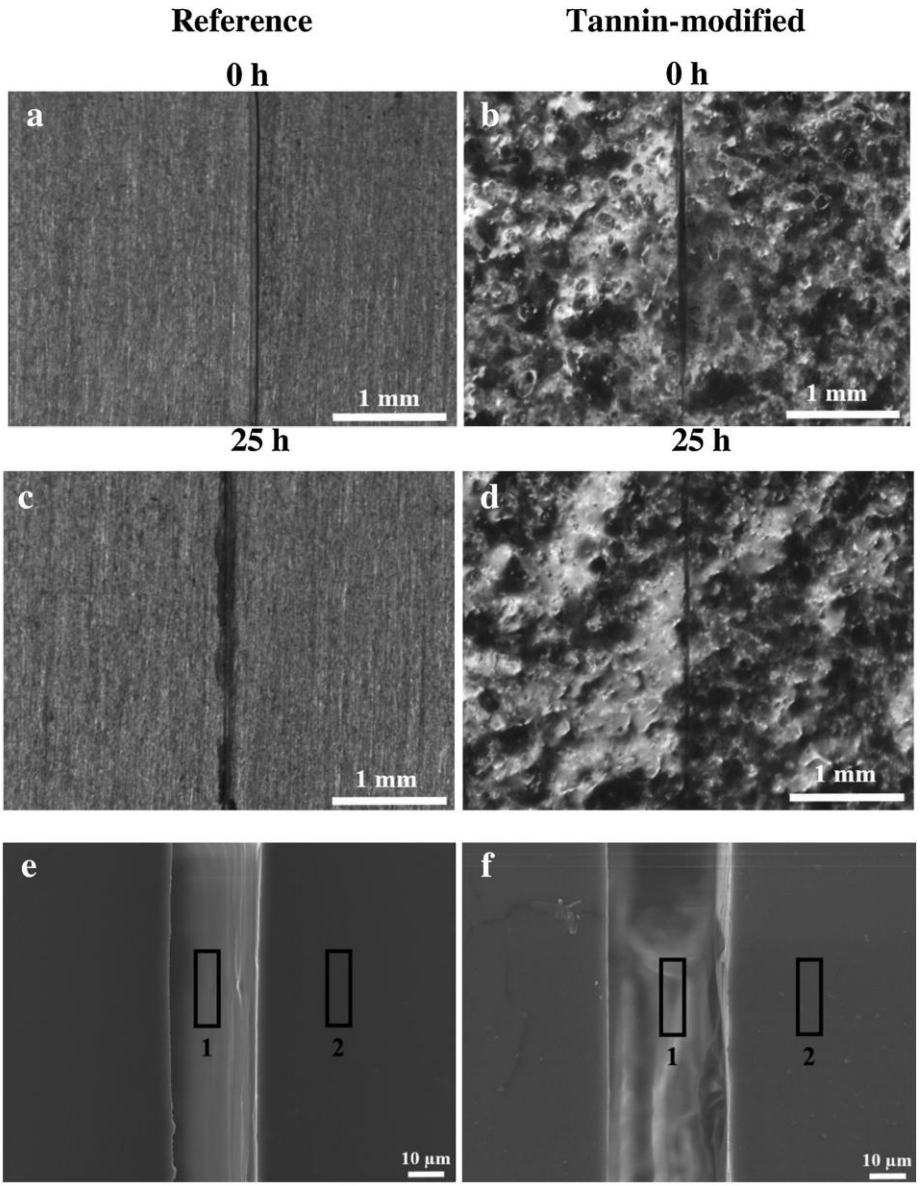

Fig. 10. Optical microscope and SEM images of artificial defects made on (a, c, e) reference, and (b, d, f) tannin-modified coating after LEIS measurements in 0.005 mol L^{-1} NaCl for 25 h.

good agreement with the LEIS results (Fig. 9).

The EDX analysis (Fig. 13a, reference coating) in spots 1 and 2 (scratch zone) shows the following elemental average composition / wt. %: C (67 ± 2); O (31 ± 2) and Al (2 ± 1), while at spot 3 (scratch-free zone) the composition / wt.% was: C (77) and O (23). The concentration of C decreased and Al increased in the scratched zone compared to the scratch-free one, indicating bare metal exposure and poor protection from the surrounding coating. For the tannin-modified coating (Fig. 13b) the elemental average composition / wt.% at spots 1, 2 and 3 (scratch zone) was: C (65 ± 4) and O (34 ± 4), while in spot 4 (scratch-free zone) the composition / wt.% was: C (71) and O (29). These results indicate that the original defect is partially healed and that tannin also prevents propagation of corrosion underneath the coating. As consequence higher amounts of species involved in corrosion.

The reference coating allowed easier propagation of the corrosion process, including, underneath the coating, from where less species was able to reach the surface. This conclusion was supported by SEM-EDX analysis (Fig. 13c, d). Thus, the results reveal an increased area affected by corrosion propagation underneath the reference coating, while in the tannin-modified coating most of the damage was located directly in the area of the defect.

In good agreement, the corrosion process underneath the coating was also evidenced both in the LEIS (Fig. 11) and SVET/SIET measurements (Fig. 12). Moreover, coating delamination could be observed at the end of localized electrochemical measurements (Fig. 13c).

Contrarily, the tannin-modified coating provides better barrier properties and the coating efficiently prevents propagation of corrosion from the defect due to its healing property imparted by the presence of tannin and increased number of −OH groups in the resulting coating matrices. Coating repair was confirmed at the end of the localized electrochemical tests (Figs. 11 and 12). Moreover, the evolution of the E_{OCP} suggested that tannin acts predominantly as anodic inhibitor for the Al alloy boosting the protective properties of the coating.

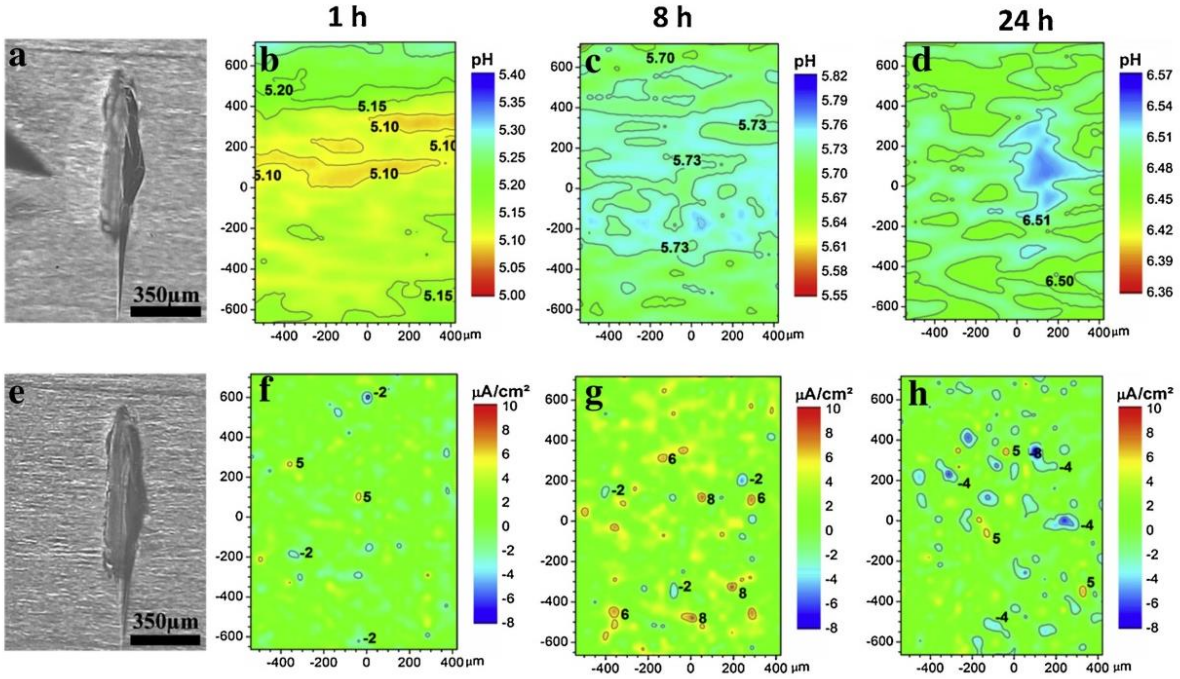

Fig. 11. a, e - Optical micrographs (corresponding to the scanned area) of the sample coated with the reference coating after 1 h and 24 h respectively; pH (b, c, d) and current density (f, g, h) distributions obtained after 1 h, 8 h and 24 h of immersion in 0.05 mol L^{-1} NaCl respectively.

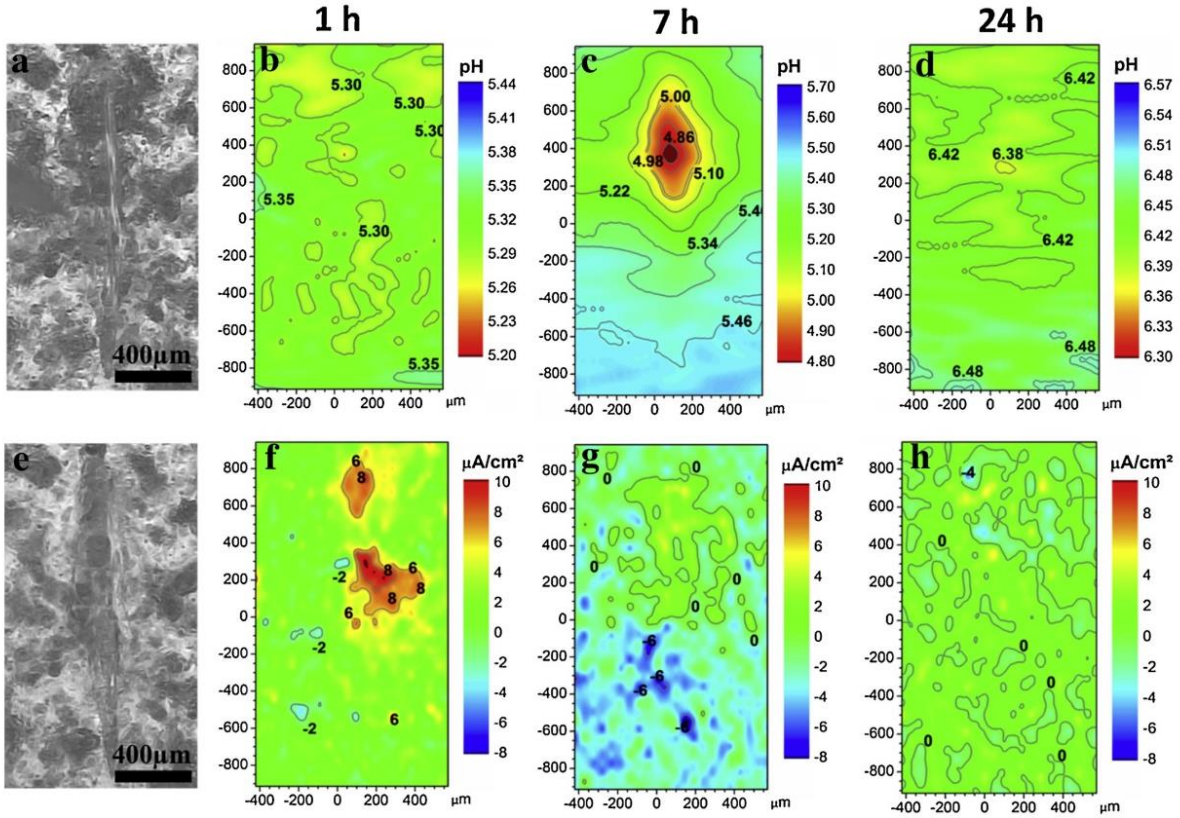

Fig. 12. a, e - Optical micrographs (corresponding to the scanned area) of the sample coated with the tannin-modified coating after 1 h and 24 h respectively; pH (b, c, d) and current density (f, g, h) distributions obtained after 1 h, 7 h and 24 h of immersion in 0.05 mol L^{-1} NaCl respectively.

The results indicate that localized electrochemical techniques provide complementary information and evidenced the self-healing effect of tannin-modified coatings. The results are consistent with reported EIS studies [23], where it was shown that the incorporation of tannin compounds efficiently improved corrosion resistance of the coated AA2024 alloy. In this work, by combining different localized

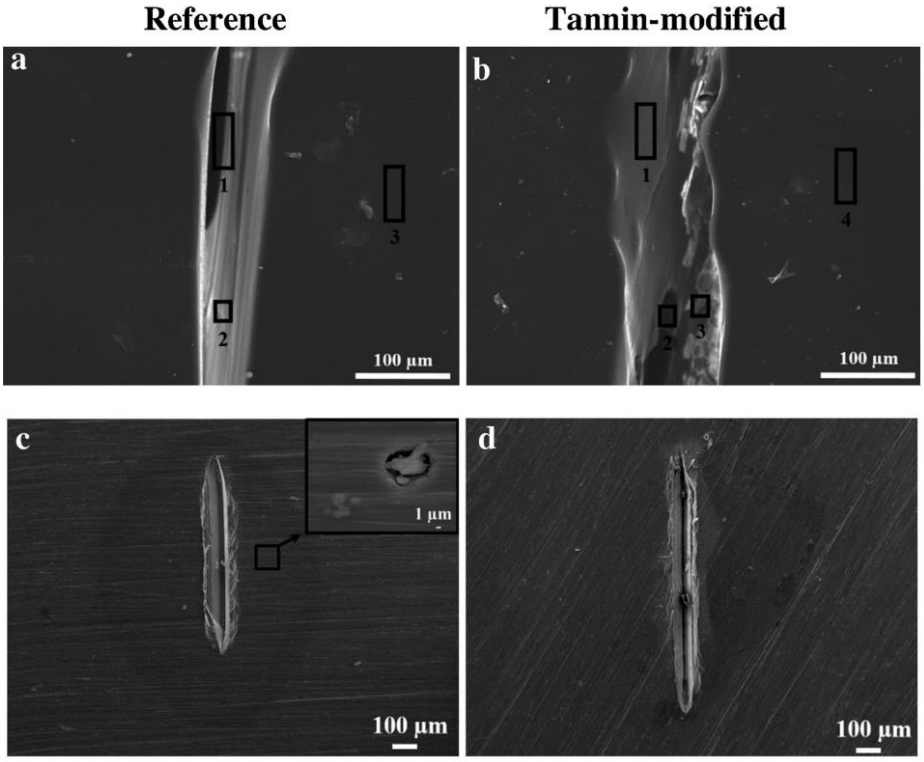

Fig. 13. SEM images of reference coating (a) and tannin-modified coating (b) applied on AA2024-T3 after SVET measurements in 0.05 mol L^{-1} NaCl solution for 24 h and (c, d) the surface after coating removal.

electrochemical techniques, it was demonstrated that the protection effectiveness in the presence of tannin was kept over scratched coating areas exposed to NaCl. The incorporation of tannin in the polyurethane-based coating introduces a high number of -OH groups, which favor cross-linking in the chemical structure of the polymer, contributing to its self-healing effect.

4. Conclusions

Polyurethane coatings derived from natural greener raw materials and their corrosion protection ability were studied by using a complementary combination of mechanical, physico-chemical and electrochemical techniques. The experimental findings evidence improved corrosion protection of the AA2024 coated with tannin-modified coatings, which delayed water uptake compared to blank polyurethane coatings. E_{OCP} values suggests that tannin is predominantly an anodic inhibitor and EIS results evidenced the high barrier properties of the coatings and showed that the pore resistance of tannin-modified coatings was one order of magnitude above the reference coating.

The combination of LEIS, SVET, pH-micropotentiometry and SEM/EDX analysis demonstrate that tannin-modified coatings are able to prevent corrosion progress, while repairing the coating over the damaged areas. Thus, tannin-modified coatings provide efficient and improved protection to the AA2024 alloy from corrosion.

Acknowledgements

J.V. Nardeli author thanks the São Paulo state agency FAPESP (Process: 2015/10554-9 and 2018/09040-9) for scholarships and TANAC S.A. by providing the inhibitors. M.F. Montemor and M. Taryba acknowledge Fundação para Ciência e Tecnologia (FCT) for the funding under the project UID/QUI/00100/2019. The authors thank Prof. Dra. E.R.P. Pinto for her collaboration in the partial synthesis of the coatings.

Appendix A. Supplementary data

Supplementary material related to this article can be found, in the online version, at doi:https://doi.org/10.1016/j.corsci.2019.108213.

References

[1] S.V. Lamaka, M.L. Zheludkevich, K.A. Yasakau, M.F. Montemor, M.G.S. Ferreira, High effective organic corrosion inhibitors for 2024 aluminium alloy, Electrochim. Acta 52 (2007) 7231–7247, https://doi.org/10.1016/j.electacta.2007.05.058.
[2] A.C. Balaskas, I.A. Kartsonakis, D. Snihirova, M.F. Montemor, G. Kordas, Improving the corrosion protection properties of organically modified silicate–epoxy coatings by incorporation of organic and inorganic inhibitors, Prog. Org. Coat. 72 (2011) 653–662, https://doi.org/10.1016/j.porgcoat.2011.07.008.
[3] D. Snihirova, L. Liphardt, G. Grundmeier, F. Montemor, Electrochemical study of the corrosion inhibition ability of "smart" coatings applied on AA2024, J. Solid State Electrochem. 17 (2013) 2183–2192, https://doi.org/10.1007/s10008-013-2078-3.
[4] K. Marcoen, P. Visser, G.F. Trindade, M.-L. Abel, J.F. Watts, J.M.C. Mol, H. Terryn, T. Hauffman, Compositional study of a corrosion protective layer formed by leachable lithium salts in a coating defect on AA2024-T3 aluminium alloys, Prog. Org. Coat. 119 (2018) 65–75, https://doi.org/10.1016/j.porgcoat.2018.02.011.
[5] M. Mrad, Y.B. Amor, L. Dhouibi, M.F. Montemor, Effect of AA2024-T3 surface pretreatment on the physicochemical properties and the anticorrosion performance of poly(γ-glycidoxypropyltrimethoxysilane) sol-gel coating, Surf. Interface Anal. 50 (2018) 335–345, https://doi.org/10.1002/sia.6373.
[6] R.G. Buchheit, H. Guan, S. Mahajanam, F. Wong, Active corrosion protection and corrosion sensing in chromate-free organic coatings, Prog. Org. Coat. 47 (2003) 174–182, https://doi.org/10.1016/j.porgcoat.2003.08.003.
[7] M. Mrad, Y.B. Amor, L. Dhouibi, M.F. Montemor, Corrosion prevention of AA2024-T3 aluminum alloy with a polyaniline/poly(γ-glycidoxypropyltrimethoxysilane) bi-layer coating: comparative study with polyaniline mono-layer feature, Surf. Coat. Technol. 337 (2018) 1–11, https://doi.org/10.1016/j.surfcoat.2017.12.053.
[8] P. Visser, H. Terryn, J.M.C. Mol, On the importance of irreversibility of corrosion inhibitors for active coating protection of AA2024-T3, Corros. Sci. 140 (2018) 272–285, https://doi.org/10.1016/j.corsci.2018.05.037.
[9] P. Visser, Y. Liu, X. Zhou, T. Hashimoto, G.E. Thompson, S.B. Lyon, L.G.J. van der Ven, A.J.M.C. Mol, H.A. Terryn, The corrosion protection of AA2024-T3 aluminium alloy by leaching of lithium-containing salts from organic coatings, Faraday Dicussions 180 (2015) 511–526, https://doi.org/10.1039/C4FD00237G.
[10] J.V. Nardeli, D.V. Snihirova, C.S. Fugivara, M.F. Montemor, E.R.P. Pinto, Y. Messaddecq, A.V. Benedetti, Localised corrosion assessement of crambe-oil-based

polyurethane coatings applied on the ASTM 1200 aluminum alloy, Corros. Sci. 111 (2016) 422–435, https://doi.org/10.1016/j.corsci.2016.05.034.
[11] O. Gharbi, S. Thomas, C. Smith, N. Birbilis, Chromate replacement: what does the future hold? Nature Mat. Degrad. 2 (2018) 1–8, https://doi.org/10.1038/s41529-018-0034-5.
[12] K. Devarayan, G. Mayakrishnan, N. Sulochana, Green inhibitors for corrosion of metals: a review, Chem. Sci. Rev. Lett. 1 (2012) 1–18.
[13] M. Abdolah Zadeh, J. Tedim, M. Zheludkevich, S. van der Zwaag, S.J. Garcia, Synergetic active corrosion protection of AA2024-T3 by 2D- anionic and 3D-cationic nanocontainers loaded with Ce and mercaptobenzothiazole, Corros. Sci. 135 (2018) 35–45, https://doi.org/10.1016/j.corsci.2018.02.018.
[14] S. Martinez, I. Stem, Inhibitory mechanism of low-carbon steel corrosion by mimosa tannin in sulphuric acid solutions, J. Appl. Electrochem. 31 (2001) 973–978, https://doi.org/10.1023/A:1017989510605.
[15] S. Martinez, I. Stern, The thermodynamic characterization of metal dissolution and inhibitor adsorption processes in the low carbon steel/mimosa tannin/sulfuric acid system, App. Surf. Sci. 199 (2002) 83–89, https://doi.org/10.1016/S0169-4332(02)00546-9.
[16] A.O. James, A.O. Atela, Aloe vera: an inhibitor of aluminium corrosion in hydrochloric acid solution, Int. J. Pure Appl. Chem. 3 (2008) 159–163.
[17] H. Gerengi, H.I. Sahin, Schinopsis lorentzii extract as a green corrosion inhibitor for low carbon steel in 1 M HCl solution, Ind. Eng. Chem. Res. 51 (2012) 780–787, https://doi.org/10.1021/ie201776q.
[18] P.M. Krishnegowda, V.T. Venkatesha, P.K.M. Krishnegowda, S.B. Shivayogiraju, Acalypha torta leaf extract as green corrosion inhibitor for mild steel in hydrochloric acid solution, Ind. Eng. Chem. Res. 52 (2013) 722–728, https://doi.org/10.1021/ie3018862.
[19] R.M. Palou, O.O. Xomelt, N.V. Likhanova, Environmentally Friendly Corrosion Inhibitors, Developments in Corrosion Protection, InTech, 2014, pp. 431–465, https://doi.org/10.5772/57252 Chapter 19.
[20] M. Aliofkhazraei, Developments in corrosion protection, InTech, 2014.
[21] J.V. Nardeli, C.S. Fugivara, M. Taryba, E.R.P. Pinto, M.F. Montemor, A.V. Benedetti, Tannin: a natural corrosion inhibitor for bare and coated aluminum alloys, Prog. Org. Coat. 135 (2019) 368–381, https://doi.org/10.1016/j.porgcoat.2019.05.035.
[22] B.E.A. Rani, B.B.J. Basu, Green inhibitors for corrosion protection of metals and alloys: an overview, Int. J. Corros. 2012 (2011) 1–15, https://doi.org/10.1155/2012/380217.
[23] V. Dalmoro, C. Santos, J.H.Z. Santos, Chap. 20: smart coatings for corrosion protetion, Book: Industrial Applications for Intelligent Polymers and Coatings, Springer, 2016, pp. 417–435, https://doi.org/10.1007/978-3-319-26893-4_20.
[24] S. Yahya, A.A. Rahim, A.M. Shah, R. Adnan, Inhibitive behaviour of corrosion of aluminium alloy in NaCl by mangrove tannin, Sains Malays. 40 (2011) 953–957 ISSN 0126-6039.
[25] A. Mirmohseni, M. Azizi, M.S.S. Dorraji, Facile synthesis of copper/reduced single layer graphene oxide as a multifunctional nanohybrid for simultaneous enhancement of antibacterial and antistatic properties of waterborne polyurethane coating, Prog. Org. Coat. 131 (2019) 322–332, https://doi.org/10.1016/j.porgcoat.2019.02.031.
[26] ASTM D3359 Standard Test Methods for Measuring Adhesion by Tape Test. West Conshohocken, American Society for Testing Materials, 2009.
[27] J.B. Jorcin, E. Aragon, C. Merlatti, N. Pébère, Delaminated areas beneath organic coating: a local electrochemical impedance approach, Corros. Sci. 48 (2006) 1779–1790, https://doi.org/10.1016/j.corsci.2005.05.031.
[28] E.A. Zdrachek, A.G. Karotkaya, V.A. Nazarov, K.A. Andronchyk, L.S. Stanishevskii, V.V. Egorov, M.G. Taryba, D. Snihirova, M. Kopylovich, S.V. Lamaka, H+-selective microelectrodes with optimized measuring range for corrosion studies, Sens. Actuators B Chem. 207 (2015) 967–975, https://doi.org/10.1016/j.snb.2014.07.106.
[29] R.G. Buchheit, R.P. Grant, P.F. Hlava, B. Mckenzie, G.L. Zender, Local dissolution phenomena associated with S phase (Al_2CuMg) particles in aluminum alloy 2024-T3, J. Electrochem. Soc. 144 (1997) 2621–2628, https://doi.org/10.1149/1.1837874.
[30] H. Shi, Z. Tian, T. Hu, F. Liu, E. Han, M. Taryba, S.V. Lamaka, Simulating corrosion of Al_2CuMg phase by measuring ionic currents, chloride concentration and pH, Corros. Sci. 88 (2014) 178–186, https://doi.org/10.1016/j.corsci.2014.07.021.
[31] C. Fang, X. Zhou, Q. Yu, S. Liu, D. Guo, R. Yu, J. Hu, Synthesis and characterization of low crystalline waterborne polyurethane for potential application in water-based ink binder, Prog. Org. Coat. 77 (2014) 61–71, https://doi.org/10.1016/j.porgcoat.2013.08.004.
[32] R.S. Peres, E. Cassel, D.S. Azambuja, Black wattle tannin as steel corrosion inhibitor, Int. Schol. Res. Net. 2012 (2012) 1–9, https://doi.org/10.5402/2012/937920.
[33] A.A. Rahim, E. Rocca, J. Steinmetz, M.J. Kassim, R. Adnan, M. Sani Ibrahim, Mangrove tannins and their flavanoid monomers as alternative steel corrosion inhibitors in acidic medium, Corros. Sci. 49 (2007) 402–417, https://doi.org/10.1016/j.corsci.2006.04.013.
[34] F.S. Grasel, M.F. Ferrão, C.R. Wolf, Development of methodology for identification the nature of the polyphenolic extracts by FTIR associated with multivariate analysis, Spectrochim. Acta Part A Mol. Biom. Spec. 153 (2016) 94–101, https://doi.org/10.1016/j.saa.2015.08.020.
[35] A.L. Missio, B. Tischer, P.S.B. Santos, C. Codevilla, C.R. Menezes, J.S. Barin, C.R. Haselein, J. Labidi, D.A. Gatto, A. Petutschnigg, G. Tondi, Analytical characterization of purified mimosa (Acacia mearnsii) industrial tannin extract: single and sequential fractionation, Sep. Purif. Technol. 186 (2017) 218–225, https://doi.org/10.1016/j.seppur.2017.06.010.
[36] R.M. Silverstein, G.C. Bassler, T.C. Morrill, Spectrometric Identification of Organic Compounds, fifth ed., John Wiley & Sons, New York, 1991.
[37] R.S. Mishra, A.S. Khanna, Formulation and performance evaluation of hydroxyl terminated hyperbranched polyesters-based poly (ester–urethane–urea) coatings on mild steel, Prog. Org. Coat. 72 (2011) 769–777, https://doi.org/10.1016/j.porgcoat.2011.08.009.
[38] A. Asefnejad, M.T. Khorasani, A. Behnamghader, B. Farsadzadeh, S. Bonakdar, Manufacturing of biodegradable polyurethane scaffolds based on polycaprolactone using a phase separation method: physical properties and in vitro assay, Int. J. Nanomed. 6 (2011) 2375–2384, https://doi.org/10.2147/IJN.S15586.
[39] D.K. Chattopadhyay, P.S.R. Prasad, B. Sreedhar, K.V.S.N. Raju, The phase mixing of moisture cured polyurethane-urea during cure, Prog. Org. Coat. 54 (2005) 296–304, https://doi.org/10.1016/j.porgcoat.2005.07.004.

Material suplementar no Apêndice III

CAPÍTULO III:

Desenvolvimento de *smart-coating* (revestimento inteligente) para proteção contra corrosão

Este capítulo foi motivado por um convite da editora em explorar o tema Smart-coating. Portanto, aqui se fornece um estudo geral utilizando um revestimento orgânico com matriz polimérica diferente e com menor proporção de tanino condensado. Neste trabalho foi avaliada a proteção contra corrosão da liga AA2024-T3 e o período de início do efeito self-healing. Esta seção é publicada como capítulo de livro: J.V. Nardeli, C.S. Fugivara, M.F. Montemor, A.V. Benedetti. "Smart coating for corrosion protection of aluminium alloys: global and localized study of anti-corrosion performance" no Livro: A Diversidade de Debates na Pesquisa em Química 2, Atena, 2020.

Reproduced with permission from [J.V. Nardeli, C.S. Fugivara, M.F. Montemor, A.V. Benedetti. Smart coating for corrosion protection of aluminium alloys: global and localized study of anti-corrosion performance. In: A Diversidade de Debates na Pesquisa em Química 2, ATENA. v.2, 2020] Copyright 2020 Atena.

CAPÍTULO 1

SMART COATING FOR CORROSION PROTECTION OF ALUMINIUM ALLOYS: GLOBAL AND LOCALIZED STUDY OF ANTI- CORROSION PERFORMANCE

Data de aceite: 04/05/2020

Data de submissão: 05/02/2020

ORCID: https://orcid.org/0000-0002-0243-6639

Jéssica Verger Nardeli
Universidade Estadual Paulista "Júlio de Mesquita Filho" – UNESP, Instituto de Química, Departamento de Físico-Química
Araraquara – São Paulo
Currículo Lattes: http://lattes.cnpq.br/1394679914888559
ORCID: http://orcid.org/0000-0003-4240-3863

Cecílio Sadao Fugivara
Universidade Estadual Paulista "Júlio de Mesquita Filho" – UNESP, Instituto de Química, Departamento de Físico-Química
Araraquara – São Paulo
Currículo Lattes: http://lattes.cnpq.br/2797127887030838
ORCID: https://orcid.org/0000-0002-2288-2601

Fátima Montemor
Centro de Química Estrutural-CQE, DEQ, Instituto Superior Técnico, Universidade de Lisboa
Lisboa – Portugal
ORCID: https://orcid.org/0000-0001-7835-6814

Assis Vicente Benedetti
Universidade Estadual Paulista "Júlio de Mesquita Filho" – UNESP, Instituto de Química, Departamento de Físico-Química
Araraquara – São Paulo
Currículo Lattes: http://lattes.cnpq.br/1769008264876945

ABSTRACT: The development of smart coating based on vegetable oils in the presence of additives have been a good alternative for corrosion protection of different metallic substrates. The AA2024 alloy is a prime material for application in aircraft parts and many others industrial parts, however, this alloy is susceptible to corrosion because the presence of sensitive S-phase, composed by copper and magnesium. The development of the coatings was based on researches of our group using tannin (natural inhibitor) for modification of the polymeric structure of polyurethane. The coatings were characterized by attenuated total reflectance Fourier transform infrared spectroscopy (FTIR-ATR), contact angle, and measurements of thickness. The barrier properties and corrosion protection ability were assessed by open circuit potential (E_{OCP}) and electrochemical impedance spectroscopy (EIS). The self-healing ability of the coatings was studied by localized impedance spectroscopy (LEIS) in the presence of scratch on coating the surface. The results demonstrate that the modified coating provides effective corrosion protection due to damaged polymer healing and the electrochemical and surface

analysis contribute to the interpretation of the corrosion inhibition mechanism.
KEYWORDS: smart coating, corrosion protection, localized impedance, coatings development.

REVESTIMENTO INTELIGENTE PARA PROTEÇÃO CONTRA CORROSÃO DE LIGAS DE ALUMÍNIO: ESTUDO GLOBAL E LOCALIZADO DO DESEMPENHO ANTICORROSÃO

RESUMO: O desenvolvimento de revestimento inteligente à base de óleos vegetais na presença de aditivos têm sido uma boa alternativa para proteção contra corrosão de diferentes substratos metálicos. A liga AA2024 é um material primordial para aplicação em peças de aeronaves e outras peças industriais, no entanto, é suscetível à corrosão devido à presença da fase-S, composta por cobre e magnésio. O desenvolvimento dos revestimentos foi baseado em pesquisas do nosso grupo, utilizando tanino (inibidor natural) para modificação da estrutura polimérica do poliuretano. Os revestimentos foram caracterizados por espectroscopia no infravermelho por transformada de Fourier com refletância total atenuada (FTIR-ATR), ângulo de contato e medidas da espessura. As propriedades de barreira e a capacidade de proteção contra corrosão foram avaliadas por medida de potencial em circuito aberto (*E*OCP) e espectroscopia de impedância eletroquímica (EIS). A capacidade de autocura dos revestimentos foi estudada por espectroscopia de impedância localizada (LEIS) na presença de defeitos artificiais na superfície do revestimento. Os resultados demonstram que o revestimento modificado fornece proteção eficaz contra a corrosão devido à cura do polímero danificado e as análises eletroquímica e de superfície contribuem na interpretação do mecanismo de inibição da corrosão.
PALAVRAS-CHAVE: revestimento inteligente, proteção contra corrosão, impedância localizada, desenvolvimento de revestimentos.

1 | INTRODUCTION

Corrosion is a natural phenomenon, in which occurs the material deterioration due to reactions with species present in the environment. Corrosion is a continuous process (JONES, 2020; MELCHERS, 2019), and thus the choice of a coating must be judicious to last throughout the expected life cycle of the system.

The aluminium alloys used in the aerospace industry have been constantly improved over the past century and now constitute about 80% of the weight of modern aircraft (DORIN; VAHID; LAMB, 2018; YASAKAU et al., 2008). However, one of the major concerns of the airline industries is the ageing of the aircraft associated with corrosion. For protecting aluminum alloys and other metallic surface against

corrosion, it is crucial to understand the fundamental aspects of the corrosion processes affecting the material.

In this context, the search for self-healing polymers has increased due to the need to extend the useful life of materials that are susceptible to corrosion. Self-healing is defined: *"Self-healing can be defined as the ability of a material to heal (recover/repair) damages automatically and autonomously, that is, without any external intervention"* (GHOSH, 2009). The self-healing effect may be related to the physical or chemical integration of repairing components of the polymer, *i.e.* (1) embedment of vessels encapsulating reactive liquids, (2) chemical integration of dynamic reformable/reversible bonds, (3) dispersion of superparamagnetic, (4) self-repair without addition of any discrete physical/chemical healing constituents, driven by interchain van der Waals (vdW) (HORNAT; URBAN, 2020; PULIKKALPARAMBIL; SIENGCHIN; PARAMESWARANPILLAI, 2018). In accordance to literature (NARDELI et al., 2019a), the reaction into polyurethane with tannin inhibitor provided more hydrogen bonds formation that favors self-healing effect in polymers, which can be schematically represented in Figure 1.

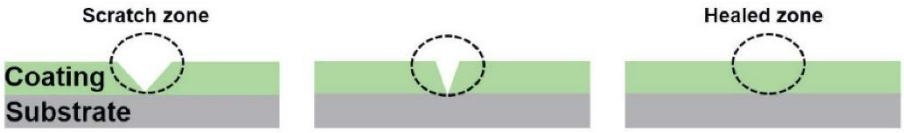

Figure 1. General self-healing mechanism in polymer coating

Different approaches using global and localized techniques are essential for the development and interpretation of new protecting systems (NARDELI et al., 2016; NARDELI et al., 2019b). The aim of this chapter is to stimulate the development of new organic coatings based on formulations (with tannin) that have already proved efficient (NARDELI et al., 2020) in the protection against corrosion of aluminum alloys.

2 | METHODOLOGY

2.1 Coatings preparation

Two different coatings were obtained based on the details of preparation reported by our group (NARDELI et al., 2016 – unmodified coating; NARDELI et al., 2020 – modified coating, however using 2.5 wt.% tannin). The unmodified coating was prepared without inhibitor (NARDELI et al., 2016 - using a proportion 1:3 (polyester:prepolymer)) and the modified coating was obtained by adding tannin

inhibitor (97.5 wt.% unmodified coating + 2.5 wt.% tannin inhibitor) (NARDELI et al., 2020). Then, the coatings were applied on the AA2024 surface, according to the literature (NARDELI et al., 2020). The substrate preparation and composition of the AA2024 substrate were previously described (NARDELI et al., 2020).

2.2 Surface characterization

2.2.1 Thickness

The average thickness of the coatings was determined in triplicate with an Elcometer in different regions of the surface to verify the homogeneity of thickness throughout the length of the film.

2.2.2 Contact angle

The hydrophobicity of the substrate and coatings surface was evaluated by a Dataphysics OCA20. Static distilled water contact angles were measured by carefully placing a 17 μL water droplet onto the substrate aluminum alloy and coating (unmodified and modified) surfaces. The measurements were performed in three replicates to check data repeatability.

2.2.3 Attenuated total reflectance Fourier transform infrared spectroscopy (FTIR-ATR)

The coatings were chemically characterized by means of Fourier Transform Infrared Attenuated Total Reflectance (FTIR-ATR) using a Nikolet IS5 spectrophotometer with an Attenuated Total Reflectance attachment (scans = 32, energy scanning from 400 to 4000 cm^{-1}, resolution = 2 cm^{-1}), however, this characterization has been extensively explored in other works (NARDELI et al., 2019a).

2.2.4 *Scanning electron microscopy (SEM)*

The coating surface was analyzed after localized electrochemical study by SEM and EDX analysis using a FEG-SEM JEOL model JSM 7001F microscope at an accelerating voltage of 15 or 20 kV. The EDX detector from FEG-SEM JEOL is a light elements detector, from Oxford (England), model INCA 250.

2.3 Anti-corrosion performance

Anti-corrosion performance can be estimated by global electrochemical response and localized electrochemical response of the coating applied on

substrate. Both studies provided information based on the response of the coating in the absence (E_{OCP} and EIS measurements) and presence of the scratch (localized electrochemical impedance spectroscopy) on the surface.

To assess self-healing property, an artificial scratch (4 mm size) using a scalpel blade was applied on the coating surface until exposing the metallic substrate. The surface was observed by optical microscopy before and after the LEIS measurements, however, SEM/EDX results will be presented, which contribute more precisely to estimate the protection mechanism according to the composition inside the scratch zone and on the scratch-free zone.

2.3.1 Global electrochemical study

2.3.1.1. Open circuit potential (EOCP) and electrochemical impedance spectroscopy (EIS)

For E_{OCP} and EIS, a conventional three-electrode electrochemical cell Model K0235 was used, which was composed by an AA2024 coated alloy (geometrical area of 1 cm² exposed to the electrolyte in the absence of scratch), the working electrode; an AgIAgClIKCl 3mol L^{-1}, the reference electrode and a Pt spiral, the auxiliary electrode. The electrolyte was 3.5% NaCl solution and the measurements were conducted at 25 oC.

E_{OCP} measurements were performed for both coatings (unmodified and modified) immersed in solution for 30 minutes. EIS measurements were performed for 2 h, 30 days, and 50 days of immersion, using a GAMRY REF 600 potentiostat/galvanostat by applying a 10 mV(r.m.s.) sinusoidal potential perturbation signal to *E*OCP, from 1×10^{5} to 5×10^{-3} Hz, and recording 10 points/frequency decade. These data were employed to evaluate the coatings performance with 1 cm^2 exposed geometrical area in the absence of scratch.

2.3.2 Localized electrochemical study

2.3.2.1. Localized electrochemical impedance spectroscopy (LEIS)

LEIS measurements were performed with a Solartron 1286 electrochemical interface with a Solartron 1250 frequency response analyzer coupled with a Uniscan electrochemical station. The LEIS system was composed of five electrodes, consisting of a conventional three-electrode arrangement (reference electrode, counter electrode, and the coated sample as working electrode under a potentiostatic control) and a Pt bi-electrode (LEIS probe) to measure the local potential gradient

in solution above the working electrode surface. The reference electrode was a saturated calomel electrode (SCE) and the counter electrode was a Pt mesh. Details on the customized configuration of the LEIS probe used in this work have been previously described (NARDELI et al., 2016). The probe was stepped across a well-defined area of the sample including the scratch. The scanned area was 5048 μm × 2000 μm for the unmodified coating and 5106 μm × 2000 μm for the modified coating. A frequency of 5 kHz was used during LEIS mapping. The LEIS maps (area scan: 32 points x 16 lines) were taken in 0.005 mol L-1 NaCl aqueous solution every hour, for 24 h of immersion.

3 | RESULTS AND DISCUSSION

3.1 Surface characterization

3.1.1 Thickness

The determined thicknesses were 445.8 μm and 741.6 μm for the unmodified coating (without tannin) and modified coating (with tannin), respectively.

3.1.2 Contact angle

Figure 2 shows the static contact angles of the surfaces of the coatings applied on AA2024 alloy. This study provided information on hydrophobicity the surface - the higher the contact angle, the greater the hydrophobicity of the surface, therefore, the less water uptake by the coating.

The addition of the organic coating on the AA2024 surface leads to an increase in the contact angle from 76.1° to 90.1°. The addition of inhibitor tannin to organic coating leads to an increase in the contact angle from 90.1° to 94.6°, demonstrated in Figure 2. Therefore, modified coating presents higher hydrophobicity.

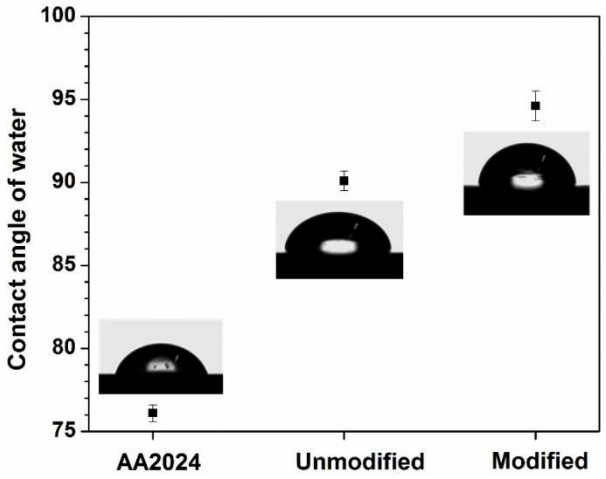

Figure 2. Static contact angles of AA2024 substrate, unmodified coating and modified coating as measured with deionized water.

3.2 Anti-corrosion performance

3.2.1 Global electrochemical study

3.2.1.1. Open circuit potential (EOCP) and electrochemical impedance spectroscopy (EIS)

Figure 3a depicts the evolution of *E*OCP *vs.* time in 3.5% NaCl solution for the substrate AA2024 alloy, and for both unmodified and modified coatings. After 30 minutes of immersion, the *E*OCP values for the bare AA2024 alloy are close to -0.57 V/AgIAgClIKCl 3mol L-1, while for the unmodified coating the value is ~-0.40 V/AgIAgClIKCl 3mol L^{-1}. When the alloy is coated with the modified coating, the *E*OCP values is ~-0.28 V/AgIAgClIKCl 3mol L^{-1}. Over the entire immersion test, the modified coating evidenced the most positive potential value that accounts for its better barrier property in relation to the modified coating.

Figure 3b and Figure 3c show a set of representatives Bode impedance modulus plots for the unmodified and modified coatings obtained after 2 h, 30 days and 50 days of immersion in 3.5% NaCl solution. These results cover the electrochemical response for an area of 1 cm2 without artificial defect, allowing to estimate |*Z*| values around 3.0 x 1010 (2 h), 2.1 x 1010 (30 days), 2.6 x 1010 (50 days) for unmodified coating, and |*Z*| values ~8.3 x 1010 (2 h), ~1.0 x 1011 (30 days), ~4.2 x 1010 (50 days) for modified coating, being always higher than those of the unmodified coating. It is worth to recall that the surface of the modified coating is more hydrophobic, therefore, has less interaction with water, and the modified coating is also thicker

than the unmodified one.

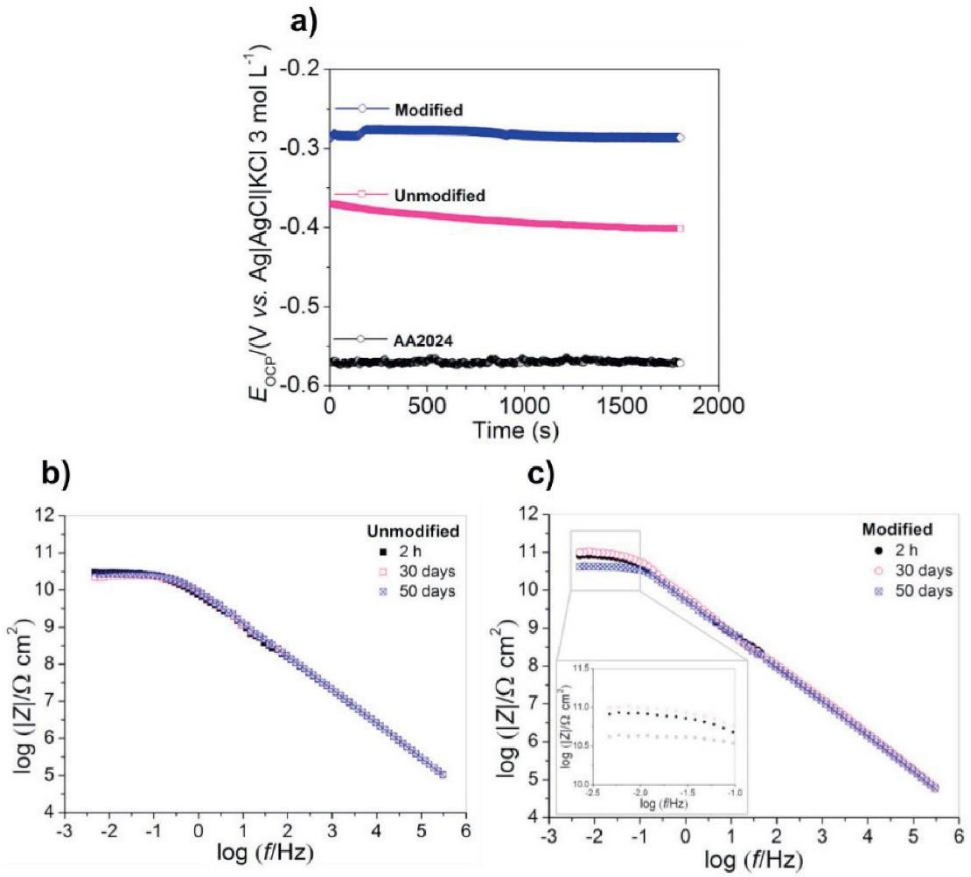

Figure 3. (a) EOCP vs. time for 1800 seconds, (b and c) electrochemical impedance Bode IZI plots taken at 2 h, 30 days, 50 days of immersion in 3.5% NaCl solution.

3.2.2 Localized electrochemical study

3.2.2.1. Localized electrochemical impedance spectroscopy (LEIS)

Figure 4 depicts the evolution of admittance above the surface of the unmodified (Figure 4a) and modified coatings (Figure 4b) provided by LEIS maps for 1 h, 15 h and 24 h of immersion in 0.005 mol L^{-1} NaCl solution. The scale range in Figure 4a is identical to that in Figure 4b to allow a rough comparison between the admittance values. The admittance for the unmodified coating (Figure 4a) increases with the immersion time, showing maximum admittance at 24 h of immersion, thus corresponding to lower impedance values. Some of the most important reactions when the aluminum alloy is exposed to the electrolyte are depicted below as represented by equations 1 - 4.

Cathodic reaction:

$$O_{2(g)} + 2H_2O_{(l)} + 4e^- \rightarrow 4OH^-_{(aq)} \quad \text{(Equation 1)}$$

Anodic reaction:

$$Al_{(s)} \rightarrow Al^{3+}_{(aq)} + 3e^- \quad \text{(Equation 2)}$$

$$Al^{3+}_{(aq)} + 3H_2O_{(l)} \rightarrow Al(OH)_{3(s)} + 3H^+ \quad \text{(Equation 3)}$$

Global reaction:

$$4Al_{(s)} + 3O_{2(g)} + 6H_2O_{(l)} \rightarrow 4Al(OH)_{3(s)} \quad \text{(Equation 4)}$$

However, for the modified coating (Figure 4b) the decrease in admittance in the scratch zone is noted. LEIS experiment was carried out for 24 h only, and it confirms the trends observed in the EIS measurements depicted in Figure 3c. In accordance to literature [ref], the coating modified with tannin provided self-repair effect in scratch zone. In comparison to other results of our group in which a greater amount of tannin was used in the coating formulation, the self-healing effect starts in a few hours (~ 5 h) of immersion, while in the present case, using a lower amount of tannin and other polymeric matrix the effect starts after 15 h of immersion.

In this way it is confirmed that by changing the polymeric matrix and decreasing the amount of tannin, the self-healing effect is maintained, however, the process starts after longer immersion time (~15 h). Therefore, for the development of the smart coating it is interesting to increase the amount of tannin, so that the self-healing effect starts at shorter time. The importance of the interaction between the polymeric matrix and the tannin is also emphasized, so that this combination improves the coating performance against corrosion.

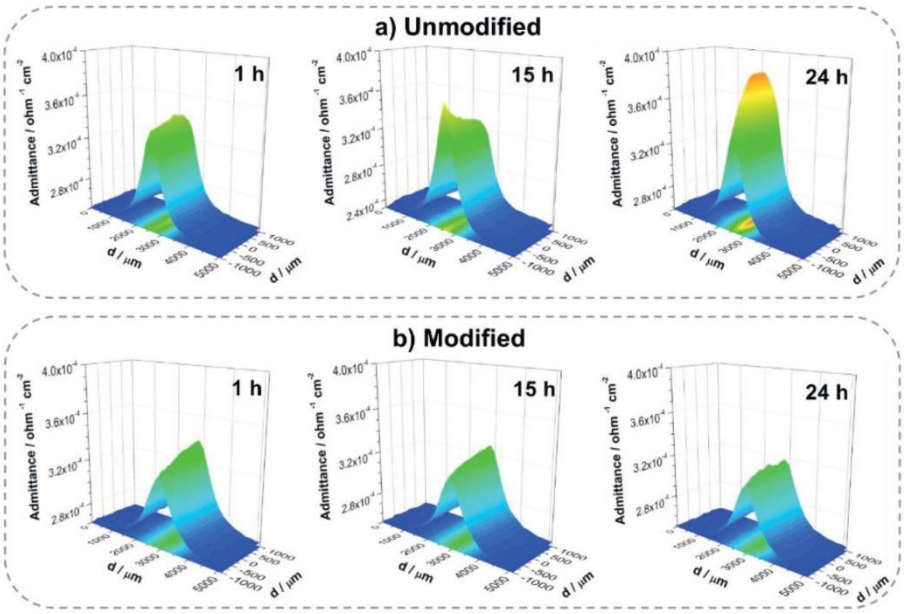

Figure 4. LEIS maps for (a) unmodified and (b) modified coatings obtained at 1 h, 15 h, 24 h of immersion in 0.005 mol L-1 NaCl solution.

Thus, by combining EIS (global electrochemical study) with LEIS (localized electrochemical study), it was possible to observe, in detail, the evolution of the various resistive parameters and the local inhibition on the scratch.

At the end of the immersion test (24 h of immersion in 0.005 mol L-1 NaCl solution) both defects were observed via SEM imaging and EDX analysis (Figure 5). Figure 5a shows that for the unmodified coating, the EDX analysis in the scratch zone confirmed the presence of aluminum. This result indicates that the corrosion process propagated from the scratch zone under the coating, attacking the substrate, in accordance to equations 1 - 4. For the modified coating (Figure 5b), the EDX analysis in the scratch zone shows the absence of aluminum, indicating that the modified coating recovers the coating in the scratch, an effect that can be attributed to the self-healing property, as suggested by the result obtained with LEIS, which shows the decrease of the admittance in the scratch zone.

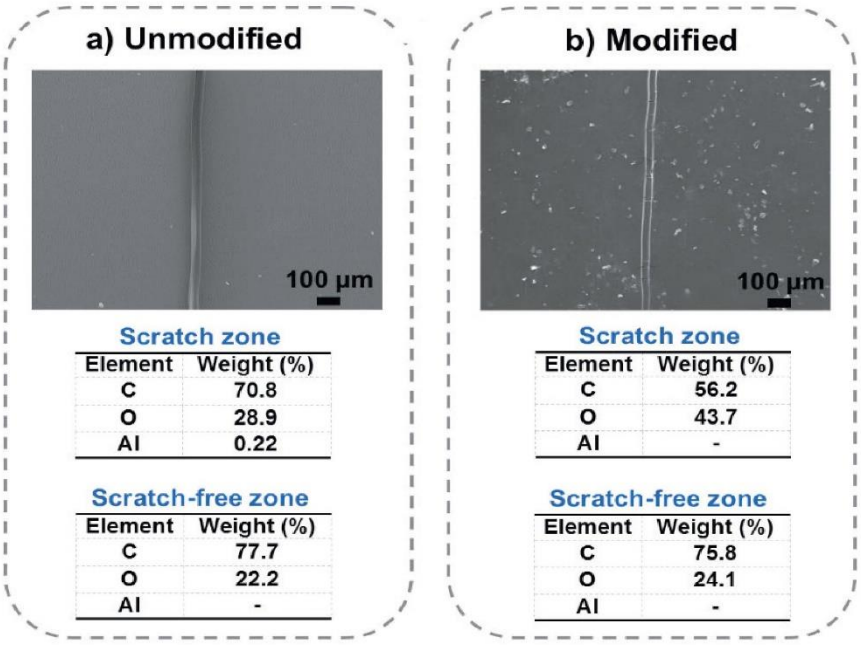

Figure 5. SEM images and EDX analysis (scratch zone and scratch-free zone) for (a) unmodified and (b) modified coatings after LEIS measurements in 0.005 mol L-1 NaCl for 24 h.

The present findings demonstrated that the self-healing effect is maintained even when the composition of the polymer matrix is varied and less tannin is used, however, the self-healing process begins after 15 h of immersion (as observed by LEIS maps, Figure 4), instead of after 5 h (NARDELI et al., 2020). Thus, in the development of smart coatings it is necessary to combine components able to increase the barrier effect and the hydrophobicity of the surface to achieve an efficient protection against corrosion. Betting on a structure with a high number of OH groups, contributes to the self-healing effect.

4 | CONCLUSION

The two coatings were produced by a method known and used in our group, however using different polymeric structure and amount of tannin. The presence of tannin increased the thickness of the coating and the contact angle, resulting in a more hydrophobic surface than the unmodified coating. EIS results showed that the barrier effect is greater for the modified coating than for the unmodified coating, while LEIS and SEM/EDX results indicated that the self-healing properties of the coatings are greatly dependent on the amount of tannin in their formulation. Lowering the content of tannin maintained the self-healing effect however it started after longer immersion time.

ACKNOWLEDGEMENTS

J. V. Nardeli author thanks the São Paulo state agency FAPESP (Process: 2015/10554-9 and 2018/09040-9) for scholarships and TANAC S.A. by providing the inhibitors.

REFERENCES

Dorin, T.; Vahid, A.; Lamb, J. Aluminium lithium alloys. In Lumley, Roger N (ed), **Fundamentals of aluminium metallurgy: recent advances**, Woodhead Publishing, Duxford, Eng., p. 387-438, 2018.

GHOSH, S. K. **Self-healing Materials: Fundamentals, Design Strategies, and Applications**. Wiley-VCH, 2009.

Hornat, C. C.; Urban, M. W. Shape memory effects in self-healing polymers. **Progress in Polymer Science**, in press, p. 101208, 2020.

JONES, M. C. Corrosion Prevention. In: Vachtsevanos, G.; Natarajan, K.; Rajamani, R.; Sandborn, P. (eds) **Corrosion Processes. Structural Integrity**, Springer, Cham, v. 13, p. 105-117, 2020.

Melchers, R. E. Predicting long-term corrosion of metal alloys in physical infrastructure. **Nature: Materials Degradation**, v. 3, p. 4, 2019.

NARDELI, J. V.; FUGIVARA, C. S.; PINTO, E. R. P. P.; POLITO, W. L.; MESSADDECQ, Y.; RIBEIRO, S. J. L.; BENEDETTI, A. V. Preparation of polyurethane monolithic resins and modified with a condensed tannin yielding self-healing property. **Polymers**, v. 11, p. 1890, 2019.

NARDELI, J. V.; FUGIVARA, C. S.; TARYBA, M.; MONTEMOR, M. F.; RIBEIRO, S. J. L.; BENEDETTI, A. V. Novel healing coatings based on natural-derived polyurethane modified with tannins for corrosion protection of AA2024-T3. **Corrosion Science**, v. 162, p. 108213, 2020.

NARDELI, J. V.; FUGIVARA, C. S.; TARYBA, M.; PINTO, E. R. P. P.; MONTEMOR, M. F.; BENEDETTI, A. V. Tannin: a natural corrosion inhibitor for bare and coated aluminum alloys. **Progress in Organic Coatings**, v. 135, p. 368-381, 2019.

NARDELI, J. V.; SNIHIROVA, D. V.; FUGIVARA, C. S.; MONTEMOR, M. F.; PINTO, E. R. P. P.; MESSADDECQ, Y.; BENEDETTI, A. V. Localised corrosion assessement of crambe-oil-based polyurethane coatings applied on the ASTM 1200 aluminum alloy. **Corrosion Science**, v. 111, p. 422-435, 2016.

Pulikkalparambil, H.; Siengchin, S.; Parameswaranpillai, J. Corrosion protective self-healing epoxy resin coatings based on inhibitor and polymeric healing agents encapsulated in organic and inorganic micro and nanocontainers. **Nano-Structures & Nano-Objects**, v. 16, p. 381-395, 2018.

Yasakau, K. A.; Zheludkevich, M. L.; Karavai, O. V.; Ferreira, M. G. S. Influence of inhibitor addition on the corrosion protection performance of sol-gel coatings on AA2024. **Progress in Organic Coatings**, v. 63, n. 3, p. 352-361, 2008.

CAPÍTULO IV:

Estudo do efeito do inibidor em solução

Este capítulo fornece um estudo detalhado da aplicação do inibidor tanino em solução na proteção contra corrosão da liga AA1200. Aborda diferentes técnicas eletroquímicas convencionais e localizadas, as quais permitem o estudo detalhado do sistema em questão. O efeito de inibição da corrosão é confirmado por meio de análises de microscopia óptica, eletrônica de varredura. Esta seção é publicada como artigo: J.V. Nardeli, C.S. Fugivara, M. Taryba, E.R.P. Pinto, M.F. Montemor, A.V. Benedetti. "Tannin: A natural corrosion inhibitor for aluminum alloys" na revista Progress in Organic Coatings v. 135, p.368-381, 2019.

Reproduced with permission from [J.V. Nardeli, C.S. Fugivara, M. Taryba, E.R.P. Pinto, M.F. Montemor, A.V. Benedetti. Tannin: A natural corrosion inhibitor for aluminum alloys. PROGRESS IN ORGANIC COATINGS. v.135, p.368-381, 2019] Copyright 2019 Elsevier Ltd. Progress in Organic Coatings.

Progress in Organic Coatings 135 (2019) 368–381

Contents lists available at ScienceDirect

Progress in Organic Coatings

journal homepage: www.elsevier.com/locate/porgcoat

Tannin: A natural corrosion inhibitor for aluminum alloys

Jéssica V. Nardeli[a,b,*], Cecilio S. Fugivara[a], Maryna Taryba[b], Elaine R.P. Pinto[a], M.F. Montemor[b], Assis V. Benedetti[a,*]

[a] Universidade Estadual Paulista-UNESP, Instituto de Química, 14800-060 Araraquara, SP, Brazil
[b] Centro de Química Estrutural-CQE, DEQ, Instituto Superior Técnico, Universidade de Lisboa, Av. Rovisco Pais, 1049-001 Lisboa, Portugal

ARTICLE INFO

Keywords:
AA1200 alloy
Tannin
Coatings
Corrosion protection
Inhibitor

ABSTRACT

This work aims at investigating the effect of tannin, a natural compound, as corrosion inhibitor for bare and coated aluminum alloys (AA1200). Tannin was characterized by Attenuated Total Reflectance Fourier Transform Infrared Spectroscopy (FTIR-ATR) and its interaction with the sample surface was evaluated by computational calculations using the density functional theory (DFT) and electrochemical measurements. The corrosion behavior was studied by open circuit potential (E_{OCP}), electrochemical impedance spectroscopy (EIS) and by the scanning vibrating electrode technique (SVET). Complementary studies were performed by scanning electron microscopy (SEM). Results demonstrated that tannin is an effective corrosion inhibitor protecting both coated and uncoated aluminum samples.

1. Introduction

Aluminum alloys are widely used as structural materials; however, they are prone to localized corrosion in NaCl containing environments. Coatings have been considered as an important route to protect Al alloys from corrosion [1,2]. Protection can be extended further by *in situ* addition of corrosion inhibitors even when coatings have been already applied onto the metal surface, i.e., after coating [3–6]. Corrosion inhibitors are active chemical species which help to slow down, delay or prevent corrosion, via different mechanisms, such as adsorption onto the metal surface that blocks active surface sites [4,7]. Usually, the polar function of organic inhibitor molecules works as reaction center in the adsorption process. The efficiency of organic inhibitors has been associated with the presence of polar groups containing S, O or N atoms, heterocyclic compounds and π-electrons with great electron density [8].

When added to solutions, organic inhibitors (OI) can adsorb on metal surfaces by displacing water according to Eq. 1 [4,9]:

$$OI_{(electrolyte)} + nH_2O_{(ads.\ surf.)} \rightleftharpoons OI_{(ads.\ surf.)} + nH_2O_{(eletrolyte)} \quad (1)$$

It has been reported that some aggressive ions (e.g. chlorides) can also be displaced by organic inhibitors, allowing more effective corrosion protection [4].

The use of natural inhibitors is presently a key requirement for protection of metallic parts against corrosion and to prevent unexpected metal losses, including coated parts that have been damaged [7].

A large number of studies have been devoted to the corrosion inhibition effect of different plant extracts in different media. These extracts include a variety of natural organic products such as essential oils, tannins (flavones, flavonoids, etc.), pigments, steroids, terpenes, among other active substances used as corrosion inhibitors [10,11]. It is of major scientific interest to identify the chemical nature of the species in the extracts and to understand their inhibition mechanism.

Tannins are complex mixtures of non-toxic, biodegradable polyphenolic compounds, extracted from plants [12,13] and comprise two different classes of polyphenolic compounds: hydrolysable and condensed tannins. Condensed tannins are found in considerable concentrations in the wood and bark of several trees, for instance, black wattle [14,15] and have been largely studied as corrosion inhibitors in different media [15–17]. Michael and Olubunmi [18] showed that the presence of electron rich heteroatoms and double bonds, favour adsorption, contributing to the inhibition effect of tannins.

In this work, tannin, molecular groupings or clusters derived from the flavan-3-ol structure (Fig. 1), resulting from the aqueous leaching of bark from black acacia, *Acacia mearnsii* de Wild (TANAC S.A.), was used as corrosion inhibitor for Al alloys. Chemically, acacia tannin is a mixture of complex substances, rich in polyphenols, which confer to the mimosa extract high antioxidant power and significant biological activity. Other substances such as sugars and hydrolysable gums are also present in the extract [15]. Although the inhibition action of natural tannins has been known for long time, only in the past decade tannins have been experimentally and theoretically investigated systematically

* Corresponding authors at: Universidade Estadual Paulista-UNESP, Instituto de Química, 14800-060 Araraquara, SP, Brazil.
E-mail addresses: jessica.nardeli@unesp.br (J.V. Nardeli), assis.v.benedetti@unesp.br (A.V. Benedetti).

https://doi.org/10.1016/j.porgcoat.2019.05.035
Received 19 January 2019; Received in revised form 22 April 2019; Accepted 21 May 2019
0300-9440/ © 2019 Elsevier B.V. All rights reserved.

Reproduced with permission from [J.V. Nardeli, C.S. Fugivara, M. Taryba, E.R.P. Pinto, M.F. Montemor, A.V. Benedetti. Tannin: A natural corrosion inhibitor for aluminum alloys. PROGRESS IN ORGANIC COATINGS. v.135, p.368-381, 2019] Copyright 2019 Elsevier Ltd. Progress in Organic Coatings.

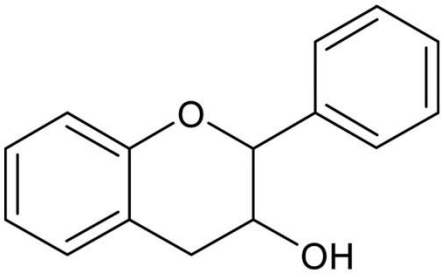

Fig. 1. Chemical structure of flavan-3-ol (tannin).

as corrosion inhibitors for metals in different media [15–19]. In this sense, knowledge contributing to develop new formulations of safer and effective inhibitors derived from tannin is of extreme relevance. One interesting point is to investigate the inhibition ability of these species in coated specimens. Soluble inhibitors added in the electrolyte (or leached from the coating and dissolved in the electrolyte during its uptake by the coating) can reach the bare metal protecting it [20].

The fundamentals of the inhibitive mechanism of tannin have been studied by means of the frontier orbital and inhibitor adsorption theories [4]. Theoretical calculations [16,17] demonstrated that in chestnut and mimosa tannins, the most relevant molecular properties responsible for their action as corrosion inhibitors were the geometrical structure of the molecule, the dipole moment (μ), **HOMO** and **LUMO** energies, and the energy gap. These results evidenced that molecular analysis using quantum chemical methods facilitate the rational selection and the design of new inhibitive formulations.

Simulations and computational calculations, using density functional theory (DFT), have been performed to estimate different intrinsic molecular properties of the structure shown in Fig. 1, e.g. dipole moment (μ), frontier molecular orbitals (*Highest Occupied Molecular Orbital*-**HOMO** and *Lowest Unoccupied Molecular Orbital*-**LUMO**), total hardness (η), number of electrons transferred (ΔN), electronegativity (χ) knowing these parameters allows to explain the inhibition effect of tannin on bare and coated aluminum surfaces [21,22]. The chemical hardness is a molecular quantity (η) and its absolute value is defined as $\eta = \frac{1}{2}(\partial\mu/\partial N)_V$, where μ = electronic chemical potential, N = number of electrons, and V the potential of the nuclei plus any external potential. However, a total or global chemical hardness (average value) is obtained from the operational and approximate definition given by the half of the difference between the ionization potential (*IP*) and electron affinity (*EA*): $\eta = 1/2(IP\text{-}EA)$. The sum of the total hardness of two reacting molecules ($\eta_C + \eta_B$) acts as a resistance for the reaction. Hard molecules have a large **HOMO-LUMO** gap and soft molecules have a small **HOMO-LUMO** gap. Dipole moment, which is the most widely used parameter to describe the polarity [23] and the energy of **HOMO** is directly related to the ionization potential, while the energy of **LUMO** is directly related to the electron affinity. The **HOMO-LUMO** gap, i.e. the difference in energy between them is an important stability index [24]. Therefore, frontier orbitals, which determine the way the molecule interacts with other species, are correlated with the electronegativity (χ) and chemical hardness (η) of the metal, since the negative of **HOMO** energy is equal to IP and the negative of **LUMO** energy is equal EA [21]. The **HOMO** is the outermost (highest energy) orbital containing electrons and may act as an electron donor while **LUMO** is the innermost (lowest energy) orbital that can accept electrons. The tannins components may present steric impediments and then it is important to know in what part of the molecule the **HOMO** and **LUMO** orbitals are localized to facilitate the explanation of experimental results. In the present, these calculations are made for the main unit flavan-3-ol.

2. Experimental

2.1. Substrate preparation

AA1200 aluminum alloy (100 mm × 100 mm × 2 mm) purchased from Belmetal S.A. with the chemical composition (wt.%): Cu (0.012), Fe (0.072) and Al balance was used as substrate. The surface of AA1200 plates was successively wet-ground down to 1200 grit using silicon carbide sandpaper and washed with distilled water and acetone and then dried in air.

2.2. Organic coatings preparation

The coating was obtained in two steps: preparation of (1) polyester (flexible segment) and (2) prepolymer (rigid segment). Two coatings (**A** and **B**) were prepared. Coating **A**: In step 1, the polyester was prepared with transesterification reaction crambe oil (CO, 997.60 g), trimethylolpropane (TMP, 670.50 g), phthalic anhydride (PhA, 444.30 g), butylated hydroxytoluene (BHT, 0.50 g) and lithium hydroxide (LiOH, 0.25 g). The reagents CO, TMP and PhA were mixed with antioxidant BHT used to protect the double bonds of crambe oil from oxidation and LiOH was the catalyst for polyester preparation. No solvent was used in this step. The reaction was performed under stirring and heating at 240 °C for 5 h, and in N_2 atmosphere. The glycerin was removed during the reaction with Dean-Stark. The progress of the reaction was monitored by methanol solubility test (3 ml methanol/1 ml polyester) and acidity index (mg KOH/g of polyester). When the polyester was totally solubilized in methanol and the acidity index was lower 30 the reaction was completed and stopped. In step 2, the prepolymer was prepared with castor oil (CAO, 191.01 g), trimethylolpropane (TMP, 71.07 g), butylated hydroxytoluene (BHT, 3.30 g), propylene glycol (PG, 19.02 g), n-Butyl acetate (BA, 667.92 g), ethyl glycol acetate (EGA, 286.78 g), hexamethylene diisocyanate (HDI, 782.11 g) under stirring and heating at 60 °C for 6 h, in N_2 atmosphere. CAO, TMP and HDI are the reagents, BHT has the same function as in step 1, and PG, BA and EGA are solvents. The products obtained in steps 1 and 2 are made to react in the presence of the catalyst stannous octoate (SO, 0.14 g) under stirring for 10 min to form coating **A**. Coating **B**: the step 1 was exactly the same as in coating **A**. In step 2, the quantity of components changed in relation to coating **A**. The prepolymer was prepared with CAO (125.35 g), TMP (46.93 g), hexamethylene diisocyanate (HDI, 521.40 g), BHT (2.20 g), PG (12.17 g), BA (444.89 g), EGA (191.63 g), under stirring and heating 60 °C for 6 h in N_2 atmosphere. Exactly as in coating **A**, the products were mixed and made to react in the presence of the catalyst stannous octoate (SO, 0.14 g) to form coating **B**.

The coatings were applied onto three aluminum panels (100 mm × 100 mm) using an adjustable applicator (TKB Erichsen instruments®), cured in a fume hood at 25 °C for 48 h and then stored in a desiccator.

2.3. Thickness, adhesion and hardness of the coating

The thickness of the coating was determined using a model 355 Elcometer Coating thickness gauge system. The adhesion of the coating was performed by the tape test, according to the standard ASTM D3359-2009 [25]. Film hardness was determined by the pencil test according to the standard ASTM D3363-2011 [26] and 6 measurements were done for each coating. These measurements were performed on three coated panels obtained for coatings **A** and **B**.

2.4. Theoretical studies

The theoretical investigation of the main unit flavan-3-ol (Fig. 1) of tannin as inhibitor (the inhibitor is commercial, so only the basic unit is

exactly known) was performed with density functional theory (DFT) and the computer program GAUSSIAN09W [27], using the B3LYP functional [28] and base set 6-31G [29]. This procedure was adopted from a previous work published elsewhere [30,31].

The geometry of the main unit flavan-3-ol of the corrosion inhibitors as well as the molecular properties such as dipole moment (μ), frontier molecular orbitals (**HOMO** and **LUMO**), volume and area occupied by the molecule were obtained by the adjustment of the geometric variables. Other variables were obtained according to literature [21] as electron fraction transferred between that unit of the inhibitor and metal (ΔN), total hardness (η) and electronegativity (χ).

2.5. Chemical and morphological analyses

2.5.1. Attenuated Total Reflectance Fourier Transform Infrared Spectroscopy (FTIR-ATR)

Both coatings and inhibitor were studied by means of Attenuated Total Reflectance Fourier Transform Infrared Spectroscopy (FTIR-ATR) using a Vertex70 Bruker spectrophotometer with an Attenuated Total Reflectance accessory (scans = 64, energy scanning from 400 to 4000 cm^{-1}, resolution $= 2\,cm^{-1}$).

2.5.2. Scanning electron microscopy (SEM)

Scanning electron micrographs of the coated and bare AA1200 Al alloy surfaces, before and after each electrochemical test, were taken using a scanning electron microscope Hitachi (SEM/S-2400) coupled to a Thermo Scientific microanalysis system. Energy dispersive X ray (EDX) microanalysis and SEM images were performed under a 20 kV voltage.

2.6. Corrosion studies

Solutions were prepared with ultrapure water (Milli-Q, resistivity > 18 MΩ cm), NaCl (Merck, p.a.) and inhibitor tannin (TANAC S.A.) and used in the electrochemical tests carried out at 25 °C. The electrochemical experiments were performed in a conventional three-electrode electrochemical cell, using the bare and the coated aluminum alloy (geometrical area of 1 cm^2) as working electrode, Ag|AgCl|KCl 3 mol L^{-1} as reference electrode, and a Pt spiral as counter electrode. All potentials are referred to the Ag|AgCl|KCl 3 mol L^{-1} reference electrode. Tannin concentrations were 4.41×10^{-2} mol L^{-1} and 4.41×10^{-3} mol L^{-1}.

2.6.1. Open circuit potential (E_{OCP}) and conventional electrochemical impedance spectroscopy (EIS) measurements

E_{OCP} *vs.* time and impedance were measured in triplicate using uncoated panels and panels coated with the different coatings. EIS measurements were performed using a GAMRY REF 600 potentiostat / galvanostat by applying a sinusoidal potential perturbation signal of 10 mV(r.m.s.) to E_{OCP}, from 300 kHz to 5 mHz recording 10 points/frequency decade. Impedance spectra were recorded as function of the immersion time until a sharp decrease of the E_{OCP} values was detected and stabilization near values expected for the substrate were attained. The sharp decrease of the E_{OCP} values indicates deterioration of the barrier properties of the coatings. Open circuit potentials were recorded between each impedance measurement and the impedance spectra were analyzed with the Zview® software.

2.6.2. Scanning vibrating electrode technique (SVET) measuring

SVET studies were performed in 0.05 mol L^{-1} NaCl aqueous solution without and with 4.41×10^{-3} mol L^{-1} tannin inhibitor for 24 h at 25 °C. The measurements were performed in duplicate using a SVET system from Applicable Electronics Inc., controlled by the ASET software (Science Wares Inc.). Samples were glued onto an epoxy holder and the exposed area (approximately 1 mm^2) was delimited by insulating the remaining surface using a mixture of beeswax. In coated samples a scratch (≈1.0 mm long × ≈ 0.2 mm large) was done with a scalpel. The exposed area was continuously monitored using a microscopic video system and the measurements were performed in a 21 × 26 grid, generating 546 points for coating **A**; 21 × 21 grid, generating 441 points for coating **B** without inhibitor; 21 × 36 grid, generating 756 points for samples tested with tannin inhibitor. An insulated Pt-Ir probe, with platinum black deposited on a spherical tip of 16 µm diameter, was used as vibrating electrode. The probe was placed 100 ± 2 µm above the surface, vibrating in the planes perpendicular (Z) and parallel (X) to the surface of the sample with the probe vibration frequencies of 124 Hz and 325 Hz, respectively. Only the vertical component of the vibration was considered.

Table 1
Thickness, adhesion and hardness of coatings measured after 2 months after cure.

Coating	Thickness / µm	Adhesion	Hardness
A	34 ± 2	5B	5H
B	42 ± 2	5B	5H

3. Results and discussion

3.1. Thickness, adhesion and hardness of the coating

Table 1 shows the thickness, adhesion and hardness values of the coatings determined at room temperature (~25 °C). Although all as-prepared coatings were deposited with identical thickness, different compositions induce different reactions occurring during cure (~25 °C), resulting in coatings with distinct thicknesses. Air moisture also influences the curing process since water reacts with free-NCO groups in the resin to form amine groups that may produce urea groups further reacting with the urethane groups and producing biurethane and allophanate bonds [32].

Table 1 shows that the thickness is lower for the coating with higher amount of prepolymer (thickness of coating **A** < coating **B**), indicating that the amount of prepolymer strongly influences the final coating thickness. Higher number of free-NCO groups (higher amount of prepolymer) accelerates the curing process [32] due to the reaction of NCO with the hydroxyl groups from polyester forming highly cross linked chains (coating **A**). Lower proportion of prepolymer slows down cure, favoring formation of other groups such as amines, biurethane and allophanates. This makes possible the formation of larger chains, resulting in a thicker coating.

The adhesion test shows maximum adhesion (5B) for both coatings indicating excellent adhesion to the aluminum alloy. The adhesion values (Table 1) are higher than the ones reported in literature for films formed by non-triglycerides [32]. Hardness is high for all coatings (Table 1).

3.2. Theoretical studies

3.2.1. Molecular orbitals

Fig. 2 shows flavan-3-ol (out-of-plan) and flavan-3-ol (in-plan) (tannins) in the lower energy spatial configuration, the location of the **HOMO** and **LUMO** orbitals, the dipole moment vector (μ) of flavan-3-ol (out-of-plan) and flavan-3-ol (in-plan) molecules obtained from quantum calculations at B3LYP/25 g in water solvent.

In the flavan-3-ol (out-of-plan) molecule, shown in Fig. 2a, the **HOMO** orbitals are located on the double bonds of the first ring and on the oxygen heteroatom of the cycle, and the **LUMO** orbital is located on the two rings, while in the flavan-3-ol (in-plan) molecule, shown in Fig. 2b, the **HOMO** orbitals are located on the double bonds of the first ring and on the oxygen heteroatom of the cycle, and the **LUMO** orbital is located on the secondring.

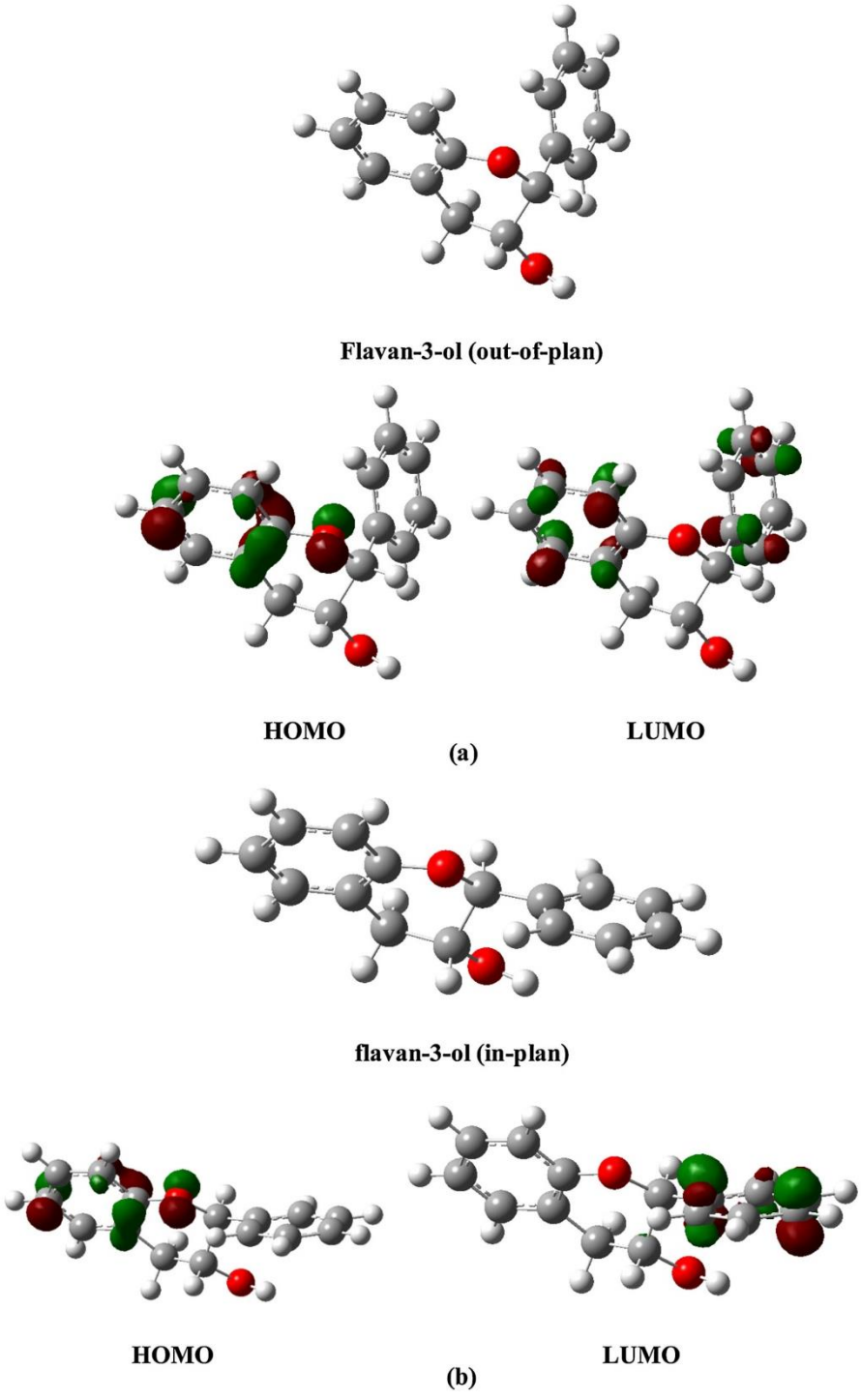

Fig. 2. Chemical structure and frontier orbitals (**HOMO** and **LUMO**) representations for the inhibitors **(a)** flavan-3-ol (tannin) (out-of-plan) and **(b)** flavan-3-ol (tannin) (in-plan) ●= oxygen, ●= carbon, ○= hydrogen.

Table 2
Quantum-chemical parameters calculated from theoretical studies.

Tannin inhibitor	HOMO (eV)	LUMO (eV)	GAP $\Delta E_{L\text{-}H}$ (eV)	$A_{occup.}$ (Å^2/molecule)	μ (Debye)	$\eta_{inhibitor}$ (eV)	$\chi_{inhibitor}$ (eV)	ΔN_{Al}
Flavan-3-ol (out-of-plan)	−6.14	−0.29	5.85	50.1	1.35	2.92	3.21	$1.75x10^{-3}$
Flavan-3-ol (in-plan)	−6.11	−0.34	5.77	50.5	1.46	2.88	3.22	$8.84x10^{-4}$

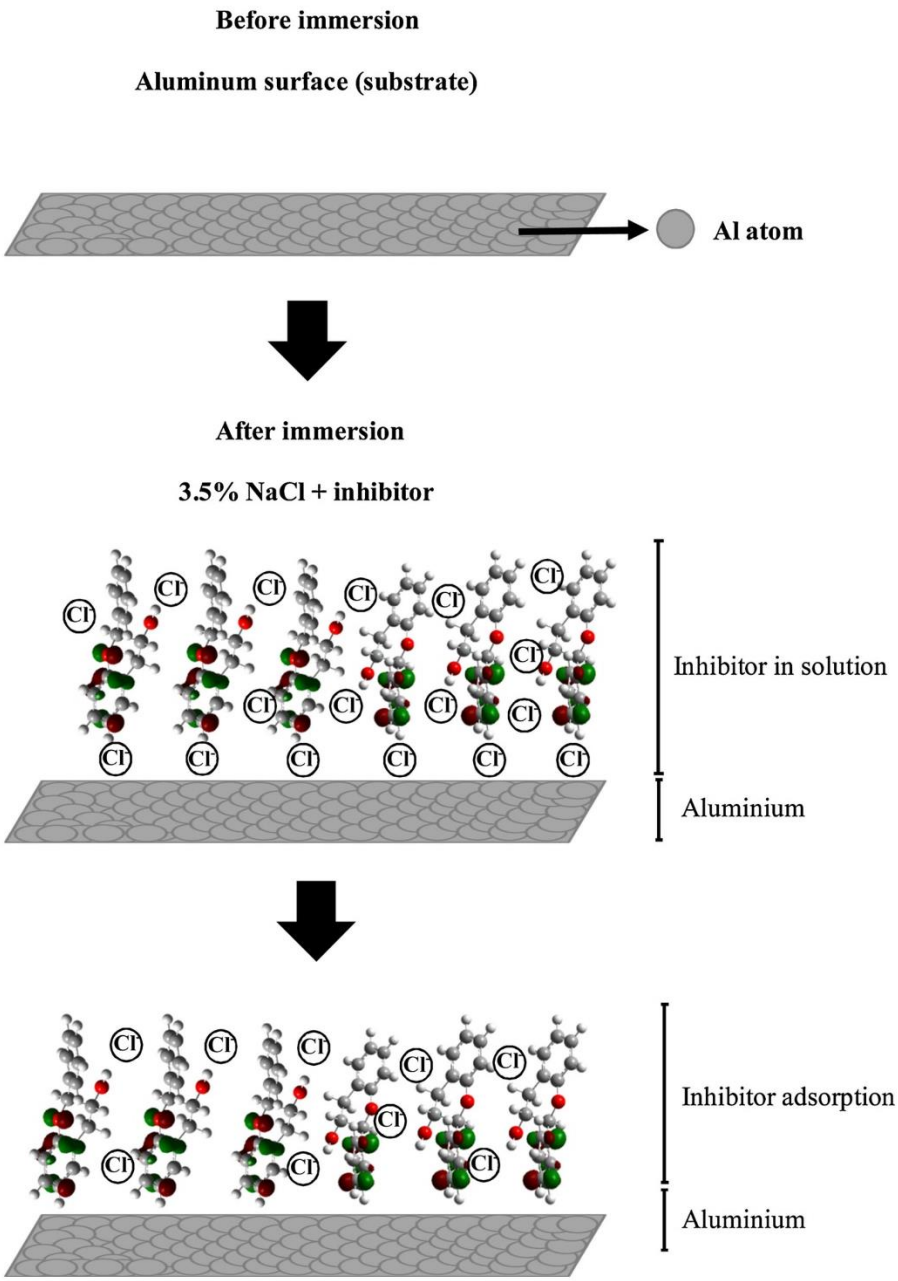

Fig. 3. Schematic representation of proposed adsorption mechanism for inhibitor after immersion in 3.5% NaCl solution with inhibitor (flavan-3-ol (in-plan)). In this model chloride ions are in solution together with the inhibitor and some ions are adsorbed on the metal surface. After some time, chloride ions are replaced by the inhibitor molecules.

The chemical-quantum parameters estimated for the inhibitor are given in Table 2. Variables as electron fraction transferred between inhibitor and metal (ΔN), total hardness (η) and electronegativity (χ) were obtained from literature [21].

Since the substrate was an aluminum alloy, data were obtained for 1 (one) aluminum atom [21] to consider the interaction between inhibitor and substrate. Data for aluminum are $IP_{Al} = 5.99$ eV; $EA_{Al} = 0.46$ eV; $\chi_{Al} = 3.23$; $\eta_{Al} = 2.77$ eV and data for the inhibitors were obtained from Eqs. 2–5.

Ionization potential (*IP*):

$$IP = -E_{HOMO} \quad (2)$$

Electron affinity (*EA*):

$$EA = -E_{LUMO} \quad (3)$$

Eletronegativity (χ):

$$\chi = \frac{IP + EA}{2} \quad (4)$$

Total hardness (η):

$$\eta = \frac{IP - EA}{2} \quad (5)$$

With this data it was possible to obtain the fraction value of electrons transferred between inhibitor and metal (ΔN) (Eq. 6) and

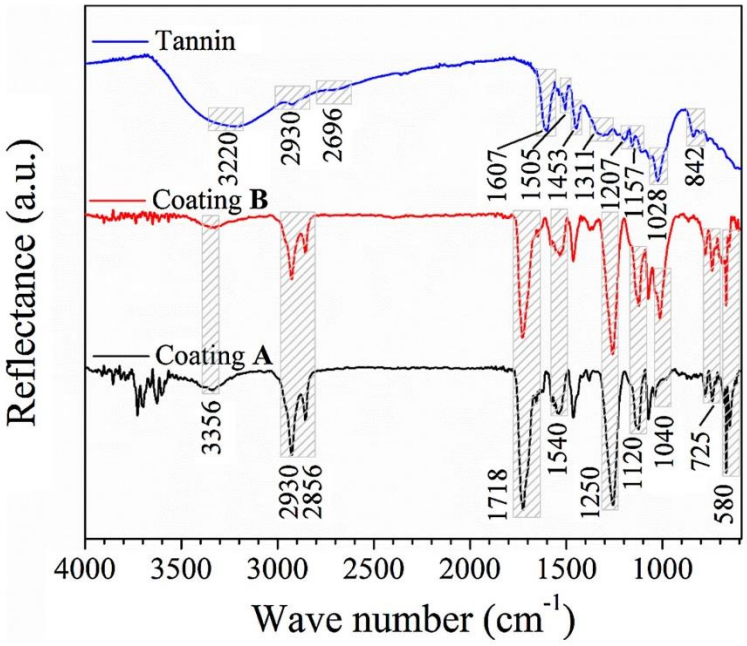

Fig. 4. FTIR-ATR spectra for coating A, coating B and tannin inhibitor samples.

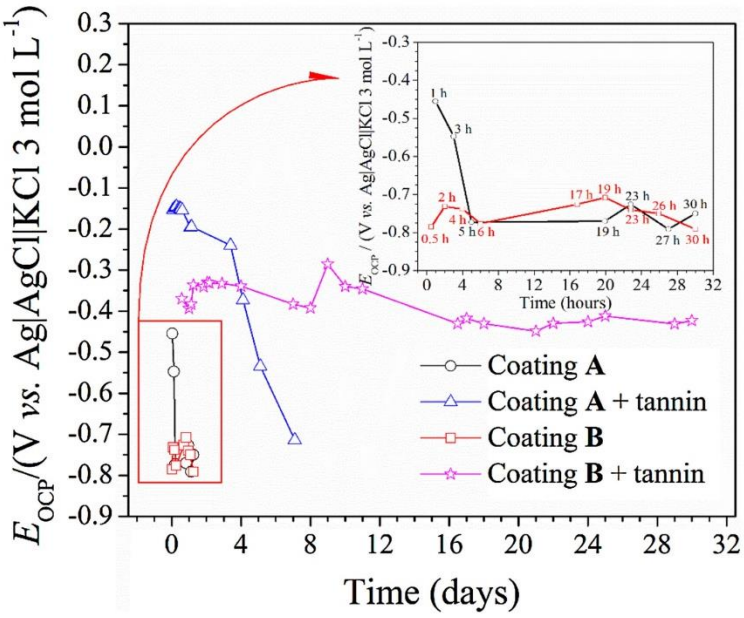

Fig. 5. E_{OCP} *vs.* time for the coatings **A** and **B** in 3.5% NaCl solution without inhibitor after 30 h (inset) and coatings **A** and **B** in 3.5% NaCl solution with 4.41×10^{-2} mol L^{-1} tannin, respectively, after 7 and 30 days of immersion.

according to the literature [21] for $\Delta N_{Al} > 3.6$ the electron transfer occurs from the metal to the inhibitor, and for $\Delta N_{Al} < 3.6$ from the inhibitor to the metal.

Electrons transferred (ΔN):

$$\Delta N = \frac{\chi_{metal} - \chi_{inhibitor}}{2(\eta_{metal} + \eta_{inhibitor})} \quad (6)$$

According to the results obtained by Eqs. 4–6, and given in Table 2, for this compound, independently of the configuration, the value of $\Delta N_{Al} < 3.6$, indicates that electron transfer occurs from the inhibitor to the metal and the tannin in-plan shows lower $\Delta E_{L\text{-}H}$ value than tannin out-of-plan. The in-plane configuration possesses a slightly higher dipole moment and is softer than the configuration out-of-plan; all these characteristics point to better inhibiting effect for the in-plane configuration.

According to this result the adsorption of inhibitor on the Al surface could occur with the main unit flavan-3-ol horizontally or vertically oriented towards the surface, considering the location of the **HOMO** orbitals. The horizontal orientation is of low probability due to the steric effects and the great number of water molecules should be replaced per one molecule of inhibitor, and the adsorption via oxygen heteroatom is also hindered due to steric effects. Then, the vertical

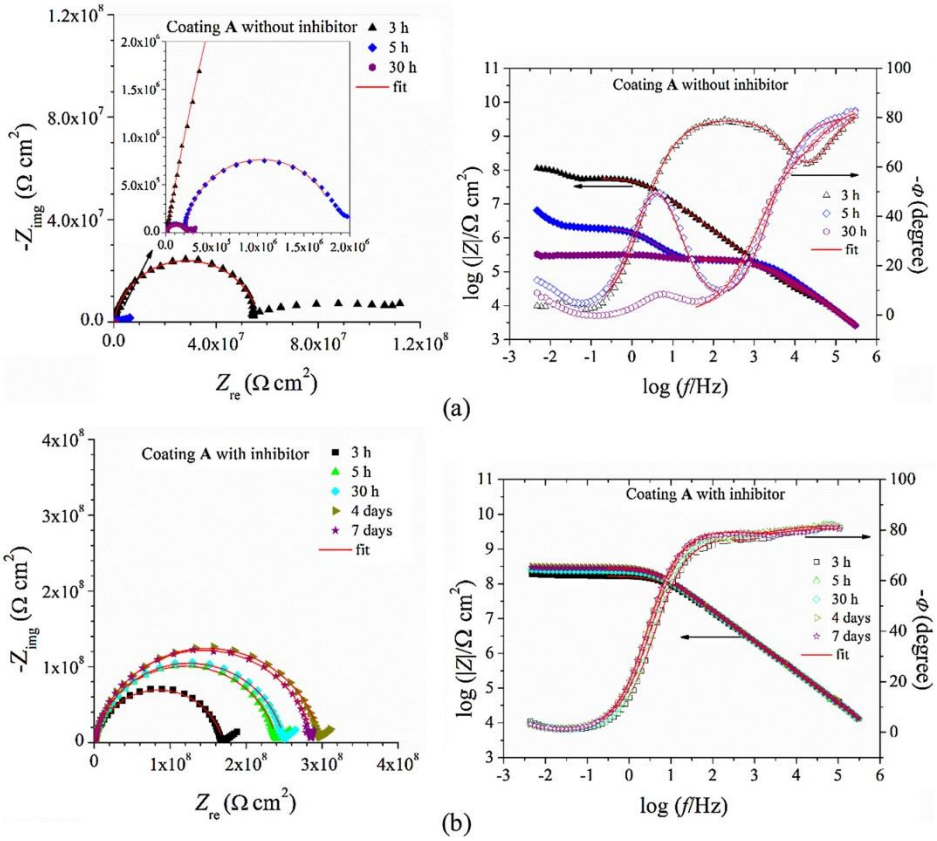

Fig. 6. Nyquist and Bode plots for coating **A** as function of the immersion time in unstirred and non-deaerated 3.5% NaCl solution: (a) without inhibitor, (b) with 4.41×10^{-2} mol L^{-1} tannin at 25 °C.

orientation of the inhibitor molecule towards the metallic surface is supposed most probable. Therefore, the adsorption of the inhibitor to the surface may occur via one alone electrons pair of a polar group like hydroxyl directly bonded to the first ring, which maintains the vertical orientation of the molecule towards the metal surface, as previously described [17]. The system is schematically represented in Fig. 3 and it is worth to note that this model considers a single aluminum atom. Teixeira et al. [30] used similar calculations to study the interaction of volatile corrosion inhibitors with zinc/zinc oxide surface, however, a more realistic metallic surface was considered with a zinc surface model (6 Å × 7 Å × 2 Å unit cell, optimized with 157 atoms) and a model of zinc oxide surface (5 Å × 5 Å × 2 Å unit cell, optimized with 207 atoms) instead of a single zinc atom.

3.3. Attenuated total reflectance Fourier transform infrared spectroscopy (FTIR-ATR)

Fig. 4 illustrates the FTIR-ATR spectra for the tannin inhibitor and for coatings A and B.

The band of hydroxyl groups, predominant in polyesters, is observed at 3356 cm^{-1}, evidencing hydrogen bonds formation [33,34]. However, it can be influenced by the urethane bond, because it has the N—H stretching from the urethane (—NH—CO—O) bond [35]. Thus, this band can be also related to the hydrogen bond of some free hydroxyl with secondary amine from urethane. The absence of the band at ca. 2270 cm^{-1} corroborates that NCO-free groups of the prepolymer were consumed during coating preparation and cure reactions [35,36]. Reactions responsible for NCO-free consumption are the ones leading to formation of allophanate and biuret bonds, and the reaction with moisture during cure.

IR bands at 1542 cm^{-1} and 1718 cm^{-1} are characteristic of the N—H vibration from the urethane (—NH—CO—O) bond and C═O bond, respectively [35]. The characteristic band of the aromatic ring in phthalic anhydride (PhA) is evidenced at 1619 cm^{-1}. Other bands between 1400-1000 cm^{-1} are attributed to the stretching of C—O(ester), and C—O—C, and angular deflection of H—O—C and C—H bonds also present in all oils and polyesters [33].

Tannin (Fig. 4) shows a band at 3220 cm^{-1} due to presence of hydroxyl groups. The two bands at 2930 cm^{-1} and 2696 cm^{-1} are characteristic of the symmetrical stretch of CH, CH_2, CH_3. Other stretching identified are the C═C—C at 1607 cm^{-1}, 1505 cm^{-1}, 1453 cm^{-1}, characteristic of aromatic compounds, C—O at 1311 cm^{-1}, 1207 cm^{-1}, 1157 cm^{-1}, and C—H in-plan and C—H out-of-plan, respectively, occurring at 1028 cm^{-1} and 842 cm^{-1} [15,19,37,38]. The features remain the same before and after immersion.

3.4. Corrosion studies

3.4.1. Open circuit potential (E_{OCP}) and electrochemical impedance spectroscopy (EIS)

For the aluminum alloy E_{OCP} is −0.71 V in the absence of tannin and −0.60 V in the presence of tannin. Fig. 5 depicts the evolution of E_{OCP} *vs.* time for both coatings **A** and **B** immersed in 3.5% NaCl solution without and with 4.41×10^{-2} mol L^{-1} tannin. For coating **A,** E_{OCP} decreases from -0.45 V to ~ −0.8 V in the absence of tannin and from ~ −0.15 V to −0.71 V in the presence of tannin during 7 days of immersion. In both conditions, the potential values reach the ones characteristic of Al alloys in chloride solution [39], indicating that the

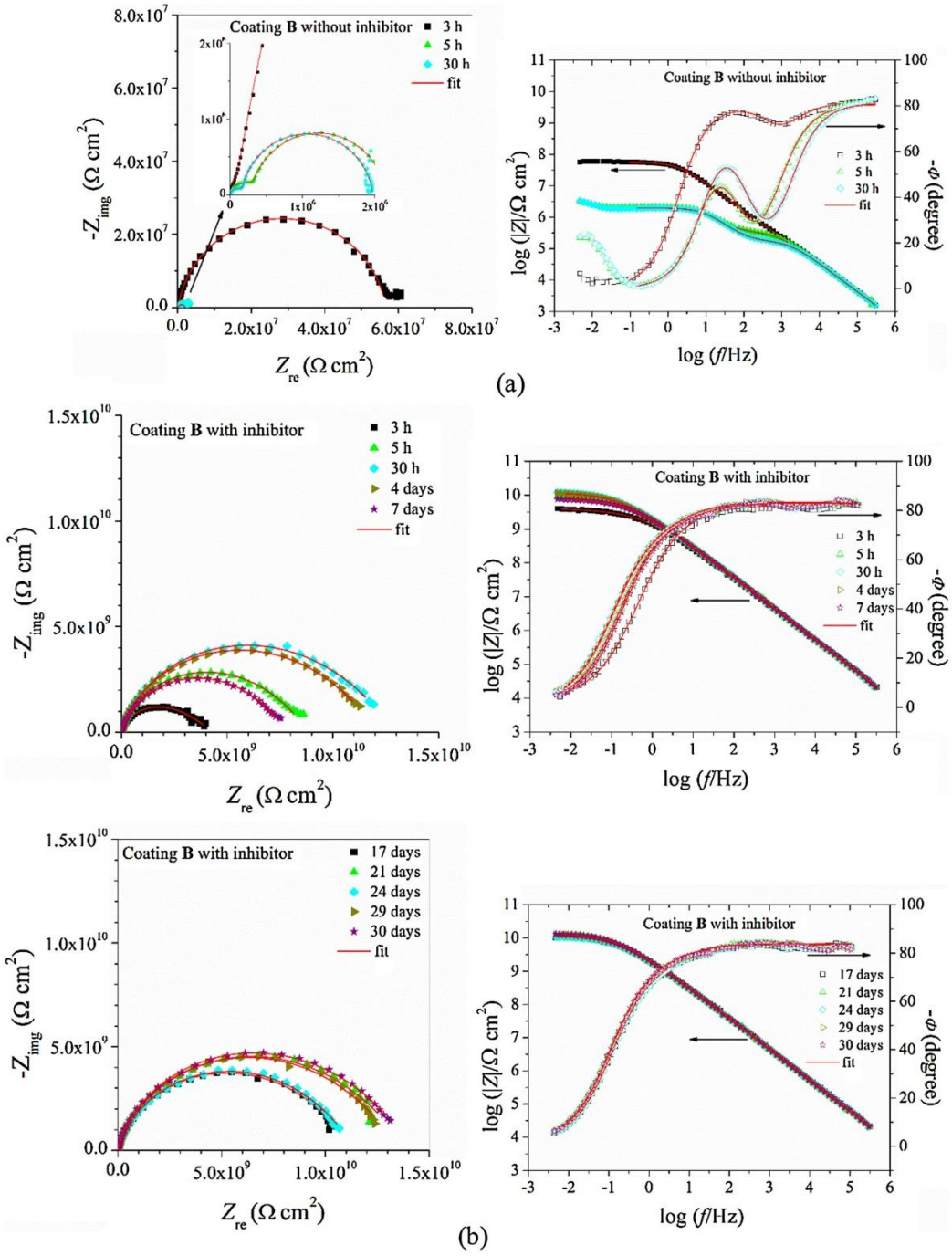

Fig. 7. Nyquist and Bode plots for coating **B** as function of the immersion time in unstirred and non-deaerated 3.5% NaCl solution: (a) without inhibitor, (b) with 4.41×10^{-2} mol L^{-1} tannin at 25 °C.

presence of tannin protects the coated substrate for few days only. In the absence of inhibitor, coating **A** protects the aluminum alloy only for few hours. Different situation can be observed for coating **B**, that in the absence of inhibitor behaves like coating **A** and in the presence of tannin seems to protect the substrate for much longer time - one month. Therefore, coating **B** shows E_{OCP} similar to the aluminum alloy in absence of inhibitor, but the values remain around −0.40 V for one month in the presence of inhibitor. This evidences that the presence of inhibitor protects the aluminum alloy in chloride medium. In a first analysis, the results seem contradictory, since in the absence of tannin the ticker coating is worse than the thinner one. However, in coating **A**, the shorter chains can be better organized on the surface than in coating **B** that forms longer chains due to slower cure. Thus, at early stage coating **A** may slow down electrolyte penetration, but being thinner, the electrolyte reaches the substrate earlier (after few hours). Tannin can protect effectively coating **A** for few days, due to its ability to adsorb on the metal surface and to protect the substrate for certain period. The inhibitor seems more efficient in the thicker coating **B** providing

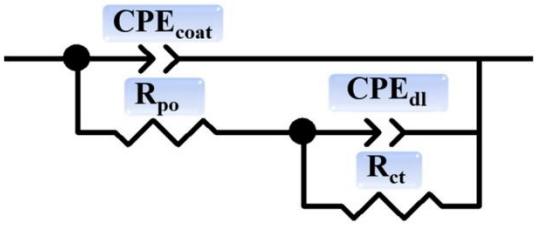

Fig. 8. Equivalent electrical circuits used to fit the organic coated aluminum alloy: (a) EEC adjusted EIS spectra of coatings **A** and **B** in the presence and absence of inhibitor.

corrosion protection for at least one month, as suggested by stabler E_{OCP} values that are approximately +300 mV more positive than the corrosion potential of the bare alloy.

Fig. 6**a** shows the Nyquist and Bode plots for coating **A** during immersion in 3.5% NaCl. The impedance values at high and medium frequencies, suggest poor substrate protection in the absence of inhibitor. Fig. 6**b** shows the Nyquist and Bode plots for coating **A** in 3.5% NaCl solution with 4.41×10^{-2} mol L^{-1} tannin and the evolution clearly indicates increased protection of the substrate. The impedance values, at low frequencies are slightly above 100 MΩ cm^2 and kept nearly constant up to 7 days of immersion.

Fig. 7**a** shows the Nyquist and Bode plots for coating **B** in 3.5% NaCl immersion. The impedance values show that the coating protects the substrate at early immersion times in absence of tannin inhibitor, however the values are slightly higher compared to the ones determined for coating **A**. Fig. 7**b** shows the Nyquist and Bode plots for coating **B** in presence of 4.41×10^{-2} mol L^{-1} tannin. The impedance values are significantly higher compared to the previous ones and after decay within the first week, there was a recovery, probably due to the presence of inhibitor at the bottom of the pores that reach the bare metal.

The Bode plots (Figs. 6a and 7a) showed phase angle values around

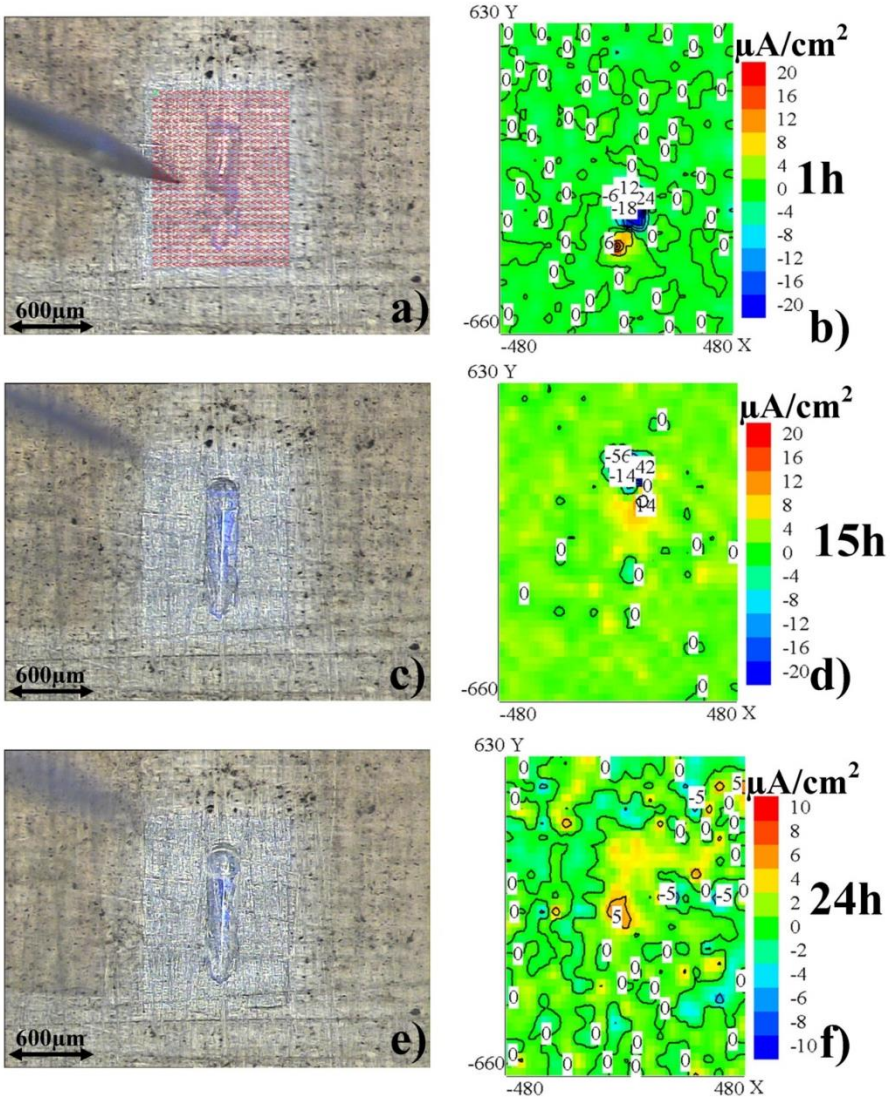

Fig. 9. Optic micrographs and current density distribution over coating **A** in chloride solution without inhibitor at different immersion times: **a)** and **b)** 1 h; **c)** and **d)** 15 h; **e)** and **f)** 24 h. Red markers in a) designate scanning points. X and Y coordinates represent the length of the scanned area in µm, respectively. (For interpretation of the references to colour in this figure legend, the reader is referred to the web version of this article.)

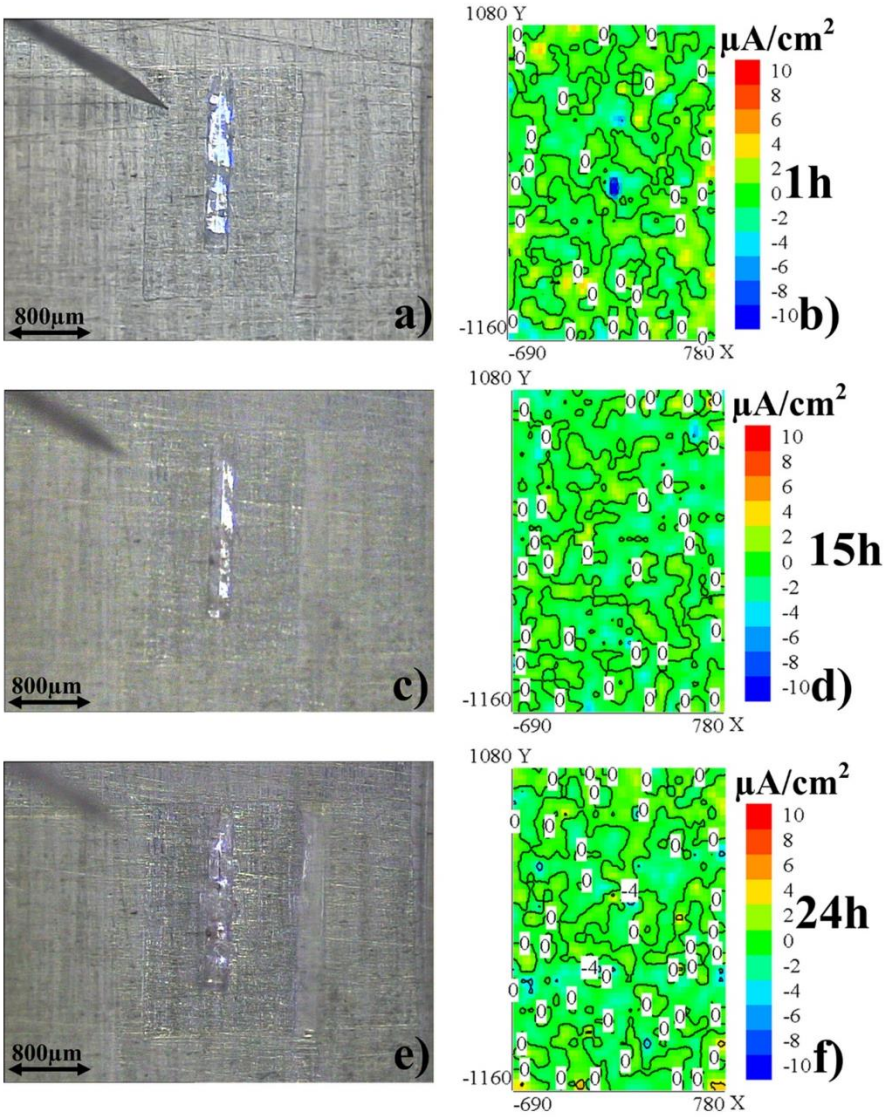

Fig. 10. Optic micrographs and current density distribution over coating **A** in chloride solution with inhibitor at different immersion times: **a)** and **b)** 1 h; **c)** and **d)** 15 h; **e)** and **f)** 24 h. Red markers in a) designate scanning points. X and Y coordinates represent the length of the scanned area in µm, respectively. (For interpretation of the references to colour in this figure legend, the reader is referred to the web version of this article.)

-80° at high frequencies. In the medium frequency range, a time constant is observed, and the phase angle becomes less negative with increasing the immersion time. These features evidence fast electrolyte uptake through the coatings and corrosion onset at the substrate in 3.5% NaCl, which in agreement with the decrease of the E_{OCP} to values close to those expected for the bare Al alloy (Fig. 5). The impedance moduli (|Z|) at low frequencies (Figs. 6**a** and 7 a) decrease more than one order of magnitude after 3 h of immersion, mainly for coating **A**, which is thinner than coating **B**. The values of $|Z|$ oscillate between 10^6 Ω cm² and 10^7 Ω cm², and the dispersion at low frequency indicates onset of corrosion activity, confirming the poor barrier effect of these coatings and corrosion activity in the absence of inhibitor.

The presence of the inhibitor in solution (Figs. 6**b** and 7 **b**) extends the protection time up to 7 days (coating **A**) and up to 30 days (coating **B**). In the presence of inhibitor, the phase angle is kept around -80 degrees in a wide frequency range for both coatings, pin pointing the good barrier effect. Furthermore, the low frequency impedance is stable, suggesting that the inhibitor may reach the metal surface slowing the charge transfer reaction, which shifted the corresponding time constant to very low frequencies compared to the spectra taken in the absence of inhibitor. The $|Z|$ values at low frequency are around 10^9 Ω cm² for coating **A** and 10^{10} Ω cm² for coating **B,** in the presence of inhibitor, demonstrating better protection in coating **B**.

EIS data were analyzed using the equivalent electrical circuits (EEC) depicted in Fig. 8. The capacitive contribution of the impedance plots was simulated using a constant phase element (CPE) instead of a pure capacitor due to the non-ideal behavior of the working electrode. The CPE has two components CPE-constant (CPE-T) related to the capacitance and CPE-power ($0 \leq n \leq 1$), the exponent. When $n = 1$ the CPE is a pure capacitance and $n = 0$ CPE is a pure resistance. CPE_{coat} means the constant phase element of the coating and R_{po} the resistance of the solution inside defects and pores of the coating. R_s was not included because it could be not assessed within the studied frequency range. The $CPE_{dl}//R_{ct}$ sub-circuit was added to the to account for the

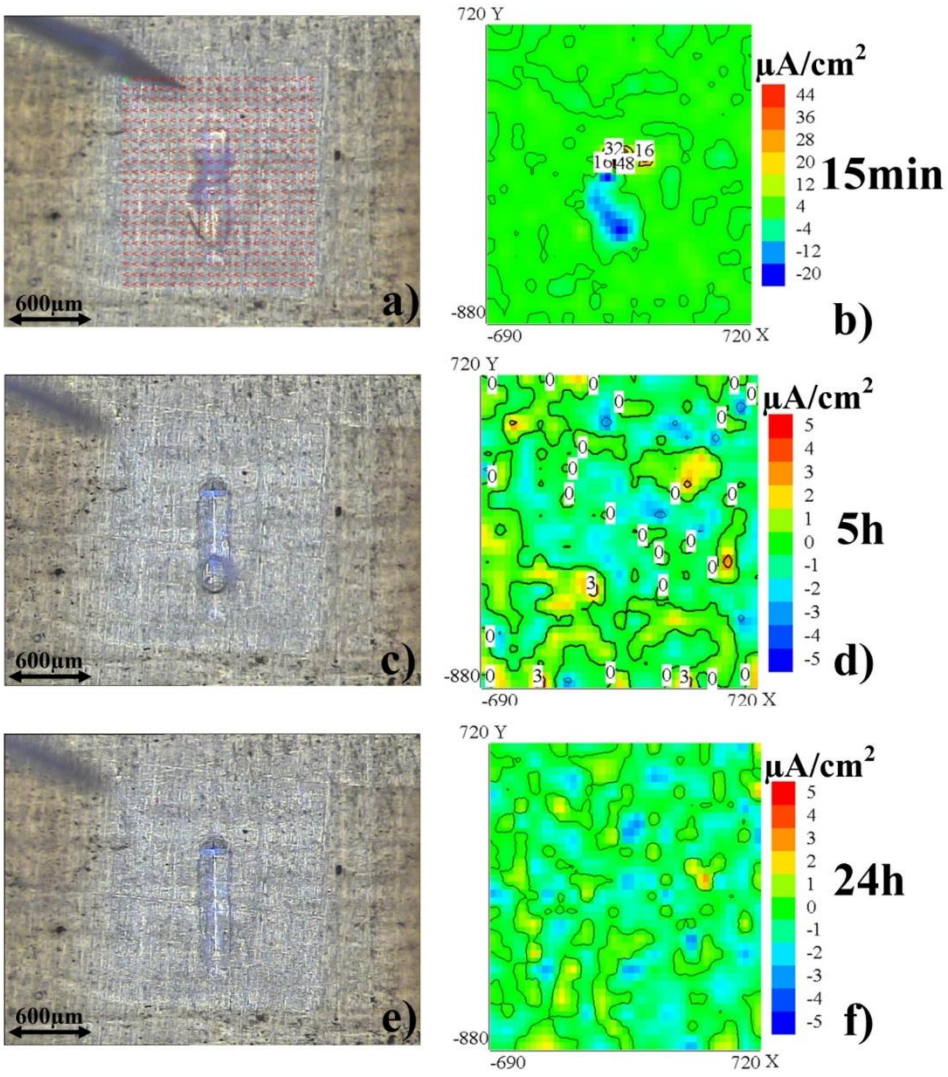

Fig. 11. Optic micrographs and current density distribution over scratched of coating **B** in chloride solution without inhibitor at different immersion times: **a)** and **b)** 15 min; **c)** and **d)** 5 h; **e)** and **f)** 24 h. Red markers in a) designate scanning points. X and Y coordinates represent the length of the scanned area in µm, respectively. (For interpretation of the references to colour in this figure legend, the reader is referred to the web version of this article.)

electrochemical reactions (aluminum oxidation and oxygen reduction) at the coating/metal interface. CPE_{dl}-T is related to the electrical double layer capacitance (C_{dl}), n_{dl} the exponent associated with the heterogeneous current distribution on the active surface area, and R_{ct} is the charge transfer resistance.

Table S1 (Supplementary Information) shows the EEC parameters used to fit the EIS data. For coating **A** the admittance of the CPE (~10^{-10} S cm^{-2} s^n) is little influenced by the addition of inhibitor, while the pore resistance increased from ~10^5 Ω cm^2 to ~10^7 Ω cm^2 in the presence of inhibitor. The admittance of the CPE of the electrical double layer (CPE-T_{dl}) decreased from ~10^{-9} S cm^{-2} s^n to ~10^{-11} S cm^{-2} s^n in presence of inhibitor, while the charge transfer resistance increased one order of magnitude (from ~10^7 Ω cm^2 to ~10^8 Ω cm^2). For coating **B**, the values of admittance for the CPE_{coat} decreased from ~10^{-9} S cm^{-2} s^n in the absence of inhibitor to 10^{-11} S cm^{-2} s^n in its presence, and the pore resistance increased from ~10^5 Ω cm^2 to ~10^8 Ω cm^2. The CPE-T_{dl} values decreased from ~10^{-8} S cm^{-2} s^n to 10^{-11} with the addition of inhibitor while R_{ct} increased from 10^6 Ω cm^2 to 10^9 Ω cm^2. For both coatings, the addition of inhibitor into the solution increased the charge transfer resistance and decreased the capacitance of the electric double layer, indicating that adsorption of inhibitor on the surface decrease the active area of the electrode. Coating **B** shows the best performance either in presence or absence of inhibitor.

3.4.2. Scanning vibrating electrode technique (SVET)

SVET measurements for coating **A** without and with inhibitor are depicted in Figs. 9 and 10, respectively, and for coating **B** without and with inhibitor in Figs. 11 and 12, respectively.

For both samples, corrosion activity is observed in the defect from the early immersion stages. Samples with coating **B** present higher corrosion activity that vanished after approximately 5 h up to the end of the experiment and no significant corrosion activity could be detected after 24 h of immersion. Samples with coating **A** remain active during 24 h of immersion, showing current density fluctuations. After approximately 16 h, current densities decrease and at the end of the measurements both anodic and cathodic activities are lower than at the earliest stages of immersion.

Fig. 13 presents SEM images and results of EDX analysis obtained

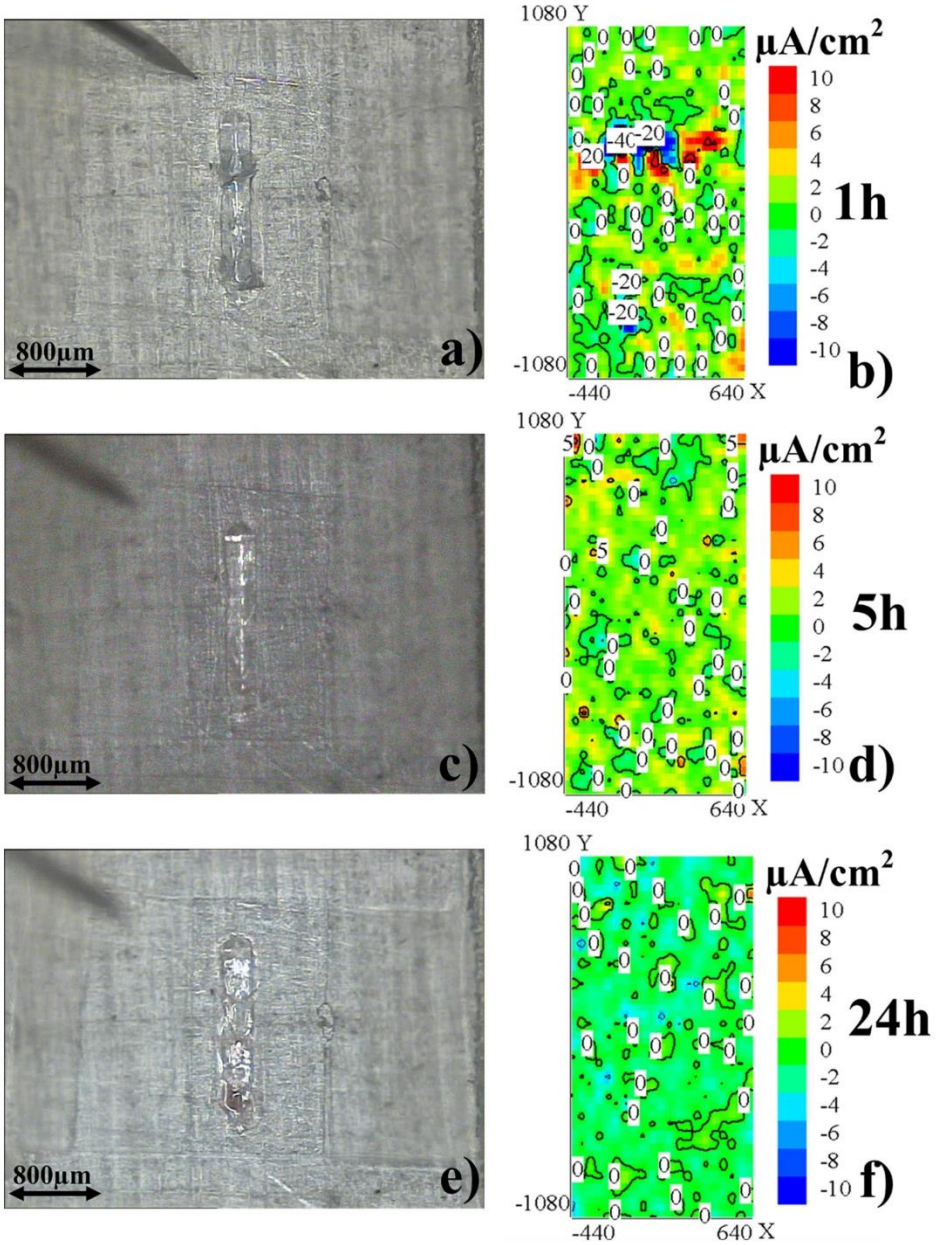

Fig. 12. Optic micrographs and current density distribution over scratched of coating **B** in chloride solution with inhibitor at different immersion times: **a)** and **b)** 1 h; **c)** and **d)** 5 h; **e)** and **f)** 24 h. Red markers in a) designate scanning points. X and Y coordinates represent the length of the scanned area in µm, respectively. (For interpretation of the references to colour in this figure legend, the reader is referred to the web version of this article.)

for coating **A** after the SVET (24 h of immersion) in the absence (Fig. 13a) and presence of inhibitor (Fig. 13b). The results evidence that the substrate has been exposed and oxidized during the exposure and that the Al concentration decreases more than half in the presence of inhibitor, probably due to adsorption of tannin in the scratch area.

4. Conclusions

The electrochemical results evidenced that tannin, a natural corrosion inhibitor, decreased corrosion activity and enhanced corrosion protection both in coated and uncoated samples. In the absence of inhibitor both coated samples showed low frequency impedance values around 10^6 Ω cm², but these values increased to ≈10^9 Ω cm² and 10^{10} Ω cm² in the presence of inhibitor for samples with coating **A** and **B**, respectively.

SVET measurements demonstrated that the presence of inhibitor improved the corrosion resistance of the exposed metal when both coatings were damaged.

For the main unit flavan-3-ol of tannin here used, the **HOMO** orbitals are located on the double bond of the first ring and oxygen heteroatom, suggesting that adsorption occurs vertically towards the surface via one alone electron pair locate at the polar group (OH) directly bonded to the first ring.

The results show that natural tannin is an efficient inhibitor for the

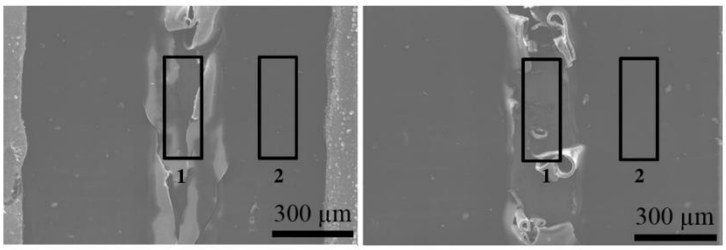

Location	C	O	Al
1	58.0	7.29	34.7
2	79.0	20.9	0.10

(a)

Location	C	O	Al
1	67.1	17.9	15.0
2	77.0	22.8	0.12

(b)

Fig. 13. SEM image and EDX analysis of coating **A** without inhibitor (a) and with inhibitor (b) after SVET measurements for 24 h followed by the elemental composition of the samples.

coated aluminum Alloy 1200 and, therefore, it has great potential to be used as anti-corrosive pigment in coatings for increased corrosion protection.

Acknowledgements

J.V. Nardeli author thanks the São Paulo state agency FAPESP (Process: 2015/10554-9 and 2018/09040-9) for scholarships and TANAC S.A. by providing the inhibitors. M.F. Montemor and M. Taryba acknowledge Fundação para Ciência e Tecnologia (FCT) for the funding under the project UID/QUI/00100/2019.

Appendix A. Supplementary data

Supplementary material related to this article can be found, in the online version, at doi:https://doi.org/10.1016/j.porgcoat.2019.05.035.

References

[1] P.A. Schweitzer, Fundamentals of Corrosion: Mechanisms, Causes, and Preventive Methods, first ed., Taylor and Francis Group, LLC, 2010 ISBN: 9781420067705.
[2] J.V. Nardeli, D.V. Snihirova, C.S. Fugivara, M.F. Montemor, E.R.P. Pinto, Y. Messaddecq, A.V. Benedetti, Localised corrosion assessement of crambe-oil-based polyurethane coatings applied on the ASTM 1200 aluminum alloy, Corros. Sci. 111 (2016) 422–435, https://doi.org/10.1016/j.corsci.2016.05.034.
[3] M. Finšgar, J. Jackson, Application of corrosion inhibitors for steels in acidic media for the oil and gas industry: a review, Corros. Sci. 86 (2014) 17–41, https://doi.org/10.1016/j.corsci.2014.04.044.
[4] M.F. Montemor, Active Protective Coatings: Fostering Green Inhibitors for Corrosion Prevention, Springer Book, 2016, https://doi.org/10.1007/978-94-017-7540-3_6.
[5] D. Snihirova, M. Taryba, S.V. Lamaka, M.F. Montemor, Corrosion inhibition synergies on a model Al-Cu-Mg sample studied by localized scanning electrochemical techniques, Corros. Sci. 112 (2016) 408–417, https://doi.org/10.1016/j.corsci.2016.08.008.
[6] E. Honarmand, H. Mostaanzadeh, M.H. Motaghedifard, M. Hadi, M. Khayadkashani, Inhibition effect of opuntia stem extract on corrosion of mild steel: a quantum computational assisted electrochemical study to determine the most effective components in inhibition, Prot. Met. Phys. Chem. Surf. 53 (2017) 560–572, https://doi.org/10.1134/S207020511703008X.
[7] J.C. da Rocha, J.A.C.P. Gomes, E. D'Elia, Corrosion inhibition of carbon steel in hydrochloric acid solution by fruit peel aqueous extracts, Corros. Sci. 52 (2010) 2341–2348, https://doi.org/10.1016/j.corsci.2010.03.033.
[8] A.K. Satapathy, G. Gunasekaran, S.C. Sahoo, K. Amit, P.V. Rodrigues, Corrosion inhibition by Justicia gendarussa plant extract in hydrochloric acid solution, Corros. Sci. 51 (2009) 2848–2856, https://doi.org/10.1016/j.corsci.2009.08.016.
[9] E. Gileadi, Electrode Kinetics for Chemists, Chemical Engineers, and Materials Scientists, VCH, 1993 ISBN: 1560815612.
[10] R.M. Palou, O.O. Xomelt, N.V. Likhanova, Environmentally friendly corrosion inhibitors, in: M. Aliofkhazraei (Ed.), Developments in Corrosion Protection, InTech, 2014, pp. 431–465, , https://doi.org/10.5772/57252.
[11] M. Aliofkhazraei, Developments in Corrosion Protection, InTech, 2014 ISBN: 978-953-51-1223-5.
[12] J.A. Jaén, J. Obaldía, M.V. Rodríguez, Application of Mössbauer spectroscopy to the study of tannins inhibition of iron and steel corrosion, Hyperfine Interact. 202 (2011) 25–38 https://10.1007/s10751-011-0337-1.
[13] J. Gust, J. Suwalski, Use of mössbauer spectroscopy to study reaction products of polyphenols and iron compounds, Corros. Sci. 50 (1994) 355–365, https://doi.org/10.5006/1.3294344.
[14] A.G. Brown, H.C. Ko, Black Wattle and Its Utilization-Abridged English Edition, RIRDC 97/72, Rural Industries Research and Development, Corporation, Barton, Australia, (1997).
[15] R.S. Peres, E. Cassel, D.S. Azambuja, Black wattle tannin as steel corrosion inhibitor, Int. Schol. Res. Net. 2012 (2012) 1–9, https://doi.org/10.5402/2012/937920.
[16] S. Martinez, I. Štagljar, Correlation between the molecular structure and the corrosion inhibition efficiency of chestnut tannin in acidic solutions, J. Molec. Struc.: Theochem. 640 (2003) 167–174, https://doi.org/10.1016/j.theochem.2003.08.126.
[17] S. Martinez, Inhibitory mechanism of mimosa tannin using molecular modeling and substitutional adsorption isotherms, Mater. Chem. Phys. 77 (2002) 97–102, https://doi.org/10.1016/S0254-0584(01)00569-7.
[18] N.C. Michael, J.A. Olubunmi, The corrosion inhibition of mild steel in sulphuric acid solution by flavonoid (catechin) separated from Nypa fruticans Wurmb leaves extract, Sci. J. Chem 2 (2014) 27–32 https://10.11648/j.sjc.20140204.11.
[19] A.A. Rahim, E. Rocca, J. Steinmetz, M.J. Kassim, R. Adnan, M. Sani Ibrahim, Mangrove tannins and their flavanoid monomers as alternative steel corrosion inhibitors in acidic medium, Corros. Sci. 49 (2007) 402–417, https://doi.org/10.1016/j.corsci.2006.04.013.
[20] R.G. Buchheit, H. Guan, S. Mahajanam, F. Wong, Active corrosion protection and corrosion sensing in chromate-free organic coatings, Prog. Org. Coat. 47 (2003) 174–182, https://doi.org/10.1016/j.porgcoat.2003.08.003.
[21] R.G. Pearson, Absolute electronegativity and hardness: application to inorganic chemistry, Inorg. Chem. 27 (1988) 734–740, https://doi.org/10.1016/j.corsci.2008.08.043.
[22] A. Dutta, S.K. Saha, U. Adhikari, P. Banerjee, D. Sukul, Effect of substitution on corrosion inhibition properties of 2-(substituted phenyl) benzimidazole derivatives on mild steel in 1 M HCl solution: a combined experimental and theoretical approach, Corros. Sci. 123 (2017) 256–266, https://doi.org/10.1016/j.corsci.2017.04.017.
[23] O. Kikuchi, Systematic QSAR procedures with quantum chemical descriptors, Quant. Struct. Act. Relat. 6 (1987) 179–184, https://doi.org/10.1002/qsar.19870060406.
[24] D.F.V. Lewis, C. Ioannides, D.V. Parke, Interaction of a series of nitriles with the alcohol-inducible isoform of P450: computer analysis of structure-activity relationships, Xenobiotica 24 (1994) 401–408, https://doi.org/10.3109/00498259409043243.
[25] ASTMD3359, Standard Test Methods for Measuring Adhesion by Tape Test, American Society for Testing Materials, West Conshohocken, 2009.
[26] ASTMD3363, Standard Test Method for Film Hardness by Pencil Test, American Society for Testing Materials, West Conshohocken, 2011.
[27] M.J. Frisch, G.W. Trucks, H.B. Schlegel, G.E. Scuseria, M.A. Robb, J.R. Cheeseman, et al., G09, Gaussian 09 (Revision D.2), Gaussian, Inc., Pittsburgh, 2009.
[28] B. Miehlick, A. Savin, H. Stoll, H. Preuss, Results obtained with the correlation energy density functionals of becke and Lee, Yang and Parr, Chem. Phys. Lett. 157 (1989) 200–206, https://doi.org/10.1016/0009-2614(89)87234-3.
[29] V.A. Rassolov, M.A. Ratner, J.A. Pople, P.C. Redfern, L.A. Curtiss, 6-31G* basis set for third-row atoms, J. Comput. Chem. 22 (2001) 976–984, https://doi.org/10.1002/jcc.1058.
[30] D.A. Teixeira, M.A.G. Valente Jr, A.V. Benedetti, G.T. Feliciano, S.C. da Silva, C.S. Fugivara, Experimental and theoretical studies of volatile corrosion inhibitors adsorption on zinc electrode, J. Braz. Chem. Soc. 26 (2015) 434–450, https://doi.org/10.5935/0103-5053.20140296.
[31] G. Gece, The use of quantum chemical methods in corrosion inhibitor studies, Corros. Sci. 50 (2008) 2981–2992, https://doi.org/10.1016/j.corsci.2008.08.043.

[32] H.R. Moeini, Synthesis and properties of novel polyurethane-urea insulating coatings from hydroxyl-terminated prepolymers and blocked isocyanate curing agent, J. Appl. Polym. Sci. 11 (2009) 3714–3720 https:\\doi.org/10.1002/app.29947.
[33] R.M. Silverstein, G.C. Bassler, T.C. Morrill, Spectrometric Identification of Organic Compounds, John Wiley & Sons, New York, 2000 ISBN: 9780471393627.
[34] R.S. Mishra, A.S. Khanna, Formulation and performance evaluation of hydroxyl terminated hyperbranched polyesters based poly (ester-urethane-urea) coatings on mild steel, Prog. Org. Coat. 72 (2011) 769–777 https:\\doi.org/10.1016/j.porgcoat.2011.08.009.
[35] A. Asefnejad, M.T. Khorasani, A. Behnamghader, B. Farsadzadeh, S. Bonakdar, Manufacturing of biodegradable polyurethane scaffolds based on polycaprolactone using a phase separation method: physical properties and in vitro assay, Int. J. Nanomed. 6 (2011) 2375–2384 https:\\doi.org/10.2147/IJN.S15586.
[36] D.K. Chattopadhyay, P.S.R. Prasad, B. Sreedhar, K.V.S.N. Raju, The phase mixing of moisture cured polyurethane-urea during cure, Prog. Org. Coat. 54 (2005) 296–304 https:\\doi.org/10.1016/j.porgcoat.2005.07.004.
[37] F.S. Grasel, M.F. Ferrão, C.R. Wolf, Development of methodology for identification the nature of the polyphenolic extracts by FTIR associated with multivariate analysis, Spectrochim. Acta Part A: Mol. Biom. Spectrosc. 153 (2016) 94–101, https://doi.org/10.1016/j.saa.2015.08.020.
[38] A.L. Missio, B. Tischer, P.S.B. Santos, C. Codevilla, C.R. Menezes, J.S. Barin, C.R. Haselein, J. Labidi, D.A. Gatto, A. Petutschnigg, G. Tondi, Analytical characterization of purified mimosa (Acacia mearnsii) industrial tannin extract: Single and sequential fractionation, Sep. Purif. Technol. 186 (2017) 218–225, https://doi.org/10.1016/j.seppur.2017.06.010.
[39] P.L. Cabot, A.H. Moreira, J.A. Garrido, A.V. Benedetti, E. Pérez, Electrochemical corrosion and microstructure of structural Al-Zn-Mg alloys, Curr. Topics Electrochem. 3 (1994) 1–18.

Material suplementar no Apêndice IV

4 Discussão

4.1 Preparação das resinas monolíticas

O estudo desenvolvido no Capítulo I demonstra um modo eficiente para obtenção das resinas / revestimentos de poliuretano. Para tal estudo foi avaliada a caracterização da matéria-prima, produtos intermediários (poliéster e pré-polímero) e produtos finais (resina monolítica) por ATR-FTIR (**Figura 9**), revelando que o espectro ATR-FTIR do óleo de crambe evidencia a ausência da banda –OH, como esperado, porque o óleo de crambe não possui hidroxila em sua estrutura; o espectro para o óleo de mamona evidencia a presença de –OH (3425 cm^{-1}). No caso do tanino condensado, a ausência da banda C=O (~ 1700 cm^{-1}) confirma que a estrutura é de tanino condensado e contribui para a inserção de OH (~ 3340 cm^{-1}) [45]. O espectro ATR-FTIR de poliéster confirma a eficácia da reação de modificação do óleo de crambe pela presença da banda –OH (3489 cm^{-1}). O espectro ATR-FTIR do pré-polímero mostra a presença da banda característica de NCO (2270 cm^{-1}) pertencente a grupos isocianato livre na estrutura química [45]. No espectro ATR-FTIR da resina PU, a banda atribuída aos grupos livres de NCO não é detectada, indicando / confirmando a reação completa entre o poliéster e o pré-polímero. As resinas de PU-modificada com tanino condensado contêm as bandas características de –OH (3346 cm^{-1}), N-H (3340 e 1527 cm^{-1}), C=O (1720 cm^{-1}), C-O (1249 cm^{-1}), O-H (1246 cm^{-1}) e –O-H (1120 cm^{-1}) ligações, que mostram claramente a formação de ligação de uretano [45].

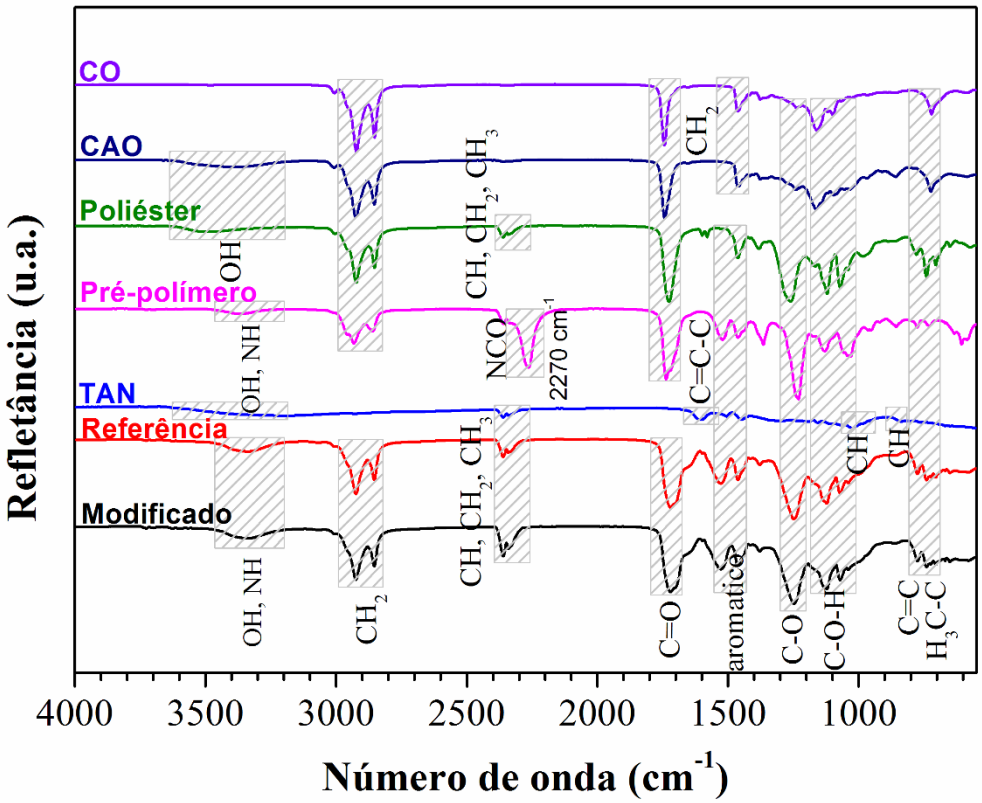

Figura 9. Espectros de ATR-FTIR para: matéria prima (óleo de crambe (CO) e mamona (CAO)), poliéster, pré-polímero, inibidor tanino condensado (TAN) e revestimentos (referência e modificado).

4.2 Aplicação dos revestimentos na proteção contra corrosão

Após o estudo desenvolvido no Capítulo I, que permitiu uma informação prévia sobre o sistema, dois estudos foram realizados visando aplicação do revestimento na proteção contra corrosão da liga AA2024-T3. Portanto, o estudo descrito no Capítulo II faz menção a aplicação dos revestimentos cuja formulação foi apresentada no item **Parte Experimental** denominados *Reference coating* e *Tannin-modified coating*. A **Figura 1**, Capítulo II mostra a micrografia SEM do mapeamento elementar da liga AA2024-T3 e EDX que evidencia os principais metais da liga: Al (**Figura 1b,** Capítulo II), Cu (**Figura 1c,** Capítulo II), Mn (**Figura 1d**, Capítulo II), Mg (**Figura 1e**, Capítulo II), Fe (**Figura 1f**, Capítulo II). A fase S (Al_2CuMg, **Figura 1g**, Capítulo II) é a fase intermetálica mais abundante na liga AA2024 e representa cerca de 60% dos precipitados e cobre cerca de 2,5-3% da área da superfície [13]. Esta abundância foi claramente

evidenciada nas **Figura 1c** e **1g** (Capítulo II) nas quais os precipitados ricos em Cu podem ser observados com dimensões abaixo de 10 µm. Esses precipitados desempenham um papel fundamental no processo de corrosão, pois atuam como locais preferenciais de nucleação de corrosão. Quando a fase S, enriquecida em Cu se dissolve, há abertura de vales na matriz de Al ao redor das partículas de Al_2CuMg, principalmente como resultado de sua autodissolução [13]. A presença de precipitados de Mn e Fe também foi observada - **Figura 1d**, Capítulo II e **Figura 1f**, Capítulo II. Esses intermetálicos também são suscetíveis à atividade de corrosão localizada. Em geral, os diferentes precipitados observados na **Figura 1** - Capítulo II, constituem locais preferenciais para o início da corrosão. A corrosão da liga AA2024 em soluções de NaCl é um processo complexo, envolvendo reações químicas e eletroquímicas que incluem a dissolução da fase S e a oxidação de Al a Al^{3+}, Mg a Mg^{2+}, oxidação e deposição de Cu, e redução de O_2 e H_2O para OH^-.

A imagem SEM da superfície dos revestimentos (**Figura 2a**, Capítulo II) revela uma superfície homogênea. A absorção de água dos monólitos (revestimento antes da aplicação na liga AA2024) representada na **Figura 2b**, Capítulo II, comprova que o revestimento referência exibe %*W* = 0,37, enquanto o revestimento modificado com tanino condensado exibe %*W* = 0,02. Este resultado sugere que a presença do tanino condensado aumenta significativamente o número de ligações de hidrogênio e, consequentemente, retarda a absorção de água. Uma das principais vantagens dos revestimentos de poliuretano à base de solventes orgânicos é a alta resistência à penetração de água, comparada aos revestimentos de poliuretano à base de água [13]. A **Figura 4** (Capítulo II) mostra a imagem da seção transversal, evidenciando a interface revestimento|AA2024 e a medida de espessura para ambos os revestimentos. A espessura média do revestimento referência é (364 ± 1) µm e o revestimento modificado com tanino condensado é (616 ± 1) µm. Os revestimentos apresentam homogeneidade, não evidenciam defeitos ou características como trincas ou buracos e de acordo com a norma da ASTM ambos os revestimentos foram classificados com adesão máxima (5B).

O estudo eletroquímico global deste sistema por meio da evolução de E_{OCP} *vs.* tempo (**Figura 5**, Capítulo II) em 0,6 mol L^{-1} NaCl para a liga AA2024 exposta a NaCl sem e com adição de tanino condensado (8,83 x 10^{-3} mol) revela

que para a liga AA2024, os valores de E_{OCP} são próximos a -0,60 V, enquanto que em NaCl contendo tanino condensado (solução) os valores são mais anódicos: ~ -0,53 V. Esse comportamento E_{OCP} sugere que, nessas condições experimentais, o tanino condensado funciona predominantemente como inibidor anódico. Este comportamento ocorre somente quando se usa a liga AA1200 [77]. Dando continuidade ao estudo eletroquímico global, a **Figura 6a** (Capítulo II) e a **Figura 6b** (Capítulo II) mostram um conjunto representativo de gráficos Nyquist e Bode para os revestimentos referência e modificado com tanino condensado, obtidos após 3 h, 336 h (2 semanas) e 672 h (4 semanas) de imersão em 0,6 mol L^{-1} NaCl. As medições de EIS refletem as mudanças que ocorrem no revestimento ou na interface metal / revestimento. Na **Figura 6a** (Capítulo II) na região de alta frequência, os gráficos Bode mostram uma constante de tempo com valores de ângulo de fase próximos a -85° e que se estende para uma grande região de frequência, como esperado quando os revestimentos fornecem boas propriedades de barreira. Em baixa frequência, um platô resistivo foi observado. A magnitude da impedância ($|Z|$) diminui de valores em torno de 1,0 x 10^{10} Ω cm^2 para valores próximos a 2,6 x 10^9 Ω cm^2 após 4 semanas de imersão para o revestimento referência (**Figura 6b,** Capítulo II). No entanto, para o revestimento modificado com tanino condensado, o valor inicial $|Z|$ foi uma ordem de magnitude maior e ao longo do tempo eles diminuíram de aproximadamente 1,0 x 10^{11} Ω cm^2 para 4,1 x 10^{10} Ω cm^2, sendo sempre acima daqueles do revestimento referência. Todos os valores confirmam as propriedades de barreira superiores dos revestimentos modificados com tanino condensado. Os circuitos elétricos equivalentes usados para quantificar os dados de impedância são mostrados na **Figura 6c, d**, Capítulo II. Nesta combinação, R_{po} e R_{tc} podem ser atribuídos, respectivamente, à resistência do poro do revestimento e à resistência de transferência de carga; R_s, a resistência da solução, não foi incluída porque não pôde ser avaliada dentro da faixa de frequência estudada; CPE_{po} e CPE_{dl} são os elementos de fase constante associados ao revestimento e à dupla camada elétrica respectivamente. Elementos de fase constante foram usados aqui em vez de capacitância pura devido aos desvios de um comportamento ideal de capacitor.

As **Figuras 7** e **8** (Capítulo II) mostram a evolução dos valores de admitância sobre o defeito artificial formado na superfície dos revestimentos de

referência e modificado com tanino condensado respectivamente. O revestimento referência - **Figura 7** (Capítulo II) mostra o aumento da atividade de corrosão ao longo do tempo, como esperado quando a liga de Al é exposta à solução de NaCl. Para o revestimento modificado com tanino condensado, há alguma atividade sobre o defeito, mas a atividade permanece baixa e tende a desaparecer com o tempo - **Figura 8**, Capítulo II.

Para melhor comparar as duas amostras, a **Figura 9** (Capítulo II) mostra a evolução da admitância determinada em cada instante em relação à admitância inicial ao longo do tempo de experimento. Ambas as amostras mostraram atividade similar nos estágios iniciais e aquela com o revestimento contendo tanino condensado mostrou atividade baixa e estável ao longo do tempo, indicando que o substrato permanece protegido, provavelmente devido à recuperação do revestimento, como confirmado por microscopia óptica e eletrônica de varredura (**Figura 10b**, Capítulo II). Para o revestimento referência, há um aumento gradual da admitância ao longo do tempo que se torna mais marcante após 20 h de imersão, sugerindo uma atividade de corrosão mais pronunciada, conforme confirmado por microscopia óptica e eletrônica de varredura (**Figura 10a**, Capítulo II).

Para o revestimento referência (**Figura 10a**, Capítulo II), a análise de EDX do ponto 1 (região de defeito) mostra a seguinte composição elementar / %massa: C (61,4), O (32,6) e Al (5,80). Sobre o ponto 2 (região livre de defeito) a composição elementar é C (75,0), O (24,6) e Al (0,29). A quantidade de Al na liga exposta é maior do que na parte revestida, como esperado. Estes resultados indicam danos no revestimento ao longo do tempo. Para o revestimento modificado com tanino condensado (**Figura 10b**, Capítulo II), a análise de EDX do ponto 1 (região de defeito, **Figura 11f**, Capítulo II) mostra a presença de C (80,3), O (19,5) e Al (0,12) e no local 2 (região livre de defeito) a composição é C (70,8), O (28,9) e Al (0,22). A quantidade de Al é similar, indicando que o revestimento modificado com tanino condensado se recuperou sobre o defeito, um efeito que pode ser atribuído à propriedade de *self-healing* introduzida pelo tanino condensado, como sugerido na **Figura 10**, Capítulo II.

As **Figuras 11** e **12** (Capítulo II) apresentam os resultados das medidas de densidade de corrente e pH quase-simultâneas (imersão em solução 0,05 mol L^{-1} NaCl) após 1, 8 e 24 h para o revestimento referência e após 1, 7 e 24 h para

o revestimento modificado com tanino condensado. A amostra revestida com o revestimento referência (**Figura 11**, Capítulo II) revelou fraca atividade de corrosão dentro do defeito durante o período de imersão. Esta atividade foi suficiente para induzir ligeira alcalinização sobre o defeito no final do teste de imersão, 24 h. Vale a pena mencionar que a atividade catódica não pôde ser detectada pela sonda SVET, provavelmente porque a espessura do revestimento dificulta a detecção de espécies carregadas negativamente formadas sob o revestimento. No entanto, os microeletrodos de pH são caracterizados por maior sensibilidade e podem detectar sinais de alcalinização, o que confirma a atividade local de corrosão.

Curiosamente, a atividade de corrosão observada sobre a amostra revestida com revestimento modificado com tanino condensado foi maior em comparação com a amostra de referência durante as primeiras 7-10 h de imersão (**Figura 12**, Capítulo II). Tanto a densidade de corrente como o pH, as distribuições indicaram um aumento precoce da atividade anódica até 7 h de imersão e, após houve uma diminuição repentina de atividade e o defeito permaneceu inativo até o final do teste de imersão.

A menor atividade sobre o defeito no revestimento referência, quando comparado com o revestimento modificado com tanino condensado, tem uma explicação possível. Devido ao defeito, a solução atinge o substrato e a dissolução anódica de Al acompanhada de redução de oxigênio ocorre localmente. Com o passar do tempo, o fenômeno se propaga sob o revestimento, levando à delaminação catódica. No entanto, as propriedades do revestimento e particularmente a sua capacidade de formar novas ligações de hidrogênio reparam as áreas danificadas do revestimento e atrasam a propagação da corrosão. Este efeito é ainda mais pronunciado na presença de tanino condensado. Tal efeito pode ser explicado pelo aumento do número de grupos -OH (confirmado por FTIR, **Figura 3** – Capítulo II) na estrutura do revestimento, que pode reparar as áreas danificadas do revestimento. É provável que o mecanismo de reparo envolva a formação de novas ligações de hidrogênio entre os grupos hidroxila do tanino condensado e / ou oxigênio dos grupos na matriz de poliuretano. Esse reparo do revestimento, em última análise inibe a atividade de corrosão sobre defeitos.

As **Figuras 13a** e **13b** (Capítulo II) apresentam as imagens SEM e os pontos de análise EDX para o revestimento referência e para o revestimento modificado com tanino condensado, respectivamente, após as medidas do SVET/SIET (24 h de imersão). Os resultados evidenciam que o substrato foi exposto e oxidado e que o teor de Al (região de defeito) é maior no revestimento referência (**Figura 13a**, Capítulo II). Para o revestimento modificado com tanino condensado (**Figura 13b**, Capítulo II), a região de defeito não revela a presença de alumínio, confirmando o efeito *self-healing*, em concordância com os resultados de LEIS (**Figura 10**, Capítulo II).

A análise EDX (**Figura 13a**, Capítulo II, revestimento referência) dos pontos 1 e 2 (região de defeito) mostrou a seguinte composição média elementar / %massa: C (67 ± 2); O (31 ± 2) e Al (2 ± 1), enquanto no local 3 (região livre de defeito) a composição / %massa foi: C (77) e O (23). A concentração de C diminuiu e o Al aumentou na região de defeito em comparação com a região livre de defeitos, indicando exposição do metal desprotegido e menos proteção do revestimento circundante. Para o revestimento modificado com tanino condensado (**Figura 13b**, Capítulo II), a composição média elementar / %massa dos pontos 1, 2 e 3 (região de defeito) foi: C (65 ± 4) e O (34 ± 4), enquanto no ponto 4 (região livre de defeito) a composição / %massa foi: C (71) e O (29). Estes resultados indicaram que o defeito original foi recoberto pelo revestimento (*self-healing*). Além disso, o revestimento modificado com tanino condensado tem um efeito benéfico, impedindo a propagação da corrosão sob o revestimento.

O revestimento referência permitiu a propagação das espécies e foram capazes de atingir a superfície. O processo de corrosão sob o revestimento e menos espécies foram capazes de atingir a superfície. Esta conclusão foi apoiada pela análise SEM / EDX após remover o revestimento da superfície (**Figuras 13c** e **13d**, Capítulo II) revelando uma área mais significativa de propagação do processo de corrosão sob o revestimento referência, enquanto no caso de revestimento modificado com tanino condensado, a maior parte do dano foi localizada diretamente na área do defeito.

O revestimento referência permitiu uma propagação mais rápida de espécies agressivas e, assim, o processo de corrosão sob o revestimento foi evidenciado tanto nas medições LEIS (**Figura 7**, Capítulo II) como SVET/SIET

(**Figura 11**, Capítulo II). Além disso, a delaminação do revestimento pode ser observada no final das medições eletroquímicas localizadas (**Figura 13c**, Capítulo II).

Contrariamente, o revestimento modificado com tanino condensado proporciona melhores propriedades de barreira e o revestimento evita eficientemente a propagação do processo de corrosão no defeito devido à sua propriedade de *self-healing* conferida pela presença de tanino condensado e maior número de grupos -OH na matriz do revestimento. O reparo do revestimento foi evidenciado ao final dos testes eletroquímicos localizados (**Figuras 10d**, **10f** e **13b**, Capítulo II). Além disso, a evolução do E_{OCP} sugeriu que o tanino condensado atua como inibidor anódico da liga Al, potencializando as propriedades protetoras do revestimento.

O estudo descrito no Capítulo III reporta a aplicação dos revestimentos cuja formulação foi apresentada no item **Parte Experimental** denominados *Unmodified coating* e *Modified coating*. Neste estudo foi utilizado outra matriz polimérica e uma concentração menor de tanino condensado.

As espessuras determinadas foram de 445,8 µm e 741,6 µm para o revestimento não modificado (sem tanino condensado) e revestimento modificado (com tanino condensado) respectivamente. A **Figura 2** (Capítulo III) mostra os ângulos de contato estáticos das superfícies: da liga AA2024 (sem revestimento e com os revestimentos). Este estudo forneceu informações sobre a hidrofobicidade da superfície - quanto maior o ângulo de contato, maior a hidrofobicidade da superfície, logo, menor absorção de água pelo revestimento. Portanto, evidencia que a aplicação do revestimento orgânico na superfície do AA2024 leva a um aumento no ângulo de contato de 76,1º para 90,1º. A adição de tanino condensado ao revestimento orgânico leva a um aumento no ângulo de contato de 90,1º para 94,6º.

O estudo eletroquímico global deste sistema por meio de medidas de E_{OCP} *vs.* tempo e EIS para os revestimentos não modificados e modificados obtidos após 2 h, 30 dias e 50 dias de imersão em solução de NaCl a 3,5% foram apresentados na **Figura 3**, Capítulo III.

A **Figura 3a** (Capítulo III) apresenta a evolução de E_{OCP} *vs.* tempo em solução de NaCl a 3,5% para a liga de substrato AA2024 e para revestimentos não modificados e modificados. Após 30 minutos de imersão (**Figura 3a**,

Capítulo III) os valores de E_{OCP} para a liga AA2024 estão próximos de -0,57 V/Ag|AgCl|KCl $_{3mol\ L-1}$, enquanto para o revestimento não modificado o valor é ~ -0,40 V/Ag|AgCl|KCl $_{3mol\ L-1}$. Quando a liga é revestida com o revestimento modificado, os valores de E_{OCP} são ~ -0,28 V/Ag|AgCl|KCl $_{3mol\ L-1}$. Durante todo o teste de imersão, o revestimento modificado apresentou um valor de potencial mais positivo que explica sua melhor propriedade de barreira em relação ao revestimento sem modificação.

A **Figura 3b** (Capítulo III) e a **Figura 3c** (Capítulo III) representam um conjunto de gráficos representativos do módulo de impedância Bode para os revestimentos não modificados e modificados obtidos após 2 h, 30 dias e 50 dias de imersão em solução de NaCl a 3,5%. Esses resultados abrangem a resposta eletroquímica para uma área de 1 cm^2 sem defeito artificial, permitindo estimar valores de $|Z|$ em torno de 3,0 x 10^{10} (2 h), 2,1 x 10^{10} (30 dias), 2,6 x 10^{10} (50 dias) para revestimento não modificado e $|Z|$ valores ~ 8,3 x 10^{10} (2 h), ~ 1,0 x 10^{11} (30 dias), ~ 4,2 x 10^{10} (50 dias) para revestimento modificado, sendo sempre mais altos que os do revestimento não modificado. Vale lembrar que a superfície do revestimento modificado é mais hidrofóbica, portanto, tem menos interação com a água.

As análises de LEIS (**Figura 4a**, Capítulo III) mostram que a admitância para o revestimento não modificado aumenta com o tempo de imersão, mostrando valor máximo após 24 h de imersão, correspondendo, assim, a valores mais baixos de impedância. No entanto, para o revestimento modificado (**Figura 4b**, Capítulo III), observa-se uma diminuição na admitância na zona do defeito artificial.

No final do teste de imersão (24 h em solução de NaCl 0,005 mol L^{-1}), ambos os defeitos foram observados por meio de imagem SEM e análise EDX (**Figura 5**, Capítulo III). A **Figura 5a** (Capítulo III) mostra que, para o revestimento não modificado, a análise EDX na região do defeito confirmou a presença de alumínio. Esse resultado indica que o processo de corrosão foi propagado da região do defeito sob o revestimento, atacando o substrato. Para o revestimento modificado (**Figura 5b**, Capítulo III), a análise EDX na zona de defeitos mostra a ausência de alumínio, indicando que o revestimento modificado apresenta o efeito *self-healing*, em concordância com os resultados de LEIS - diminuição da admitância na região do defeito.

De acordo com a literatura [13] e com o estudo demonstrado no Capítulo II, o revestimento modificado com tanino condensado proporcionou efeito *self-healing* na região do defeito. Em comparação com os resultados do Capítulo II (revestimento com maior quantidade de tanino condensado), o efeito *self-healing* inicia-se em ~5 h de imersão (Capítulo II - resultados de LEIS, **Figura 8**), enquanto no presente estudo (Capítulo III - resultados de LEIS, **Figura 4**), usando uma quantidade menor de tanino condensado e outra matriz polimérica, o efeito inicia-se após 15 h de imersão. A **Figura 10** apresenta uma ilustração da inicialização do efeito *self-healing* para ambos os sistemas (Capítulos II e III). Na **Figura 10a** nota-se menor propagação da corrosão na área ativa (região do defeito), enquanto que na **Figura 10b** nota-se uma região ativa mais intensa por toda extensão do defeito, e que diminui ao longo do tempo de imersão 15 h - 24 h de imersão.

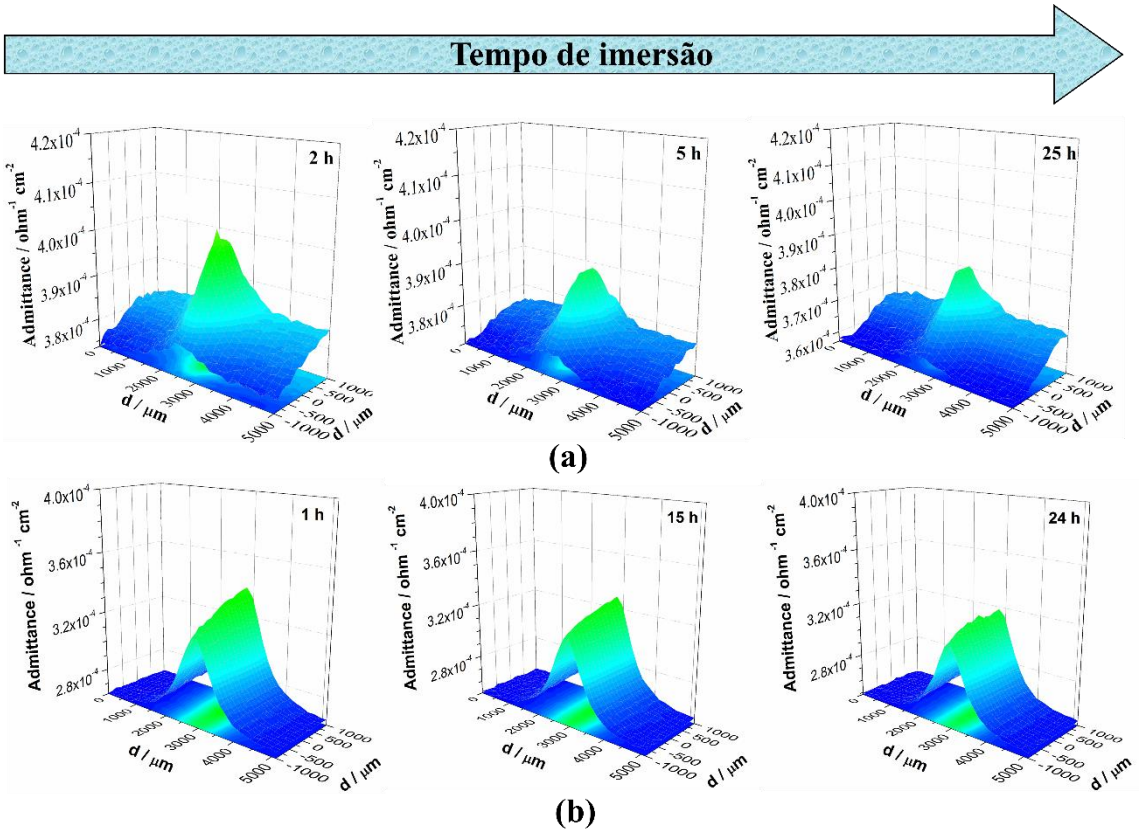

Figura 10. Inicialização do efeito *self-healing* para os revestimentos apresentados nos (a) Capítulo II – maior concentração de tanino e (b) Capítulo III – menor concentração de tanino.

Dessa forma, confirma-se que, alterando a matriz polimérica e diminuindo a quantidade de tanino condensado, o efeito *self-healing* é mantido; no entanto, o processo inicia-se após um tempo mais longo de imersão (~15 h). Portanto, para o desenvolvimento do revestimento inteligente é interessante aumentar a quantidade de tanino condensado, para que o efeito *self-healing* inicie em tempos mais curtos de imersão. Também é enfatizada a importância da interação entre a matriz polimérica e o tanino condensado, para que essa combinação melhore o desempenho do revestimento contra a corrosão.

Resumindo, a incorporação de tanino condensado no revestimento à base de poliuretano introduz um elevado número de grupos -OH, que favorecem a reticulação na estrutura química do polímero, contribuindo para o seu efeito *self-healing*. A **Figura 11** ilustra o mecanismo de proteção proposto para esse sistema. O efeito *self-healing* foi monitorado e registrado por meio de imagens de microscópio e um vídeo é apresentado no Apêndice III.

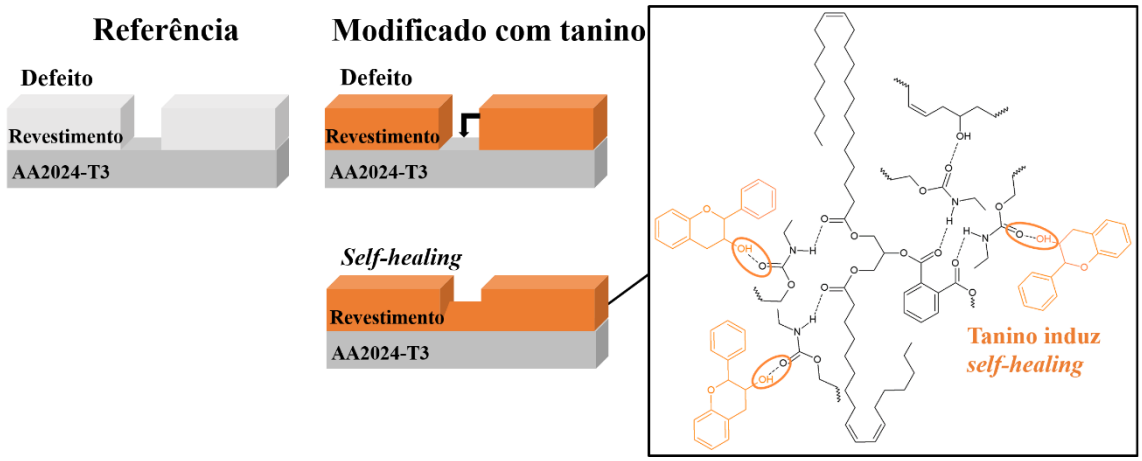

Figura 11. Ilustração do mecanismo de proteção quando aplicado um defeito artificial na superfície do revestimento referência e revestimento modificado com tanino condensado.

Com isso, os estudos desenvolvidos nesta tese contribuem, sobretudo, no entendimento dos fenômenos de corrosão e efeito *self-healing* nos revestimentos orgânicos quando incorporado inibidor de corrosão na formulação, que demonstram elevado interesse tecnológico.

Os resultados indicam que as técnicas localizadas fornecem informações complementares e evidenciam o efeito *self-healing* do revestimento à base de tanino condensado. Os resultados são consistentes com estudos de EIS relatados [79], em que foi mostrado que a incorporação de tanino condensado melhorou a resistência à corrosão da liga AA2024 revestida. Neste trabalho, combinando diferentes técnicas localizadas, foi demonstrado que a eficácia da proteção foi mantida sobre áreas de revestimento riscado na presença de NaCl.

5 Conclusões

Esta tese demonstrou a viabilidade da preparação de resinas monolíticas de poliuretano que possibilitam um estudo prévio do sistema antes de ser aplicado à superfície metálica. Novas abordagens como a incorporação de inibidor de corrosão (tanino condensado) foram capazes de produzir resinas e revestimentos orgânicos com propriedades *self-healing*. Em especial destaca-se por conter uma variedade de formulações que utilizam como matéria-prima produtos naturais (óleo de crambe, óleo de mamona, inibidor de corrosão – tanino condensado) e que oferecem efeito *self-healing* a estrutura do revestimento. Assim, os resultados obtidos permitem as seguintes afirmações:

1) As resinas de poliuretano (PU) produzidas a partir de óleos vegetais e a resina PU modificada com tanino condensado foram obtidos com sucesso e caracterizadas por diferentes técnicas químicas. Os espectros de ATR-FTIR possibilitaram a caracterização da matéria-prima (óleos e inibidor de corrosão) e a confirmação da formação do poliéster, pré-polímero, resina de PU e resina de PU modificada com tanino condensado.
2) Os revestimentos de PU e sua capacidade de proteção contra corrosão foram estudados usando uma combinação de multitécnicas: físico-químicas e eletroquímicas. Os revestimentos de PU modificados com tanino condensado forneceram evidências experimentais de melhoria da proteção contra a corrosão da liga AA2024-T3 revestida. Os revestimentos modificados retardaram a absorção de água em comparação com os revestimentos de PU sem incorporação de tanino condensado. Os valores de E_{OCP} sugerem que o tanino condensado é predominantemente um inibidor anódico e os resultados de EIS evidenciaram as excelentes propriedades de barreira dos revestimentos e que a resistência dos poros dos revestimentos modificados era uma ordem de magnitude acima do revestimento sem tanino condensado.
3) A combinação das análises LEIS, SVET / SIET e SEM / EDX demonstram que os revestimentos modificados com tanino condensado são capazes de impedir o progresso da corrosão, enquanto reparam o revestimento nas áreas danificadas. Assim, os revestimentos modificados com tanino

condensado fornecem proteção eficiente e aprimorada à liga AA2024-T3 contra a corrosão.

4) As resinas monolíticas e revestimentos produzidos pela incorporação de tanino condensado, exibem efeito *self-healing* após algumas horas de imersão. O efeito foi confirmado por meio de técnicas de microscopia óptica e SEM / EDX.
5) Esses estudos abrem grandes possibilidades para novas formulações de poliuretano à base de óleos vegetais e revestimentos de poliuretano modificados com tanino condensado ou outros inibidores de corrosão que podem ser usados para prolongar a vida útil de diferentes superfícies metálicas.

Perspectivas futuras do trabalho

- Avaliar a influência da quantidade de tanino condensado no revestimento e inicialização do efeito *self-healing*, utilizando outros substratos metálicos.
- Explorar as propriedades dos revestimentos em outras condições experimentais (baixa temperatura, câmara de névoa salina – *Salt Spray*).
- Explorar as propriedades dos revestimentos com inibidores encapsulados.
- Testar outras metodologias para depositar o revestimento na superfície do substrato.

Referências bibliográficas

[1] DAVIS, J. R. **ASM specialty handbook**: aluminum and aluminum alloys. 2nd ed. Materials Park: ASM International, 1993. Chapter 2, p. 1-31.

[2] ALCOA: ASSOCIAÇÃO BRASILEIRA DO ALUMÍNIO. **Fundamentos e aplicações do alumínio**. São Paulo, 2007. (Acervo de publicações). Disponível em: <http://www.abal.org.br/biblioteca/acervo-abal/>. Acesso em: 01 nov. 2019.

[3] MINATEL, R. **Um estudo comparativo sobre a recristalização de chapas de alumínio AA1200 e AA3003 obtidas por lingotamento contínuo *(twin roll caster)* e por fundição de placas *(direct chill)***. 2009. 63 f. Dissertação (Mestrado em Engenharia Metalúrgica e de Materiais) - Escola Politécnica, Universidade de São Paulo, São Paulo, 2009.

[4] ABNT NBR ISO 209:2010: Alumínio e suas ligas - Classificação da composição química / Aluminum and its alloys - Chemical composition classification, ABNT - Associação Brasileira de Normas Técnicas (2010).

[5] POSTAL, M. **Materiais para construção mecânica**. Uberlândia: Centro Nacional de Tecnologia em Alimentos, “Fábio de Araújo Motta, Serviço Nacional de Aprendizagem Industrial, 1999. 98 p.

[6] GOMES, M. R.; BRESCIANI, E. Propriedades e usos de metais não ferrosos, ABM, São Paulo, 1987.

[7] HATCH, J. E. **Aluminum**: properties and physical metallurgy. Materials Park: **American Society Metals**, 320 p., 1984.

[8] BUCHHEIT, R. G. A compilation of corrosion potentials reported for intermetallic phases in aluminum alloys. **Journal of the Electrochemical Society**, v. 142, p. 3994–3996, 1995.
https://doi.org/10.1149/1.2048447

[9] BIRBILIS, N.; BUCHHEIT, R. G. Electrochemical characteristics of intermetallic phases in aluminum alloys na experimental survey and discussion. **Journal of the Electrochemical Society**, v. 152. p. B140–B151, 2005.
https://doi.org/10.1149/1.1869984

[10] DORIN, T.; VAHID, A.; LAMB, J. (2018). Aluminium Lithium Alloys. 10.1016/B978-0-08-102063-0.00011-4.

[11] DURSUN, T.; SOUTIS, C. Recent developments in advanced aircraft aluminium alloys. **Materials and Design**, n. 56, p. 962-871, 2014.

[12] LAMAKA, S. V.; ZHELUDKEVICH, M. L.; YASAKAU, K. A.; MONTEMOR, M. F.; FERREIRA, M. G. S. High effective organic corrosion inhibitors for 2024 aluminium alloy. **Electrochimica Acta**, v. 52, p. 7231-7247, 2007.
https://doi.org/10.1016/j.electacta.2007.05.058

[13] NARDELI, J. V.; FUGIVARA, C. S.; TARYBA, M.; MONTEMOR, M. F.; RIBEIRO, S. J. L.; BENEDETTI, A. V. Novel healing coatings based on natural-derived polyurethane modified with tannins for corrosion protection of AA2024-T3. **Corrosion Science**, v. 162, p. 108213, 2020.
https://doi.org/10.1016/j.corsci.2019.108213

[14] SHI, H.; TIAN, Z.; HU, T.; LIU, F.; HAN, E.; TARYBA, M.; LAMAKA, S. V. Simulating corrosion of Al_2CuMg phase by measuring ionic currents, chloride concentration and pH. **Corrosion Science**, v. 88, p. 178-186, 2014.
https://doi.org/10.1016/j.corsci.2014.07.021

[15] BALASKAS, A. C.; KARTSONAKIS, I. A.; SNIHIROVA, D.; MONTEMOR, M. F.; KORDAS, G. Improving the corrosion protection properties of organically modified silicate–epoxy coatings by incorporation of organic and inorganic inhibitors. **Progress in Organic Coatings**, v. 72, p. 653-662, 2011.
https://doi.org/10.1016/j.porgcoat.2011.07.008

[16] SNIHIROVA, D.; LIPHARDT, L.; GRUNDMEIER, G.; MONTEMOR, M. F. Electrochemical study of the corrosion inhibition ability of “smart” coatings applied on AA2024. **Journal of Solid State Electrochemistry**, v. 17, p. 2183-2192, 2013.
https://doi.org/10.1007/s10008-013-2078-3

[17] MARCOEN, K.; VISSER, P.; TRINDADE, G. F.; ABEL, M. -L.; WATTS, J. F.; MOL, J. M. C.; TERRYN, H.; HAUFFMAN T. Compositional study of a corrosion protective layer formed by leachable lithium salts in a coating defect on AA2024-T3 aluminium alloys. **Progress in Organic Coatings**, v. 119, p. 65-75, 2018.
https://doi.org/10.1016/j.porgcoat.2018.02.011

[18] MRAD, M.; AMOR, Y. B.; DHOUIBI, L.; MONTEMOR, M. F. Effect of AA2024-T3 surface pretreatment on the physicochemical properties and the anticorrosion performance of poly(γ-glycidoxypropyltrimethoxysilane) sol-gel coating. **Surface and Interface Analysis**, v. 50, p. 335-345, 2018.
https://doi.org/10.1002/sia.6373

[19] BUCHHEIT, R. G.; GUAN, H.; MAHAJANAM, S.; WONG, F. Active corrosion protection and corrosion sensing in chromate-free organic coatings. **Progress in Organic Coatings**, v. 47, p. 174-182, 2003.
https://doi.org/10.1016/j.porgcoat.2003.08.003

[20] MRAD, M.; AMOR, Y. B.; DHOUIBI, L.; MONTEMOR, M. F. Corrosion prevention of AA2024-T3 aluminum alloy with a polyaniline/poly(γ-glycidoxypropyltrimethoxysilane) bi-layer coating: Comparative study with polyaniline mono-layer feature. **Surface and Coatings Technology**, v. 337, p. 1-11, 2018.
https://doi.org/10.1016/j.surfcoat.2017.12.053

[21] VISSER, P.; TERRYN, H.; MOL, J. M. C. On the importance of irreversibility of corrosion inhibitors for active coating protection of AA2024-T3. **Corrosion Science**, v. 140, p. 272-285, 2018.
https://doi.org/10.1016/j.corsci.2018.05.037

[22] VISSER, P.; LIU, Y.; ZHOU, X.; HASHIMOTO, T.; THOMPSON, G. E.; LYON, S. B.; VAN DER VEN, L. G. J.; MOL, A. J. M. C.; TERRYN, H. A. The corrosion protection of AA2024-T3 aluminium alloy by leaching of lithium-containing salts from organic coatings. **Faraday Discussions**, v. 180, p. 511-526, 2015.
https://doi.org/10.1039/C4FD00237G

[23] NARDELI, J. V.; SNIHIROVA, D. V.; FUGIVARA, C. S.; MONTEMOR, M. F.; PINTO, E. R. P.; MESSADDECQ, Y.; BENEDETTI, A. V. Localised corrosion assessement of crambe-oil-based polyurethane coatings applied on the ASTM 1200 aluminum alloy. **Corrosion Science**, v. 111, p. 422-435, 2016.
https://doi.org/10.1016/j.corsci.2016.05.034

[24] ZHU, Y.; ROMAIN, C.; WILLIAMS, C. K. Sustainable polymers from renewable resources. **Nature**, v. 540, p. 354-362, 2016.
https://doi.org/10.1038/nature21001

[25] RAHMAN, M. M.; RABBANI M. M.; SAHA J. K. Polyurethane and Its Derivatives. In: JAFAR M. M., SHEARDOWN, H.; AL-AHMED, A. (eds) Functional Polymers. Polymers and Polymeric Composites: A Reference Series. Springer, Cham. **2019**.
https://doi.org/10.1007/978-3-319-92067-2_7-1

[26] SZMECHTYK, T.; SIENKIEWICZ, N.; WOŹNIAK, J.; STRZELEC, K. Polyurethanes as self-healing materials. **Current Chemistry Letters**, v. 4, p. 61-66, 2015.
https://doi.org/10.5267/j.ccl.2015.3.001

[27] YANG, Z.; SHUAI, B.; ZHANG, X.; YU, H.; ZHANG, H.; JIA, Y.; ZHANG, C.; GUAN, X. Fabrication and performance of a polyurethane hybrid composite with waste red mud. **Polymer Composites**, v. 40, p. 2424-2431, 2019.
https://doi.org/10.1002/pc.25107

[28] KHALID, T.; ALBASHA; L.; QADDOUMI, N.; YEHIA, S. Feasibility Study of Using Electrically Conductive Concrete for Electromagnetic Shielding Applications as a Substitute for Carbon-Laced Polyurethane Absorbers in Anechoic Chambers. **IEEE Transactions on Antennas and Propagation**, v. 65, p. 2428-2435, 2017.
https://10.1109/TAP.2017.2670538

[29] ZHANG, C.; SHUAI, B.; ZHANG, X.; HU, X.; ZHANG, H.; JIA, Y.; YANG, Z.; GUAN, X. Polyurethane/Red Mud Composites with Flexibility, Stretchability, and Flame Retardancy for Grouting. **Polymers**, v. 10, p. 1-9, 2018.
https://10.3390/polym10080906

[30] XIANG, X. J., QIAN, J. W., YANG, W. Y., FANG, M. H.; QIAN, X. Q. Synthesis and properties of nanosilica-reinforced polyurethane for grouting. **Journal of Applied Polymer Science**, v. 100, p. 4333-4337, 2006.
https://doi.org/10.1002/app.23306

[31] YANG, Z.; ZHANG, X.; LIU, X.; GUAN, X.; ZHANG, C.; NIU, Y. Flexible and stretchable polyurethane/waterglass grouting material. **Construction and Building Materials**, v. 138, p. 240-246, 2017.
https://doi.org/10.1016/j.conbuildmat.2017.01.113

[32] ZAIMAHWATI; YUNIATI; JALAL, R. RIHAYAT, T.; ZHAFIRI, S. Synthesis and Characterization Thermal of Polyurethane/MMT from Castor Oil Polyols for Coating. **IOP Conference Series: Materials Science and Engineering**, v. 536, p. 1-8, 2019.
https://doi.org/10.1088/1757-899X/536/1/012037

[33] ZHAO, Z.; GUO, L.; FENG, L.; LU, H.; XU, Y.; WANG, J.; XIANG, B.; ZOU, X. Polydopamine functionalized graphene oxide nanocomposites reinforced the corrosion protection and adhesion properties of waterborne polyurethane coatings. **European Polymer Journal**, v. 120, p. 109249, 2019.
https://doi.org/10.1016/j.eurpolymj.2019.109249

[34] YE, X.; WANG, Z.; MA, L. QIANTING WANG, ANNI CHU, Zinc oxide array/polyurethane nanocomposite coating: Fabrication, characterization and corrosion resistance. **Surface and Coatings Technology**, v. 358, p. 497-504, 2019.
https://doi.org/10.1016/j.surfcoat.2018.11.080

[35] GARRISON, T. F.; KESSLER, M. R. Chap 3 - Plant Oil-Based Polyurethanes, Editor(s): MADBOULY, S.A.; ZHANG, C.; KESSLER, M. R. Bio-Based Plant Oil Polymers and Composites, William Andrew Publishing, p. 37-54, 2016.
https://doi.org/10.1016/B978-0-323-35833-0.00003-7

[36] ALAM, M.; AKRAM, D.; SHARMIN, E.; ZAFAR, F.; AHMAD, S. Vegetable oil based eco-friendly coating materials: A review article. **Arabian Journal of Chemistry**, v. 7, p. 469-479, 2014.
https://doi.org/10.1016/j.arabjc.2013.12.023

[37] PFISTER, D. P.; XIA, Y.; LAROCK, R. C. Recent advances in vegetable oil-based polyurethanes. **ChemSusChem**, v. 4, p. 703-717, 2011.
https://doi.org/10.1002/cssc.201000378

[38] PANDA, S. S.; PANDA, B. P.; NAYAK, S. K.; MOHANTY, S. A Review on Waterborne Thermosetting Polyurethane Coatings Based on Castor Oil: Synthesis, Characterization, and Application. **Polymer-Plastics Technology Engineering**, v. 57, p. 500-522, 2018.
https://doi.org/10.1080/03602559.2016.1275681

[39] GÄLLSTEDT, M.; PETTERSSON, H.; JOHANSSON, T.; NEWSON, W. R.; JOHANSSON, E.; HEDENQVIST, M. S. Film Extrusion of Crambe abyssinica/Wheat Gluten Blends. **Journal of Visualized Experiments**, v. 119, p. e54770, 2017.
https://doi.org/10.3791/54770

[40] RASEL, H.; JOHANSSON T.; GÄLLSTEDT, M.; NEWSON, W.; JOHANSSON, E.; HEDENQVISTINC, M. Development of bioplastics based on agricultural side-stream products: Film extrusion of Crambe abyssinica/wheat gluten blends for packaging purposes. **Journal of Applied Polymer Science**, v. 133, p. 42442, 2016.
https://doi.org/10.1002/app.42442

[41] ARBENZ, A.; AVÉROUS, L. Tannins: A Resource to Elaborate Aromatic and Biobased Polymers. In: Biodegradable and Biobased Polymers for Environmental and Biomedical Applications, Susheel Kalia and Luc Avérous (Eds.), Chapter 4, Wiley, 2016.
https://doi.org/10.1002/9781119117360.ch4

[42] MADBOULY, S. A.; OTAIGBE, J. U. Rheokinetics of thermal-induced gelation of waterborne plyurethane dispersions. **Macromolecules**, v. 38, p. 10178-10184, 2005.
https://doi.org/10.1021/ma0511088

[42] MADBOULY, S. A.; XIA, Y.; KESSLER, M. R. Rheological behavior of environmentally friendly castor oil-based waterborne polyurethane dispersions. **Macromolecules**, v. 46, p. 4606-4616, 2013.
https://doi.org/10.1021/ma400200y

[44] KARAK, N.; RANA, S.; CHO, J. W. Synthesis and characterization of castor-oil-modified hyperbranched polyurethanes. **Applied Surface Science**, v. 112, p. 736-743, 2009.
https://doi.org/10.1002/app.29468

[45] NARDELI, J. V.; FUGIVARA, C. S.; PINTO, E. R. P. P.; POLITO, W. L.; MESSADDECQ, Y.; RIBEIRO, S. J. L.; BENEDETTI, A. V. Preparation of polyurethane monolithic resins and modified with a condensed tannin yielding self-healing property. **Polymers**, v. 11, p. 1890, 2019.
https://doi.org/10.3390/polym11111890

[46] NARDELI, J. V.; FUGIVARA, C. S.; BENEDETTI, A. V. Environmentally Friendly coatings applied on aluminum alloy ASTM 1200. In Annual Meeting of the International Society of Electrochemistry, 64th, Santiago de Querétaro. Surface treatments. Switzerland: International Society of Electrochemistry, 1, 2013.

[47] NARDELI, J. V.; FUGIVARA, C. S.; TARYBA, M.; MONTEMOR, M. F.; BENEDETTI, A. V. Zn containing polymer coatings for AA7475: localized study of anti-corrosion performance. In The European Corrosion Congress – EUROCORR, Sevilha, Espanha, 1, 2019.

[48] TALBERT, R. Paint technology Handbook. CRC Press, 2007. ISBN: 9781574447033.

[49] FAZENDA, J. M. R. Tintas, ciência e tecnologia. Abrafati, São Paulo, 2009. ISBN: 9788521204749.

[50] XIE, F.; ZHANG, T.; BRYANT, P.; KURUSINGAL, V.; COLWELL, J. M.; LAYCOCK, B. Degradation and stabilization of polyurethane elastomers. **Progress in Polymer Science**, v. 90, p. 211-268, 2019. https://doi.org/10.1016/j.progpolymsci.2018.12.003

[51] ROSU, D.; ROSU, L.; CASCAVAL, C. N. IR-change and yellowing of polyurethane as a result of UV irradiation. **Polymer Degradation and Stability**, v. 94, p. 591-596, 2009. https://doi.org/10.1016/j.polymdegradstab.2009.01.013

[52] The chemistry of polyurethane coatings – a general reference manual, Bayer® material science. Available online: http://digitalcollections.library.cmu.edu/awweb/awarchive?type=file&item=488891 (accessed on 01 may 2019).

[53] GOLLING, F. E.; PIRES, R.; HECKING, A.; WEIKARD, J.; RICHTER, F.; DANIELMEIER, K.; DIJKSTRA, D. Polyurethanes for corrosion & adhesives – chemistry & applications. **Polymer International**, v. 68, p. 848-855, 2019. https://doi.org/10.1002/pi.5665

[54] GHOSH, S. K. **Self-healing Materials: Fundamentals, Design Strategies, and Applications**. Wiley-VCH, 2009.

[55] HORNAT, C. C.; URBAN, M. W. Shape memory effects in self-healing polymers. **Progress in Polymer Science**, in press, p. 101208, 2020.

[56] PULIKKALPARAMBIL, H.; SIENGCHIN, S.; PARAMESWARANPILLAI, J. Corrosion protective self-healing epoxy resin coatings based on inhibitor and polymeric healing agents encapsulated in organic and inorganic micro and nanocontainers. **Nano-Structures & Nano-Objects**, v. 16, p. 381-395, 2018. https://doi.org/10.1016/j.nanoso.2018.09.010

[57] NARDELI, J. V.; FUGIVARA, C. S.; MONTEMOR, F.; BENEDETTI, A. V. Smart coating for corrosion protection of aluminium alloys: global and localized study of anti- corrosion performance, A diversidade de debates na pesquisa em química v. 2. Atena, 2020.

[58] ODARCZENKO, M.; THAKARE, D.; LI, W.; YANG, K.; TANG, S.; VENKATESWARAN, S. P.; SOTTOS, N. R.; WHITE, S. R. Self-Protecting Epoxy Coatings with Anticorrosion Microcapsules, **ACS Omega**, v. 3, n. 10, p. 14157-14164, 2018. https://doi.org/10.1021/acsomega.8b01950

[59] VIMALANANDAN, A.; LV, L.-P.; TRAN, T. H.; LANDFESTER, K.; CRESPY, D.; ROHWERDER, M. Redox-Responsive Self-Healing for Corrosion Protection. **Advanced Materials**, v. 25, p. 6980-6984, 2013.
https://doi.org/10.1002/adma.201302989

[60] GARCÍA, S. J.; FISCHER, H. R.; WHITE, P. A.; MARDEL, J.; GONZALEZ-´ GARCÍA, Y.; MOL, J. M. C.; HUGHES, A. E. Self-Healing Anticorrosive Organic Coating Based on an Encapsulated Water Reactive Silyl Ester: Synthesis and Proof of Concept. **Progress in Organic Coatings**, v. 70, p. 142-149, 2011.
https://doi.org/10.1016/j.porgcoat.2010.11.021

[61] DIELEMAN, C. D.; DENISSEN, P. J.; GARCIA, S. J. Long-Term Active Corrosion Protection of Damaged Coated-AA2024-T3 by Embedded Electrospun Inhibiting Nanonetworks. **Advanced Materials Interfaces**, v. 5, p. 1800176, 2018.
https://doi.org/10.1002/admi.201800176

[62] ZHELUDKEVICH, M. L.; YASAKAU, K. A.; BASTOS, A. C.; KARAVAI, O. V.; FERREIRA, M. G. S. On the application of electrochemical impedance spectroscopy to study the self-healing properties of protective coatings. **Electrochemistry Communications**, v. 9, n. 10, p. 2622-2628, 2007.
https://doi.org/10.1016/j.elecom.2007.08.012

[63] WANG, X.; LIU, F.; ZHENG, X.; SUN, J. Water-Enabled Self-Healing of Polyelectrolyte Multilayer Coatings. **Angewandte Chemie**, v. 50, p. 11378-11381, 2011.
https://doi.org/10.1002/ange.201105822

[64] MONTEMOR, M. F.; FERREIRA, M. G. S. Electrochemical study of modified bis-[triethoxysilylpropyl] tetrasulfide silane films applied on the AZ31 Mg alloy, **Electrochimica Acta**, v. 52, p. 7486-7495, 2007.
https://doi.org/10.1016/j.electacta.2006.12.086

[65] GARCIA-HERAS, M.; JIMENEZ-MORALES, A.; CASAL, B.; GALVAN, J. C.; RADZKI, S.; VILLEGAS, M. A. Preparation and electrochemical study of cerium–silica sol-gel thin films. **Journal of Alloys and Compounds**, v. 380, p. 219-224, 2004.
https://doi.org/10.1016/j.jallcom.2004.03.047

[66] SHCHUKIN, D. G.; ZHELUDKEVICH, M.; YASAKAU, K.; LAMAKA, S.; FERREIRA, M. G. S.; MÖHWALD, H. Layer-by-Layer Assembled Nanocontainers for Self-Healing Corrosion Protection. **Advanced Materials**, v. 18, p. 1672-1678, 2006.
https://doi.org/10.1002/adma.200502053

[67] GHARBI, O.; THOMAS, S.; SMITH, C.; BIRBILIS, N. Chromate replacement: what does the future hold? **Nature Materials Degradation**, v. 2, p. 1-8, 2018.
https://doi.org/10.1038/s41529-018-0034-5

[68] DEVARAYAN, K.; MAYAKRISHNAN, G.; SULOCHANA, N. Green Inhibitors for Corrosion of Metals: A Review. **Chemical Science Review and Letters**, v. 1, p. 1-18, 2012.

[69] ZADEH, M. A.; TEDIM, J.; ZHELUDKEVICH, M.; ZWAAG, S. V. D.; GARCIA, S. J. Synergetic active corrosion protection of AA2024-T3 by 2D- anionic and 3D-cationic nanocontainers loaded with Ce and mercaptobenzothiazole. **Corrosion Science**, v. 135, p. 35-45, 2018.
https://doi.org/10.1016/j.corsci.2018.02.018

[70] MARTINEZ, S.; STEM, I. Inhibitory mechanism of low-carbon steel corrosion by mimosa tannin in sulphuric acid solutions. **Journal of Applied Electrochemistry**, v. 31, p. 973-978, 2001.
http://dx.doi.org/10.1023/A:1017989510605

[71] S. MARTINEZ, I. STERN, The thermodynamic characterization of metal dissolution and inhibitor adsorption processes in the low carbon steel/mimosa tannin/sulfuric acid system. **Applied Surface Science**, v. 199, p. 83-89, 2002.
https://doi.org/10.1016/S0169-4332(02)00546-9

[72] JAMES, A. O.; ATELA, A. O. Aloe vera: an inhibitor of aluminium corrosion in hydrochloric acid solution. **Pure and Applied Chemistry**, v. 3, p. 159-163, 2008.

[73] GERENGI, H.; SAHIN, H. I. Schinopsis lorentzii extract as a green corrosion inhibitor for low carbon steel in 1 M HCl solution. **Industrial & Engineering Chemistry Research**, v. 51, p. 780-787, 2012.
http://dx.doi.org/10.1021/ie201776q

[74] KRISHNEGOWDA, P. M.; VENKATESHA, V. T.; KRISHNEGOWDA, P. K. M.; SHIVAYOGIRAJU, S. B. Acalypha torta leaf extract as green corrosion inhibitor for mild steel in hydrochloric acid solution. **Industrial & Engineering Chemistry Research**, v. 52, p. 722-728, 2013.
http://dx.doi.org/10.1021/ie3018862

[75] PALOU, R. M.; XOMELT, O. O.; LIKHANOVA, N. V. **Environmentally friendly corrosion inhibitors, Developments in corrosion protection**, InTech, Chapter 19, p. 431-465, 2014.
https://dx.doi.org/10.5772/57252

[76] ALIOFKHAZRAEI, M. Developments in Corrosion Protection, InTech, 2014.

[77] NARDELI, J. V.; FUGIVARA, C. S.; TARYBA, M.; PINTO, E. R. P.; MONTEMOR, M. F.; BENEDETTI, A. V. Tannin: a natural corrosion inhibitor for bare and coated aluminum alloys. **Progress in Organic Coatings**, v. 135, p. 368-381, 2019.
https://doi.org/10.1016/j.porgcoat.2019.05.035

[78] RANI, B. E. A.; BASU, B. B. J. Green Inhibitors for Corrosion Protection of Metals and Alloys: An Overview. **International Journal of Corrosion**, v. 2012, p. 1-15, 2011.
https://dx.doi.org/10.1155/2012/380217

[79] DALMORO, V.; SANTOS, C.; SANTOS, J. H. Z. **Smart coatings for corrosion protetion, in book: Industrial Applications for intelligent Polymers and Coatings**, Chapter 20, p. 417-435, Springer, 2016.
https://doi.org/10.1007/978-3-319-26893-4_20

[80] YAHYA, S.; RAHIM, A. A.; SHAH, A. M.; ADNAN, R. Inhibitive behaviour of corrosion of aluminium alloy in NaCl by mangrove tannin. **Sains Malaysiana**, v. 40, p. 953-957, 2011.

[81] HERNES, P. J.; BENNER, R.; COWIE, G. L.; GOÑI, M. A.; BERGAMASCHI, B. A.; HEDGES, J. I. Tannin diagenesis in mangrove leaves from a tropical estuary: a novel molecular approach. **Geochimica Cosmochimica Acta**, v. 65, p. 3109-3122, 2001.
https://doi.org/10.1016/S0016-7037(01)00641-X

[82] PIZZI, A. Tannin-Based Biofoams-A Review, **Journal of Renewable Materials**, v. 7, p. 477-492, 2019.
https://doi.org/10.32604/jrm.2019.06511

[83] TONDI, G. Tannin-Based Copolymer Resins: Synthesis and Characterization by Solid State 13C NMR and FT-IR Spectroscopy. **Polymers**, v. 9, n. 6, p. 223, 2017.
https://doi.org/10.3390/polym9060223

[84] BANU, K.; SHIMURA, T.; SADEGHI, S. Selective detection and recovery of gold at tannin-immobilized non-conducting electrode. **Analytica Chimica Acta**, v. 853, p. 207-213, 2015.
https://doi.org/10.1016/j.aca.2014.09.030

[85] PERES, R. S.; CASSEL, E.; AZAMBUJA, D. S. Black wattle tannin as steel corrosion inhibitor. **International Scholarly Research Notices**, v. 2012, p. 1-9, 2012.
http://dx.doi.org/10.5402/2012/937920

[86] MARTINEZ, S.; ŠTAGLJAR, I. Correlation between the molecular structure and the corrosion inhibition efficiency of chestnut tannin in acidic solutions. **Journal of Molecular Structure: THEOCHEM**, v. 640, p. 167-174, 2003.
http://dx.doi.org/10.1016/j.theochem.2003.08.126

[87] MARTINEZ, S. Inhibitory mechanism of mimosa tannin using molecular modeling and substitutional adsorption isotherms. **Materials Chemistry and Physics**, v. 77, n. 1, p. 97-102, 2002.
http://dx.doi.org/10.1016/S0254-0584(01)00569-7

[88] MICHAEL, N. C.; OLUBUNMI, J. A. The corrosion inhibition of mild steel in sulphuric acid solution by flavonoid (catechin) separated from Nypa fruticans Wurmb leaves extract. **Science Journal of Chemistry**, v. 2, p. 27-32, 2014. https://10.11648/j.sjc.20140204.11

[89] RAHIM, A. A.; ROCCA, E.; STEINMETZ, J.; KASSIM, M. J.; ADNAN, R.; IBRAHIM, M. S. Mangrove tannins and their flavanoid monomers as alternative steel corrosion inhibitors in acidic medium. **Corrosion Science**, v. 49, p. 402-417, 2007.
http://dx.doi.org/10.1016/j.corsci.2006.04.013

[90] MATAMALA, G.; SMELTZER, W.; DROGUETT, G. Comparison of steel anticorrosive protection formulated with natural tannins extracted from acacia and from pine bark. **Corrosion Science**, v. 42, p. 1351-1362, 2000.
https://doi.org/10.1016/S0010-938X(99)00137-7

[91] PINTO, E. R. P. **Modificação de óleos vegetais e de origem animal para síntese de poliésteres e poliuretanos com baixo teor de compostos orgânicos voláteis**. 2012. 203 f. Tese (Doutorado em Química) – Instituto de Química, Universidade Estadual Paulista, Araraquara, 2012.

[92] COELHO, L. B.; TARYBA, M.; ALVES, M.; NOIRFALISE, X.; MONTEMOR, M. F.; OLIVIER, M. -G. The corrosion inhibition mechanisms of Ce(III) ions and triethanolamine on graphite-AA2024-T3 galvanic couples revealed by localised electrochemical techniques, **Corrosion Science**, v. 150, p. 207-217, 2019.
https://doi.org/10.1016/j.corsci.2019.02.007

[93] HUANG, V. M.; WU, S-L.; ORAZEM, M. E.; PÉBÈRE, N.; TRIBOLLET, B.; VIVIER, V. Local electrochemical impedance spectroscopy: A review and some recent developments, **Electrochimica Acta**, v. 56, p. 8048-8057, 2011.
https://doi.org/10.1016/j.electacta.2011.03.018

[94] INDIRA, K.; NISHIMURA, T. In-Situ electrochemical monitoring and ex-Situ chemical analysis of epoxy coated steels in sodium chloride environment using various spectroscopic techniques. **Transactions of the Indian Institute Metals**, v. 70, p. 2347-2360, 2017.
https://doi.org/10.1007/s12666-017-1096-8

[95] TING, W.; JUAN, D.; SHENG, Y.; LINGHUA, T.; JIAJUN, F. Triple stimuli-responsive smart nanocontainers enhanced self-healing anticorrosion coatings for protection of aluminum alloy. **ACS Applied Materials & Interfaces**, v. 11, p. 4425-4438, 2019.
https://doi.org/10.1021/acsami.8b19950

[96] BIERWAGEN, G.; BATTOCCHI, D.; SIMÕES, A.; STAMNESS, A.; TALLMAN, D. The use of multiple electrochemical techniques to characterize Mg-rich primers for Al alloys. **Progress in Organic Coatings**, v. 59, p. 172-178, 2007.
https://doi.org/10.1016/j.porgcoat.2007.01.022

[97] JADHAV, N.; GELLING, V. J. Review-The Use of Localized Electrochemical Techniques for Corrosion Studies, **Journal of the Electrochemical Society**, v. 166, n. 11, p. C3461-C3476, 2019.
https://doi.org/10.1149/2.0541911jes

[98] GALVÃO, T. L. P.; BOUALI, A. C.; SERDECHNOVA, M.; YASAKAU, K. A.; ZHELUDKEVICH, M. L.; TEDIM, J. Chapter 16 - Anticorrosion thin film smart coatings for aluminum alloys, Editor(s): MAKHLOUF, A. S. H.; ABU-THABIT, N. Y. Advances in Smart Coatings and Thin Films for Future Industrial and Biomedical Engineering Applications, Elsevier, p. 429-454, 2020.
https://doi.org/10.1016/B978-0-12-849870-5.00007-0

[99] AMERICAN SOCIETY FOR TESTING AND MATERIALS. **ASTM D3359-09**: Standard test methods for measuring adhesion by tape test. West Conshohocken, 2009.

[100] ALENCAR, M.A.S.; BENEDETTI, A.V.; FUGIVARA, C.S.; MESSADDEQ, Y. Construção de célula eletroquímica para observação de amostras in situ em estereomicroscópio. **Química Nova**, v. 33, n. 6, p. 1394-1397, 2010.
https://doi.org/10.1590/S0100-40422010000600031

Apêndice I

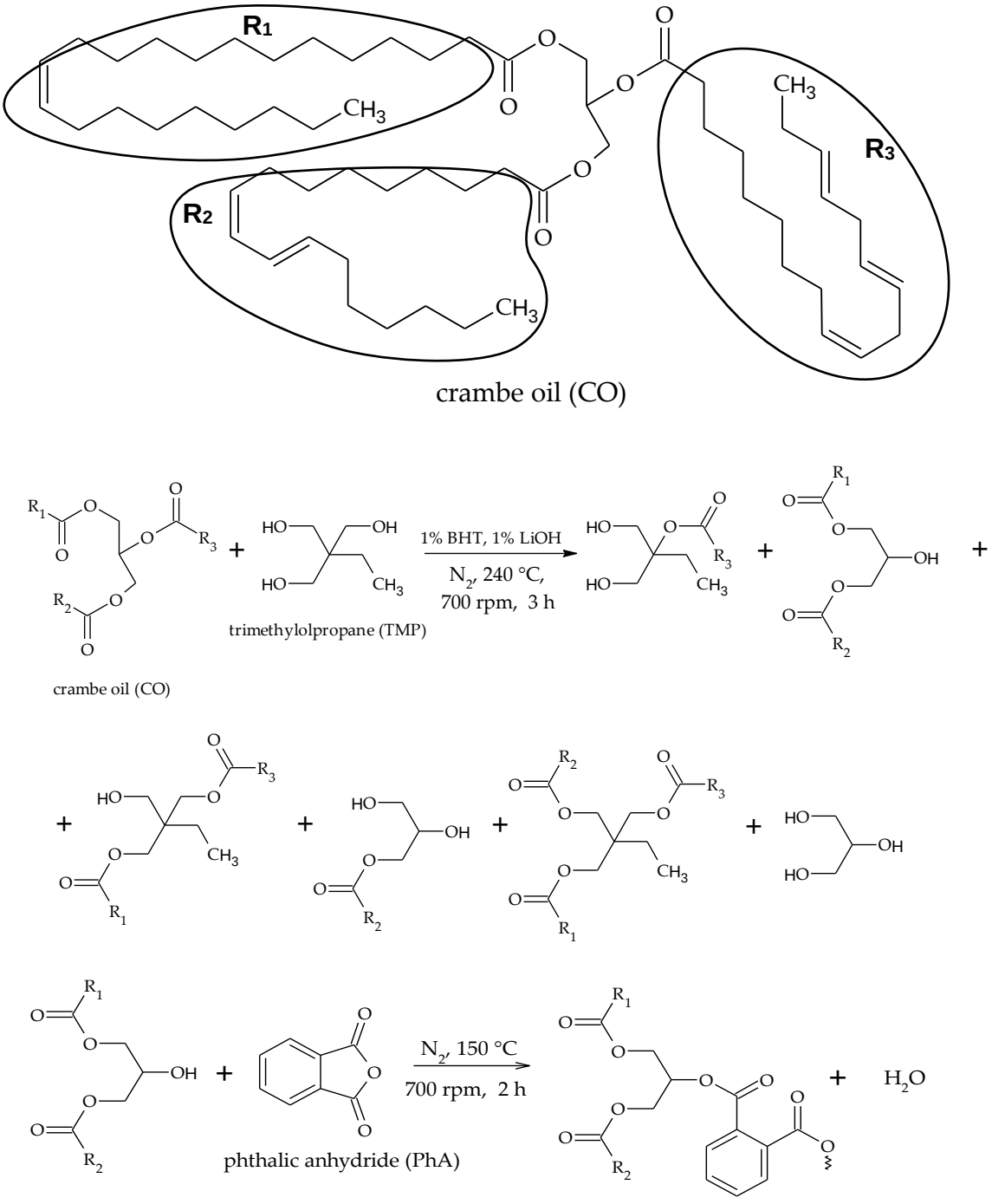

Figura 12A. Reações de obtenção do poliéster por meio da modificação do óleo de crambe.

Reproduced with permission from [J.V. Nardeli, C.S. Fugivara, E.R.P. Pinto, W.L. Polito, Y. Messaddeq, S.J.L. Ribeiro, A.V. Benedetti. Preparation of polyurethane monolithic resins and modification with condensed tannin yielding self-healing property. POLYMERS. v.11, p.1890, 2019] Copyright 2019 MDPI Polymers.

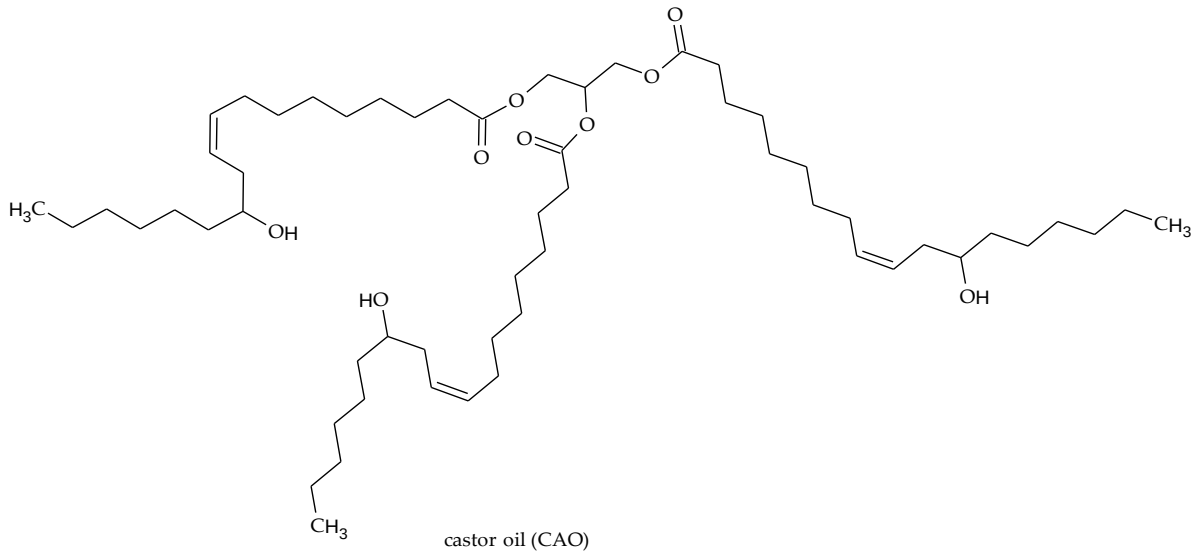

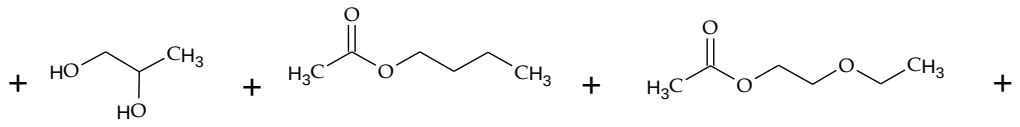

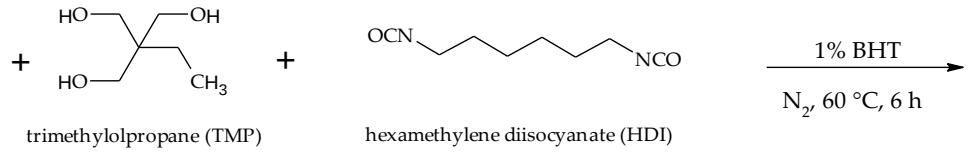

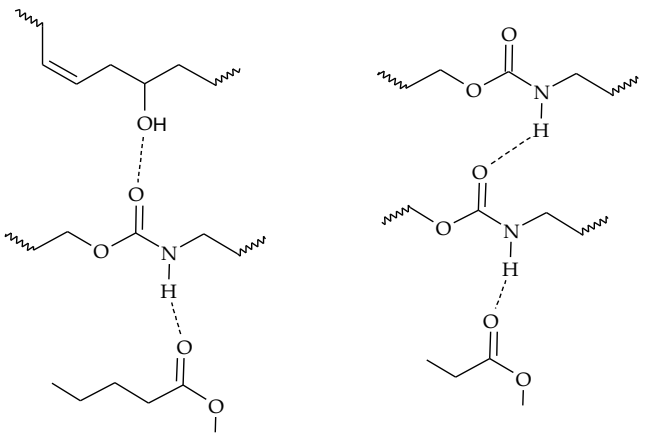

hydrogen bonds formed in the polyurethanes

Figura 13A. Reações de obtenção do pré-polímero por meio da modificação do óleo de mamona.

Reproduced with permission from [J.V. Nardeli, C.S. Fugivara, E.R.P. Pinto, W.L. Polito, Y. Messaddeq, S.J.L. Ribeiro, A.V. Benedetti. Preparation of polyurethane monolithic resins and

modification with condensed tannin yielding self-healing property. POLYMERS. v.11, p.1890, 2019] Copyright 2019 MDPI Polymers.

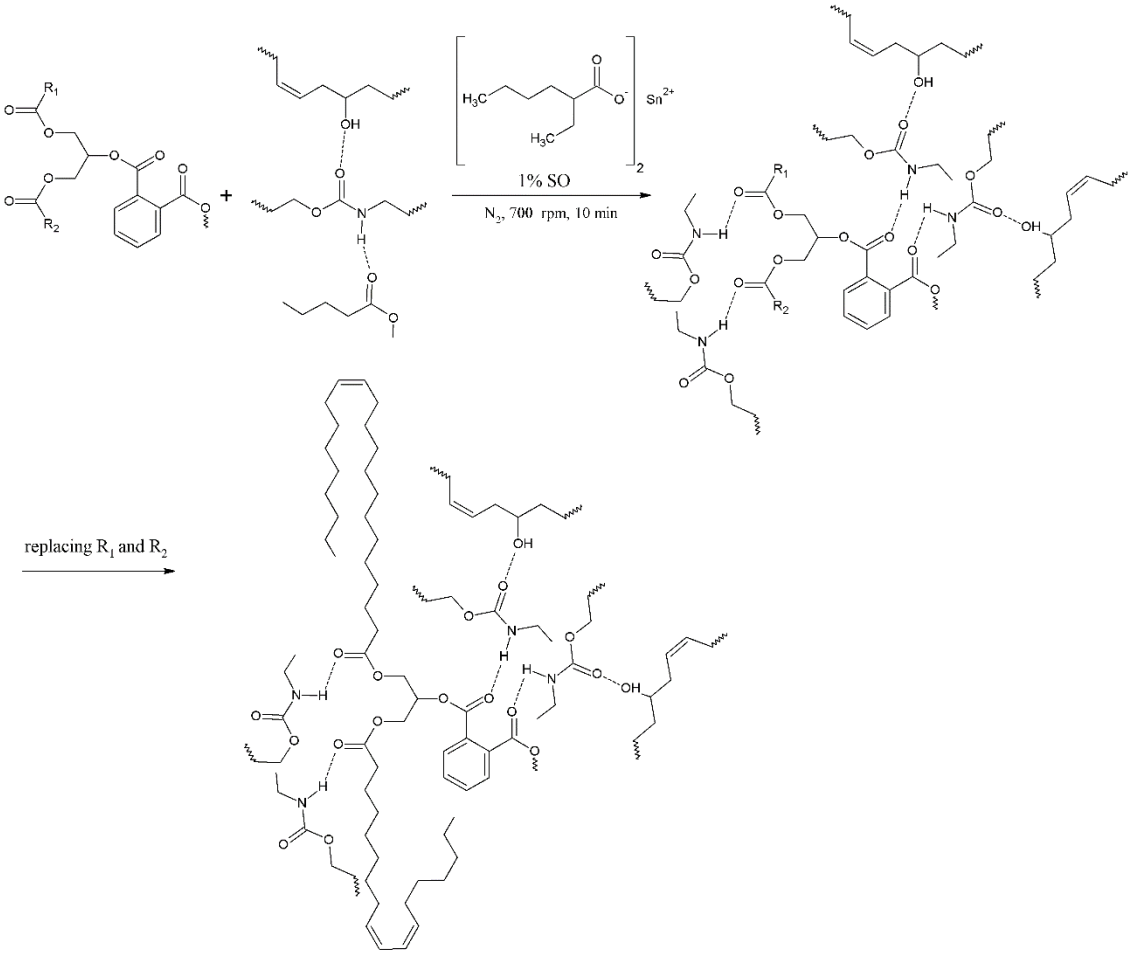

Figura 14A. Reações de obtenção da resina de PU.

Reproduced with permission from [J.V. Nardeli, C.S. Fugivara, E.R.P. Pinto, W.L. Polito, Y. Messaddeq, S.J.L. Ribeiro, A.V. Benedetti. Preparation of polyurethane monolithic resins and

modification with condensed tannin yielding self-healing property. POLYMERS. v.11, p.1890, 2019] Copyright 2019 MDPI Polymers.

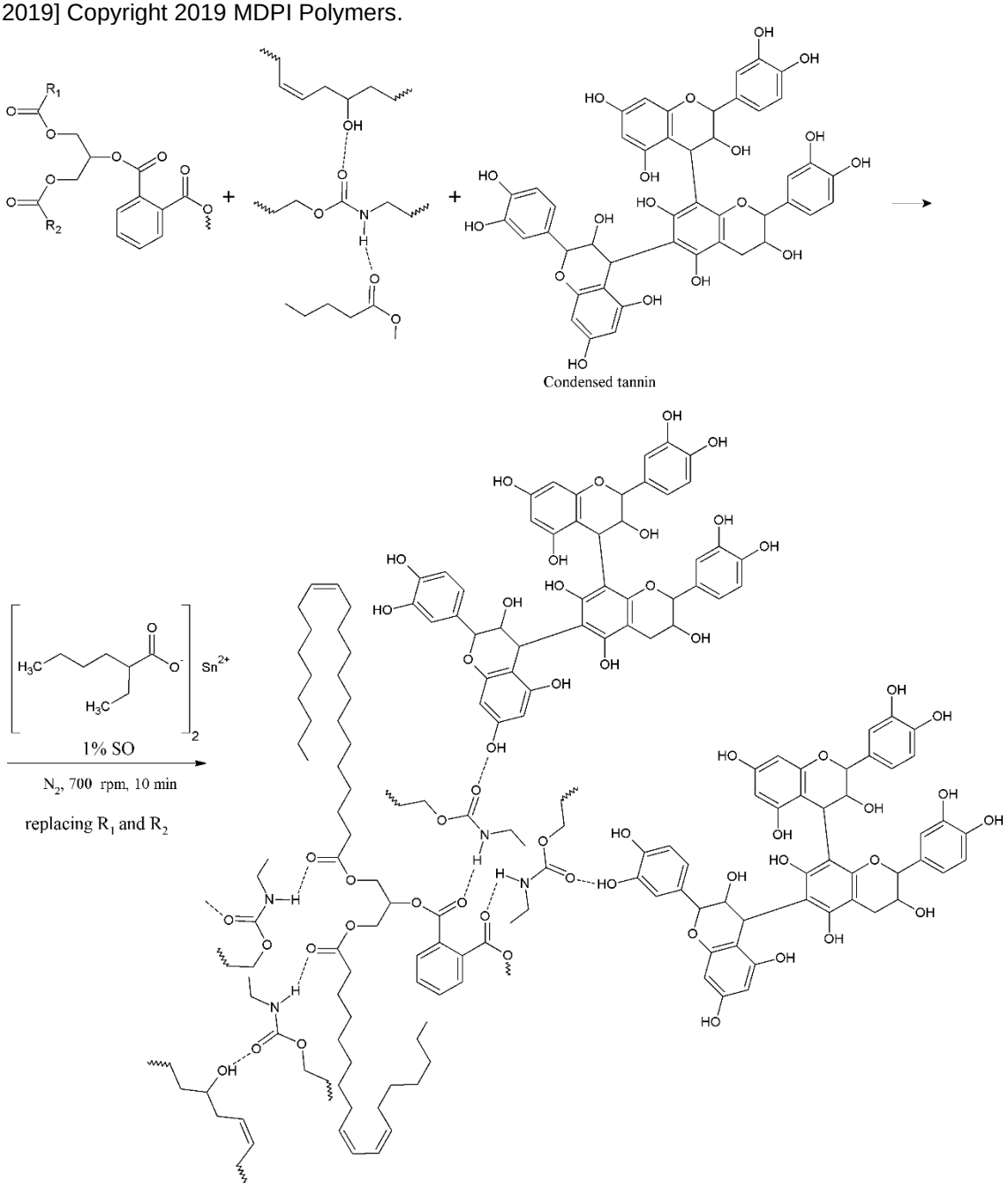

Figura 15A. Reações de obtenção da resina de PU-modificado com tanino condensado.

Reproduced with permission from [J.V. Nardeli, C.S. Fugivara, E.R.P. Pinto, W.L. Polito, Y. Messaddeq, S.J.L. Ribeiro, A.V. Benedetti. Preparation of polyurethane monolithic resins and

modification with condensed tannin yielding self-healing property. POLYMERS. v.11, p.1890, 2019] Copyright 2019 MDPI Polymers.

Apêndice II

Supplementary Material

Preparation of Polyurethane Monolithic Resins and Modification with a Condensed Tannin-Yielding Self-Healing Property

Jéssica Verger Nardeli [1,*], Cecílio Sadao Fugivara [1], Elaine Ruzgus Pereira Pinto [2], Wagner Luiz Polito [2], Younes Messaddeq [2], Sidney José Lima Ribeiro [2] and Assis Vicente Benedetti [1,*]

[1] São Paulo State University (UNESP), Institute of Chemistry, Department of Physical-chemistry, PO Box 355, Araraquara, 14801-970, SP, Brazil
[2] São Paulo State University (UNESP), Institute of Chemistry, Department of General and Inorganic Chemistry, PO Box 355, Araraquara, 14801-970, SP, Brazil
* Correspondence: jeh.nardeli@gmail.com (J.V.N.), assis.v.benedetti@unesp.br (A.V.B.)

video-a video-b

Figure S1. Videos of PU (**a**) and condensed tannin-modified PU (**b**) monoliths after applying an artificial defect during all immersion time in deionized water.

Vídeos: https://www.mdpi.com/2073-4360/11/11/1890#supplementary

Reproduced with permission from [J.V. Nardeli, C.S. Fugivara, E.R.P. Pinto, W.L. Polito, Y. Messaddeq, S.J.L. Ribeiro, A.V. Benedetti. Preparation of polyurethane monolithic resins and modification with condensed tannin yielding self-healing property. POLYMERS. v.11, p.1890, 2019] Copyright 2019 MDPI Polymers.

Apêndice III

Supplementary material
Novel healing coatings based on natural-derived polyurethane modified with tannins for corrosion protection of AA2024-T3

Jéssica V. Nardeli[a,b], Cecilio S. Fugivara[a], Maryna Taryba[b],
M.F. Montemor[b], Sidney J.L. Ribeiro[a], Assis V. Benedetti[a,*]

[a] Universidade Estadual Paulista-UNESP, Instituto de Química, 14800-060 Araraquara/SP, Brazil

[b] Centro de Química Estrutural-CQE, DEQ, Instituto Superior Técnico, Universidade de Lisboa, Av. Rovisco Pais, 1049-001 Lisboa, Portugal

[*] Corresponding author.
E-mail: jessica.nardeli@unesp.br (Jéssica V. Nardeli), assis.v.benedetti@unesp.br (Assis V. Benedetti)

Reproduced with permission from [J.V. Nardeli, C.S. Fugivara, M. Taryba, M.F. Montemor, S.J.L. Ribeiro, A.V. Benedetti. Novel healing coatings based on natural-derived polyurethane modified with tannins for corrosion protection of AA2024-T3. CORROSION SCIENCE. v.162, p.108213, 2020] Copyright 2019 Elsevier Ltd. Corrosion Science.

Additionally, a specific experiment was performed with a dedicated cell [M. A. Silva Alencar, A.V. Benedetti, C.S. Fugivara, Y. Messaddeq, Construção de célula eletroquímica para observação de amostras *in situ* em estereomicroscópio, Quim. Nova, 33 (2010) 1394-1397] containing the sample and a thin layer of 0.005 mol L^{-1} NaCl solution (same concentration used in LEIS). The surface was recorded during 25 h using a stereomicroscope coupled to a computer and TOP VIEW® software.

Fig. S1. Film (total time 25 h) indicating the self-heling effect.

Vídeos:
https://www.sciencedirect.com/science/article/pii/S0010938X19311175#sec0150

Reproduced with permission from [J.V. Nardeli, C.S. Fugivara, M. Taryba, M.F. Montemor, S.J.L. Ribeiro, A.V. Benedetti. Novel healing coatings based on natural-derived polyurethane modified with tannins for corrosion protection of AA2024-T3. CORROSION SCIENCE. v.162, p.108213, 2020] Copyright 2019 Elsevier Ltd. Corrosion Science.

Apêndice IV

Supplementary Information
Tannin: a natural corrosion inhibitor for aluminum alloys

Jéssica V. Nardeli[a,b], Cecilio S. Fugivara[a], Maryna Taryba[b], Elaine R.P. Pinto[a]
M.F. Montemor[b], Assis V. Benedetti[a,*]

[a] Universidade Estadual Paulista-UNESP, Instituto de Química, 14800-060 Araraquara/SP, Brazil

[b] Centro de Química Estrutural-CQE, DEQ, Instituto Superior Técnico, Universidade de Lisboa, Av. Rovisco Pais, 1049-001 Lisboa, Portugal

[*] Corresponding author.

E-mail: assis.v.benedetti@unesp.br (Assis V. Benedetti), jessica.nardeli@unesp.br (Jéssica V. Nardeli)

Reproduced with permission from [J.V. Nardeli, C.S. Fugivara, M. Taryba, E.R.P. Pinto, M.F. Montemor, A.V. Benedetti. Tannin: A natural corrosion inhibitor for aluminum alloys. PROGRESS IN ORGANIC COATINGS. v.135, p.368-381, 2019] Copyright 2019 Elsevier Ltd. Progress in Organic Coatings.

Table S1

EEC parameters used to fit the EIS diagrams obtained in 3.5% NaCl solution without and with 4.41×10^{-2} mol L^{-1} tannin for the different coatings applied on AA1200.

Coating **A** without inhibitor

Time	Elements						
	$CPE\text{-}T_{coat}/10^{-10}$ (S cm^{-2} s^n)	n_1	$R_{po}/10^5$ (Ω cm^2)	$CPE\text{-}T_{dl}/10^{-9}$ (S cm^{-2} s^n)	n_2	$R_{ct}/10^7$ (Ω m^2)	$\chi^2/10^{-3}$
3 h	4.62	0.93	0.31	1.52	0.86	5.72	0.54
(%error)	(7.05)	(0.53)	(2.98)	(2.67)	(0.18)	(0.43)	
5 h	8.47	0.89	2.16	82.5	0.95	0.16	0.96
(%error)	(2.25)	(0.20)	(0.44)	(1.58)	(0.47)	(0.96)	
30 h	4.73	0.93	0.50	5.42	0.71	0.019	0.26
(%error)	(6.19)	(0.45)	(6.71)	(6.41)	(1.11)	(2.04)	

Coating **A** with inhibitor

Time	Elements						
	$CPE\text{-}T_{coat}/10^{-10}$ (S cm^{-2} s^n)	n_1	$R_{po}/10^6$ (Ω cm^2)	$CPE\text{-}T_{dl}/10^{-11}$ (S cm^{-2} s^n)	n_2	$R_{ct}/10^8$ (Ω m^2)	$\chi^2/10^{-3}$
3 h	1.57	0.90	6.23	8.87	0.79	1.63	0.68
(%error)	(2.82)	(0.24)	(13.3)	(7.62)	(1.00)	(0.75)	
5 h	1.44	0.90	6.46	5.00	0.81	2.33	0.47
(%error)	(2.60)	(0.21)	(15.7)	(10.0)	(0.98)	(0.62)	
30 h	1.42	0.90	6.06	5.29	0.80	2.44	0.38
(%error)	(2.46)	(0.20)	(15.4)	(8.91)	(0.84)	(0.56)	
4 days	1.39	0.90	6.51	5.42	0.78	2.92	0.41
(%error)	(2.51)	(0.20)	(17.0)	(8.70)	(0.84)	(0.58)	
7 days	1.67	0.89	6.68	2.04	0.87	2.81	0.36
(%error)	(2.80)	(0.23)	(22.1)	(25.0)	(2.12)	(0.63)	

Coating **B** without inhibitor

Time	Elements						
	$CPE\text{-}T_{coat}/10^{-9}$ (S cm^{-2} s^n)	n_1	$R_{po}/10^5$ (Ω cm^2)	$CPE\text{-}T_{dl}/10^{-8}$ (S cm^{-2} s^n)	n_2	$R_{ct}/10^6$ (Ω m^2)	$\chi^2/10^{-3}$
3 h	1.26	0.90	7.77	0.059	0.90	55.7	0.40
(%error)	(1.63)	(0.14)	(3.87)	(3.98)	(0.47)	(0.29)	
5 h	1.43	0.89	3.61	1.40	0.92	1.78	1.60
(%error)	(2.28)	(0.21)	(0.99)	(3.14)	(0.71)	(0.70)	
30 h	1.34	0.90	1.95	1.21	0.92	1.77	0.44
(%error)	(1.43)	(0.12)	(0.52)	(1.43)	(0.29)	(0.32)	

Coating **B** with inhibitor

Time	Elements						
	$CPE\text{-}T_{coat}/10^{-11}$ (S cm^{-2} s^n)	n_1	$R_{po}/10^8$ (Ω cm^2)	$CPE\text{-}T_{dl}/10^{-11}$ (S cm^{-2} s^n)	n_2	$R_{ct}/10^9$ (Ω m^2)	$\chi^2/10^{-3}$
3 h	8.02	0.90	7.35	11.3	0.57	2.46	9.54
(%error)	(1.78)	(0.15)	(25.4)	(12.8)	(12.8)	(15.9)	
5 h	7.05	0.92	6.38	7.54	0.52	8.26	1.20
(%error)	(0.92)	(0.11)	(25.6)	(3.74)	(2.52)	(2.73)	
30 h	6.64	0.92	10.6	7.01	0.54	11.9	1.16
(%error)	(0.98)	(0.09)	(17.5)	(3.22)	(2.39)	(2.46)	
4 days	6.61	0.92	10.7	7.15	0.55	11.0	1.13
(%error)	(0.95)	(0.09)	(16.0)	(3.19)	(6.33)	(2.39)	
7 days	7.03	0.92	6.25	7.56	0.54	7.22	1.26
(%error)	(1.22)	(0.11)	(24.3)	(3.88)	(2.54)	(2.78)	

17 days	6.68	0.92	9.61	6.65	0.55	10.4	1.22
(%error)	(1.04)	(0.10)	(18.9)	(3.40)	(2.40)	(2.51)	
21 days	6.35	0.93	11.0	6.48	0.55	12.8	1.30
(%error)	(0.99)	(0.09)	(17.5)	(3.09)	(2.34)	(2.38)	
24 days	6.56	0.92	10.8	6.82	0.57	10.4	1.05
(%error)	(0.89)	(0.09)	(14.3)	(2.96)	(2.13)	(2.19)	
29 days	6.34	0.93	8.70	5.92	0.55	12.7	1.37
(%error)	(1.13)	(0.11)	(22.8)	(3.03)	(2.30)	(2.36)	
30 days	6.43	0.93	11.9	5.84	0.54	13.1	1.39
(%error)	(1.04)	(0.10)	(21.9)	(4.04)	(2.75)	(2.90)	